

**Studies on the separation of Cesium and Strontium
from acidic solutions using liquid membranes**

By

**Pankaj Kandwal
(CHEM01200704002)**

**Bhabha Atomic Research Centre,
Mumbai 400085, India**

*A thesis submitted to the
Board of Studies in Chemical Sciences
In partial fulfillment of requirements
For the Degree of*

Doctor of Philosophy

of

HOMI BHABHA NATIONAL INSTITUTE



May, 2012

Homi Bhabha National Institute

Recommendations of the Viva Voce Board

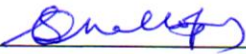
As members of the Viva Voce Board, we certify that we have read the dissertation prepared by Pankaj Kandwal entitled "Studies on the separation of Cesium and Strontium from acidic solutions using liquid membranes" and recommend that it may be accepted as fulfilling the dissertation requirement for the Degree of Doctor of Philosophy.

Chairman: Dr. A. Goswami  Date: 05.11.2012

Guide: Dr. P.K. Mohapatra  Date: 05.11.2012

Co-guide: Dr. (Smt.) S. Mukhopadhyay  Date: 05.11.2012

External Examiner: Prof. A.K. Singh  Date: 5.11.2012

Member 2: Dr. S. Chattopadhyay  Date:

Member 3: Dr. Manmohan Kumar  Date: 5/11/2012

Final approval and acceptance of this dissertation is contingent upon the candidate's submission of the final copies of the dissertation to HBNI.

I hereby certify that I have read this dissertation prepared under my direction and recommend that it may be accepted as fulfilling the dissertation requirement.

Guide:  Date: 05.11.2012

Co-guide:  Date: 05.11.2012

STATEMENT BY AUTHOR

This dissertation has been submitted in partial fulfillment of requirements for an advanced degree at Homi Bhabha National Institute (HBNI) and is deposited in the Library to be made available to borrowers under rules of the HBNI.

Brief quotations from this dissertation are allowable without special permission, provided that accurate acknowledgement of source is made. Requests for permission for extended quotation from or reproduction of this manuscript in whole or in part may be granted by the Competent Authority of HBNI when in his or her judgment the proposed use of the material is in the interests of scholarship. In all other instances, however, permission must be obtained from the author.

(Pankaj Kandwal)

DECLARATION

I, hereby declare that the investigations presented in this Thesis has been carried out by me. The work is original and has not been submitted earlier in whole or part for a degree / diploma to this or any other Institution / University.

(Pankaj Kandwal)

Dedicated to my Parents and Family

ACKNOWLEDGMENTS

I wish to express my sincere gratitude to my research guide Prof. P.K. Mohapatra and co-guide Dr.(Smt.) Sulekha Mukhopadhyay for their valuable guidance and constant encouragement throughout the work. I am also very thankful to them for helping me out of the difficulties found during research journey.

It is my great privilege to thank Prof. V.K. Manchanda for his keen interest in my work and giving me valuable suggestion and encouraging me to learn the subject more deeply. The Chairman (Dr. A. Goswami) and members of doctoral committee are deeply acknowledged for their critical analysis and valuable suggestions provided during the review presentations and pre-synopsis viva-voce.

It is my pleasure to thank Dr. M.S. Murali, Dr. P.N. Pathak and Dr. A. Bhattacharya for their encouraging discussions during the course of my doctoral research.

I am greatly thankful to Dr. S.A. Ansari, Dr. D.R. Raut, Shri D.R. Prabhu, Shri Rajesh Gujar, Shri Avinash Kanekar and Smt. Smita Dixit for their help and encouragement throughout this Thesis work. I would like to acknowledge my sincere gratitude to my labmates and friends Ajay Patil, Rakesh Shinde, Neelam Kumari, Praveen Verma, Rupali Lagad, Sharayu Kasar, Dr. Sadananda Das, Prakash Gope, Sandeep Wagh and Rohan Chinchale for their support and help throughout my doctoral research. I feel extremely fortunate to have Rohit, Naveen, Sunil, Nitendra, Arvind, Debes, Lokesh gambhir, Anuvab, Nazir Khan, Manoj Adhikari and Vijay as my friends who, be it a scientific or personal matter, were always be with me in any situation. I also thank Dr. Neha Pandey for her useful discussions and encouragement. I would like to express my

gratitude to my dear friend Arpita for giving me support through continuous encouraging me for the best of my research work.

Ever encouraging and motivating words from Sanjay Sir are always be a self sustaining power for me. I am specially thankful to him for his continuous help and support which lead me to the final goal of my life. Finally, I wish to acknowledge my Parents and family for their love and support during the research work and making me successful in achieving my dream.

May, 2012

Pankaj Kandwal

CONTENTS

| | |
|-----------------------------------------------------------------------------------------------------------|-----|
| SYNOPSIS | I |
| LIST OF FIGURES | X |
| LIST OF TABLES | XXI |
| CHAPTER 1: GENERAL INTRODUCTION | 1 |
| 1.1 Nuclear fission and nuclear energy: The concept of nuclear reactor | 2 |
| 1.2 Nuclear fuel cycle | 4 |
| 1.2.1 Wastes originating from the front-end of the fuel cycle | 5 |
| 1.2.2 Wastes originating from the back-end of the fuel cycle | 5 |
| 1.3 Classification of the nuclear waste | 6 |
| 1.3.1 Low level waste | 7 |
| 1.3.2 Intermediate level waste | 7 |
| 1.3.3 High level waste | 7 |
| 1.4 ^{137}Cs and ^{90}Sr: Source and impact on environment | 8 |
| 1.4.1 Isotopes of Cesium and Strontium | 9 |
| 1.4.2 Environmental hazards by Cesium and Strontium | 10 |
| 1.4.2.1 Radiocesium | 10 |
| 1.4.2.2 Radiostrontium | 11 |
| 1.4.3 Applications of ^{137}Cs | 11 |
| 1.4.4 Applications of ^{90}Sr | 12 |
| 1.5 Methods and reagents for extraction of Cesium and Strontium | 13 |
| 1.5.1 Separation of radiocesium | 13 |
| 1.5.1.1 Precipitation method | 13 |

| | | |
|----------------|------------------------------------------------------|----|
| 1.5.1.2 | Ion-exchange methods | 14 |
| 1.5.1.2.1 | Ferrocyanides and Phosphates | 15 |
| 1.5.1.2.2 | Titanates | 15 |
| 1.5.1.2.3 | AMP | 16 |
| 1.5.1.2.4 | Flexible sulphide framework for Cesium recovery | 17 |
| 1.5.1.3 | Solvent extraction | 18 |
| 1.5.1.3.1 | Crown ethers | 18 |
| 1.5.1.3.2 | Calixarenes and calix-crown ethers | 22 |
| 1.5.1.3.3 | Chlorinated cobalt dicarbollides (CCD) | 24 |
| 1.5.2 | Separation methods for radiostrontium | 25 |
| 1.5.2.1 | Precipitation method | 26 |
| 1.5.2.2 | Ion-exchange methods | 26 |
| 1.5.2.3 | Solvent extraction methods | 26 |
| 1.6 | Various techniques for recovery of metal ions | 29 |
| 1.6.1 | Solvent extraction | 29 |
| 1.6.2 | Ion-exchange technique | 33 |
| 1.6.3 | Extraction chromatography | 34 |
| 1.6.4 | Membrane based techniques | 34 |
| 1.6.4.1 | Non-supported liquid membranes | 35 |
| 1.6.4.1.1 | Bulk liquid membranes (BLM) | 35 |
| 1.6.4.1.2 | Liquid emulsion membranes (LEM) | 36 |
| 1.6.4.2 | Supported liquid membranes | 37 |
| 1.6.4.2.1 | Flat-sheet supported liquid membrane (FSSLM) | 38 |
| 1.6.4.2.2 | Hollow fibre supported liquid membrane (HFSLM) | 38 |

| | | |
|--------------------------------------------------------|-------------------------------------------------------------------|----|
| 1.7 | Mathematical modeling of mass-transport | 40 |
| 1.8 | Scope of the Thesis | 43 |
| CHAPTER 2: REAGENTS AND EXPERIMENTAL TECHNIQUES | | 46 |
| 2.1 | Radiotracers | 46 |
| 2.1.1 | Decay characteristics of ^{137}Cs and ^{90}Sr | 46 |
| 2.1.2 | Radiotracers | 48 |
| 2.2 | Materials and reagents | 49 |
| 2.2.1 | Crown ether | 49 |
| 2.2.2 | Calix-crown | 49 |
| 2.2.3 | Chlorinated cobalt dicarbollide (CCD) | 50 |
| 2.2.4 | PC-88A | 50 |
| 2.2.5 | Chemicals | 51 |
| 2.2.6 | Membranes | 52 |
| 2.2.7 | Preparation of Simulated High-Level Waste (SHLW) | 52 |
| 2.2.8 | Preparation of CCD solution | 53 |
| 2.3 | Analytical techniques | 54 |
| 2.3.1 | NaI (Tl) detector | 54 |
| 2.3.2 | High-Purity Germanium (HPGE) detector | 55 |
| 2.3.3 | Liquid scintillation counter | 56 |
| 2.3.4 | Viscometer | 57 |
| 2.3.5 | Inductively coupled plasma-atomic emission spectroscopy (ICP-AES) | 58 |
| 2.4 | Experimental methods | 59 |
| 2.4.1 | Solvent extraction | 60 |

| | | |
|---------------------------------------------------------------------------------|------------------------------------------------------------|----|
| 2.4.2 | Irradiation studies | 61 |
| 2.4.3 | Membrane transport studies | 61 |
| 2.4.3.1 | Flat-sheet supported liquid membrane (FSSLM) | 61 |
| 2.4.3.2 | Hollow fibre supported liquid membrane (HFSLM) | 63 |
| 2.5 | Mathematical modeling | 66 |
| CHAPTER 3: RECOVERY OF Cs BY Calix[4]arene-bis-(2,3-naphtho)-crown-6 | | 68 |
| 3.1 | Introduction | 68 |
| 3.2 | Distribution studies | 70 |
| 3.3 | Membrane transport studies | 74 |
| 3.3.1 | Transport profile of Cs(I) | 75 |
| 3.3.2 | Effect of carrier concentration | 79 |
| 3.3.3 | Effect of the feed acidity | 82 |
| 3.3.4 | Effect of cesium concentration | 84 |
| 3.3.5 | Transport of cesium from simulated high level waste (SHLW) | 85 |
| 3.3.6 | Effect of the flow rate | 88 |
| 3.4 | Conclusions | 89 |
| CHAPTER 4: STUDIES ON LIQUID MEMBRANE TRANSPORT OF STRONTIUM | | 92 |
| 4.1 | Introduction | 92 |
| 4.2 | Distribution studies | 95 |
| 4.3 | Hollow fibre supported liquid membrane studies | 96 |
| 4.3.1 | Transport of Sr(II) through HFSLM | 96 |

| | | |
|---------|-----------------------------------------------------------------------------------------------|-----|
| 4.3.2 | Effect of the feed acidity | 100 |
| 4.3.3 | Effect of the metal ion concentration | 102 |
| 4.3.4 | Transport of Sr from SHLW feed solution | 103 |
| 4.3.5 | Effect of the acid co-transport on the transport of Sr(II) | 104 |
| 4.4 | Separation of carrier free ^{90}Y from mixture of ^{90}Sr - ^{90}Y | 106 |
| 4.4.1 | Solvent extraction studies | 107 |
| 4.4.2 | Membrane studies | 112 |
| 4.4.2.1 | Flat sheet SLM transport | 112 |
| 4.4.2.2 | Hollow fibre SLM transport | 114 |
| 4.4.2.3 | Separation of ^{90}Sr and ^{90}Y and purity of the product | 116 |
| 4.4.2.4 | Radiation stability | 118 |
| 4.5 | Conclusions | 120 |

CHAPTER 5: MATHEMATICAL MODELING FOR MASS TRANSPORT IN LIQUID MEMBRANES 123

| | | |
|---------|-------------------------------------------------------------|-----|
| 5.1 | Introduction | 123 |
| 5.2 | Model development | 124 |
| 5.2.1 | Basic process of mass transport | 124 |
| 5.2.2 | Conditions for transport modeling | 127 |
| 5.2.3 | Diffusion and factors affecting diffusion | 128 |
| 5.2.3.1 | Wilke-Chang equation | 128 |
| 5.2.3.2 | Stokes-Einstein correlation | 129 |
| 5.2.4 | Mathematical modeling of cesium transport through FSSLM | 129 |
| 5.2.5 | Mathematical modeling of cesium ion transport in HFSLM mode | 133 |

| | | |
|------------------------------------------------------------------------------------------------------------------------------------------|-------------------------------------------------------------|-----|
| 5.3 | Procedure of solving differential equations in MATLAB | 135 |
| 5.4 | Model prediction and comparison results | 137 |
| 5.4.1 | Modeling of mass transfer across FSSLM | 137 |
| 5.4.1.1 | Solvent extraction studies | 137 |
| 5.4.1.2 | Liquid membrane studies | 138 |
| 5.4.1.2.1 | Calculation of mass transfer coefficients | 138 |
| 5.4.1.2.2 | Model validation using transport experiments | 140 |
| 5.4.1.2.2.1 | Effect of carrier concentration | 140 |
| 5.4.1.2.2.2 | Effect of feed acidity on transport profile of Cs(I) | 142 |
| 5.4.1.2.2.3 | Effect of feed metal ion concentration | 143 |
| 5.4.1.2.2.4 | Effect of diluent (NPOE and <i>n</i> -dodecane) composition | 146 |
| 5.4.2 | Modeling of mass transfer across HFSLM | 147 |
| 5.4.2.1 | Effect of carrier concentration | 148 |
| 5.4.2.2 | Effect of the feed acidity | 149 |
| 5.4.2.3 | Effect of feed metal ion loading | 150 |
| 5.4.2.4 | Effect of flow rate | 151 |
| 5.5 | Modeling of other membrane transport system | 152 |
| 5.6 | Conclusions | 153 |
| CHAPTER 6: DEVELOPMENT OF ALTERNATIVE DILUENT SYSTEM FOR SIMULTANEOUS RECOVERY OF CESIUM AND STRONTIUM BY CCD AND PEG MIXTURE | | 155 |
| 6.1 | Introduction | 155 |

| | |
|-----------------------------------------------------------------------|-----|
| 6.2 Solvent extraction studies | 158 |
| 6.2.1 Diluent composition optimization | 158 |
| 6.2.2 Kinetics of equilibrium | 160 |
| 6.2.3 The effect of HNO₃ concentration | 161 |
| 6.2.4 The effect of CCD concentration | 162 |
| 6.2.5 Addition of PEG-400 with CCD | 163 |
| 6.2.6 Co-current extraction of Cs(I) | 166 |
| 6.2.7 Reusability of the solvent | 166 |
| 6.2.8 Radiation stability of the solvent | 167 |
| 6.3 Membrane transport studies | 168 |
| 6.3.1 Diluent composition optimization | 169 |
| 6.3.2 Effect of feed acidity on the transport profile of Cs(I) | 171 |
| 6.3.3 Effect of CCD concentration on the transport of Cs(I) | 173 |
| 6.3.4 Membrane thickness variation | 174 |
| 6.3.5 Calculation of diffusivity by time-lag method | 175 |
| 6.3.6 Transport of Cs and Sr by CCD and PEG-400 mixture | 176 |
| 6.4 Conclusions | 178 |
| | |
| CHAPTER 7: SUMMARY AND CONCLUSIONS | 180 |
| | |
| REFERENCES | 186 |
| | |
| PUBLICATIONS | 202 |

“Studies on the separation of Cesium and Strontium from acidic solutions using liquid membranes”

In view of increasing demand for energy in developing countries like India, the quest for new resources of energy is quite reasonable. Nuclear energy is considered to be one of the best alternatives to the conventional sources of energy. The discovery of nuclear fission by Otto Hahn (known as the father of nuclear chemistry) gave a new direction towards the fulfillment of increasing demands of energy. Nuclear fission of few grams of ^{235}U by thermal neutrons gives an energy equivalent to burning of tones of coal and since it produces significantly lower amount of pollutants, it can be considered to be ‘green technology’. In nuclear power plants, controlled nuclear fission is carried out in nuclear reactors and the nuclear energy is used for electricity production. It is estimated that about 15-20 % of the world’s electricity requirement is fulfilled by the 430 nuclear power plants installed all over the world [1].

In closed nuclear fuel cycle, U and Pu are recovered from the spent fuel by the well known PUREX process. After reprocessing of the spent fuel, the safe management of nuclear waste is a challenge for nuclear scientists. The nuclear waste contains heat emitting fission products like ^{137}Cs , ^{90}Sr , minor actinides (^{241}Am , ^{243}Am , ^{245}Cm and ^{237}Np) and unrecovered U and Pu. Along with this, structural elements like Fe, Cr, Zr etc., are also present in the waste. The fission products ^{137}Cs ($t_{1/2}= 30.1$ y) and ^{90}Sr ($t_{1/2}=28.5$ y), due to their long half life and large heat output (^{137}Cs : 0.42 W/g and ^{90}Sr : 0.90 W/g), may create deformation of the glass matrix and hence increase the risk of leaching out of the radionuclides from the vitrified blocks. Therefore, regular surveillance of the disposal sites may be required leading to an increase in the overall expenditures of waste management. Also, leaching out of radionuclides from the repositories can be hazardous to the environment. Along with this, the chemical similarity of Sr with Ca and that of Cs with Na can lead to serious problem of interference of these nuclides in the biological system of human beings. Hence, on one hand, the separation of such radiotoxic nuclides reduces the waste volume in the vitrified blocks and hence will

minimize the MANREM problems while on the other, it will reduce the risk generated due to their toxicity to the biological system.

Long half life and high energy gamma rays emitted from ^{137}Cs make this radionuclide a viable alternative source for gamma irradiators to replace the commonly used ^{60}Co ($t_{1/2}=5.2$ y, $\gamma = 1173$ keV and 1332 keV) for the sterilization of medical accessories, food preservation, sewage sludge treatment, etc. Similarly, ^{90}Sr , due to its high heat output, has applications in various useful purposes like as heat source for thermo-electric and thermo-mechanical power generators (RTGs and RTMGs) in remote areas, military applications, etc [2,3,4].

Various reagents have been used for the separation of cesium and strontium from acidic as well as basic solutions. Precipitation of cesium has been carried out by using phosphotungstic acid, tetraphenyl borate anion, metal ferrocyanide / ferricyanide, etc. while lead sulfate as carrier was used for the precipitation of strontium from acidic solutions [4]. Ion-exchange methods have also been developed for the recovery of these metal ions. Inorganic ion-exchangers like zirconium phosphate, AMP etc., have been employed for the removal of cesium from solutions but the high cost and non-availability of these materials limit their use in larger scale. Recently, a new class of ion exchangers composed of combination of $[(\text{CH}_3)_2\text{NH}_2]^+$ and $[\text{Ga}_2\text{Sb}_2\text{S}_7]^{2-}$ ions have been found to be highly selective for cesium [5]. Zeolites and crystalline silicotitanate have also been found to be highly selective for cesium in the presence of large concentration of sodium and other alkali metals. Antimonic acid was used as ion-exchanger for strontium removal from wide range of acidity of aqueous solution. Simultaneous recovery of Cs and Sr has been carried out by adding PEG-400 with CCD in diluents like nitrobenzene / FS-13 [6, 7]. Recently, crown ethers and calix-crowns have drawn attention due to their high selectivity for a particular metal ion and ease of operation. Substituted 18 crown 6 ethers have been found to be selective extractants for Sr(II) from acidic solution [8]. These compounds are soluble in polar diluents like nitrobenzene, 1-octanol etc. However, the toxic nature of these diluents makes them less suitable for large scale processing.

Techniques like solvent extraction, ion-exchange, extraction chromatography and liquid membranes have been utilized for the recovery of metal ions from solutions. Out of

these, liquid membrane techniques are important in view of the fact that a very less amount of solvent is required for carrying out separation studies and simultaneous extraction and stripping is possible. Hence, expensive and exotic chemicals can be used in liquid membrane based separation methods. On the other hand, process modeling is an important aspect when we talk about large scale application of a process. Modeling of a process is important as a) it helps in better understanding of the process, b) optimization of process can be done with much less human efforts and, c) the scale up of the process can be achieved with less experimental trials. Various mathematical models are present in literature but the complexities of those models make their use very complicated [9].

In view of these, the main objectives of present work are to develop liquid membrane techniques (particularly hollow fibre supported liquid membrane, HFSLM) for the recovery of Cs and Sr from the acidic solution under the pressurized heavy water reactor-simulated high level waste (PHWR-SHLW) conditions. Various experimental conditions have been optimized by varying system compositions. It was also of interest to develop alternative diluent system to the toxic / corrosive diluents for the simultaneous recovery of Cs and Sr by the CCD and PEG mixture. Finally, it was also required to develop HFSLM technique for the separation of carrier free ^{90}Y from a mixture of ^{90}Sr - ^{90}Y for its therapeutic uses. A mathematical model was developed for transport modeling of metal ion through HFSLMs to simulate the transport processes.

Chapter 1: General Introduction

This Chapter gives an overview of the nuclear fuel cycle and sources of radio-caesium and radio-strontium. Various types of nuclear wastes generated during the reprocessing and their impact on the environment have been elaborated. The Chapter also describes the various separation methods viz., solvent extraction, ion-exchange, precipitation and liquid membranes etc., for the recovery of Cs and Sr from different waste solutions. Various challenges for recovery of these metals and their important applications have also been described. The advantages associated with calix-crowns and crown ethers over other reagents and challenges in their use have been elaborated. The merits of liquid

membranes including hollow fibre supported liquid membrane over other conventional techniques have been summarized. A brief comparison has been made on the different transport models for the transport of Cs and Sr in liquid membrane. The well known UNEX (UNiversal solvent EXtraction) process for the simultaneous recovery of Cs, Sr and minor actinides have been discussed in the light of the available literature [6]. The recent developments in the direction of recovery of Cs and Sr from aqueous solutions have been elaborated. This Chapter also lists the aims and objectives of the present study.

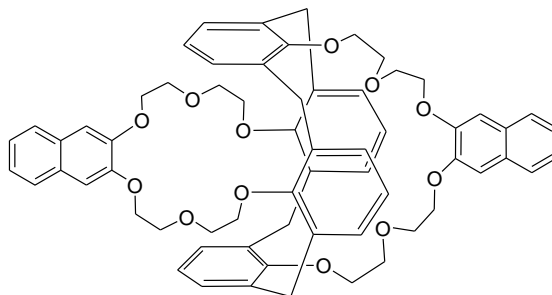
Chapter 2: Experimental

A general outline about different experimental techniques and instrumentations, used throughout the work, has been elaborated in this Chapter. Distribution studies have been carried out by equilibrating known volumes of organic and aqueous phases in stoppered glass tubes at constant temperature in a thermostated bath. Flat-sheet supported liquid membrane studies are performed with two-component Pyrex glass transport cells. The details of hollow fibre supported liquid membrane and impregnation of carrier solvent in the pores of the hollow fibre have been described in this Chapter. The sources of different radiotracers used in the present work along with their assaying methods have also been discussed. The estimation of gamma-emitting radiotracers was carried out by gamma counting employing NaI(Tl) and HPGe detectors. The assay of beta-emitting isotopes was performed by liquid scintillation counter. The basic principle and working of these detectors have been elaborated in this Chapter. A detailed description of the mathematical model developed and used in the present work has also been described.

Chapter 3: Recovery of Cs by calix[4]arene-bis-(2,3-naphtho)-crown-6

This Chapter elaborates on the recovery of cesium from acidic feed solutions using the cesium selective calix[4]arene-bis-(2,3-naphtho)-crown-6 (CNC) as the carrier ligand in the supported liquid membrane. Various parameters for the efficient transport of Cs were optimized in batch solvent extraction studies. A concentration of 1 mM CNC in 80% NPOE + 20% *n*-dodecane was optimized as the best carrier composition. Flat Sheet

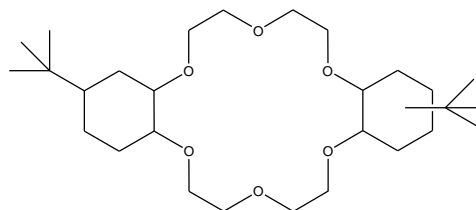
Supported Liquid Membrane (FSSLM) studies on 20 ml scale indicated that ~ 90% of cesium transport was possible in 24 hours from 3 M HNO₃ as the feed and distilled water as the strip solution. On the other hand, > 99.9% Cs transport could be achieved in 6 hours on 500 ml scale using Hollow Fibre Supported Liquid Membrane (HFSLM) under the optimized condition. Effect of feed acidity, ligand concentration and feed composition on the transport in HFSLM was studied and the results have been described in this Chapter. About 90% recovery of Cs was achieved from Pressurized Heavy-Water Reactor-Simulated High Level Waste (PHWR-SHLW) on 500 ml scale with excellent selectivity from the other metal ions present in the SHLW. The membrane stability was excellent and the results suggested possible application of the present technique for the recovery of Cs from nuclear waste solutions.



Calix[4]arene-bis(2,3-naphtho)-18-crown-6

Chapter 4: Transport studies on Strontium by liquid membrane

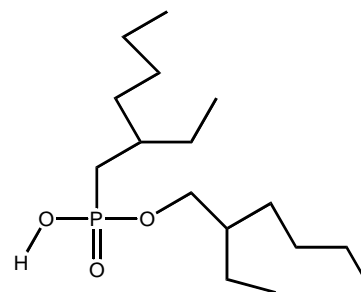
This Chapter describes the transport behaviour of Sr by HFSLM containing di-*tert*-butylcyclohexano 18-crown-6 (DTBuCH18C6) as the selective carrier for strontium. The batch solvent extraction studies as well as literature data suggested 0.1 M DTBuCH18C6 in 80% NPOE + 20% *n*-dodecane as the suitable carrier solvent composition for polypropylene hollow fibre membrane. Various experiments were performed to see the effect of feed acidity, metal ion concentration and feed composition on the transport of Sr. The results suggested that ~ 94 % recovery of Sr can be achieved in 3 hours from PHWR-SHLW under the optimized conditions. Quantitative transport of Sr was not possible and was ascribed to the significant amount of acid



**4,4'(5')di-*tert*-butylcyclohexano
18-crown-6**

transport from feed to strip phase solution. Due to higher acid transport to the strip side, the back transport of Sr was also observed. The back transport of Sr was prevented by neutralizing the strip phase acidity with NaOH at regular interval. Efforts were made to improve the transport efficiency of Sr using different strip solutions.

^{90}Y , a daughter product of ^{90}Sr , is an important radiopharmaceutical isotope due to its short half life (64.1 hours) and suitable beta-energy. In literature, different techniques have been reported for the purification of ^{90}Y from a mixture of $^{90}\text{Sr} / ^{90}\text{Y}$ at a relatively smaller scale (5-10 ml scale) [10]. HFSLM technique was successfully developed for the separation of carrier free ^{90}Y from the mixture of $^{90}\text{Sr} / ^{90}\text{Y}$ at litres scale using bis(2-ethylhexyl) phosphonic acid (PC-88A) as the carrier. Solvent extraction studies indicated that Y(III) can be selectively extracted by PC-88A at 0.1 M HNO_3 with D.F. values with respect to Sr(II) > 1000 . The extracted Y(III) could be back extracted with > 3 M HNO_3 . With the optimized experimental parameters, the ^{90}Y was selectively transported into the receiver phase by HFSLM, containing 20% (v/v) PC-88A, leaving behind the entire amount of ^{90}Sr in the feed solution. The purity of ^{90}Y was ascertained by various techniques and was found to be in the range of acceptable level. Hence, HFSLM technique can be used for the separation of carrier free ^{90}Y at liters scale with the required purity.



**bis(2-ethylhexyl) phosphonic acid
(PC-88A)**

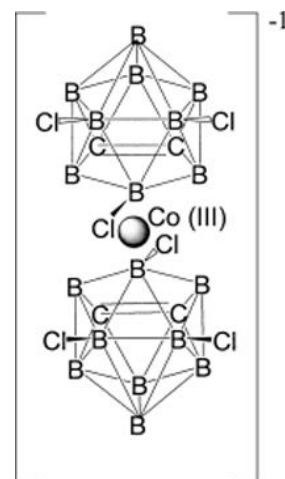
Chapter 5: Mathematical modeling for mass transport in liquid membranes

This Chapter describes the mathematical models developed for the mass transport phenomena in FSSLM and HFSLM. The models have been developed based on different diffusional parameters of the transported chemical species. Various assumptions have been made for the simplification of transport process and the basic fundamental behind the process are discussed in detail. Many of the mass transfer models found in literature

are very complicated and hence it was required to develop a simple model to simulate the mass transport through liquid membranes. The Chapter describes the procedure to formulate the equations by using mass-balance in the liquid membrane phase. The mathematical model developed to predict the transport behaviour of different metal ions was successfully validated by the experimental data. The proposed model can be used to predict the transport behaviour of Cs and Sr by HFSLM technique from different waste solutions.

Chapter 6: Simultaneous recovery of Cs and Sr by CCD and PEG

There is a world wide interest in the simultaneous recovery of Cs and Sr from the HLW using CCD (chlorinated cobalt dicarbollide) and PEG (polyethylene glycol) as the extractants in nitrobenzene or FS-13 (Phenyl trifluoro methyl sulphone) as the diluent. However, the toxicity of nitrobenzene and corrosive nature of the fluorinated diluent (FS-13) pose serious limitations on their large scale applications. Now a days, due to strict environmental regulations, these toxic and corrosive diluents are not recommended for large scale uses. In this context, it was required to develop a new diluent for CCD and PEG, which can be an alternative to these toxic diluents. Mixtures of NPOE and *n*-dodecane were evaluated as the diluent systems and the results are discussed in this Chapter. With 0.01 M CCD as the carrier, different compositions of diluent (NPOE + *n*-dodecane) were studied and it was found that with the lowering of NPOE percentage in the diluent, the distribution ratio of cesium increases with a regular trend. This is probably due to the possible interaction of CCD with NPOE which will be affecting the free CCD concentration in the organic phase thereby decreasing the distribution ratio. Effect of acidity and ligand concentration on the distribution behaviour of cesium has also been studied. The ligand variation studies revealed the 1:1 stoichiometry of the extracted species. In addition, simultaneous recovery of Cs and



Chlorinated cobalt dicarbollide (CCD)

Sr was carried out by adding PEG with CCD. Addition of PEG increases the strontium extraction while cesium extraction was found to be decreasing. Based on these results, membrane transport studies were carried out taking 0.01 M CCD in 60% NPOE + 40% *n*-dodecane as the carrier solvent with 1 M HNO₃ as feed while 8 M HNO₃ was employed as the strip phase. It was found that > 97% recovery of cesium was possible in 24 hours of operation. Other studies regarding stability of the liquid membrane, effect of system composition, effect of CCD concentration and feed acidity have been discussed thoroughly. The results show the possible recovery of cesium and strontium in NPOE and *n*-dodecane mixture.

Chapter 7: Summary and conclusions

The present research work deals with the separation of cesium and strontium from nuclear waste solutions by supported liquid membrane techniques. CNC (calix[4]arene-bis-2,3-naphtho 18-crown-6) has been used as a selective extractant for cesium which shows 1000 times better selectivity for Cs as compared to other alkali metal ions such as Na, K etc. On the other hand, di-*tert*-butylcyclohexano 18-crown-6 (DTBuCH18C6) has been successfully employed as selective carrier ligand for strontium. The separation of Cs and Sr has been successfully demonstrated on 500 ml scale using of PHWR-SHLW by the HFSLM technique. A HFSLM method has also been developed for the carrier free separation of ⁹⁰Y from ⁹⁰Sr with the required purity of ⁹⁰Y. In an approach to recover Cs and Sr simultaneously, a new solvent system (NPOE + *n*-dodecane) has been developed for CCD and PEG as successfully demonstrated in solvent extraction as well as supported liquid membrane techniques. The major findings of the present research work are summarized in this Chapter along with the future perspectives.

References:

1. IAEA Nuclear Technology Review **2009**, IAEA, Vienna, 3.
2. IAEA Technical Report Series No.356, IAEA, Vienna, (**1993**) 5.

-
3. Strontium-90 heat sources, R. Shor, R. H. Lafferty, Jr. P. S. Baker, ORNL-11C-36, May (1971).
 4. L.A. Bray, U.S. AEC Report BNWL-288, Battelle Pacific Northwest Laboratory, Richland, WA, 1967.
 5. Nan Ding and Mercouri G. Kanatzidis, *Nature Chemistry*, 2 (2010) 187.
 6. Jack D. Law, R. Scott Herbst, Terry A. Todd, Valeriy N. Romanovskiy, Vasily A. Babain, Vyatcheslav M. Esimantovskiy, Igor V. Smirnov, and Boris N. Zaitsev, *Solv. Extr. Ion Exch.*, 19 (2001) 23.
 7. M.S. Murali, D.R. Raut, D.R. Prabhu, P.K. Mohapatra, B.S. Tomar, V.K. Manchanda, *J. Radioanal. Nucl. Chem.*, xx (2011) xx.
 8. E.P. Horwitz, M.L. Dietz, D.E. Fisher, *Solv. Extr. Ion Exch.*, 8 (1990) 557.
 9. E. Bringas, M.F. San Roman, J.A. Irabien, I. Ortiz, *J. Chem. Technol. Biotechnol.*, 84 (2009) 1583.
 10. P.S. Dhama, P.W. Naik, N.L. Dudwadkar, R. Kannan, P.V. Achuthan, A.D. Moorthy, U. Jambunathan, S.K. Munshi and P.K. Dey, *Sep. Sci. Technol.*, 42 (2007) 1107.

LIST OF FIGURES

Figure 1.1: Worldwide production of energy by various sources. Source of data: RENEWABLES IN GLOBAL ENERGY SUPPLY.

Figure 1.2: Thermal neutron fission yield curve of U-235.

Figure 1.3: Schematic of Nuclear fuel cycle.

Figure 1.4: Structural formulae of various crown ethers relevant for alkali / alkaline earth metal ion complexation.

Figure 1.5: Cation-dipole interactions between metal ion and crown ether.

Figure 1.6: Structural formula of *bis*-(4,4'(5')-[1-hydroxy-2-ethylhexyl]-benzo)-18-crown-6.

Figure 1.7: Structural representation of different calixarenes.

Figure 1.8: Different conformations of calixarenes.

Figure 1.9: Structural formula of calix[4]arene-bis-crown-6.

Figure 1.10: Structural formula of calix[4]arene-bis(2,3-naphtho)-18-crown-6.

Figure 1.11: Structural formula of chlorinated cobalt dicarbollide.

Figure 1.12: Structural formula of *bis*-4,4'(5') [1-hydroxyheptyl]-cyclohexano-18-crown-6.

Figure 1.13: Schematic diagrams of BLM configurations: (a) beaker in beaker arrangement (b) U-tube arrangement.

Figure 1.14: Liquid Emulsion Membrane (LEM).

Figure 1.15: Flat-Sheet Supported Liquid Membrane.

Figure 1.16: Schematic representation of HFSLM set-up.

Figure 2.1: Decay scheme for ^{137}Cs .

Figure 2.2: Decay scheme for ^{90}Sr .

Figure 2.3: Structural formula of DtBuCH18C6.

Figure 2.4: Structural formula of Calix[4]arene-bis(2,3-naphtho)-crown-6.

Figure 2.5: Structural formula of CCD.

Figure 2.6: Structural formula of PC-88A.

Figure 2.7: NaI(Tl) detector Set-up.

Figure 2.8: The High-purity germanium detector (HPGe).

Figure 2.9: The Anton Paar Viscometer used for the viscosity measurements.

Figure 2.10: Thermostat bath for maintaining the temperature.

Figure 2.11: The transport cell used for the FSSLM studies.

Figure 2.12: Schematic diagram of HFSLM transport process.

Figure 2.13: The HFSLM experimental setup.

Figure 3.1: Structural formulae of (a) calix[4]-arene-bis(crown-6), (b) calix[4]-arene-bis(o-benzocrown-6) and (c) calix[4]-arene-bis(naphthocrown-6).

Figure 3.2: Variation of $K_{d,Cs}$ with the calix-crown ligand concentration. Aq. phase: 3 M HNO_3 ; Org. phase: CNC in 80% NPOE + 20% *n*-dodecane.

Figure 3.3: (a) Transport of Cs(I) by HFSLM and (b) $\ln(C_t/C_0)$ vs. 't' plot; Carrier: 1.0×10^{-3} M CNC in 80% (v/v) NPOE + 20% (v/v) *n*-dodecane + 0.4% Alamine 336; Feed: 3 M HNO_3 spiked with ^{137}Cs (500mL); Strip: Distilled water; Flow rate: 200 mL/min; Temperature: 25°C.

Figure 3.4: Gamma spectrum of the radionuclides in the feed, strip and raffinate solutions showing the selective transport of ^{137}Cs in HFSLM after 5 hours of operation; Carrier: 1.0×10^{-3} M CNC in 80% NPOE + 20% *n*-dodecane + 0.4% (v/v) Alamine 336; Feed: 3 M HNO_3 spiked with various radiotracers (500mL); Strip: Distilled water (500 mL); Flow rate: 200mL/min; Temperature: 25°C.

Figure 3.5: Linear plots of $\ln(C_t/C_0)$ vs. time for calculation of permeability coefficient; Carrier: Varying concentration of CNC in 80% NPOE + 20% *n*-dodecane containing 0.4% Alamine 336; Feed: 3 M HNO_3 spiked with ^{137}Cs tracer (500 mL); Receiver: Distilled water (500 mL); Flow rate: 200 mL/min. Temperature: 25°C.

Figure 3.6: Plot of $1/P$ vs $1/K_{ex}[NO_3^-]_{aq} \cdot [L]_{org}$ for the calculation of permeability parameters.

Figure 3.7: Transport profile of Cs(I) under various feed acidity. Carrier: 1.0×10^{-3} M CNC in 80% NPOE + 20% *n*-dodecane + 0.4% (v/v) Alamine 336, Strip: Distilled water, Flow rate: 200 mL/min.

Figure 3.8: Transport of Cs(I) by HFSLM at different cesium concentration. Carrier: 1.0×10^{-3} M CNC in 80% NPOE + 20% *n*-dodecane + 0.4% (v/v) Alamine-336; Feed: 3 M HNO₃ (500 mL); Receiver: Distilled water (500 mL); Flow rate: 200 mL/min.

Figure 3.9: Transport profile of Cs(I). Strip: Distilled water; Carrier: 1.0×10^{-3} M CNC in 80% NPOE + 20% *n*-dodecane containing 0.4% Alamine 336; Flow rate: 200 mL / min.

Figure 3.10: Acid transport profile with SHLW as feed (500 mL). Strip: Distilled water (500 mL), Carrier: 1.0×10^{-3} M CNC in 80% NPOE + 20% *n*-dodecane + 0.4% (v/v) Alamine 336, Flow rate: 200 mL/min.

Figure 3.11: Transport of Cs from SHLW; Carrier: 1.0×10^{-3} M CNC; Feed: SHLW spiked with ¹³⁷Cs tracer (500 mL); Strip: Distilled water (500 mL); Flow rate: 200 mL/min; Strip phases: □ distilled water, ○ acetate buffer at pH 5, and Δ dist. water neutralized with NaOH at 2 h intervals.

Figure 3.12: Variation of permeability coefficient (P) with flow rate; Carrier: 1×10^{-3} M of CNC; Feed: 3 M HNO₃ spiked with ¹³⁷Cs tracer (500 mL); Receiver: Distilled water (500 mL); Temperature: 25°C.

Figure 4.1: Structural formula of di-*tert*-butylcyclohexano 18-crown-6.

Figure 4.2: Transport profile of Sr(II) through HFSLM. Feed: 3 M HNO₃, Strip: Distilled water, Carrier: 0.1 M DtBuCH18C6 in 80% NPOE + 20% *n*-dodecane, Flow rate: 200 mL/min.

Figure 4.3: Transport of H⁺ by DtBuCH18C6 through HFSLM. Feed: 3 M HNO₃ spiked with ¹³⁷Cs; Strip: Distilled water; Carrier: 0.1 M DtBuCH18C6 in 80% NPOE + 20% *n*-dodecane; Flow rate: 200 mL / min.

Figure 4.4: Transport profile of Sr(II) at different feed acidity. Strip: Distilled water, Carrier: 0.1 M DtBuCH18C6 in 80% NPOE + 20% *n*-dodecane, Flow rate: 200 mL/min.

Figure 4.5: Sr transport profile at various metal ion loading. Feed: 3 M HNO₃ at varying HNO₃ acidity; Strip: Distilled water; Carrier: 0.1 M DtBuCH18C6 in 80% NPOE + 20% *n*-dodecane; Flow rate: 200 ml/min.

Figure 4.6: Comparative transport profile of Sr. Feed: SHLW or 3 M HNO₃; Strip: Distilled water; Carrier: 0.1 M DtBuCH18C6 in 80% NPOE + 20% *n*-dodecane; Flow rate: 200 mL/min.

Figure 4.7: Transport profile of Sr without and with the neutralization of strip phase acidity by NaOH. Feed: SHLW solution; Strip: Distilled water; Carrier: 0.1 M DtBuCH18C6 in 80% NPOE + 20% *n*-dodecane; Flow rate: 200 mL/min.

Figure 4.8: The effect of [H⁺] variation in feed on transport profile of Sr(II). Feed: Varying H⁺ at fixed 3 M NO₃⁻; Strip: Distilled water, Carrier: 0.1 M DtBuCH18C6 in 80% NPOE + 20% *n*-dodecane. Flow rate: 200 mL/min.

Figure 4.9: Structural formula of PC-88A.

Figure 4.10: Kinetics of equilibrium for extraction of Y(III) by 0.63 M PC-88A in *n*-dodecane. Aq. phase: 0.5 M HNO₃.

Figure 4.11: Plot of logK_{d,Y} vs. log[PC-88A]. Aqueous phase: 0.5 M HNO₃; Equilibration time: 1 hr.

Figure 4.12: Plot of logK_{d,Y} vs. log[H⁺]. Organic Phase: 0.63 moles /L PC-88A in *n*-dodecane, Aqueous phase: 3 M NO₃⁻; Equilibration time: 1 hour.

Figure 4.13: Distribution of Y(III) and Sr(II) from nitric acid medium by PC-88A. Organic phase: 0.63 M PC-88A; Diluent: *n*-dodecane; Equilibration time: 1 hour; Temperature: 25°C.

Figure 4.14: Transport of Sr(II) and Y(III) by PC-88A in FSSLM; Membrane support: 0.45µm PTFE; Carrier: 0.63 Mol/L PC88A; Diluent: *n*-dodecane; Feed: 0.1 M HNO₃ spiked with ⁹⁰Y and ^{85,89}Sr tracers (20mL); Strip: 3 M HNO₃ (20mL); Temperature: 25°C.

Figure 4.15: Transport of Y(III) and Sr(II) in HFSLM; Carrier: 0.63 M PC-88A; Diluent: *n*-dodecane; Feed: 0.1 M HNO₃ spiked with ⁹⁰Y and ^{85,89}Sr tracers (500 ml); Strip: 3 M HNO₃ (500 ml); Flow rate: 200 ml/min; Temperature: 25°C.

Figure 4.16: Plot of 1/P vs. 1/K_{d,Y} for the calculation of mass transfer coefficients.

Figure 4.17: log(N_t/N₀) vs. time plot for calculation of half life of radionuclide.

Figure 4.18: Purity analysis of ^{90}Y product after the HFSLM separation by the half-life method.

Figure 4.19: Effect of radiation dose on the permeation of Y(III) in FSSLM. Membrane support: 0.45 μm PTFE; Carrier: 0.63 M PC-88A; Diluent: *n*-dodecane; Feed: 0.1 M HNO_3 spiked with ^{90}Y and $^{85,89}\text{Sr}$ tracers (20 mL); Strip: 3 M HNO_3 (20 mL); Temperature: 25°C.

Figure 5.1: Schematic diagram showing concentration profiles across various zones of the supported liquid membrane transport system.

Figure 5.2: Schematic diagram showing the metal ion transport process by neutral extractant across a supported liquid membrane. $\text{M}^{\text{x}+}$ represents the metal ion; L stands for the carrier ligand.

Figure 5.3: Schematic diagram showing mass balance in fibre and feed tank.

Figure 5.4: Log-log plot of variation of $K_{\text{d,Cs}}$ with the ligand concentration. Aqueous phase: 3 M HNO_3 spiked with ^{137}Cs ; Organic phase: Varying concentration of CNC in 80% NPOE + 20% *n*-dodecane as the diluent.

Figure 5.5: Calculation of mass transfer coefficients. Feed: 3 M HNO_3 ; Strip: Distilled water; Carrier: 1.0×10^{-3} CNC in 80% NPOE + 20% *n*-dodecane.

Figure 5.6: Transport of Cs under varying ligand concentrations. Symbols \blacktriangledown , +, \blacktriangle , \bullet and \blacksquare are for 0.25×10^{-3} M, 0.5×10^{-3} M, 1×10^{-3} M, 2×10^{-3} M and 3×10^{-3} M concentrations

of CNC, respectively. Feed: 3 M HNO₃, Strip: Distilled water; Diluent: 80% NPOE + 20% *n*-dodecane + 0.4% Alamine 336.

Figure 5.7: Effect of feed acidity on transport of cesium. Symbols ■, ▲ and * represents 1, 2 and 3 M feed acidity respectively. Strip: Distilled water; Carrier solvent: 1.0×10⁻³ M CNC in 80% NPOE + 20% *n*-dodecane+ 0.4% Alamine 336.

Figure 5.8: Figure showing the effect of loading of cesium ion on the transport. Symbols ■, ▲ and * represents the case of 0.3 g/L, 0.1 g/L and 0.05 g/L feed cesium ion concentration. Carrier: 1.0×10⁻³ M CNC in 80% NPOE + 20% *n*-dodecane + 0.4% Alamine 336.

Figure 5.9: Transport profile of Cs(I) at varying diluent composition. Symbols ■, ▲, * and ▼ represents the diluent composition of 50-50%, 60-40%, 80-20% of NPOE- *n*-dodecane and 100 % pure NPOE. Carrier solvent: 1.0×10⁻³ M CNC; Feed: 3 M HNO₃; Strip: distilled water.

Figure 5.10: Transport of Cs(I) through HFSLM. Feed: Cs(I) in 3M HNO₃; Strip: distilled water; Carrier solvent: Varying concentration of CNC in 80% NPOE + 20% *n*-dodecane + 0.4% Alamine 336; Flow rate: 200ml/min.

Figure 5.11: Transport of Cs(I) at different feed acidity. Feed: Cs(I) in different conc. of HNO₃; Strip: Distilled water; Carrier solvent: 1.0×10⁻³ M CNC in 80% NPOE + 20% *n*-dodecane + 0.4% Alamine 336; Flow rate: 200 ml/min.

Figure 5.12: Cs(I) transport profile at varying CsNO₃ concentration in feed. Feed: Cs(I) in 3 M HNO₃; Strip: Distilled water; Carrier solvent: 1.0x10⁻³ M CNC in 80% NPOE + 20% *n*-dodecane + 0.4% Alamine 336; Flow rate: 200 ml/min.

Figure 5.13: Experimental and prediction results for Sr(II) transport through HFSLM containing 0.1 M DtBuCH18C6. Feed: 3 M HNO₃; Strip phase: Distilled water.

Figure 6.1: Structural representation of (a) 1,2-dicarbollide dianion and (b) transition metal bis-dicarbollide complex ion.

Figure 6.2: Structural formula of chlorinated cobalt dicarbollide (CCD).

Figure 6.3: Variation of distribution ratio of Cs(I) with varying diluent composition. Aqueous phase: 1 M HNO₃ containing ¹³⁷Cs tracer; Organic phase: 0.01 M CCD in NPOE + *n*-dodecane; Equilibration time: 1 hour.

Figure 6.4: Kinetics of extraction of Cs(I) by CCD. Aqueous phase: 1 M HNO₃ spiked containing ¹³⁷Cs; [CCD]: 0.01 M in 40% NPOE + 60% *n*-dodecane.

Figure 6.5: Variation of D_{Cs} with the nitric acid concentration. Organic phase: 0.01 M CCD in FS-13 or 40% NPOE + 60% *n*-dodecane; Aqueous phase: Varying concentration of HNO₃ containing ¹³⁷Cs tracer; Equilibration time: 1 hour.

Figure 6.6: log-log plot of D_{Cs} vs. CCD concentration. Aqueous phase: 1 M HNO₃; Diluent: 40% NPOE + 60% *n*-dodecane; Equilibration time: 1 hour.

Figure 6.7: Extraction of Cs(I) and Sr(II) by a mixture of CCD and PEG-400. Aqueous phase: 1 M HNO₃; Organic phase: 0.01 M CCD + varying concentration of PEG-400; Equilibration time: 1 hour.

Figure 6.8: Log-log plot of D_{Sr} vs. CCD concentration. Aqueous phase: 1 M HNO₃; Organic phase: Varying concentration of CCD + 0.04% (v/v) PEG-400; Equilibration time: 1 hour.

Figure 6.9: Successive extraction and stripping distribution ratio values using the fresh feed and strip solutions but regenerated solvent. Aqueous phase: 1 M HNO₃; Organic phase: 0.01 M CCD in 40% NPOE + 60% *n*-dodecane; Equilibration time: 1 hour.

Figure 6.10: Comparison of transport profile of Cs(I) through FSSLM at 1st and 5th day. Feed: 1 M HNO₃; Strip: 8 M HNO₃; Carrier: 0.01 M CCD in (a) 40% NPOE + 60% *n*-dodecane, (b) 60% NPOE + 40% *n*-dodecane, (c) 80% NPOE + 20% *n*-dodecane and (d) 100% NPOE.

Figure 6.11: Transport profile of Cs(I) at different feed acidity. Feed: HNO₃ at varying concentration; Strip: 8 M HNO₃; Carrier: 0.01 M CCD in 60% NPOE + 40% *n*-dodecane.

Figure 6.12: Transport profile of Cs(I) at varying CCD concentration. Feed: 1 M HNO₃; Strip: 8 M HNO₃; Carrier: CCD in 60% NPOE + 40% *n*-dodecane.

Figure 6.13: Transport profile of ¹³⁷Cs as a function of time. Feed: 1 M HNO₃; Strip: 8 M HNO₃; Carrier: 0.01 M CCD in 60% NPOE + 40% *n*-dodecane.

Figure 6.14: Transport profile of Cs and Sr. Feed: 1 M HNO₃; Strip: 8 M HNO₃; Carrier: 0.01 M CCD + 0.04% (v/v) PEG-400 in 60% NPOE + 40% *n*-dodecane.

LIST OF TABLES

Table 1.1: Composition of Pressurized Heavy Water Reactor Simulated High Level Waste.

Table 1.2: Various isotopes of Cesium and Strontium.

Table 1.3: Ionic size of various alkali / alkaline earth metal ions and cavity size of different crown ethers.

Table 2.1: Decay mode and analytical technique used for counting for various Radioisotopes.

Table 2.2: The list of various chemicals and reagents used in the studies.

Table 2.3: Details of hollow fibre membrane contactor (LiquiCel[®] X50: 2.5x8 Membrane Contactor) used in the present work.

Table 3.1: Measured value of viscosity, density and distribution ratio (K_d) for pure NPOE, *n*-dodecane and mixture of both as diluent.

Table 3.2: Variation of distribution ratio of metal ion with the metal ion loading. Feed: 3 M HNO₃ with different concentration of Cs(I), Organic Phase: 1.0×10^{-3} M CNC in 80% NPOE + 20% *n*-dodecane + 0.4% Alamine 336, Equilibration time: 1 h.

Table 3.3: % Transport and calculated permeability coefficient for five cascaded HFSLM runs. Feed: 3 M HNO₃ spiked with ¹³⁷Cs; Strip: Distilled water; Carrier: 1.0×10^{-3} M CNC in 80% NPOE + 20% *n*-dodecane + 0.4% Alamine336; Flow rate: 200 mL/min.

Table 3.4: Transport of Cs(I) by HFSLM and respective decontamination factor (D.F.) values with respect to various elements; Carrier: 1.0×10^{-3} M CNC in 80% (v/v) NPOE + 20% (v/v) *n*-dodecane + 0.4% (v/v) Alamine 336; Feed: 3 M HNO₃ spiked with ¹³⁷Cs (500 mL); Strip: Distilled water; Flow rate: 200 mL/min; Temperature: 25°C.

Table 3.5: Variation of distribution ratio ($K_{d,Cs}$) and Permeability coefficient (P) with the ligand concentration. Carrier: Varying concentrations of CNC; feed: 3 M HNO₃ spiked with ¹³⁷Cs tracer (500 mL); receiver: distilled water (500 mL); flow rate: 200 mL/min.

Table 3.6: Transport of acid at different feed acidity. Carrier: 1.0×10^{-3} M CNC in 80% NPOE + 20% *n*-dodecane + 0.4% (v/v) Alamine 336; Feed: HNO₃ of different acidity (500 mL); Strip: distilled water; Flow rate: 200 mL/min; Temperature: 25°C.

Table 3.7: Effect of Cs(I) concentration in feed solution on its transport rate; Carrier: 1.0×10^{-3} M calix[4]arene-bis-naphthocrown-6; Feed: CsNO₃ in 3 M HNO₃ spiked with ¹³⁷Cs tracer (500 mL); Receiver: Distilled water (500 mL); Flow rate: 200 mL/min.

Table 3.8: Cs and acid transport data during the FSSLM and HFSLM transport studies using tracer. Feed: 3 M HNO₃ spiked with ¹³⁷Cs; strip: distilled water. Flow rate for HFSLM: 200 mL/min; Temperature: 25°C.

Table 4.1: % Transport of various metal ions from PHWR-SHLW by HFSLM after 3 hours of operation. Strip: Distilled water; Carrier: 0.1 M DtBuCH18C6 in 80% NPOE + 20% *n*-dodecane; Flow rate: 200 mL/min.

Table 4.2: Transport of H^+ at varying feed acidity. Feed: HNO_3 at different concentration; Strip: Distilled water; Carrier: 0.1 M DtBuCH18C6 in 80% NPOE + 20% *n*-dodecane; Flow rate: 200 mL/min.

Table 4.3: Extraction of Y(III) and Sr(II) with PC-88A; Organic phase: 0.63 M PC-88A; Aqueous phase: HNO_3 ; Diluent: *n*-dodecane; Temperature: 25°C.

Table 4.4: Permeability coefficient (P) of Y(III) in FSSLM by irradiated solvent; Carrier: 0.63 Mol/L PC-88A in *n*-dodecane; Feed: 0.1 M HNO_3 ; Strip: 3 M HNO_3 ; Temperature: 25°C.

Table 4.5: Overview of the various literature reports and results obtained with present system.

Table 5.1: Variation of membrane mass-transfer coefficient and the viscosity of solvent with the variation in carrier concentration. Feed: 3 M HNO_3 ; Strip: Distilled water; Diluent: 80% NPOE + 20% *n*-dodecane.

Table 5.2: Distribution ratio of cesium at different cesium concentration in the feed. Carrier: 1.0×10^{-3} M CNC in 80% NPOE + 20% *n*-dodecane + 0.4% Alamine 336.

Table 5.3: The simulation results of cesium ion transport at different cesium concentration in feed. Simulation parameters: Feed: 3 M HNO_3 ; Strip: distilled water; Carrier: 1.0×10^{-3} M in 80% NPOE + 20% *n*-dodecane + 0.4% Alamine 336; Flow rate: 200 mL/min.

Table 5.4: Variation of extraction equilibrium constant (K_{eq}) and membrane mass-transfer co-efficient (k_{org}) with the variation in diluent composition. [CNC]: 1.0×10^{-3} M.

Table 6.1: Measured value of viscosity of various compositions of NPOE and *n*-dodecane.

Table 6.2: Co-current extraction of Cs(I) by CCD. Aqueous phase: 1 M HNO₃; Organic phase: 0.01 M CCD in 40% NPOE + 60% *n*-dodecane, Equilibration time: 1 hour.

Table 6.3: The effect of radiation dose on the distribution ratio of Cs(I) ion by CCD. Aqueous phase: 1 M HNO₃; Organic phase: 0.01 M CCD in 40% NPOE + 60% *n*-dodecane.

Table 6.4: % transport of Cs(I) after 6 h through FSSLM. Feed: 1 M HNO₃ spiked with Cs; Strip: 8 M HNO₃; Carrier: 0.01 M CCD in varying composition of NPOE + *n*-dodecane.

Table 6.5: Variation of % transport after 6 h and permeability coefficient with the membrane thickness. Feed: 1 M HNO₃; Strip: 8 M HNO₃; Carrier: 0.01 M CCD in 60% NPOE + 40% *n*-dodecane.

CHAPTER 1: General Introduction

For a large country like India with its over one billion population and rapid economic growth rate, no single energy resource or technology constitutes a panacea to address all issues related to availability of fuel supplies, environmental impact (particularly, climate change) and health externalities. Therefore, it is necessary that all non-carbon emitting resources become an integral part of an energy mix – as diversified as possible – to ensure energy security to a country like India during the present century. Available sources are low carbon fossil fuels, renewable and nuclear energy and all these should be subject of increased level of research, development, demonstration and deployment. Till now only about 6% of world's energy requirement is fulfilled by nuclear sources while oil and coal are used as major source of energy production [1].

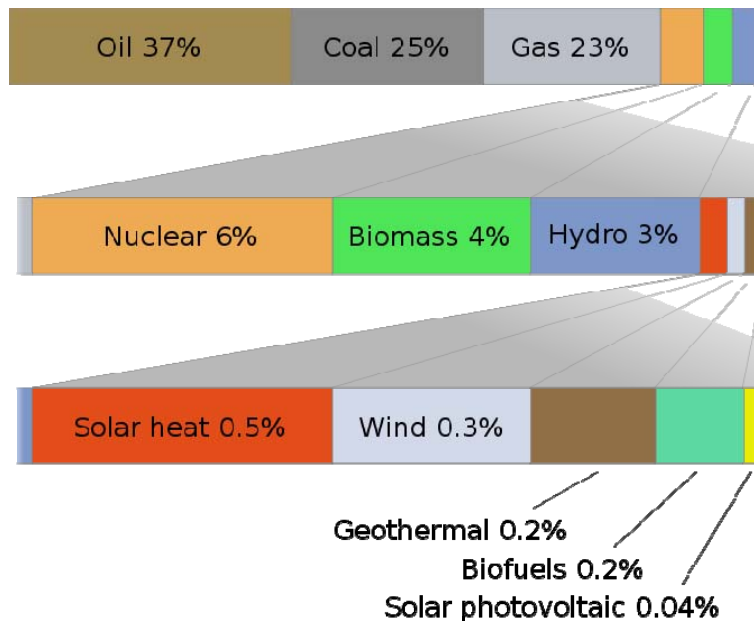


Fig. 1.1: Worldwide production of energy by various sources.

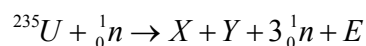
Source of data: RENEWABLES IN GLOBAL ENERGY SUPPLY [1]

Since coal and oils are non-renewable sources of energy, there is always a quest for viable alternative options. In this respect, nuclear energy is considered to be one of the green processes with significantly lower pollutant emission and can be a suitable alternative to conventional sources of energy.

1.1 NUCLEAR FISSION AND NUCLEAR ENERGY: THE CONCEPT OF NUCLEAR REACTOR

The discovery of nuclear fission is an important landmark in the history of nuclear science. ^{235}U when bombarded by thermal neutrons ($E_n < 0.025 \text{ eV}$), produces enormous amount of energy ($\sim 200 \text{ MeV}$ per fission per atom) along with a number of fission fragments. The mass loss in this process appears as the huge energy according to the Einstein's mass-energy relation.

The following equation shows the fission process



where X, Y represents fission products and E denotes the amount of energy released per fission per atom of ^{235}U . In nuclear fission, a number of fission products are produced as a result of unsymmetrical fragmentation of fissioning nuclides. Mass-yield curve of thermal neutron fission of ^{235}U has been shown in figure 1.2. It can be seen that in the fission-yield curve, two maxima occur around mass number of 95 and 140.

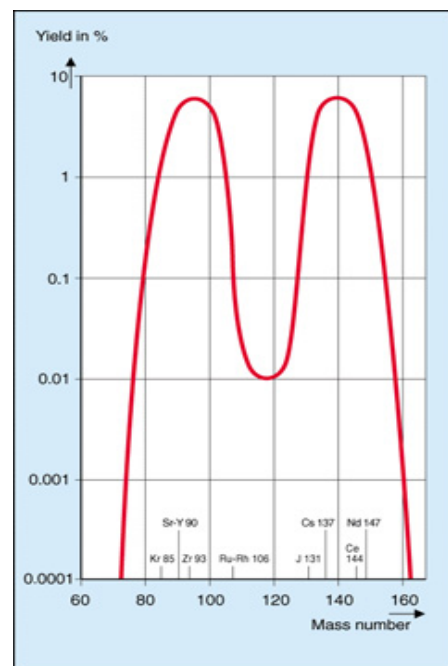


Figure 1.2: Thermal neutron fission yield curve of U-235

In nuclear fission, approximately 2.5 fast neutrons are produced per fission, which after thermalization can further take part in fission process. This shows that nuclear fission is a self-sustained process. But, if sufficient amount of fissile material is available, uncontrolled chain reaction can take place leading to explosive situation with the production of enormously large amounts of energy. Hence, it was thought to have some material that can absorb the extra neutron produced in the fission so that the net availability of neutron is just sufficient to sustain the chain reaction. This fundamental concept was used in designing the nuclear reactor to obtain controlled release of energy which can be subsequently used for electricity production.

Now a days, in pressurized heavy water reactor (PHWR), natural uranium (0.7 atom % of ^{235}U and 99.3% ^{238}U) is used as the fuel and heavy water is employed as the moderator to thermalize the fast neutron. Nuclear fuel coming from reactor contains a huge amount of unfissioned uranium and several radioactive elements formed due to the fission reaction. Countries like USA, where the uranium availability is sufficient, do not bother about the uranium and hence they adopted the once through nuclear fuel cycle in which the fuel is directly disposed into the deep repositories in remote areas. In a country like India, due to the limited natural sources of fissile material (^{235}U), the future of nuclear energy program is dependent on the availability of artificially made fissile elements like ^{233}U and ^{239}Pu . Therefore, closed nuclear fuel cycle is the required option in which valuable U and Pu are recovered from the spent nuclear fuel by the well known PUREX process. Further, it is required to carry out the safe management of the large volumes of radioactive wastes emanating from the PUREX cycle. Hence, the benefits of nuclear energy lie primarily in the safe management of nuclear waste.

1.2 NUCLEAR FUEL CYCLE

The combined process of mining and milling of fuel, enrichment of fissile element in fuel, fabrication into fuel rods, burning in reactor and management of nuclear waste is known as the complete nuclear fuel cycle. The schematic of the complete nuclear fuel cycle is shown in fig. 1.3. The fuel cycle is divided into two parts; initial part is known as the front-end of fuel cycle while the later one is termed as the back-end of nuclear fuel cycle.

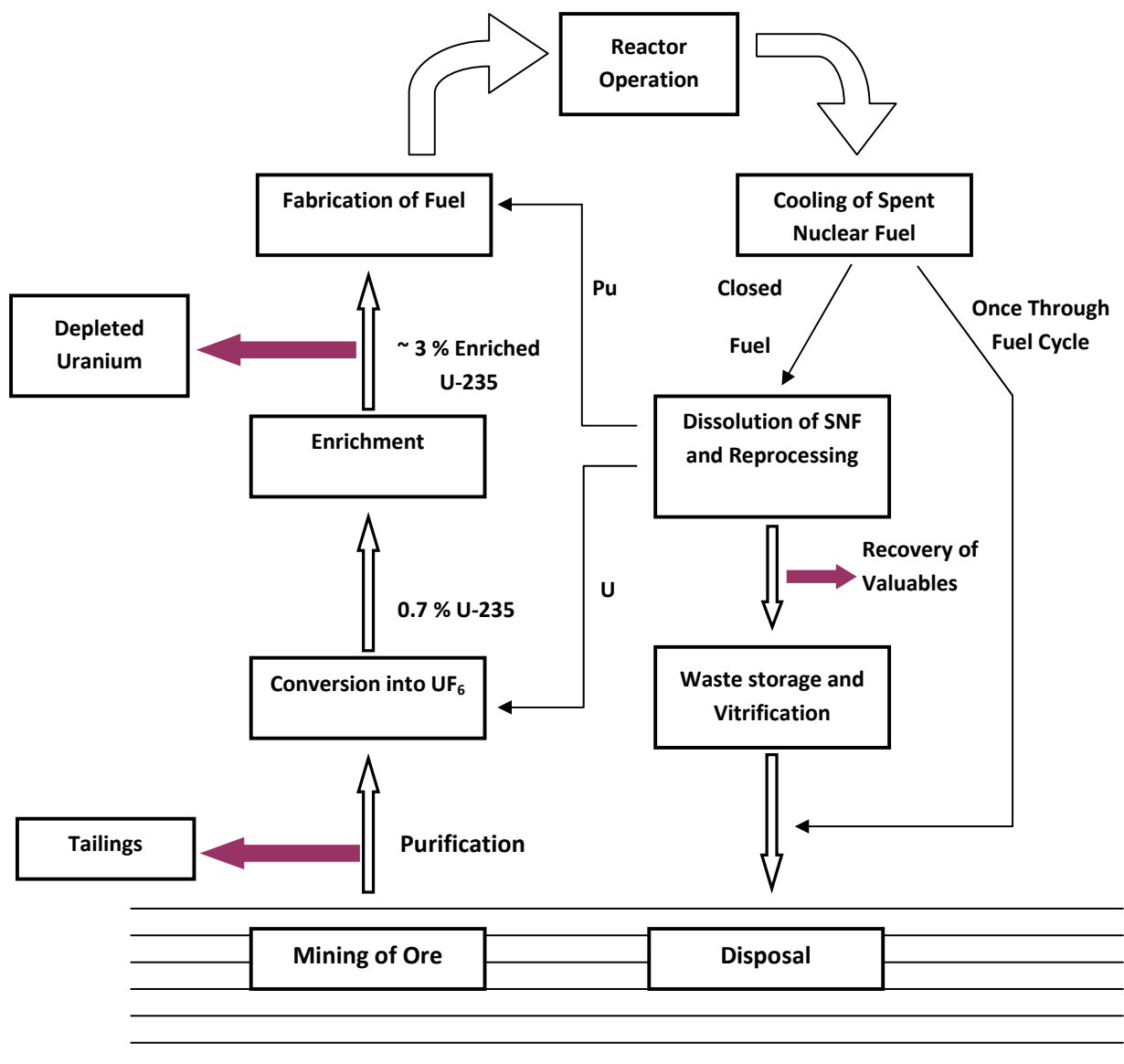


Figure 1.3: Schematic of Nuclear fuel cycle

1.2.1 Wastes originating from the front-end of the fuel cycle

The front-end of the nuclear fuel cycle consists of the process of mining and milling of fuel and fabrication of fuel into fuel rods. The waste originating from the mining process consists of the decay products of $^{235}\text{U}/^{238}\text{U}$. Waste from milling of mined ore contains mainly radium which is sent back to the mining sites where it is covered with rocks and clays. The “Uranium cake” produced after milling process is almost free from all decay products as most of them are removed through tailings.

1.2.2 Wastes originating from the back-end of the fuel cycle

The fuel rods coming after burning in the reactor contain highly radioactive elements generated through the fission and activation reactions. These rods are dissolved in concentrated nitric acid and the resulting solution is called ‘dissolver solution’. U/Pu is recovered from the dissolver solution by the PUREX process using TBP as the extractant. After the recovery of U and Pu, the PUREX raffinate contains the unrecovered U and Pu along with fission products, alpha-emitting activation products viz., ^{237}Np , ^{241}Am , ^{243}Am and ^{245}Cm , structural elements like Fe, Cr, Zr etc and process chemicals. The acidity of solution is adjusted at 3-4 M nitric acid and this highly radioactive solution is referred to as high level waste (HLW). The composition of PHWR-HLW is given in Table 1.1. The highly toxic nature of the elements in HLW requires big concern about the safe management of nuclear waste generated in the back-end of the nuclear fuel cycle.

Table 1.1: Composition of Pressurized Heavy Water Reactor Simulated High Level Waste [2]

| Element | Concentration (g/L) | Element | Concentration (g/L) |
|----------------|--------------------------------|----------------|--------------------------------|
| Na | 5.50 | Mo | 0.14 |
| K | 0.22 | Cs | 0.32 |
| Cr | 0.12 | Ba | 0.06 |
| Mn | 0.43 | La | 0.18 |
| Fe | 0.72 | Ce | 0.06 |
| Ni | 0.11 | Pr | 0.09 |
| Sr | 0.03 | Nd | 0.12 |
| Y | 0.06 | Sm | 0.086 |
| Zr | 0.004 | U | 6.34 |

1.3 CLASSIFICATION OF THE NUCLEAR WASTE

The nuclear waste from the back-end of the nuclear fuel cycle can be classified on various grounds. For example, based on the physical state, nuclear waste can be classified as solid nuclear waste and liquid nuclear waste while it can also be characterized by the type of radiation field (alpha, beta or gamma radiation) being produced or the radioactivity present in the waste stream. Also, waste can be categorized for specific purposes (special nuclear materials), in view of safety of working personnel or transportation etc. Worldwide, the nuclear waste is categorized depending on the radioactivity level of the wastes (high level waste, intermediate level waste and low level waste). This has been described in the next section.

1.3.1 Low level waste

The activity level in Low Level Waste (LLW) solution is less than millicurie per liter of solution. It is generated in various streams in nuclear waste as well as from radioactive laboratories, hospitals and industries. It mostly contains small amount of short lived radioactive elements associated in wastes like papers, bags, filters, tools, lean waste solution streams etc. The LLW is dumped in the superficial sites after reducing the waste volume.

1.3.2 Intermediate level waste

When the radioactivity level of waste ranges from millicurie to curie per liter, it is termed as Intermediate Level waste (ILW). It contains 7 % volume and 4 % radioactivity of total radioactive wastes in the world. Generally, ILW composed of materials originating from the treatment of high active wastes, resins used for concentration of activity, components of nuclear reactor etc. It requires more careful attention compared to LLW due to higher radioactivity level and it cannot be dispersed on the surface of disposal sites. It can be solidified in matrices like concrete or bitumen and then buried in the repositories.

1.3.3 High level waste

If the radioactivity level of waste is higher than curie per liter, the waste is known as High Level Waste (HLW). Due to significantly high levels of radioactivity, HLW is handled in proper shielded hot cells equipped with remote handling facilities. It comprises of the wastes originating from spent nuclear fuel processing, various liquid streams of reprocessing the spent fuel etc. The major radioactivity of nuclear waste is concentrated in HLW. Although it occupies 3% of total

volume, yet > 95% of total radioactivity is contributed by HLW. Special care is taken while handling and transportation of such waste solutions. Highly shielded containers are used to avoid radiation exposure to the working personnel. The 'concentration and containment' (CC) strategy is proposed for the safe management of HLW. In this process, the HLW is immobilized in glass matrices followed by containment in stainless steel canisters and then disposed off in deep geological repositories. Regular surveillance of the disposal sites is required for any kind of radioactivity leakage into the environment. Due to various heat emitting radioisotopes (e.g. ^{137}Cs , ^{90}Sr etc.) present in the HLW, there is a significant risk of deformation of glass matrices and leaching out of radionuclides into the environment which may be hazardous for living beings. Hence special attention has to be given for management for disposal of HLW.

1.4 ^{137}Cs AND ^{90}Sr : SOURCE AND IMPACT ON ENVIRONMENT

Cesium-137 and Strontium-90 are produced in nuclear reactor as a result of nuclear fission of the fissile elements. As can be seen in the fig.1.2, the two maxima occur at around mass-number of 95 and 140 and hence, these two radionuclides are produced in high yield during fission reaction in the reactor. These radionuclides are also found in environment due to the nuclear fallout from weapon testing or any nuclear activity or by mishandling of radiation sources of these elements. As of 2005, cesium-137 is the principal source of radiation in the zone of alienation around the Chernobyl nuclear power plant. Together with ^{134}Cs , ^{131}I and ^{90}Sr , ^{137}Cs was among the isotopes, distributed by the reactor explosion, which constitute the greatest risk to human health. ^{137}Cs and ^{90}Sr contribute towards major radioactivity and heat output of HLW and hence the removal of ^{137}Cs and ^{90}Sr from the HLW, prior to its disposal, is very important. Out of the various fission products, ^{137}Cs and ^{90}Sr are of significant long half life (^{137}Cs : 30.1 y, ^{90}Sr :

28.5 y). ^{137}Cs emits gamma radiation ($E_\gamma = 661 \text{ KeV}$) while ^{90}Sr emits beta particles and gets converted to ^{90}Y which is a pure beta emitting radionuclide ($E_\beta = 2.28 \text{ MeV}$) ultimately decaying to the stable ^{90}Zr . Chemical similarity of cesium with sodium and that of strontium with calcium may create problem with the biological system of various living beings. Sr (like Ca) is a bone seeker and so, if ^{90}Sr enters in the body, it may ultimately be deposited in the bones and produce un-necessary radiation exposure to the person which may cause bone cancer [3]. Hence, removal of these radionuclides would not only reduce the cost to regular surveillance of waste disposal sites but also reduce the waste volume to be disposed [4].

1.4.1 ISOTOPES OF CESIUM AND STRONTIUM

The various isotopes of cesium and strontium produced in the nuclear reactor along with their half-lives have been given in Table 1.2. Naturally occurring isotope of cesium is the stable ^{133}Cs while all the other isotopes of cesium are radioactive and are formed in nuclear reactor as a result of fission or other nuclear reaction. ^{133}Cs , ^{134}Cs , ^{135}Cs and ^{137}Cs are major isotopes of cesium produced in the reactor, with ^{137}Cs accounting for almost 43% of the total cesium. Strontium in freshly discharged spent fuel as a result of nuclear fission consists of stable isotope ^{88}Sr and radioactive isotopes ^{89}Sr , ^{90}Sr and ^{91}Sr , with ^{90}Sr accounting for about 60% of total strontium production by fission.

The major heat output of HLW is contributed by ^{137}Cs (0.417 W/g) and ^{90}Sr (0.93 W/g) present in the waste. The removal of these two long-lived isotopes may produce significant cooling to the waste and reduces the risk of matrix deformation, thereby reducing the risk generated by leaching out of the radioactive elements from the repositories.

Table 1.2: Various isotopes of Cesium and Strontium

| Radioisotope | T_{1/2} | Radioisotope | T_{1/2} |
|---------------------|-------------------------|---------------------|------------------------|
| ¹²⁹ Cs | 1.33 d | ⁸² Sr | 25.5 d |
| ¹³⁰ Cs | 29.2 min | ⁸⁴ Sr | Stable |
| ¹³¹ Cs | 9.7 d | ⁸⁵ Sr | 64.8 d |
| ¹³² Cs | 6.5 d | ⁸⁶ Sr | Stable |
| ¹³³ Cs | Stable | ⁸⁷ Sr | 2.8 h |
| ¹³⁴ Cs | 2.1 y | ⁸⁸ Sr | Stable |
| ¹³⁵ Cs | 2.3 × 10 ⁶ y | ⁸⁹ Sr | 50.5 d |
| ¹³⁶ Cs | 13.2 d | ⁹⁰ Sr | 28.5 y |
| ¹³⁷ Cs | 30.1 y | ⁹¹ Sr | 9.63 h |
| | | ⁹² Sr | 2.71 h |

1.4.2 ENVIRONMENTAL HAZARDS BY CESIUM AND STRONTIUM

The presence of ¹³⁷Cs and ⁹⁰Sr in the environment may adversely affect the ecological and biological systems. These elements can be adsorbed on the surface of sediments, soils and can enter the food chain. A report on Chernobyl accident states that approximately 5.4×10⁵ Ci of Cs-134 and 1.1×10⁵ Ci of ¹³⁷Cs along with 2.2×10⁶ Ci of ⁹⁰Sr activity was found to be dispersed around the Europe region [5].

1.4.2.1 RADIOCESIUM

The presence of radiocesium in ecological system may lead to severe problems. High radiation exposure due to radioactive cesium is a great problem for working personnel in

radiation fields (called MANREM problem). Cesium can enter in the human body by inhalation, ingestion or by penetration through skin. Due to the chemical similarity of cesium with sodium, radio-cesium can damage living cells by its high energy gamma rays. Experiments with dogs showed that a single dose of 3800 $\mu\text{Ci/kg}$ (140 MBq/kg, or approximately 44 $\mu\text{g/kg}$) is lethal within three weeks. External hazards due to the radiation field of ^{134}Cs and ^{137}Cs are even more harmful. The radiation effect due to these isotopes is as hazardous as high radiation exposure due to some ionizing radiation. Accidental ingestion of ^{137}Cs can be treated with Prussian blue, which binds to it chemically and then speeds its expulsion from the body.

1.4.2.2 RADIOSTRONTIUM

^{90}Sr is among the most dangerous radionuclide with serious health impacts. ^{90}Sr is a “bone seeker” that exhibits biochemical properties similar to calcium. After entering in the organism, most often by ingestion with contaminated food or water, about 70-80% of the dose is excreted. Virtually all of the remaining ^{90}Sr is deposited in the bone and bone marrow, with remaining 1% in the blood and soft tissues [6]. Its presence in the bone may cause bone cancer, cancer of the nearby tissues, or even leukemia. Exposure to ^{90}Sr can be tested by bioassay, most commonly by urine analysis.

1.4.3 APPLICATIONS OF ^{137}Cs

Long half life and high heat output of ^{137}Cs makes it a suitable radiation source in gamma irradiators to replace ^{60}Co ($t_{1/2} = 5.2$ years, $E_{\gamma} = 1.173, 1.332$ MeV). This will reduce the shielding requirement and frequency of source replenishment in the irradiators. The gamma irradiators are used for various purposes as given below [7]:

1. Gamma radiation by ^{137}Cs can be used for the preservation of foodstuffs by killing bacterial growth using gamma rays
2. Sterilization of medical accessories is carried out using gamma radiation
3. ^{137}Cs is also used in brachytherapy for treatment of certain types of cancer
4. Gamma sources are also used to make scintillation cameras
5. ^{137}Cs is also used industrially in gauges for measuring liquid flows and the thickness of materials

1.4.4 APPLICATIONS OF RADIO STRONTIUM

^{90}Sr finds extensive use in various fields due to its suitably high heat output and long half life. It is purely beta-emitting isotopes which give it special importance in various fields as listed below

1. ^{90}Sr is used in medical industries, as a radioactive source for thickness gauges and for superficial radiotherapy of some cancers. Controlled amounts of ^{90}Sr and ^{89}Sr can be used in treatment of bone cancer.
2. The daughter product of ^{90}Sr is ^{90}Y which is again a pure beta-emitting radioisotope. High purity ^{90}Y is used in radiopharmaceuticals for treatment of certain types of cancers due to its suitable radiological half life.
3. It is also used as a radioactive tracer in medicine and agriculture fields.
4. As the radioactive decay of ^{90}Sr generates significant amount of heat, and is cheaper than the alternative ^{238}Pu .

5. It is used as a heat source in many radioisotope thermoelectric generators, usually in the form of strontium fluoride. Due to high heat output (0.93 W/g), ^{90}Sr is viable candidate as fuel for thermoelectric and thermo-mechanical power generators (RTGs and RTMGs). It is also used in SNAP (system for Nuclear Auxiliary Power) systems which are used at remote and inaccessible areas, remote weather station or spacecrafts [8].

1.5 METHODS AND REAGENTS FOR EXTRACTION OF CESIUM AND STRONTIUM

Various experimental methods have been developed for the recovery of cesium and strontium from acidic as well as alkaline solution [9]. Methods and reagents have been developed and modified for the co-recovery of cesium and strontium as well as their independent extraction from the waste solution phases. These methods include precipitation by suitable reagents, ion-exchange, solvent extraction, etc.

1.5.1 SEPARATION OF RADIOCESIUM

Various methods have been developed for the extraction of cesium from alkaline / acidic media. Exhaustive work has been reported in the literature for the selective and efficient recovery of cesium from solution phase. The following part describes various methods developed.

1.5.1.1 PRECIPITATION METHOD

Phosphotungstate anion can be used to precipitate cesium ion from the solution at moderate acidity (0.5 to 2M). Sodium phosphotungstic acid, $\text{Na}_3[\text{P}(\text{W}_3\text{O}_{10})_4\cdot 4\text{H}_2\text{O}]$, has been used for this purpose to extract cesium at the Hanford site, USA [10]. The precipitate can be

dissolved in alkali (like NaOH) to recover cesium in the solution form. Alum co-precipitation was used at the Oak Ridge National Laboratory (ORNL) to separate cesium for commercial use (Rupp 1955, [11]). Since the goal was commercial use, purity rather than yield was of primary importance. In the published flow sheet for the removal of ruthenium, rare earths, strontium, and cesium, co-precipitation of cesium with ammonium alum or potassium alum followed removal of the other elements. In one batch contact, over 99% of the cesium was removed from solution. It was suggested that the cesium co-precipitation process might precede removal of other elements. The exact pH during the co-precipitation process was not reported, simply that a pH 2.5 solution was acidified. The presence of sulfate in the cesium-alum precipitate is not desirable in vitrification. Barton et al. [12] noted that cesium alum precipitates are bulky and non-selective.

1.5.1.2 ION-EXCHANGE METHOD

Ion exchange methods have also been employed for the recovery of cesium from aqueous solutions. Inorganic as well as organic ion-exchangers were found to be quite effective for radiocesium removal from waste solutions. The various inorganic ion-exchangers used for the recovery of cesium include phosphates, titanates, ferrocyanides, oxides, etc. Copper ferrocyanides ($[\text{CuFe}(\text{CN})_6] \cdot n\text{H}_2\text{O}$), some heteropolyacids (ammonium molybdophosphates, AMP), ammonium tungstophosphates and Zeolites (e.g. clinoptilolite and modernite) have been shown to be effective ion-exchanger for cesium recovery [13]. Inorganic ion-exchangers offer several advantages like stability to high radiation dose, good selectivity, reproducible stoichiometry and compatibility with glass or ceramic waste materials. But the high costs of these inorganic ion-exchangers have been the limiting factor in the application of these methods on plant scale operations.

1.5.1.2.1 Ferrocyanides and Phosphates

Copper and tungsten ferrocyanides have been found to be excellent with respect to the kinetics of uptake, ion-exchange capacity and selectivity for cesium ion but the chemical instability of this ion-exchanger in the acidity range of 0.5-1.0 M is one of the major disadvantages of these materials. Molybdenum ferrocyanide is found to be much more unstable under acidic conditions. The poor selectivity of these ferrocyanides is another serious issue [14]. Zirconium hydrogen phosphate has been found to be an excellent sorbent for cesium in the pH range of 2-10 [15].

1.5.1.2.2 Titanates

During 1975-78, studies on various titanates and silicotitanates were carried out by the researchers at Sandia National Laboratory and the use of sodium titanate material was done at Hanford during the same time period [16, 17]. It was possible to impregnate sodium titanate onto a resin. Although the capacity for cesium was not high enough, loading higher concentration of sodium titanate onto resin could improve the Cs uptake capacity. Crystalline silicotitanates (CST), and phosphorous / molybdenum or tungsten compounds have been applied for radiocesium recovery from the high-level tank wastes at Hanford. Zeolite materials were also tested for the recovery of Cs from actual tank wastes. Although silicotitanates worked well they could not be accepted due to less characterized data available at that time but the Zeolite materials were not accepted due to poor loading capacity for cesium (~ 1 g/Kg of Zeolite) compared to other materials like AMP. Recovery of cesium from the exchanger was not efficient and hence loaded exchanger is treated as final waste form. Commercially, the CST exchangers are available as trade name IONSIV[®] IE-911 and have been explored by research groups at

INEEL [18, 19]. The issues regarding the stability of these exchangers and elution properties are yet to be investigated in detail.

1.5.1.2.3 AMP

Ammonium molybdophosphate (AMP) is a crystalline dark yellow compound having the chemical formula $(\text{NH}_4)_3\text{PMo}_{12}\text{O}_{40}\cdot 3\text{H}_2\text{O}$. The polyhedra consist of porous sphere of 12 MoO_3 octahedra with phosphate group at the centre [20]. It is well known that ammonium molybdophosphate (AMP) is quite a selective ion-exchanger for cesium removal from salt loaded acidic solutions [21, 22]. The cesium exchange mechanism has been explained as exchange of cesium with the ammonium ion in the crystal lattice [23]. The selectivity for cesium over other alkali metal ions has been reported by Smit et al. [24] Before using AMP in column mode, it is immobilized on some solid support (called “binder”). The main disadvantage of ammonium molybdophosphate is its microcrystalline structure which makes the column operation difficult. The exchanger, ammonium molybdophosphate-alumina (AMP-A1203) in which alumina acts as a binder, showed better characteristics like better flow rates, radiation stability, performance of adsorption desorption cycles [25]. Poly-acrylo nitrile (PAN) has also been used as binder for AMP by various research groups [26, 27]. The support material has been found to have no affect on the cesium uptake behaviour by AMP. At INEEL, recovery of cesium from synthetic high level nuclear waste (acidity $\sim 3\text{M}$) had been studied. Once the column is loaded, AMP is separated and dissolved in NaOH solution, thus yielding a much smaller volume of HLW.

Various groups have investigated the radiation stability of AMP and found it to be quite good upto 1MGy dose. The cesium uptake behaviour has been found to be unaffected while

radiation affects the binding ability of AMP with the solid support. At higher radiation doses leaching of AMP from the support is reported which results in the degradation of the resin.

The advantages of AMP are,

- Sufficiently high distribution coefficient in moderately high acidic medium
- High Cs-loading capacity compared to other ion-exchangers
- High selectivity for Cs(I) ion
- Faster Cs-uptake
- Easily soluble in alkaline solution

However, certain disadvantages are,

- Difficulty of elution of absorbed Cs(I)
- Microcrystalline nature of AMP makes column operation difficult
- The high loading in the AMP results in high radiation doses in and hot spots on column.

1.5.1.2.4 Flexible sulphide framework for cesium recovery

A new class of inorganic ion-exchanger consisting of combination of $[(\text{CH}_3)_2\text{NH}_2]^+$ and $[\text{Ga}_2\text{Sb}_2\text{S}_7]^{2-}$ ions has been reported for cesium recovery [28]. The framework composed of $[(\text{CH}_3)_2\text{NH}_2]^+$ and $[\text{Ga}_2\text{Sb}_2\text{S}_7]^{2+}$ layers perforated with holes. Shape selectivity couples with framework flexibility, allowing the compound to respond to the ion-exchange process. The size, shape and flexibility of the holes allow Cs^+ ions in an aqueous solution to selectively pass through and enter the material *via* an ion-exchange process. Following capture, the structure dynamically closes its holes in a manner reminiscent of a Venus flytrap [29], which prevents the

Cs ions from leaching out. The back extraction of cesium from the loaded exchanger is a difficult task in this case also, which is the major drawback of this material. This study improves our understanding of selective ion capture and points to new insights on how to design compounds for practical applications such as the removal of radioactive ^{137}Cs from nuclear waste.

1.5.1.3 SOLVENT EXTRACTION

Solvent extraction methods have been widely used for cesium extraction using various reagents. High throughput, ease of operation, high selectivity are some of the advantages of solvent extraction methods which make them more attractive for separation scientists. Cesium ion being monovalent in nature is very difficult to extract from the solution using common extractants. Since the size of cesium ion is large compared to other alkali metal ions, it is the least hydrated ion in the solution. This property is made use of in extraction of cesium by hydrophobic anions like chlorinated cobalt dicarbollide. On the other hand, crown ethers have been found to be size-selective extractants which bind selectively with a particular alkali / alkaline earth metal ion having size compatibility with the cavity size of a suitable crown ether. This has been described in the next section.

1.5.1.3.1 Crown ethers

The discovery of crown ethers by Pederson [30] was a pioneering effort in the field of supramolecular chemistry. Crown ethers are cyclic polyethers forming a cavity having crown like shape hence the name crown ether is given to this class of molecules. Various crown ethers have been synthesized and are named according to the number of total atoms and number of oxygen atoms in the cyclic ring e.g. 15-crown-5 stands for a crown ether having 15 atoms

(carbon and oxygen) and 5 oxygen atom in the cyclic ring of crown ether. Figure 1.4 shows structures of various crown ether molecules.

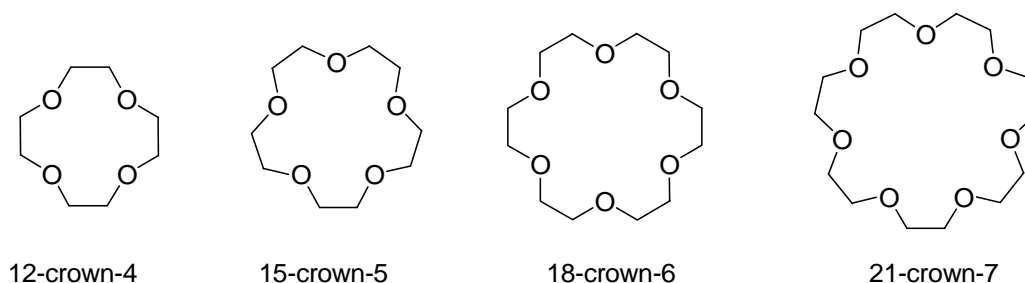


Figure 1.4: Structural formulae of various crown ethers relevant for alkali / alkaline earth metal ion complexation

The major factors governing the binding of metal ion with the crown ether are: 1) cavity size of the crown ether, 2) the hydration of metal ion in the solution and 3) substituents on the crown ether ring. Cavity size of crown ether plays an important role in the binding of the metal ion. It had been observed that metal ions having good size compatibility with the cavity of crown ether, bind more strongly. Cation-dipole interactions are responsible for the metal ion complexation with crown ethers (Figure 1.5).

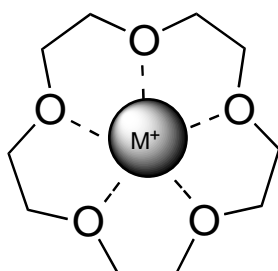


Fig. 1.5: Cation-dipole interactions between metal ion and crown ether

The cavity sizes of different crown ethers had been calculated by various groups using CPK model. The cavity size of different crown ethers and ionic size of various ions are given in Table 1.3. Crown ethers are stereospecific extractants as they have a cavity structure that can be

highly selective for the Cs⁺ or Sr²⁺ cations. The substituents on the crown ether ring have been found to have crucial effects on the extraction chemistry of metal ions.

Table 1.3: Ionic size of various alkali / alkaline earth metal ions and cavity size of different crown ethers

| Metal ion | Ionic size (Å) | Crown ether | Cavity radius (Å) |
|------------------|----------------|-------------|-------------------|
| Na ⁺ | 0.95 | 12-crown-4 | 0.67 ± 0.07 |
| K ⁺ | 1.33 | 15-crown-5 | 0.97 ± 0.12 |
| Rb ⁺ | 1.48 | 18-crown-6 | 1.45 ± 0.15 |
| Cs ⁺ | 1.69 | 21-crown-7 | 1.92 ± 0.23 |
| Sr ²⁺ | 1.13 | 24-crown-8 | 2.25 ± 0.28 |
| Ba ²⁺ | 1.43 | | |

Early work on crown ethers as extractants for cesium and strontium was performed by Gerow et al. [31] at the University of South Carolina and also by Kinard et al. [32] at Oak Ridge national Laboratory. Researchers at Argonne National Laboratory developed dibenzo-substituted 18-crown-6 ether for the selective recovery of cesium. The substituent groups make the geometry of the crown ether molecule rigid and thereby making it more selective for a particular metal ion. The interaction between the *pi*-electron cloud of benzo group and the cesium ion is considered to be one of the reasons for the higher selectivity of dibenzo-18-crown-6 for cesium ion over other alkali metal ion. Since the size of Cs⁺ ion is bigger than the cavity size of this crown ether, it is observed that the cesium ion sits above the cavity of molecule and coordinate with two crown rings in a sandwich type structure. McDowell et al. (1992) suggested di-*tert*-butyl-21-crown-7 to be a better extractant for cesium compared to their unsubstituted homologues. Their studies using

feasible process for the recovery of Cs and/or Sr which can be applied on plant scale based solely on crown ethers.

1.5.1.3.2 Calixarenes and Calix-crown ethers

Calixarenes are another class of macrocyclic compounds that have been used for the selective metal ion extraction. Calixarenes are formed by coupling of benzene moieties via methylene ($>CH_2$). Some typical calixarene structures are shown in figure 1.7.

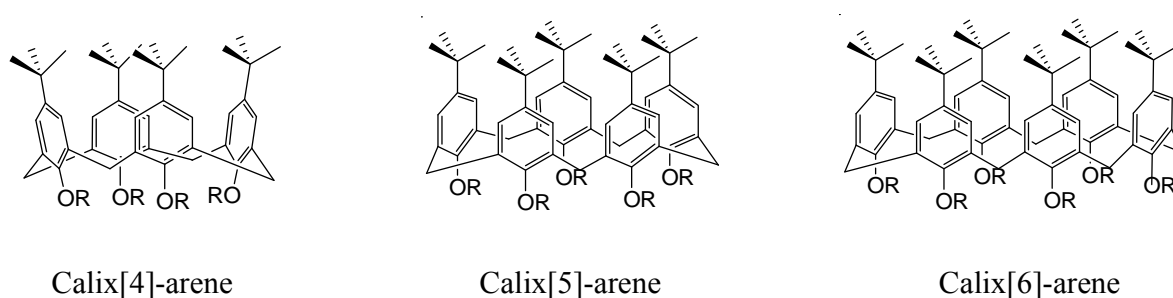


Figure 1.7: Structural representation of different calixarenes.

Calixarenes are found in various conformations viz., cone, partial cone, 1, 2-alternate, 1, 3-alternate conformations as shown in Figure 1.8.

Earlier studies of Zinke et al. [37], suggested that the calixarenes are capable of extracting alkali or alkaline earth metal ions. The substituents on calixarene framework are responsible for the extraction of different metal ions. Introduction of *p-tert*-butyl group on the molecule increases the cesium extraction by the calixarene. The substitution by ketone / ester group on calix[4]-arene makes it susceptible for alkali metal ion extraction.

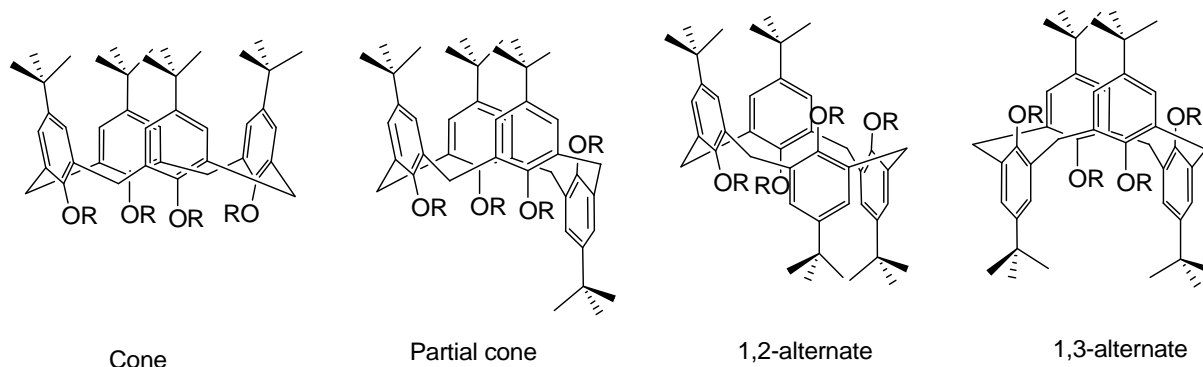


Figure 1.8 Different conformations of calixarenes

Izatt et al. were first to report the recovery of cesium and other alkali metal ions by *p-tert*-butyl substituted calixarenes using bulk liquid membranes [38].

These calixarenes offer certain advantages viz., lower water solubility, radiation stability, selective nature etc. Calixarenes are soluble in polar organic diluents like nitrobenzene, dichloromethane etc. and have been used for cesium recovery. The efficiency of metal ion extraction decreases with increase in the size of calixarene in the following order: calix[6]-arene < calix[5]-arene < calix[4]-arene. This may be due to more flexibility of the

larger size molecule making the complexation weaker.

In the subsequent modifications, calixarenes have been coupled with the crown ether molecules which are named as calix-crowns. Various calix-crowns

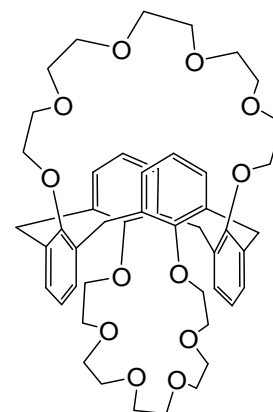


**Figure 1.9
Structural formula of
calix[4]arene-bis-
crown-6**

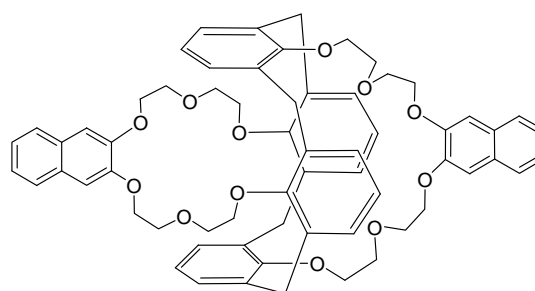


**Figure 1.10 Structural formula of calix[4]arene-
bis(2,3-naphtho)-18-crown-6**

have been synthesized and tested for metal ion extraction. Calix[4]-arene in 1,3-alternate conformation coupled with two crown-6 rings (Figure 1.9) has been found to be highly selective for cesium ion [39-41]. This is attributed to the favorable cavity size of crown ring and the cation- π interaction between cesium ion and benzene rings [42].

Substitution on crown ether ring affects the extraction ability of the calix-crown ligands to a greater extent. Substitution on crown ring by benzene group enhances the cesium extraction many folds. The benzene ring can be assumed to be increasing the organophilicity of the cesium-complex thereby facilitating the extraction of cesium. Haverlock et al. [43], have examined calix[4]-arene-bis(2,3-naphtho)-crown-6 (to be abbreviated henceforth as CNC, Fig. 1.10) for cesium recovery from waste solution and found that even at a very low concentration of this ligand, cesium can be selectively recovered from the solution with decontamination factor values $> 10^2$ for sodium and other metal ions. In case of calix-crowns, the ease of extraction and stripping are the major advantage. The studies revealed the possible application of calix-crown ethers for the recovery of radio-cesium from the nuclear waste of PUREX origin [44].

1.5.1.3.3 Chlorinated cobalt dicarbollides (CCD)

The first transition metal dicarbollide (CCD) was reported by Hawthorne et al. (1965) and has been subsequently studied by Czech researchers [45, 46]. It is a hydrophobic anion formed by coupling of two chlorine substituted-dicarbollide anions with Co(III). The protonated form of this anion is found to be highly selective for cesium ion from low acidic solutions. The structure of CCD is

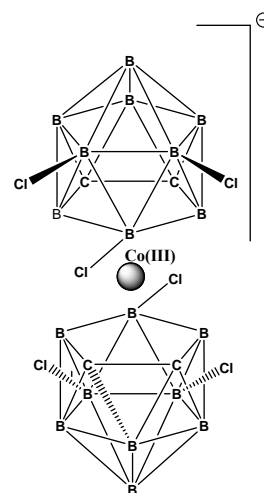


Figure 1.11
Structural formula of
chlorinated cobalt
dicarbollide (CCD)

shown in figure 1.11. It is soluble in polar organic diluents like nitrobenzene or fluorinated diluents (like phenyl trifluoro methyl sulphone or FS-13). The hazardous nature of these diluents has always been the major drawback of using the CCD for cesium recovery on large scale.

CCD is found to be a highly selective extractant for cesium from acidic medium. The Czech researchers determined that strontium could also be extracted along with cesium by adding polyethylene glycol (PEG) to the CCD dissolved in nitrobenzene [47]. Cesium ion is the least hydrated ion in aqueous solutions compared to other metal ions and combines to the poorly hydrated CCD anion and gets transferred to the organic phase. Addition of PEG is considered to dehydrate the strontium ion and thereby facilitating the extraction of Sr along with Cs. In the UNiversal solvent EXtraction (UNEX) process, cesium and strontium are extracted together along with all lanthanides and actinides by using a mixture of 0.08 M CCD + 0.1 % (v/v) PEG-400 + 0.2 M CMPO in FS-13 / nitrobenzene.

CCD has main advantage of being highly radiation resistant which makes it a viable candidate for its use in the treatment of nuclear waste [48]. The major limitation of the UNEX process is the use of toxic / corrosive diluents. Hence, there is a need for alternative diluent to be explored for CCD and PEG mixture for Cs and Sr co-recovery from radioactive wastes on large scale.

1.5.2 SEPARATION OF RADIOSTRONTIUM

Various methods and reagents have been investigated for the recovery of Sr from nuclear waste solutions. Similar to cesium recovery, precipitation method, ion-exchange, solvents extraction methods have been developed for strontium removal. A variety of reagents have been tested and suitably applied for the recovery of strontium.

1.5.2.1 Precipitation method

In 1961, researchers at the Hanford site recovered mega-curies of ^{90}Sr from HLW solution using lead sulphate carrier in the pH range of 1-2. The recovery of strontium from the precipitate was not possible and thereby generated large volumes of secondary waste. The lead sulfate carrier precipitation technology was also used to recover ^{90}Sr from mildly acidic solutions of dissolved sludge [49].

1.5.2.2 Ion-exchange methods

Antimonic acid had been used by European investigators for recovery of ^{90}Sr from highly acidic solution and HLW [50, 51]. Antimonic acid is highly efficient and selective ion-exchanger for strontium sorption. It suffers from disadvantages like poor loading kinetics and inefficient elution of the loaded ^{90}Sr from the ion-exchanger. Monosodium titanate as ion-exchanger has also been used for the recovery of Sr along with actinides from the alkaline wastes of Savannah River site origin [52].

1.5.2.3 Solvent extraction methods

Various liquid-liquid extraction methods have been described for the recovery of radiostrontium from the nuclear waste during the last several decades. Di-(2-ethylhexyl) phosphoric acid (D2EHPA) diluted with TBP and hydrocarbon diluent has been shown to be an efficient system for strontium recovery. This system was first developed by Horner [53] at Oak Ridge National Laboratory and later on modified by Schulz and Richardson for large scale operations [54]. Due to the lack of specificity in metal ion extraction, this process requires addition of large concentration of various complexing agents (like EDTA, oxalic acid, etc) to the aqueous phase to suppress the extraction of aluminum, iron and other metal ions.

As described earlier, crown ethers are found to be attractive for the extraction of strontium from acidic solutions due to their selective nature and ease of extraction and stripping. The ionic size of Sr^{2+} is 1.13 Å which is compatible with the cavity size of 18-crown-6 molecule which makes it viable candidate for the recovery of Sr^{2+} [55]. The transfer of the metal ion from the aqueous phase to the organic phase requires the dehydration of the metal ion, complexation of the metal ion with the crown ether and then finally transfer of the complex to the organic phase along with the counter anion. Large molar volume anions e.g. picrate, tetra phenyl borate anion facilitate the transfer of the metal-ligand complex into the organic phase compared to the smaller (or hard) anions like nitrate etc [56]. This is due to the less energy required to dehydrate poorly hydrated larger anions and hence the transfer of metal ion becomes energetically favorable process.

Gerow et al. [31], reported that the 4-component mixture of 0.02 M bis-4,4'(5') [1-hydroxyheptyl]-cyclohexano-18-crown-6 (Figure 1.12) in 5% nonyl-naphthalene sulphonic (NNS) + 27% TBP-68% kerosene can selectively extract Sr^{2+} from simulated PUREX HLW (3 M HNO_3). Their study indicated that Sr, Zr and Ba were also extracted by TBP.

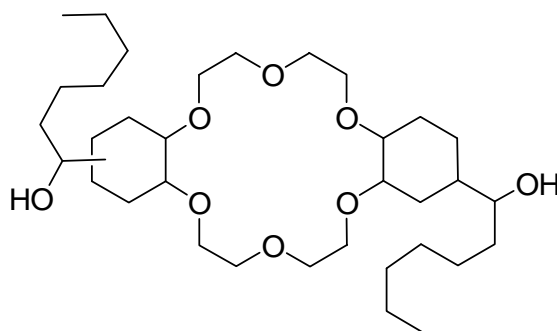


Figure 1.12 Structural formula of bis-4,4'(5') [1-hydroxyheptyl]-cyclohexano-18-crown-6

In the 1990's, researcher at the Argonne National Laboratory, proposed a process for strontium recovery using dicyclohexano-18-crown-6 in 1-octanol [57]. Strontium extraction is highly dependent on the nitric acid concentration in the feed, typically requiring 3-6 M acidity for efficient extraction. Significant acid uptake was observed by this extraction system which contained 1-octanol. Modifications were made to reduce the solubility of crown ether in aqueous phase [58]. Subsequently, Horwitz *et al.* [57] proposed a process called SREX (Strontium EXtraction) for strontium recovery by 4,4'(5')-di-*tert*-butyl-cyclohexano-18-crown-6 (DtBuCH18C6) in 1-octanol as the diluent. The SREX process was also tested on simulated INEEL tank wastes, which contained significant amounts of competing ions such as sodium and potassium [59]. In this process, strontium is extracted from acidic (≥ 1 M HNO₃) solution using a 0.2 M solution of DtBuCH18C6 in 1-octanol. The extracted strontium was readily stripped from the organic phase using either water or dilute (~ 0.05 M) HNO₃. It extracted Sr(II) effectively from the simulated sludge solution (Sr(II) = 1.3×10^{-3} M). Within three contacts, >99.7% Sr(II) recovery was achieved. The solvent exhibited good radiolytic stability. However, Ba(II) and Tc showed distribution ratio values higher than 1. The problem with the SREX process was the use of 1-octanol as the diluent which extracted significant amounts of nitric acid. The SREX solvent composition was later changed to incorporate tri-*n*-butyl phosphate (TBP) as the phase modifier in Isopar L® similar to the Transuranium Extraction (TRUEX) process. Extensive tests *via* laboratory batch contacts and in centrifugal contactors with simulated and actual acidic tank waste and dissolved calcine solutions have been performed at the INEEL [57]. Kumar et al. [60], reported that the reagent inventory can be drastically reduced by using a more polar diluent mixture, such as 80% 1-butanol and 20% 1-octanol. SREX process led to the development of Sr-specific resin which was subsequently commercialized. In order to minimize the acid uptake, a

mixture of 1-octanol and toluene has been tested where 0.025 M DtBuCH18C6 was used in 20% 1-octanol + 80% toluene as the diluent [61]. This system showed better performance than the SREX process solvent because of better extraction and stripping, lower acid uptake, lesser viscosity, good radiation stability and higher Sr loading capacity. In spite of these studies, the quest for new diluent systems with lesser acid and/or water uptake continues.

1.6 VARIOUS TECHNIQUES FOR RECOVERY OF METAL IONS

Solvent extraction techniques have been applied for the recovery of metal ions from aqueous feed solutions for a very long time. The ease of handling and less operation time are few of the advantages associated with this technique. Various other techniques having several advantages have also been developed. These include ion-exchange, extraction chromatography and liquid membrane methods. The advantages and drawbacks of these methods have been discussed in the following Sections.

1.6.1 SOLVENT EXTRACTION

This is the most widely used technique for the separation of any metal ion from solutions. This method is based on the distribution of metal ion between two immiscible liquids one of which is usually an aqueous phase and other is some water-insoluble organic solvent. The thermodynamics of distribution of metal ion can be explained by the Phase rule [62] which can be written as

$$C - P + 2 = F \quad (1.1)$$

where C, P and F denotes the number of components, number of phases and degrees of freedom respectively. For a binary system such as liquid-liquid extraction where only one solute is

present, number of phase is two ($P = 2$) and three components are present ($C = 3$). Hence by the equation (1.1), three degrees of freedom are associated with the system which means that at particular temperature and pressure, the concentration of solute in any phase can be found out by knowing its concentration in the other phase. Therefore, the ratio of concentration of solute in the two phases is constant as long as the temperature and pressure of system remain the same. The distribution of solute is governed by the Nernst's distribution law. The equilibrium can be represented as-



If the solute species remains same in both the phases, the ratio of solute concentration in the organic phase to that in the aqueous phase is termed as the “distribution coefficient” (k_d) or “partition coefficient” and is written as

$$k_d = \frac{[\text{Solute}]_{\text{org}}}{[\text{Solute}]_{\text{aq}}} \quad (1.3)$$

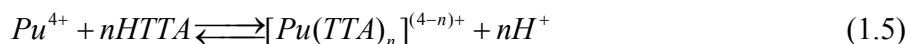
where k_d represents the partition coefficient of a particular solute specie. However, in the metal ion separation using organic extractants, the ligand forms a complex with the metal ion and then gets transferred to the organic phase. In such cases, the chemical species of the metal ion in the two phases are not the same. Hence, a term “distribution ratio” is coined to define the ratio of total concentration of the metal ion in the organic phase to that in the aqueous phase.

$$D = \frac{\sum [\text{M}]_{\text{org}}}{\sum [\text{M}]_{\text{aq}}} \quad (1.4)$$

where, [M] represents concentration of the metal ion in the respective phase. The extraction of the metal ion by the organic extractants involves the following steps (1) dehydration of metal ion, (2) complexation of metal ion with ligand, (3) transfer of metal-ligand complex to the organic phase.

The mechanism of extraction of metal ion can be any of the following types-

- (i) **Solvation mechanism:** The metal ion can be transferred into the organic phase if the ligand molecules can solvate the metal ion. The extraction of the metal ions by neutral ligands is followed by solvation in which the extraction process proceeds by the displacement of water molecules from the inner coordination sphere of metal ions by basic donor atoms such as 'O' or 'N' of the ligand molecules. The extraction of U(VI) by tri-*n*-butyl phosphate (TBP) from nitric acid medium is one of the most common examples of metal ion extraction by the solvation mechanism [63].
- (ii) **Chelation mechanism:** A chelating ligand forms a cyclic complex with the metal ion (which is entropically more stable) thereby making it more lipophilic. The best example of this is extraction of tetravalent plutonium ion by thenoyltrifluoroacetone (HTTA) in benzene (equation 1.5).



- (iii) **Ion-pair mechanism:** This mechanism is followed in case of anionic ligands which bind with metal ions and forms neutral ion-pair and also in case of metal ion complexation by crown ethers and related compounds. The ion-pair complexes are stabilized in the polar

diluents like nitrobenzene, dichloromethane, etc. which provides better metal ion extraction.

This solvent extraction technique has been applied on pilot as well as plant scale. It is associated with certain advantages and disadvantages. The advantages are:

1. The ease of handling and processing
2. Offers better selectivity
3. % Extraction can be increased by simply increasing the organic / aqueous volume ratio
4. Relatively faster mass transfer

However, it suffers with some drawbacks also, such as

1. It requires large inventories of ligands and diluents which are invariably toxic or inflammable
2. Extraction and stripping (and sometimes scrubbing) of metal ion is carried out in separate steps
3. Large volumes of secondary waste are generated due to large solvent inventory used for metal ion recovery

In spite of suffering from various limitations, solvent extraction methods are still used in large scale processing of waste streams. However, there is always a need to find alternative techniques for the recovery of metal ions from different kinds of waste solutions. Separation of cesium or strontium is carried out by calix-crowns or crown ethers which are quite expensive.

Hence techniques offering advantages such as lower ligand inventory, less operational time, etc. need to be developed.

1.6.2 ION-EXCHANGE TECHNIQUE

Ion exchange is another widely used separation technique which has been applied for the separation and purification in food and beverage industries, pharmaceutical industries, nuclear industries, etc. [64] Ion-exchange materials, normally in the form of beads, is made of water insoluble polymers. The surface of polymer has suitably developed pores with specific structure in which the extractant or the binder can be encapsulated. The extractant / binder have exchange sites where metal ion is exchanged with proton or any other cation and hence the technique is named as ion-exchange. Column properties are influenced by the particle size of the ion-exchanger. The smaller sized particles have larger surface area and hence good exchange capacity but have the drawback of higher head loss during the column operations. Cross-linking of polymer also affects properties of ion-exchanger. Ammonium molybdophosphate (AMP) is widely used as an inorganic ion-exchanger for cesium recovery from acidic feeds. In the exchange process, ammonium ions (NH_4^+) are exchanged with cesium ions stoichiometrically.

The k_d value of ion-exchange resin is determined by equilibrating the exchanger with the feed solutions containing metal ion for a given time interval. The metal ion concentration is measured before and after the equilibration and the k_d value is calculated using the formula

$$k_d = \frac{(C_0 - C_{eq})}{C_{eq}} \times \frac{V}{w} \quad (1.6)$$

where C_0 , C_{eq} represents concentration of metal ion initially (at $t=0$) and at equilibrium and V and w denote the volume of aqueous phase and weight of ion-exchange material, respectively.

1.6.3 EXTRACTION CHROMATOGRAPHY

Extraction chromatography, although not as popular as ion-exchange chromatography, has been extensively evaluated for metal ion separation by different research groups. This is an attractive method due to the lack of commercial chelating resins available for removal of specific metal ions. Extraction chromatographic materials are sometimes called solvent impregnated resins. This method is particularly important due to the specificity over the ion-exchange technique which is less specific because of the similar chemistry of elements of the same group. To prepare the extraction chromatographic resins, the chelating extractant is attached to the polymer matrix by chemical or physical means. The polymer matrix acts as the solid support while the pores contain the extractant. The removal of various elements from high- or medium-level wastes using extraction chromatography has been demonstrated [65, 66]. These elements are various gamma or beta emitting radioisotopes including $^{134,137}\text{Cs}$, ^{125}Sb , ^{106}Ru and $^{154,155}\text{Eu}$. Separation of Sr from tank solutions / sludges has also been demonstrated using extraction chromatography [66, 67]. The extraction chromatographic columns contain an inert support material loaded with an extractant such as the crown ether (di-*tert*-butylcyclohexano-18-crown-6). The performance of such resin has been proved to be quite good [68].

1.6.4 MEMBRANE BASED TECHNIQUES

Liquid membranes have been traditionally used for mass transfer from feed solution and successfully employed in industrial, analytical and biomedical fields as well as in water

treatment, gas separation etc. [69-76]. The membrane techniques are quite attractive due to the following reasons-

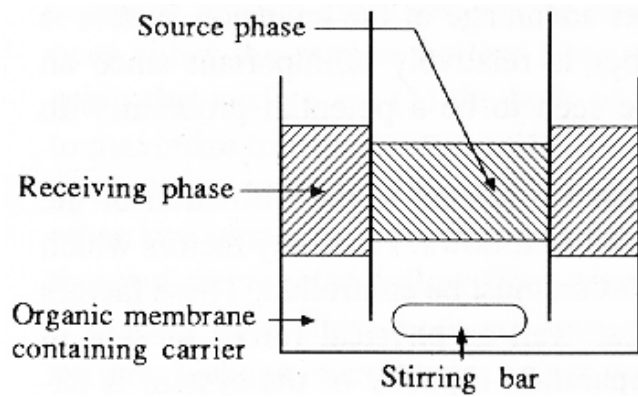
- Low operating costs
- Low capital costs
- Continuous in nature
- Remote handling is possible while processing radioactive waste solutions, reducing the radiation exposure to the personnel

In liquid membrane separation methods, organic phase is kept in between the two aqueous phases; one phase containing metal ion (feed or source phase) and the other which receives the metal ion (strip or receiver phase). Several types of membranes are extensively studied such as: supported liquid membranes and non-supported liquid membranes. Various types of membranes are described in the following Sections.

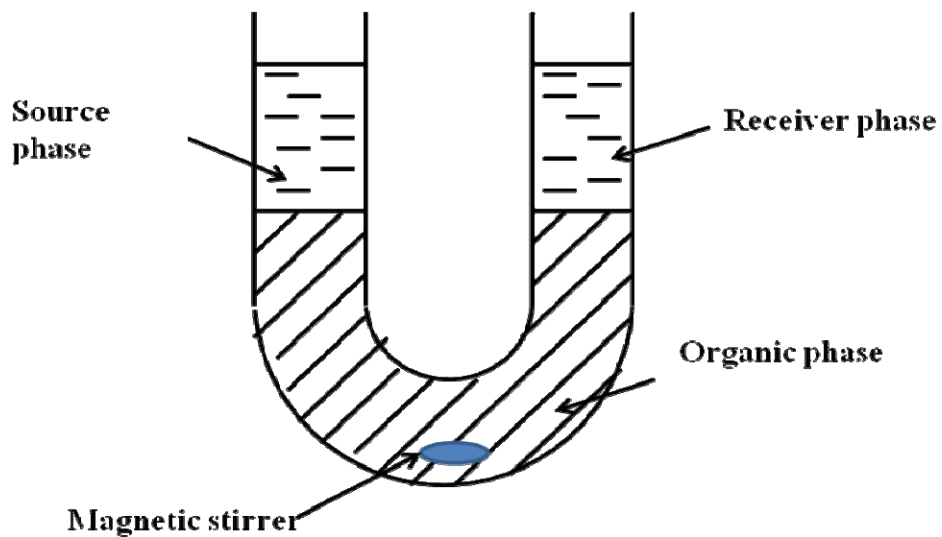
1.6.4.1 NON-SUPPORTED LIQUID MEMBRANES

1.6.4.1.1 Bulk Liquid Membranes (BLM)

In this type of liquid membranes, the bulk of organic phase is sandwiched between the feed and the strip solution and the membrane phase is agitated slowly for the effective transport of metal ion from the feed to the strip phase. The density of the organic phase should be higher than both of the aqueous phases.



(a)



(b)

Figure 1.13: Schematic diagrams of BLM configurations: (a) beaker in beaker arrangement (b) U-tube arrangement

1.6.4.1.2 Liquid Emulsion Membranes (LEM)

In this membrane configuration, the strip solution is dispersed in the continuously stirred organic phase in which some emulsifier is added. The organic phase is dispersed as droplets inside which the strip phase is contained. The emulsion is kept in contact with the feed phase

(also called the external phase) and stirred for effective transport of metal ion from external phase to internal phase through the liquid membrane phase (Fig. 1.14).

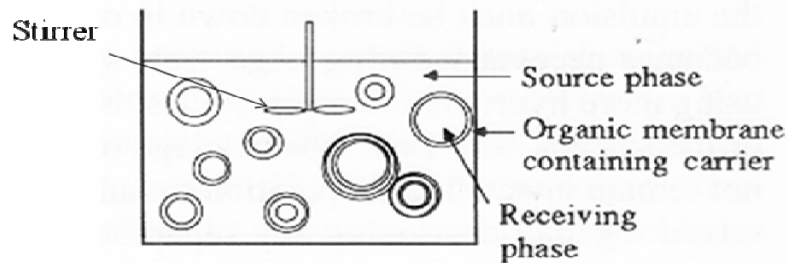


Figure 1.14: Liquid Emulsion Membrane (LEM)

After complete transport of the metal ion, the emulsion is separated from the solution and then demulsified by various methods viz. thermal decomposition, chemical decomposition, demulsification by centrifugal methods etc. After demulsification, the strip phase is recovered from the organic phase. By this technique, concentration of metal ion into the strip phase is carried out by suitably changing the internal phase to external phase volume ratio. The technique offers fast mass transport fluxes due to the smaller size of drops which provides larger surface area.

1.6.4.2 SUPPORTED LIQUID MEMBRANES

In supported liquid membranes, a polymeric matrix is used as solid support for organic solvent and is placed in between the feed and strip solutions. The stability of membrane depends upon various factors like nature of polymer and solvent, the pressure difference across the liquid membrane, the solubility of carrier extractant in the aqueous phases, etc. Two types of supported liquid membranes are commonly used viz. flat sheet supported liquid membrane and hollow fibre supported liquid membrane.

1.6.4.2.1 Flat-Sheet Supported Liquid Membrane (FSSLM)

In Flat-Sheet supported liquid membrane, a polymer sheet is placed between the two compartments, one containing the feed solution while the other containing the receiver or strip solution (Fig. 1.15). The polymer sheet is impregnated with the organic carrier solution and the phases are continuously stirred using magnetic stirrers to reduce the aqueous boundary layer resistance for mass-transfer. Since the small surface area is available for mass-transfer, hence the mass fluxes are lower. Also, this technique cannot be applied on larger scale because a small pressure difference in that case would result in the blowing out of the organic solvent from the pores of liquid membrane. Hence, FSSLM's have been applied on small scales only (generally, few mL to several hundred mL).

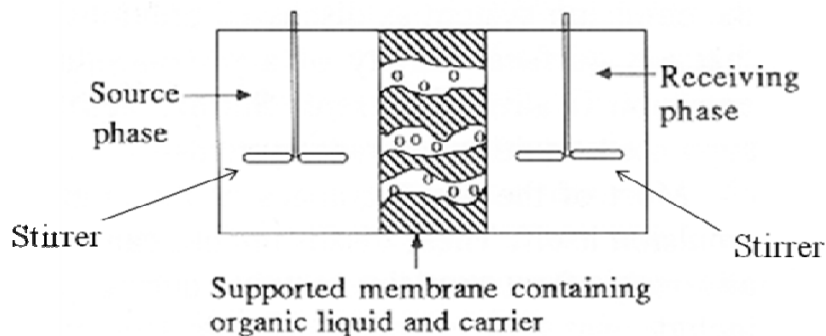


Figure 1.15: Flat-Sheet Supported Liquid Membrane

1.6.4.2.2 Hollow Fibre Supported Liquid Membrane (HFSLM)

As has been discussed, the drawbacks of FSSLM include lower transport fluxes and physical instability of membrane at higher volumes of feed and strip. The mass fluxes can be increased by increasing the surface area of contact per unit volume. From this point of view, Hollow Fibre Supported Liquid Membrane (HFSLM) is an attractive configuration for higher

flux. HFSLM module (Fig. 1.16) consists of thousands of single hollow fibres which are cylindrical in geometry. The feed and strip solutions are passed through the inside and outside of hollow fibres. Due to compactness of the system, a very large surface area per unit volume is available which provides larger mass fluxes using HFSLM technique. The relative flow of feed and strip solutions gives rise to two modes of operation: co-current flow and counter-current flow.

There are various advantages associated with this technique as listed below.

- The large surface area and small membrane thickness provide rapid mass transfer
- The source/receiving phases are more easily recoverable than the emulsion system
- The entire source and receiving phase are not in contact with the membrane at any given instant
- Leakage and contamination are easily contained

Apart from the various advantages, there are several drawbacks as listed below

- Hydrophobic membrane solvents are required to maintain integrity
- Hollow fiber system must be cleaned between uses or there will be aqueous and contaminant buildup
- Pore fouling, often occurs due to surface effects and particles in the system.

In spite of the various disadvantages are associated with HFSLM technique, yet the faster transport rate and ease of scaling up of process makes it a promising option for using this technology in the treatment of waste solutions.

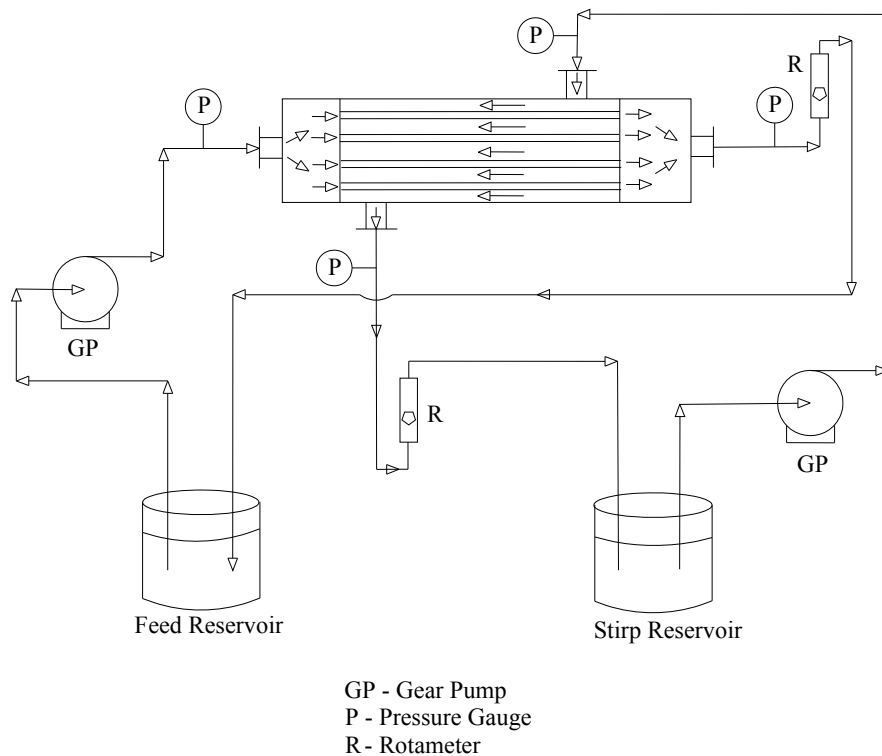


Fig. 1.16: Schematic representation of the HFSLM set-up.

1.7 MATHEMATICAL MODELING OF MASS-TRANSPORT

The development of mathematical model, optimization of experimental parameters and design parameters viz. mass-transfer coefficient, dynamic or kinetic parameters related to interfacial interactions are very important for scaling-up the process to larger scale. Additionally, the modeling of process gives better insight which improves the basic understanding and fundamental relations of various parameters. Various mathematical models have been proposed for mass-transfer process of metal ions across liquid membranes. The collection of model can be categorized as (i) simplified approach model and (ii) rigorous model.

In the simplified approach, the over all mass-transfer coefficients are calculated unlike calculation of individual mass-transfer coefficients in more rigorous models (will be described in later part of this section). The first simplified model for the mass-transport fittings was proposed by Danesi *et al.* [77]. Aqueous boundary layers were considered across the membrane and the model was developed based on diffusional mass-transport of species. Lin and Juang [78] studied the mass transport in hollow fibre contactors for extraction and stripping (back-extraction) of copper with LIX64N carriers. The authors defined two overall mass transfer coefficients for the extraction and stripping steps. The proposed model takes into account the kinetic resistance of the interfacial extraction reaction and three mass transfer resistances in the aqueous phase stagnant layer, the membrane and the organic phase. The stripping step was described in a similar way. The contribution of the individual mass transport resistances to the overall one was performed for different values of the operation variables. The authors concluded that for the extraction process, the resistance of organic layer diffusion and membrane diffusion can be neglected, with the controlling steps both aqueous-layer diffusion and interfacial reaction. For the back-extraction process, the contribution of interfacial reaction and organic-layer diffusion can be ignored, with the process dominantly governed by membrane diffusion.

Gupta *et al.* [79] reported the applicability of non-dispersive solvent extraction to the recovery of U(VI) from oxalate supernatant waste using TBP (tri-*n*-butylphosphate) and HNO₃ as extraction and back extraction agents respectively. The extraction reaction was considered instantaneous and described by the chemical equilibrium parameter and the mass transfer was assumed to be controlled by diffusion through the liquid membrane. The overall mass transfer coefficients for the extraction and back extraction steps were obtained by linear fitting of the experimental data to the simplified integrated expression derived by D'Elia *et al.* [80] from the

solution of the solute mass balances in the aqueous and stripping solutions. The above described models were simple in nature but many of them were associated with the lack of incorporation of various hydrometallurgical parameters viz. effect of flow rate, effect of variation of metal ion concentration on the distribution coefficient, etc.

Very few models have been reported on rigorous modeling of mass-transfer across HFSLM due to the complexity of solution of mass-transfer equations formed. Kim and Stroeve [81-84] studied the theoretical aspect of mass-transfer of species describing the velocity and concentration profiles through the liquid membrane. Alhusseini and Ajbar [85] reported a 'steady state' rigorous model for the transport of copper ion by LIX84 across ceramic tube supported liquid membrane where the aqueous feed phase was passed through the inside and the strip solution flowed through the shell side of tube. The mass transport is described by a coupled facilitated counter-transport model that takes into account the resistances offered by diffusion across the boundary layers of the feed and strip solutions, diffusion across the liquid membrane and non-equilibrium interfacial reactions that are described by the expression reported by Komasaawa *et al.* [86]

Garea *et al.* [87] analysed the phenol separation concentration process with hydrophobic hollow fibre supported liquid membranes using Cyanex 923 and NaOH as selective extractant and stripping agent, respectively. In this work, the experimentally obtained overall Sherwood number (Sh_o) was evaluated for different extractant concentrations leading to an empirical relationship between Sh_w and the Cyanex-923 concentration. The model described above suffers with the complexity in their formulation and subsequently in solving the equations obtained in the process. Hence, need for a simplified model which can predict the transport profile across the HFSLM is still present

1.8 SCOPE OF THE THESIS

The research work presented in this Thesis includes the application of Hollow Fibre Supported Liquid Membrane (HFSLM) for the recovery of Cs and Sr from simulated high level waste solutions using calix-crowns and crown ethers as the carrier extractants. Apart from this, a mathematical model has also been presented which is developed based on various parameter considerations and using basic fundamental relation to predict the mass-transfer profile of metal ions. The major highlights of the Thesis can be summarized as follows:

- (i) Basic studies were carried out for process optimization to observe the distribution of cesium under various experimental conditions. Calix[4]arene-bis(2,3-naphtho)-crown-6 have been evaluated extensively as the selective extractant for cesium ion from the acidic and simulated high level waste (SHLW) conditions. HFSLM transport studies have been carried out to evaluate the possible applicability of this technique for the recovery of radiocesium from the actual HLW solutions.
- (ii) Studies involving the separation of Sr from the SHLW solution by di-*tert*-butylcyclohexano-18-crown-6 in 80% 2-nitrophenyl-octyl ether (NPOE) + 20% *n*-dodecane using HFSLM technique were also carried out. The problem of acid co-transport by the crown ether extractant was examined and the addition of NaOH to neutralize the strip side acidity was found to be one of the optimum solutions for this problem. The successful recovery of Sr from the SHLW was demonstrated which suggested possibility of scaling up of the system for radiostrontium recovery from actual waste solutions.

- (iii) A mathematical model has been developed for the mass-transfer of metal ion through the membranes including both FSSLM and HFSLM. The model is relatively simple and incorporate various experimental and system parameters and uses fundamental relations to simulate the mass transport process. The experimental results of previous studies have been simulated by the model. The predicted data from the model were compared with those obtained experimentally and the results are presented in the Thesis. It has been found that under various experimental conditions, the mathematical model can be applied to predict the mass-transport through FSSLM as well as HFSLM.

- (iv) Co-recovery of Cs and Sr has been demonstrated by UNEX process where a mixture of chlorinated cobalt dicarbollide (CCD) and polyethylene glycol (PEG) has been used in nitrobenzene / FS-13. Work has been carried out to develop diluents alternative to toxic / corrosive diluent system for cesium and strontium co-recovery by CCD. Previous studies have indicated that NPOE is a less toxic diluent which can be employed as an alternative to nitrobenzene. Hence, NPOE – *n*-dodecane system has been used as the diluent composition. Solvent extraction and liquid membrane studies have been carried out to see the application of developed system for the co-recovery of cesium and strontium from the acidic waste solutions. The results are found to be promising for the simultaneous extraction Cs and Sr.

The studies of this Thesis are important as far as the recovery of valuables from the HLW is concerned. The results can be used to develop flow-sheet for the recovery of Cs and Sr from the HLW using liquid membrane methods. The developed model is tested on the present system

and found to be working quite satisfactorily. The model can be applied to any system by suitably modifying the procedure and incorporating relevant information.

CHAPTER 2: REAGENTS AND EXPERIMENTAL TECHNIQUES

Solvent extraction and supported liquid membrane (SLM) transport of Cs and Sr has been the main objectives of the work presented in this Thesis. SLM (flat sheet supported liquid membrane as well as hollow fibre supported liquid membrane) techniques have been utilized for studying the transport behaviour of Cs and Sr by calix-crowns and crown ethers, respectively under various experimental conditions. Apart from this, a mathematical model has been developed to simulate and predict the transport profiles of the metal ions through the supported liquid membrane techniques. Various reagents used in the studies and the techniques involved throughout the work have been discussed in this Chapter.

2.1 RADIOTRACERS

Major part of the work has been carried out on ^{137}Cs and ^{90}Sr radiotracers. $^{85,89}\text{Sr}$ has been used as the surrogate of ^{90}Sr in major part of the experiments. Nuclear properties of ^{90}Sr and ^{137}Cs are discussed as follows.

2.1.1 Decay characteristics of ^{137}Cs AND ^{90}Sr

^{137}Cs and ^{90}Sr are produced in nuclear reactor as a result of nuclear fission. These are produced in the reactor in high fission yields and are some of the high heat emitting isotopes. As

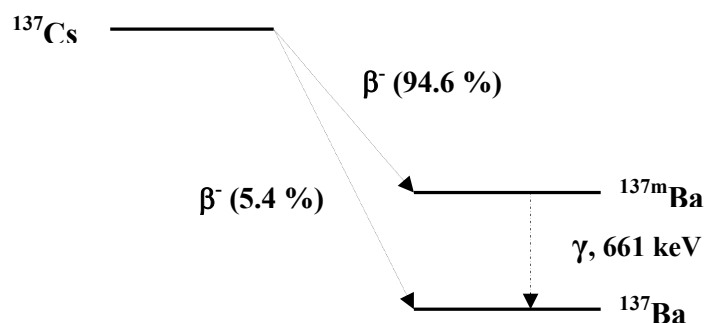


Figure 2.1 Decay scheme for ^{137}Cs

shown in the decay scheme (Figure 2.1), ^{137}Cs decays to the metastable $^{137\text{m}}\text{Ba}$ by emitting a β -particle of energy 0.514 MeV with 94.6% abundance while a fraction of it can also decay directly to ^{137}Ba by emitting a 1.175 MeV β -particle with only 5.4 % probability. The metastable state ($^{137\text{m}}\text{Ba}$) has finite half-life of 2.55 minutes. After decaying to $^{137\text{m}}\text{Ba}$, the excess energy is dissipated in the form of gamma radiation ($E_\gamma = 661 \text{ KeV}$, 90 %) or the energy can be absorbed by any orbiting electron causing the ejection of electron, by the process called Internal Conversion (IC). Hence, a secular equilibrium exists between ^{137}Cs and $^{137\text{m}}\text{Ba}$ which will attain steady state after time calculated by the following equation (2.1) [88],

$$t_{\max} = \frac{\ln(\lambda_2 / \lambda_1)}{\lambda_2 - \lambda_1} \quad (2.1)$$

where, λ_1 and λ_2 are decay constant for ^{137}Cs and $^{137\text{m}}\text{Ba}$, respectively. The value of t_{\max} is calculated to be ~ 23 minutes. The necessary precautions

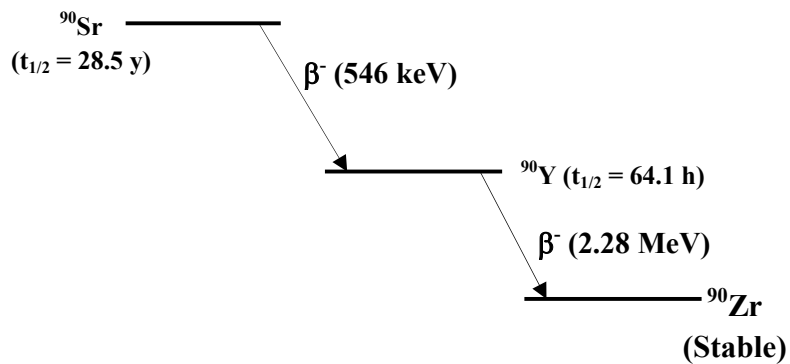


Figure 2.2 Decay scheme for ^{90}Sr

have been taken throughout the work by allowing the samples to be kept for a couple of hours prior to gamma counting.

^{90}Sr is a pure beta-emitting radio nuclide which decays to ^{90}Y which, in turn, emits a high energy beta particle of 2.28 MeV energy. The complete decay pattern has been shown in the

figure 2.2. Secular equilibrium is established in ~ 32 days after which the activity due to ^{90}Sr and ^{90}Y becomes equal.

2.1.2 Radiotracers

The nuclear properties of various radioisotopes have been listed in the Table 2.1. For most studies involving Sr, $^{85,89}\text{Sr}$ was used as a surrogate of ^{90}Sr . The radiotracers used in the present studies have been procured from Board of Radiation and Isotope Technology (BRIT), Mumbai.

Table 2.1: Decay mode and analytical technique used for counting for various Radioisotopes

| Nuclide | Decay mode | Half-life | Energy (keV) | Counting technique |
|-------------------|----------------------|------------|------------------------------|----------------------------------|
| ^{137}Cs | β^- , γ | 30.2 years | 661 | γ counting |
| ^{85}Sr | EC*, γ | 64.85 days | 514 | γ counting |
| ^{89}Sr | γ | 50.57 days | 909 | γ counting |
| ^{90}Sr | β^- | 28.5 years | 546 (β_{max}) | Liquid Scintillation counting |
| ^{59}Fe | β^- , γ | 44.5 days | 1099, 1291 | γ counting |
| ^{95}Zr | β^- , γ | 64 days | 724, 756 | γ counting |
| ^{22}Na | β^- , γ | 373 days | 511 | γ counting |
| ^{241}Am | α , γ | 432 years | 60 | γ counting |

* EC: Electron Capture

The radiochemical purity of ^{137}Cs and $^{85,89}\text{Sr}$ was ascertained by gamma-ray spectrometry using high-resolution germanium detector (HPGe). ^{90}Y is recovered from a mixture of ^{90}Sr - ^{90}Y by commercially available chromatographic column (under the name Sr-SPEC[®]). The column is

made from a commercial resin containing di-*tert*-butylcyclohexano-18-crown-6. The mixture of ^{90}Sr - ^{90}Y in 3 M HNO_3 is passed through the column and ^{90}Y is eluted out leaving ^{90}Sr held in the column. ^{241}Am was received and purified using the procedure described elsewhere [89].

2.2 MATERIALS

2.2.1 Crown ether

Strontium selective crown ether 4,4'(5')-di-*tert*-butylcyclohexano-18-crown-6 (DtBuCH18C6, figure 2.3) has been procured from Fluka Chemie AG (Switzerland) and was used as received. The received compound is a mixture of various isomers of the molecule.

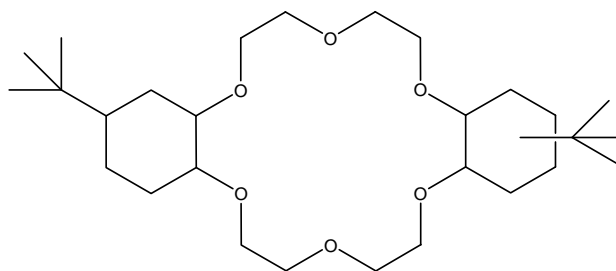


Figure 2.3 Structural formula of DtBuCH18C6

2.2.2 Calix-crown

Calix[4]arene-bis(2,3-naphtho)-crown-6 (CNC, figure 2.4) has been employed as cesium selective carrier extractant in the work and it has been obtained from Across organics, Belgium. The calix-crown has been used without further purification. The reported purity of the calix-crown is > 95 %.

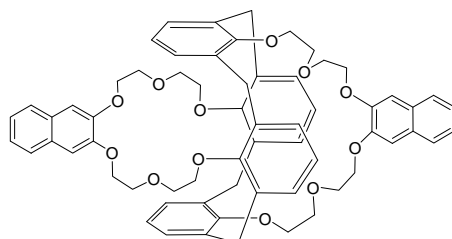


Figure 2.4 Structural formula of calix[4]arene-bis(2,3-naphtho)-crown-6

2.2.3 Chlorinated cobalt dicarbollide

Chlorinated cobalt dicarbollide (CCD, figure 2.5) was procured from KatChem Co., Czech Republic and was used as received. It was obtained in the form of its cesium salt and hence, a procedure was followed to convert it to the protonated form which will be discussed in the later part of the Thesis.

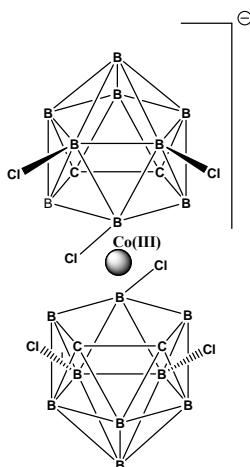


Figure 2.5 Structural formula of CCD

2.2.4 PC-88A

Bis(2-ethylhexyl) phosphonic acid (PC-88A, figure 2.6) was obtained from Daihachi Chemical Industry Co. Ltd., Japan, and was used as received.

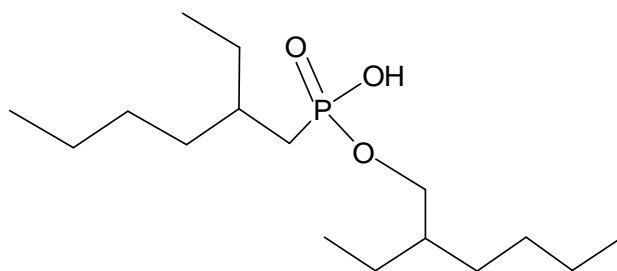


Figure 2.6 Structural formula of PC-88A

2.2.5 Chemicals

The list of the various chemicals used in the present work is given in Table 2.2

Table 2.2: The list of various chemicals and reagents used in the studies

| Chemical | Supplier | Purity |
|----------------------------------|-----------------------------|---------|
| Cesium Nitrate | Apex chemicals, Mumbai | > 99% |
| Strontium nitrate | Apex chemicals, Mumbai | > 99% |
| 2-Nitrophenyl octyl ether (NPOE) | Fluka, Switzerland | > 99% |
| Nitrobenzene | Merck, Germany | > 99% |
| <i>n</i> -Dodecane | Lancaster, UK | > 99% |
| Nitric Acid | S.D. Fine Chemicals, Mumbai | 69-71 % |
| Perchloric acid | S.D. Fine Chemicals, Mumbai | 60 % |

2.2.6 Membranes

For FSSLM experiments, PTFE membrane sheets having 85 μm thickness, 0.45 μm pore sizes and 72 % membrane porosity, have been procured from Sartorius, Germany. The thickness of the membranes was ascertained by measuring it with a digimatic micrometer (Mitutoyo Corporation, Japan).

The hollow fibre membrane contactor used in the present work was procured from Alting, France and made up of hydrophobic microporous polypropylene hollow fibres enclosed in a polypropylene shell of 2.5'' \times 8'' dimension. The module contained about 10,000 fibres of 0.03 μm pore size and 40 % porosity (wall thickness of 30 μm and fibre outer diameter 300 μm) and had an effective surface area of 1.4 m^2 . The complete specification has been given in Table 2.3.

2.2.7 Preparation of Simulated High-Level Waste (SHLW)

The composition of Pressurized Heavy Water Reactor-Simulated High Level Waste (PHWR-SHLW) is given in the Table 1.1 (Chapter 1). SHLW solution is prepared by dissolving the metal nitrate salts in the respective amount into nitric acid solution. The composition of SHLW is ascertained by ICP-AES as well as by EDXRF technique. The final acidity of SHLW was confirmed by acid-base titration in the saturated solution of potassium oxalate (which was used to complex with interfering metal ions). The acidity of PHWR-SHLW was usually in the range of 3-4 M HNO_3 .

Table 2.3 Details of hollow fibre membrane contactor (LiquiCel® X50: 2.5x8 Membrane Contactor) used in the present work.

| Parameter | Specification |
|-------------------------------------------|----------------------|
| Fibre material | Polypropylene |
| Number of fibres | 9950 |
| Fibre internal diameter (μm) | 240 |
| Fibre outer diameter (μm) | 300 |
| Fibre wall thickness (μm) | 30 |
| Effective pore size (μm) | 0.03 |
| Porosity (%) | 40 |
| Tortuosity | 2.5 |
| Effective fibre length (cm) | 15 |
| Effective surface area (m^2) | 1.4 |

2.2.8 Preparation of CCD solution

Preparation of solution was carried out by dissolving cesium salt of CCD (which is commercially available) into 2-nitrophenyloctyl ether (NPOE). The solution is continuously stirred under ultra-sonication to dissolve the CCD in the NPOE. After complete dissolution, the solution was contacted 5-6 times with 1:1 solution of perchloric acid and water to convert it into the protonated form. The main stock solution was then diluted with *n*-dodecane to get the desired diluent composition and ligand concentration.

2.3 ANALYTICAL TECHNIQUES

The various techniques used for the analysis of radionuclides were gamma ray counting using NaI(Tl), HPGe and β -counting using a liquid scintillation counter. The basic principles and working has been explained in the next Section.

2.3.1 NaI(Tl) DETECTOR

It is the most widely used inorganic scintillator for the assay of gamma ray emitting radionuclides. The main component of detector is sodium iodide activated with 0.1 – 0.2 % of thallium. Salient features of the detector include its low cost, ease of operation and ruggedness [90]. The band gap in NaI crystal is of the order of 5-6 eV. When a charged particle (or gamma ray) falls on the detector, its energy is consumed in the crystal either for excitation of the electrons from the valence band to the conduction band or for the ionization of the atom. De-excitation of the electrons from conduction band to the valence band leads to the emission of photons in the UV region as the band gap is large. To shift the wavelength (or energy) of the emitted gamma photons to the visible region, which is required for detection by photo multiplier tube (PMT), NaI crystal is doped with an activator impurity like thallium (Tl) which forms the intermediate level conduction band. The resolution of NaI(Tl) detector is about 7 % at 661 KeV. In the present work, a 3" x 3" well type NaI(Tl) detector coupled with a multichannel analyzer (Figure 2.7) has been used for gamma ray counting. Nearly 100 % detection efficiency for moderate energy photons in a well type NaI(Tl) detector offers great advantages for the counting of low radioactive samples. Suitable aliquots (usually 0.1 ml) of the desired analyte solution were taken in glass counting tubes which were then placed in the well of the detector. Each

sample was counted for sufficient time so as to get more than 10,000 counts to restrict the counting error to $< \pm 1\%$.



Figure 2.7 NaI(Tl) detector set-up

2.3.2 HIGH-PURITY GERMANIUM (HPGe) DETECTOR

In the present work, high purity germanium (HPGe) detector coupled to a multichannel analyzer has been employed for gamma ray spectroscopy to check the radiochemical purity of the radionuclides. The HPGe detector is made up of highly pure germanium crystal in which the impurity level is around 10^{10} atoms/cc of the crystal. This is referred to as high purity germanium which approaches the theoretically pure semiconductor. HPGe is one of the most widely used semiconductor detectors for gamma ray spectrometry and can be considered as the workhorse of gamma ray spectroscopy. The high energy resolution (typically 1.9keV at 1332 keV) is the key feature of this detector due to low energy band gap (0.7eV). The major advantage of HPGe detector over Ge(Li) detector is that it can be stored at room temperature [91]. However, while operating it has to be cooled to liquid nitrogen temperature. HPGe detectors are of two types, p-type and n-type. In case of p-type the outer surface of the germanium crystal is heavily doped with n-type impurity. As a result the detection efficiency falls drastically below 100keV. On the

other hand, n-type detectors are sensitive to wider range of photon energy. The n-type detector has the added advantage in that it is more resistant to radiation damage in a neutron field as compared to a p-type detector.



Figure 2.8 The High-purity germanium detector (HPGe)

2.3.3 LIQUID SCINTILLATION COUNTER

Liquid scintillation counter is mostly used for the quantitative analysis of alpha / beta emitting radionuclides. Nearly 100% detection efficiency of this detector is of great advantage and as low as a few Bq of alpha activity can be assayed with good precision. A scintillator is a material that luminesces in a suitable wavelength region when ionizing radiation interacts with it. The interaction of charged particles (alpha or beta particles) with the scintillator results in the emission of photons and the intensity of the emitted light is a quantitative measure of the incident radiation. The light emitted from scintillator is then collected by the photomultiplier tube (PMT) which produces signal representative of the primary radiation. When the scintillator emits photons in UV region, a wavelength shifter is added to the scintillator cocktail which has intermediate energy levels. In such cases the de-excitation takes place via these intermediate energy levels and hence the wavelength of the emitted photons is shifted from UV to visible

region which is subsequently recorded in the PMT. The liquid scintillation counter is used to monitor gross alpha activity as it can not distinguish between alpha energies and thus can not be used for alpha spectrometry.

Many organic compounds are versatile scintillators for radiation measurements [92, 93]. The liquid scintillation cocktail comprises of a solvent like dioxane or toluene, a scintillator like PPO (2,5-diphenyl oxazole) and a wavelength shifter such as POPOP [1,4-bis-2-(5-phenyl oxazolyl)-benzene]. The solvent is the main stopping medium for radiation and must be chosen to give efficient energy transfer to the scintillating solute. In case of toluene based scintillator, a suitable extractant such as di(2-ethylhexyl) phosphoric acid (HD2EHP) is also added which facilitates the aqueous samples determinations by transferring the radionuclides from the aqueous phase to the organic phase. In the present work, generally toluene based liquid scintillator was employed which consisted of 10% (v/v) HD2EHP, 0.7% (w/v) PPO and 0.03%(w/v) POPOP. Suitable aliquots (25-100 μ L) containing alpha / beta activity were taken in glass vials containing liquid scintillator solution. When aqueous phase was added to the toluene scintillator, the two phases were mixed vigorously using an ultrasonic agitator to transfer the radionuclides into the organic phase. Each sample was counted for sufficient time so as to get more than 10,000 counts to restrict the statistical counting error within $\pm 1\%$.

2.3.4 VISCOMETER

The kinematic viscosity and the density of liquid samples were measured by a viscometer procured from Anton Paar, Austria (model number SVM 3000, Figure 2.9).



Figure 2.9 The Anton Paar Viscometer used for the viscosity measurements.

2.3.5 INDUCTIVELY COUPLED PLASMA-ATOMIC EMISSION SPECTROSCOPY (ICP-AES)

Inductively Coupled Plasma-Atomic Emission Spectrometry (ICP-AES) is an emission spectrophotometric technique, working on the fact that the excited electrons emit energy at a given wavelength as they return to ground state after excitation by high temperature Argon Plasma [94, 95]. The fundamental characteristic of this process is that each element emits energy at specific wavelengths peculiar to its atomic character. The energy transfer for electrons when they fall back to ground state is unique to each element as it depends upon the electronic configuration of the orbital. The energy transfer is inversely proportional to the wavelength of the electromagnetic radiation,

$$E = hc/\lambda \quad (2.2)$$

(where h is Planck's constant, c the velocity of light and λ is wavelength), and hence the wavelength of light emitted is also unique.

Although each element emits energy at multiple wavelengths, in the ICP-AES technique it is most common to select a single wavelength (or a very few) for a given element. The intensity

of the energy emitted at the chosen wavelength is proportional to the amount (concentration) of that element in the sample being analyzed. Thus, by determining which wavelengths are emitted by a sample and by determining their intensities, the analyst can qualitatively and quantitatively find the elements from the given sample relative to a reference standard.

The wavelengths used in the AES measurements ranges from the upper part of the vacuum ultraviolet (160 nm) to the limit of visible light (800 nm). As borosilicate glass absorbs light below 310 nm and oxygen in air absorbs light below 200 nm, optical lenses and prisms are generally fabricated from quartz glass and optical paths are evacuated or filled by a non absorbing gas such as Argon. In present studies, Ultima HR ICP-AES has been used for the determination of metal ion concentration in samples.

2.4 EXPERIMENTAL METHODS

Although several experimental techniques for the separation of metal ions are well known, techniques such as solvent extraction and liquid membrane were employed in the present studies. The aqueous metal-ligand complexation, ligand nitric acid complexation etc. were studied by the solvent extraction method. The possibility of the separation process on large scale was demonstrated by performing liquid membrane transport experiments. The fundamental understanding for the transport of metal ions through liquid membrane was developed on batch studies using a two-compartment transport cell. Liquid membrane separation on a relatively larger scale was demonstrated by using HFSLM contactor. Various experimental setups and methodologies used in the present work are elaborated in this Section.

2.4.1 SOLVENT EXTRACTION

For distribution studies, suitable volume (0.5-2 mL) of aqueous phase at the desired acidity containing the required metal ion tracer was equilibrated in glass stoppered equilibration tube with equal volume of organic phase containing desired concentration of extractant in the suitable diluent system. For all the studies, except stated otherwise, the organic phase was pre-equilibrated with the respective acid solutions to eliminate the effect of acid uptake. The agitation of the two phases was carried out by rotary motion in a thermostated water bath (Figure 2.10) maintained at $25 \pm 0.1^\circ\text{C}$. After equilibration, the two phases were centrifuged and assayed by aliquoting suitable volumes (25-500 μL) from both the phases.



Figure 2.10 Thermostat bath for maintaining the temperature

The distribution ratio of the metal ions was calculated as the concentration of metal ions (in terms of counts per unit time per unit volume) in the organic phase to that in the aqueous phase. During acid distribution studies, the hydrogen ion concentrations in the two phases were obtained by titration with standard alkali solution using phenolphthalein as the indicator. The organic phase was titrated in aqueous ethanol medium previously neutralized to phenolphthalein

end point. Each distribution value was obtained in duplicate or triplicate and the agreement between these values was within $\pm 2\%$. A good material balance ($\geq 95\%$) was usually obtained in all the experiments.

2.4.2 IRRADIATION STUDIES

In order to study the irradiation stability of PC-88A and CCD-NPOE solutions, a ^{60}Co gamma source of ~ 2 KGy/h dose rate was used. These chemicals were kept in the chamber for required time interval to get desired radiation dose.

2.4.3 MEMBRANE TRANSPORT STUDIES

The supported liquid membrane transport studies were carried out either in the flat-sheet or the hollow fibre configuration. The basic optimized experimental conditions were used for transport experiments for both Cs and Sr transport studies and the experimental details are given below.

2.4.3.1 FLAT-SHEET SUPPORTED LIQUID MEMBRANE (FSSLM)

Flat Sheet Supported Liquid Membrane (FSSLM) technique was used for the recovery of metal ions (Cs and Sr) from acidic feed solutions at a relatively smaller scale (20 ml). The transport experiments with flat-sheet supported liquid membrane (SLM) were carried out using a Pyrex glass cell consisting of two compartments, viz. the feed side and the strip side. As shown in Fig. 2.11, both the compartments of the glass cell were joined by glass flanges along with the PTFE flat sheet membrane placed in between. The two phases were stirred using high speed magnetic stirrer equipped with precise speed control to minimize the effect of thickness of the aqueous diffusion boundary layers without damaging the membrane wall [96]. The volumes of

the aqueous feed and strip solutions were kept constant (about 20 ml) in all the experiments. The membrane is prepared by placing microporous polypropylene or PTFE membrane filters in the carrier solvent (calix-crown or crown ether in NPOE-*n*-dodecane diluent) for the required time period to ensure the complete soaking of the membrane.

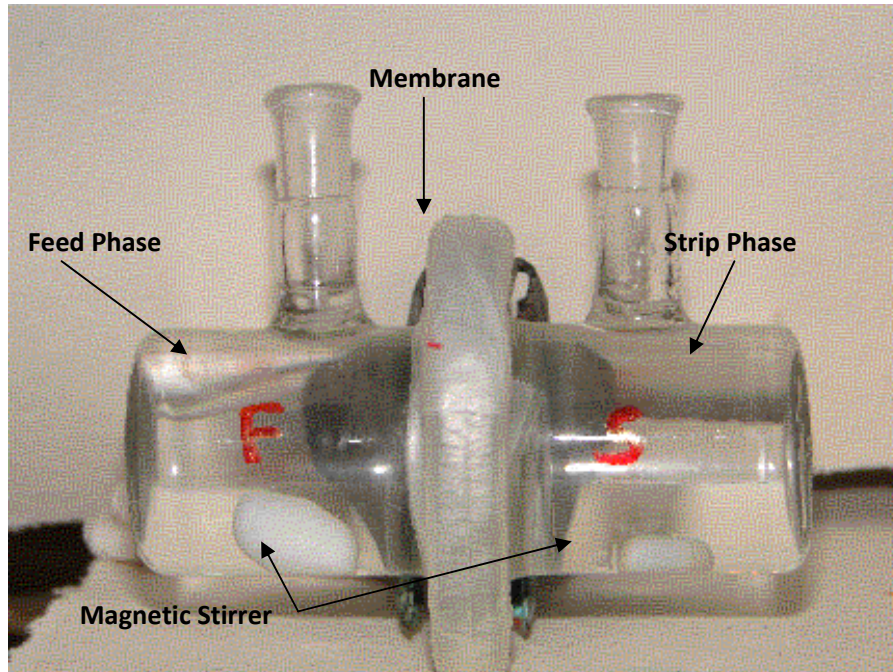


Figure 2.11 The transport cell used for the FSSLM studies

The cumulative transport (% T) of the metal ions at a given time was determined from the following equation,

$$\%T = \frac{C_0 - C_t}{C_0} \times 100 \quad (2.3)$$

where C_0 and C_t are the concentration of the metal ions in the aqueous feed at the start of experiment ($t = 0$) and at time t , respectively. The permeability coefficient (P) was obtained using the following equation [70],

$$\ln \frac{C_t}{C_0} = -P \left(\frac{Q}{V} \right) t \quad (2.4)$$

where, Q is the effective membrane area obtained from the total exposed membrane surface area A and the porosity ε ($Q = A \cdot \varepsilon$), V is the volume of the feed solution in cm^3 . A plot $\ln(C_t / C_0)$ versus time was used to calculate the P value from the slope of the linear fit. It should be noted that the above equation is valid only when the carrier is not saturated and the flux decreases linearly with time. In the present work, since all the experiments were carried out at tracer metal concentration (except stated otherwise), equation (2.4) was applicable for the calculation of P.

2.4.3.2 HOLLOW FIBRE SUPPORTED LIQUID MEMBRANE

Applicability of liquid membrane for the recovery of cesium / strontium was demonstrated on larger scale using Hollow Fibre contactors. The specifications of the hollow fibre module used in the present work are summarized earlier in Table 2.3. The Hollow Fibre Supported Liquid Membrane (HFSLM) was prepared by pumping the ligand solution through the lumen side of the module at a pressure of 3-4 psi in the recycling mode. To ensure the complete soaking of the membrane pores, the ligand solution was circulated for ~ 25 min until the solvent started percolating from lumen side to the shell side. After complete soaking, the excess ligand solution was washed out with plenty of distilled water. The pre-conditioning of system was carried out prior to the introduction of the actual feed and strip solutions. The feed solution was passed through lumen side while the strip solution was passed through the shell side of the module in all the experiments. The flow rates of the feed and strip solutions were maintained constant at 200 mL/min with the help of gear pumps equipped with precise flow controllers. A schematic

diagram of hollow fibre unit is shown in Fig. 2.12. The hollow fibre system employed in the present work is shown in Fig. 2.13.

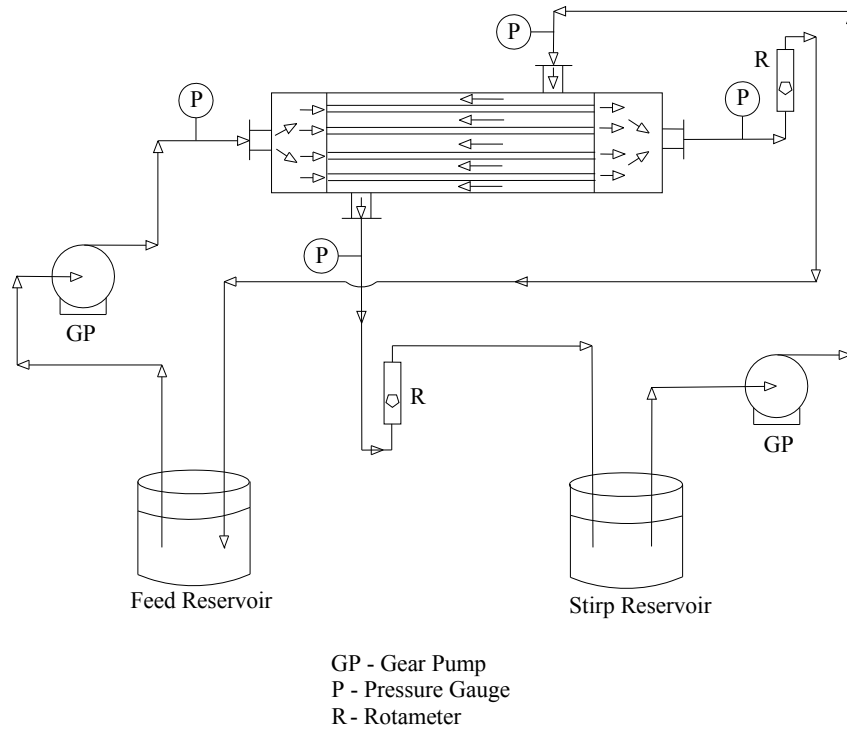


Figure 2.12 Schematic diagram of HFSLM transport process

The permeability coefficient is calculated by using the following equation as suggested by Danesi [77],

$$\ln \frac{C_t}{C_0} = -P \left(\frac{Q}{V} \right) \left(\frac{\phi}{\phi+1} \right) t \quad (2.5)$$

where, P is the overall permeability coefficient of the transported species, C_t and C_0 are the respective concentrations of the metal ions in the feed solution at an elapsed time t (min) and at zero time, and V is the total volume of the feed solution (mL). Here, the parameter A represents

the total effective surface area of the hollow fibre (cm^2) which is calculated from the following equation:

$$A = 2\pi r_i L N \epsilon \quad (2.6)$$

where, r_i is the internal radius of the fibre (cm), L is the length of the fibre (cm), N is the number of fibres and ϵ is the membrane porosity.

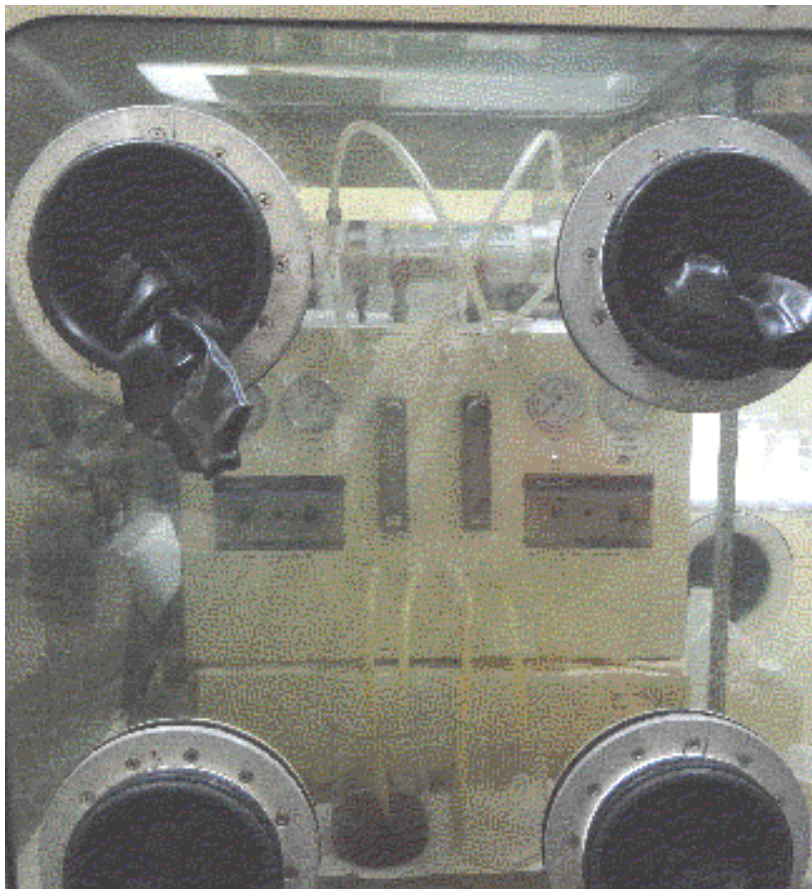


Figure 2.13 The HFSLM experimental setup

The parameter, ϕ for a module containing N number of fibres is expressed as follows,

$$\phi = Q_T / P r_i L N \quad (2.7)$$

where, Q_T is the total flow rate of the feed solution (mL/min). By plotting $\ln(C_i/C_o)$ as a function of t a straight line is expected, and according to Eqs. (2.6) and (2.7), the P value for the given system can be obtained from the fitted slope of Eq. (2.5).

2.5 MATHEMATICAL MODELING

As has been already discussed in Chapter 1, various models have been proposed in literature for the mass transfer of metal ion transport through liquid membranes. Some of the authors have developed the model consisting of rigorous mathematical complexity which is generally a difficult problem to cope with [97-103]. In this view, it was the aim to develop mathematical models which can be applied to a variety of transport problems and can work effectively. Hence, mathematical model have been developed for metal ion mass-transfer across FSSLM and HFSLM.

The present models have been developed on the basis of diffusional mass-transport phenomena. Various parameters have been assumed while developing the model and the effect of system composition is also incorporated in the model. The basic fundamental for both types of membrane transport processes is similar viz. diffusion of metal-ligand complex through the membrane phase. The following basic assumptions have been made while developing the models.

1. Aqueous boundary layers exist on both interfaces namely feed-membrane interface and strip-membrane interface
2. The concentration gradients are linear
3. The diffusion of the chemical species through the membrane phase is the rate-limiting step

4. Stripping is instantaneous which means there is no mass-accumulation inside the membrane phase

The mass-flux equations have been developed by Fick's equation and considering the mass balance of carrier ligand in the membrane phase and feed phase. The equations are simultaneously solved using mathematical software MATLAB-6.5. The detailed description of model development has been given in the respective Sections.

CHAPTER 3: Recovery of Cs by Calix[4]arene-bis-(2,3-naphtho)-crown-6

3.1. INTRODUCTION

Public acceptance of nuclear energy depends largely on the safe management of the hazardous nuclear wastes emanating from various fuel cycle operations. The high level nuclear waste of Pressurized Heavy Water Reactor (PHWR) contains a host of elements including long lived heat emitting radioisotopes viz. ^{137}Cs ($t_{1/2} = 30.1$ years) and ^{90}Sr ($t_{1/2} = 28.5$ years). The presence of these radio-nuclides poses serious issues due to the radiation induced degradation of the vitrified blocks in which the high level waste (HLW) is embedded prior to its disposal in deep geological repositories. Also, ^{137}Cs and ^{90}Sr find their many useful applications as radiation or energy sources as described earlier [9]. Therefore, selective and efficient recovery of ^{137}Cs and ^{90}Sr from high level waste is important for the safe management of radioactive waste as well as resource exploitation.

Being an alkali metal ion, cesium recovery from solution has always been a challenging problem especially in the presence of different metal ions including large concentration of sodium ion. Several reagents have been used for the recovery of radio cesium from acidic as well as alkaline solutions e.g. chlorinated cobalt dicarbollide (CCD) [45-48], ammonium molybdophosphate (AMP) coated resins [20-23, 26, 27, 104, 105], ion-exchange materials [13, 15, 17, 18, 28], crown ethers [31-34] and calix-crowns etc. [37-43, 106]. A major drawback of the AMP and CCD methods is the difficulties in stripping which is reflected in poor reusability of these reagents. Out of the many reagents used for cesium extraction, 18-membered crown ether derivatives have been found to be highly selective for Cs extraction from acidic feeds [107,108]. High concentration of 18-membered crown-ether molecule required to get sufficiently

good D_{Cs} value is one of the limitations. The name “calixarene” was coined by Gutsche for cyclic oligomers obtained by the condensation of formaldehyde with *p*-alkyl phenols [109,110]. Calixarenes offer several advantages as carrier viz., low water solubility, formation of neutral complexes by exchanging metal ion with proton, potentiality of coupling metal ion transport and reverse proton transport. Calix-crowns are the moieties obtained by grafting crown ether rings onto the phenyl rings of the calix-arenes [37]. Recent studies have indicated, however, that substituted calix-crown ligands are more attractive due to high separation factor for cesium over other alkali metal ions and possibility of easy stripping [111]. The cavity size of the calix-crowns (3.2-3.5 Å) is highly complementary to the size of Cs(I) ion as compared to the other alkali metal ions in calix[4]-arene bis-crown-6 ligands and makes it very selective for the former. Other studies employing X-ray crystallography have also shown the cation–pi interaction between metal-arene rings and exceptional selectivity of these calix-crowns for cesium by the bonding interactions with the four benzene units of the calix[4]arene [42, 112-114]. This indicates the favorable interaction of the calixarene moiety with the cesium ion that enables the selective separation of Cs(I) with a reasonably high separation factor with respect to other metals. Calix-[4]-arene-bis-crown-6 molecules in 1,3-alternate configuration have been reported to be selective for cesium metal ions in a very large concentration of sodium. The complementarity between crown ether ring size and Cs(I) ion have been reported to be quite important for the selectivity observed in case of calix-crown molecules [115]. Increasing or decreasing the crown ether ring size resulted in the decreased distribution ratio of cesium.

The high cost and toxic nature of the calix-crowns have been the main limiting factors in their use at large scale. Hence, methods with low ligand inventory are required for the treatment of large volume of solution. In this regard, we have investigated transport behavior of cesium ion

through supported liquid membranes under various experimental conditions including those involving SHLW feed conditions. The results have been discussed in detail in this Chapter.

3.2. DISTRIBUTION STUDIES

Mohapatra et al. [116] have investigated various calix-crowns for Cs extraction including calix[4]-arene-bis(crwon-6), calix[4]-arene-bis(o-benzocrwon-6) and calix[4]-arene-bis(2,3-naphthocrwon-6). Naptho-group has been observed to give better extraction of cesium because of more organophilicity incorporated in the molecule. Hence, calix[4]-arene-bis(naphthocrwon-6) (abbreviated as CNC, figure 3.1) has been found to be the most efficient out of the three molecules investigated.

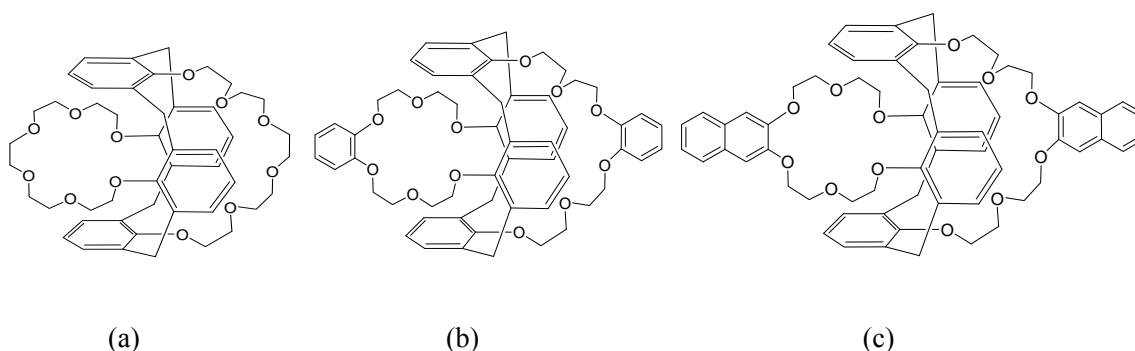


Figure 3.1 Structural formulae of (a) calix[4]-arene-bis(crwon-6), (b) calix[4]-arene-bis(o-benzocrwon-6) and (c) calix[4]-arene-bis(naphthocrwon-6).

To investigate the basic complexation process of Cs(I) by calix[4]arene-bis(2,3-naphtho)-crown-6, solvent extraction studies were carried out and effect of various factors have been observed. The basic process involved in the liquid membrane transport is simultaneous extraction and stripping of the metal ions. Hence, distribution studies were carried out to optimize the suitable experimental conditions. The following equilibrium can be written for the Cs⁺ ion extraction,



where, L and n denote CNC molecule and average number of CNC molecules bound per metal ion in the extracted complex, respectively. The subscripts 'aq' and 'org' represent the species present in the aqueous and the organic phases, respectively. The equilibrium extraction constant is given as,

$$K_{ex} = \frac{[(Cs^{+}.nL)(NO_{3}^{-})]_{org}}{[Cs^{+}]_{aq} \cdot [NO_{3}^{-}]_{f,aq} \cdot [L]_{f,org}^n}$$

or,

$$K_{ex} = \frac{D}{[NO_{3}^{-}]_{f,aq} \cdot [L]_{f,org}^n} \quad (3.2)$$

where subscript 'f' represents the species in free state. K_d is the distribution ratio of metal ion and is given by

$$K_d = \frac{[(Cs^{+}.nL)(NO_{3}^{-})]_{org}}{[Cs^{+}]_{aq}} \quad (3.3)$$

Taking logarithm of equation (3.2), obtains

$$\log K_d = \log K_{ex} + \log[NO_{3}^{-}]_{f,aq} + n \cdot \log[L]_{f,org} \quad (3.4)$$

Solvent extraction studies have indicated a linear dependence of $K_{d,Cs}$ with the concentration of calix[4]-bis-(2,3-naphtho)crown-6 with a positive slope (n) of 1.05 ± 0.05 (Fig. 3.2). This conforms to the following two-phase equilibrium (3.5) for the extraction of Cs(I) using calix[4]-bis-2,3-naphtho-crown-6, as reported in an earlier publication [117, 118]:

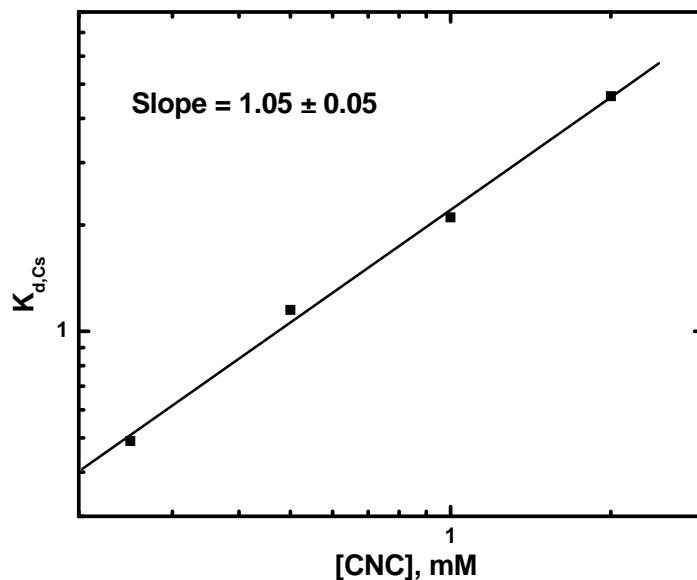


Figure 3.2 Variation of $K_{d,Cs}$ with the calix-crown ligand concentration. Aq. Phase: 3 M HNO_3 ; Org. phase: CNC in 80% NPOE + 20% *n*-dodecane.

The extraction of Cs(I) by calix-crown ligands followed the ion-pair extraction mechanism as reported earlier [116, 119] in presence of a polar diluent and Alamine-336 was found to facilitate the stripping of Cs [120]. Accordingly, NPOE, a polar diluent, along with 0.4% Alamine 336 was used for the present transport studies. In view of relatively high viscosity of NPOE (13.4 mPa.s), 20% *n*-dodecane was added which led to significantly improved transport rates [44]. Moreover, though NPOE was found to have good diluent properties due to its high dielectric constant which can stabilize the ion-pair, for transport experiments, it was required to use a modifier which can provide stable membrane system. It was found that addition of 20% *n*-dodecane to NPOE led to a viscosity decrease of $\sim 20\%$ as compared to pure NPOE that could facilitate mass transfer more efficiently (Table 3.1). Further increase in the *n*-dodecane fraction had adverse effects on the solubility of the extractant in the modified diluent. The addition of

Alamine 336 which helped in metal ion stripping, however caused a significant decrease in the $K_{d,Cs}$ values as follows: $K_{d,Cs}$ was 4.85 for 1×10^{-3} M calix[4]-bis-2,3-naphtho-crown-6 in 80% NPOE + 20% *n*-dodecane, while it was 2.10 in the presence of 0.4% Alamine 336. Alamine 336 is tertiary amine which is protonated in presence of nitric acid and form $(R_3NH)^+(NO_3)^-$ thereby nitric acid extracted in the organic phase is reduced by Alamine and the stripping becomes much facile in the presence of Alamine 336 in the organic phase. Same is true for extraction also.

Table 3.1: Measured value of viscosity, density and distribution ratio (K_d) for pure NPOE, *n*-dodecane and mixture of both as diluent.

| Diluent | Viscosity (mPa.s) | Density (g/cc) | $K_{d,Cs}^*$ (at 3 M HNO ₃) |
|-----------------------------------|----------------------|-------------------|--------------------------------------------|
| NPOE | 13.417 | 0.8745 | 8.12 |
| <i>n</i> -dodecane | 1.3038 | 0.7461 | ** |
| 80% NPOE + 20% <i>n</i> -dodecane | 11.0875 | 0.8534 | 4.85 |

* Using 1×10^{-3} M CNC without Alamine 336; ** CNC solubility was very poor

In PHWR-HLW, as much as 0.32 g/L of total cesium is present which is quite significant from radiotoxicity point of view. Hence, it was pertinent to investigate the effect of metal ion loading on distribution ratio of cesium. The distribution ratio for Cs was found to be decreasing with the increase in the metal ion concentration from tracer level to a concentration of 0.5 g/L. The experimental results have been listed in Table 3.2. At higher metal ion concentration, the concentration of free ligand (in eq. 3.2) is significantly lower and hence K_d value decreases accordingly to maintain constancy of K_{ex} .

Table 3.2: Variation of distribution ratio of metal ion with the metal ion loading. Feed: 3 M HNO₃ with different concentration of Cs(I), Organic Phase: 1.0×10⁻³ M CNC in 80% NPOE + 20% *n*-dodecane + 0.4% Alamine 336, Equilibration time: 1 hour

| [Cs], g/L | K _{d,Cs} |
|-----------|-------------------|
| Tracer | 2.10 ± 0.03 |
| 0.01 | 1.99 ± 0.02 |
| 0.1 | 1.15 ± 0.01 |
| 0.2 | 0.61 ± 0.01 |
| 0.3 | 0.42 ± 0.01 |
| 0.5 | 0.25 ± 0.01 |

3.3 MEMBRANE TRANSPORT STUDIES

In view of various advantages of supported liquid membranes over other methods, the aim of the present study was to develop suitable liquid membrane technique for the recovery of cesium from acidic solutions. The transport of cesium through flat-sheet supported liquid membrane has been investigated by Raut et al. [118]. At tracer level of metal ion, almost 90% transport of cesium was observed in 24 hours by 5×10⁻⁴ M CNC where 3 M HNO₃ and distilled water were used as the feed and the strip phases, respectively. The experiments were performed at ~ 20 mL volumes of the feed and strip phases. Hence, it was of interest to increase the throughput of the process and simultaneously reduce the time of operation by using hollow fiber

configuration. After performing sufficient basic extraction data evaluation, the transport of cesium by hollow fibre supported liquid membrane was thoroughly investigated.

3.3.1 Transport profile of Cs(I)

In Hollow Fiber Supported Liquid Membrane (HFSLM) transport experiments, 1.0×10^{-3} M CNC in 80% NPOE + 20% *n*-dodecane + 0.4% (v/v) Alamine-336 was used as the organic phase (membrane phase) and 3 M HNO₃ was employed as the feed while distilled water was taken as the strip. ¹³⁷Cs, at tracer concentration, was used and the metal ion transport through the membrane was monitored. Flow rate of both feed and strip solutions was kept fixed at 200 mL/min with the precise flow controllers. This was optimized by carrying out a series of experiments using different transport systems. The figure 3.3(a) depicts the average cumulative transport profile of five replicate transport experiments. By plotting $\ln(C_t/C_0)$ against 't' (figure 3.3 (b)), the value of permeability was calculated to be $(9.35 \pm 0.35) \times 10^{-4}$ cm/min. It had been found that > 99% cesium can be transported from the feed phase to the strip phase in only 6 hours of continuous operations which was only 90% in 24 hours with FSSLM configuration at 20 mL scale [118]. Also, the rate of acid transport in case of FSSLM was also slow probably due to small surface area per unit volume available for mass transfer. Table 3.3 summarized the % transport and permeability coefficients for 5 successive runs in HFSLM mode indicating the excellent stability of the hollow fiber supported liquid membrane.

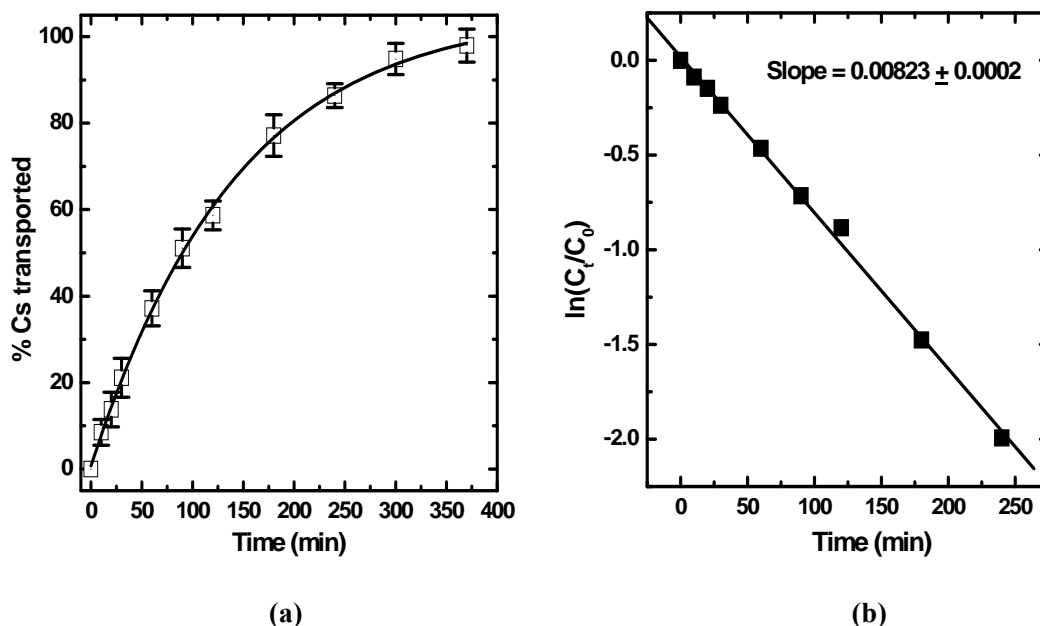


Fig. 3.3 (a) Transport of Cs(I) by HFSLM and (b) $\ln(C_t/C_0)$ vs. ‘t’ plot; Carrier: 1.0×10^{-3} M CNC in 80% (v/v) NPOE + 20% (v/v) *n*-dodecane + 0.4% Alamine 336; Feed: 3 M HNO_3 spiked with ^{137}Cs (500 mL); Strip: Distilled water; Flow rate: 200 mL/min; Temperature: 25°C.

Table 3.3: % Transport and calculated permeability coefficient for five cascaded HFSLM runs. Feed: 3 M HNO_3 spiked with ^{137}Cs ; Strip: Distilled water; Carrier: 1.0×10^{-3} M CNC in 80% NPOE + 20% *n*-dodecane + 0.4% Alamine336; Flow rate: 200 mL/min.

| Run | % T (5 h) | $P \times 10^4$ (cm/min) |
|-----------------|-----------|--------------------------|
| 1 st | 93.8 | 9.20 ± 0.25 |
| 2 nd | 92.6 | 9.12 ± 0.30 |
| 3 rd | 94.5 | 9.35 ± 0.32 |
| 4 th | 95.2 | 9.10 ± 0.26 |
| 5 th | 92.5 | 9.05 ± 0.32 |

For the selectivity studies, the feed solution was taken as 3 M HNO₃ containing various other radiotracers (²⁴¹Am, ¹⁵⁴Eu, ¹³⁷Cs, ^{85,89}Sr, ⁵⁹Fe and ⁵¹Cr) and distilled water was taken as the strip phase. The transport of various metal ions was measured after 5 hours of operation. Fig. 3.4 represents the gamma spectrum of the radionuclides at various stages of the experiment recorded using an HPGe detector inter-phased with a multi-channel analyzer. It was observed that only ¹³⁷Cs was transported into the strip phase and other metal ions such as Am, Eu, Sr, Fe and Cr were not transported to any significant extent. The strip aqueous solution exhibited only one prominent peak due to ¹³⁷Cs activity suggesting highly selective and effective transport of cesium ions.

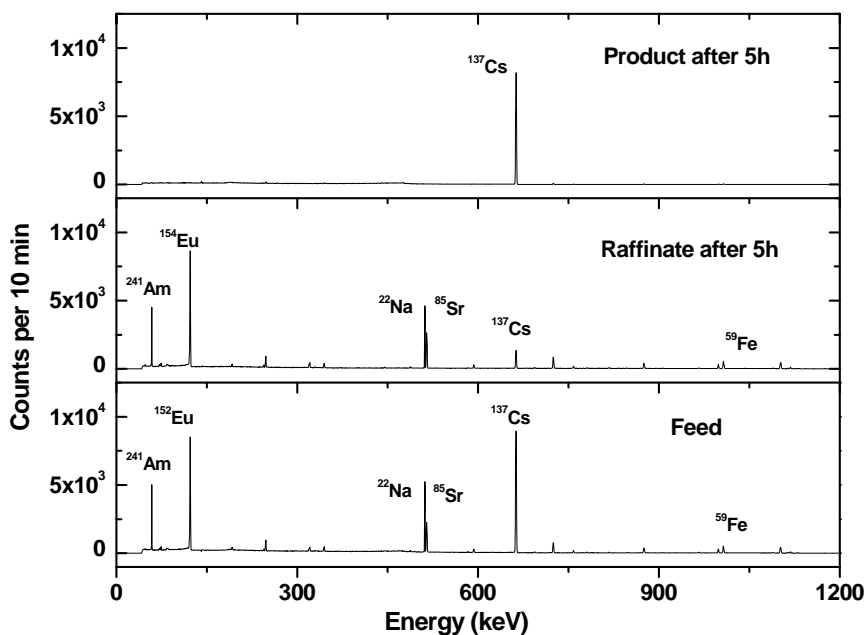


Fig. 3.4 Gamma spectrum of the radionuclides in the feed, strip and raffinate solutions showing the selective transport of ¹³⁷Cs in HFSLM after 5 hours of operation; Carrier: 1.0×10⁻³ M CNC in 80% NPOE + 20% *n*-dodecane + 0.4% (v/v) Alamine 336; Feed: 3 M HNO₃ spiked with various radiotracers (500 mL); Strip: Distilled water (500 mL); Flow rate: 200 mL/min; Temperature: 25°C

It is particularly interesting to note that no transport of Sr(II) was seen even though its ionic size has good compatibility with the 18-membered crown ligands. Hence, a good decontamination is achieved for Cs(I) with respect to other elements. Decontamination factor (D.F.) is defined as the ratio of distribution ratio of a particular metal ion to the distribution ratio of other metal ions at the same experimental conditions. The decontamination factor values for Cs(I), with respect to other metal ions are listed in Table 3.4. The decontamination factors for all the metal ions were > 500, which is quite encouraging for process scale applications. Hence selective recovery of cesium ion can be effectively achieved from acidic solutions using hollow fiber supported liquid membrane containing CNC as the carrier solvent. The results show the possibility of using HFSLM method as a promising alternative for Cs recovery from wastes. Further experiments were carried out to investigate the transport behavior of cesium under HFSLM mode.

Table 3.4: Transport of Cs(I) by HFSLM and respective decontamination factor (D.F.) values with respect to various elements; Carrier: 1.0×10^{-3} M CNC in 80% (v/v) NPOE + 20% (v/v) *n*-dodecane + 0.4% (v/v) Alamine 336; Feed: 3 M HNO₃ spiked with ¹³⁷Cs (500 mL); Strip: Distilled water; Flow rate: 200 mL/min; Temperature: 25°C.

| Elements | % Transport (5 h) | D.F. values |
|----------|-------------------|-------------|
| Cs(I) | 94.9 | - |
| Sr(II) | 0.10 | 860 |
| Am(III) | 0.15 | 595 |
| Eu(III) | 0.10 | 890 |
| Fe(III) | 0.17 | 540 |
| Cr(VI) | 0.14 | 625 |

3.3.2 Effect of carrier concentration

The effect of ligand concentration was examined at CNC concentration of 0.25 mM, 0.5 mM and 1 mM. It was observed that with increasing the CNC concentration, the rate of cesium ion transport increased. The experimental results have been listed in the table 3.5 and figure 3.5 shows a plot of $\ln(C_t/C_0)$ against time 't'. An increase in carrier concentration in membrane results in the increase in distribution ratio of metal ion at the feed-membrane interface and hence extraction of metal ion increases. This result in the higher % transport of cesium achieved at a particular time of operation (Table 3.5). In figure 3.5, the slope of linear fit of plot gives the indication about the overall permeability of metal ion through the membrane. The permeability coefficients have also been calculated and are listed in the Table 3.5.

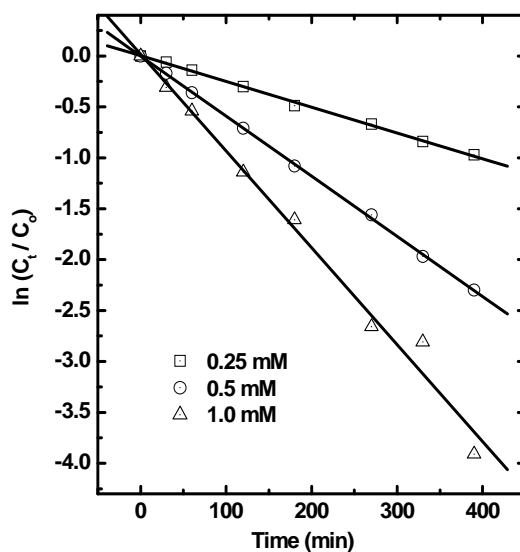


Figure 3.5 Linear plots of $\ln(C_t/C_0)$ vs. time for calculation of permeability coefficient; Carrier: Varying concentration of CNC in 80% NPOE + 20% *n*-dodecane containing 0.4% Alamine 336; Feed: 3 M HNO₃ spiked with ¹³⁷Cs tracer (500 mL); Receiver: Distilled water (500 mL); Flow rate: 200 mL/min. Temperature: 25°C.

The reciprocal of overall permeability coefficient ($1/P$) is related to other parameters by the following equation [121],

$$\frac{1}{P} = \frac{1}{k_f} + \frac{r_i}{r_{lm}P_m} + \frac{r_i}{r_o k_r} \quad (3.6)$$

where r_i , r_o and r_{lm} are the internal radius, outer radius and log-mean radius of the hollow fiber tube, respectively. P_m is the membrane permeability; k_f is the feed phase mass transfer coefficient in the tube side (feed side), and k_r is the receiver phase mass transfer coefficient in the shell side (receiver/strip side). Assuming that the stripping reaction is instantaneous at the membrane-strip interface, the contribution of the shell side aqueous phase resistance is neglected. Therefore, Eq. (3.6) can be reduced to the following equation;

$$\frac{1}{P} = \frac{1}{k_f} + \frac{r_i}{r_{lm}P_m} \quad (3.7)$$

Table 3.5: Variation of distribution ratio ($K_{d,Cs}$) and Permeability coefficient (P) with the ligand concentration. Carrier: Varying concentrations of CNC; feed: 3 M HNO₃ spiked with ¹³⁷Cs tracer (500 mL); receiver: distilled water (500 mL); flow rate: 200 mL/min.

| Ligand, mM | $K_{d,Cs}$ | $P \times 10^4$ (cm/min) | % Transport (after 6 h) |
|------------|-----------------|--------------------------|-------------------------|
| 0.25 | 0.49 ± 0.08 | 2.81 ± 0.05 | 62 |
| 0.5 | 1.15 ± 0.12 | 6.57 ± 0.08 | 90 |
| 1 | 2.10 ± 0.26 | 9.35 ± 0.35 | > 98 |

The membrane permeability (P_m) is related to the distribution ratio (K_D) by $P_m = K_d \cdot k_m$, where, k_m is the membrane mass transfer coefficient. Substituting the value of K_d from Eq. (3.2), Eq. (3.7) can be re-written as,

$$\frac{1}{P} = \frac{1}{k_f} + \frac{r_i}{\eta_m \cdot k_m \cdot K_{ex} \cdot [NO_3]_{aq} \cdot [L]_{org}} \quad (3.8)$$

From Eq. (3.8), the mass transfer rate controlling step can be predicted. When liquid membrane is an organic extractant with low distribution coefficient of the metal ions, the contribution of the aqueous feed mass transfer coefficient (k_f) to P is negligible and the membrane diffusion resistance may control the mass transport rate. Similarly, if the organic extractant in the liquid membrane has high distribution coefficient of the metal ions, k_f will have significant role in the rate controlling step.

Fig. 3.6 shows the plot of $1/P$ vs. $1/K_{ex}[NO_3^-]_{aq}[L]_{org}$. The values of k_f and k_m were calculated as 1.03×10^{-3} cm/s and 5.24×10^{-6} cm/s from intercept and slope of the plot, respectively. The value of k_f was much higher as compared to k_m , suggesting that the membrane mass transfer is the rate controlling step.

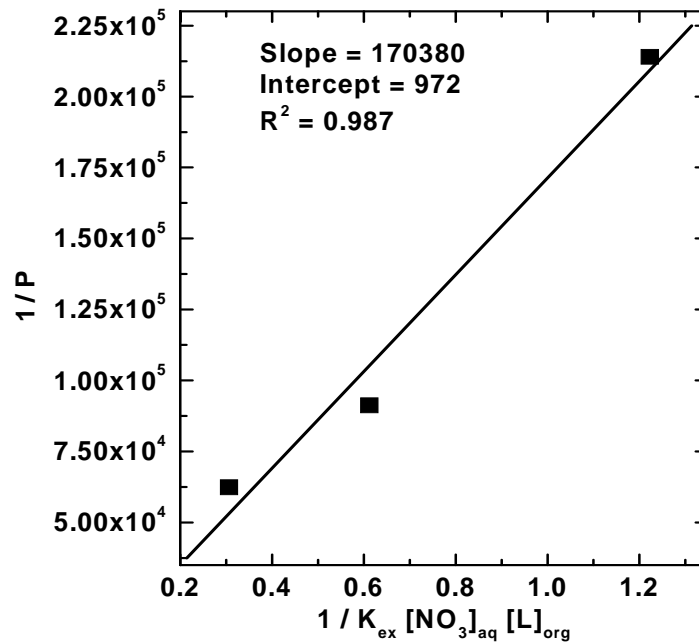


Figure 3.6 Plot of $1/P$ vs $1/K_{ex}[NO_3^-]_{aq}[L]_{org}$ for the calculation of permeability parameters.

3.3.3 Effect of the feed acidity

Cesium transport studies have also been carried out at different feed acidities in the range of 1-4 M HNO₃ keeping other parameters constant and the experimental results are shown in figure 3.7. Although the rate of transport was observed to be increasing with increase in the feed acidity up to 3 M due to increasing nitrate ion concentration which results in an increase in the extraction of the metal ion from the feed solution, a further increase in acidity to 4 M decreases the rate of transport probably due to competition of H⁺ ion with Cs⁺ ion for ligand molecule. The binding of H⁺ with crown ethers have been reported earlier by Kriz et al. [122, 123] and where the proton binding with crown ether was reported to be *via* formation of H₃O⁺, as per the following equilibrium,

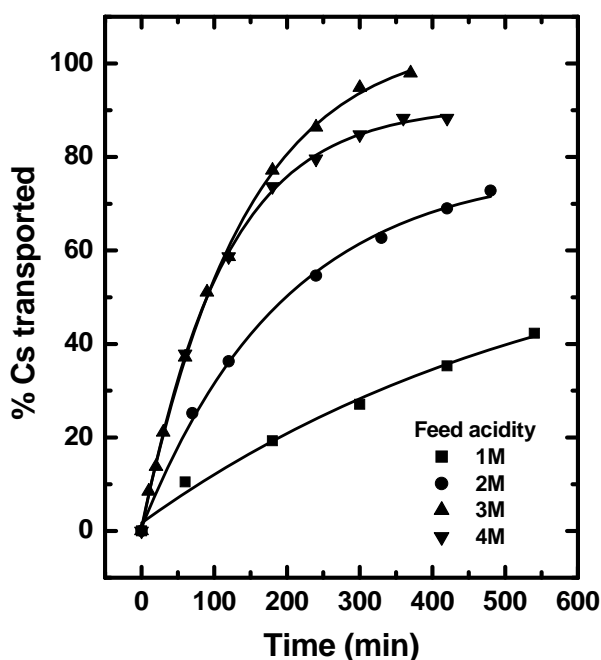
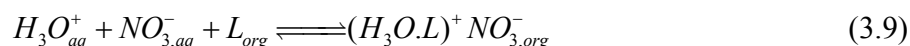


Figure 3.7 Transport profile of Cs(I) under various feed acidity. Carrier: 1.0×10^{-3} M CNC in 80% NPOE + 20% *n*-dodecane + 0.4% (v/v) Alamine 336, Strip: Distilled water, Flow rate: 200 mL/min.

As per the equilibrium (3.9), the increase in the feed acidity may be enhancing the competing equilibrium of nitric acid extraction by the calix-crown-6 ligand to the forward direction. To confirm this aspect, acid concentration in the strip phase was titrated with respect to time and the results are given in Table 3.6. It was seen that with increasing the feed phase acidity, rate of acid transport was faster with maximum transport being observed at 4 M HNO₃ thereby reducing the rate of cesium ion transport in this case. However, a big jump in acid transport rate observed while increasing the feed acidity from 3 to 4 M HNO₃ confirms the hydronium ion transport mechanism as suggested above (Eq. (3.9)) and this affected the transport rates in two ways; firstly, by decreasing the effective concentration of the extractant in the membrane phase and secondly, by affecting the stripping due to increased strip phase acidity.

Table 3.6: Transport of acid at different feed acidity. Carrier: 1.0×10^{-3} M CNC in 80% NPOE + 20% *n*-dodecane + 0.4% (v/v) Alamine 336; Feed: HNO₃ of different acidity (500 mL); Strip: distilled water; Flow rate: 200 mL/min; Temperature: 25°C

| Time (min) | Transport of acid to the strip side at the following feed phase acidities (M) | | | |
|---------------|-------------------------------------------------------------------------------|----------------------|----------------------|----------------------|
| | 1 M HNO ₃ | 2 M HNO ₃ | 3 M HNO ₃ | 4 M HNO ₃ |
| 0 | 0.00 | 0.00 | 0.00 | 0.00 |
| 60 | 0.05 | 0.09 | 0.11 | 0.22 |
| 120 | 0.10 | 0.12 | 0.15 | 0.37 |
| 180 | 0.12 | 0.15 | 0.18 | 0.53 |
| 240 | 0.16 | 0.20 | 0.22 | 0.67 |
| 360 | 0.23 | 0.27 | 0.30 | 0.90 |

3.3.4 Effect of cesium concentration

The concentration of cesium in PHWR-SHLW is approximately 0.3 g/L. Therefore, it was required to investigate the cesium loading effect on the transport profile of the metal ion. Transport experiments were carried out at cesium concentrations of 0.1 g/L, 0.3 g/L and 0.5 g/L. As shown in figure 3.8, although the rate of metal ion transport (mass-flux) is higher at higher feed metal concentration (Fick's law of diffusion), the % transport decreased significantly in the presence of Cs(I) salt from > 99.9% at tracer level to 51.2% at 0.5 g/L after 6 hours.

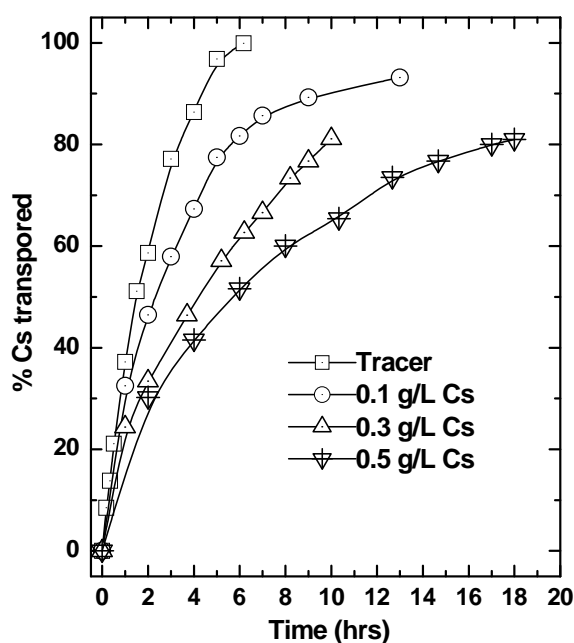


Figure 3.8 Transport of Cs(I) by HFSLM at different cesium concentration. Carrier: 1.0×10^{-3} M CNC in 80% NPOE + 20% *n*-dodecane + 0.4% (v/v) Alamine-336; Feed: 3 M HNO₃ (500 mL); Receiver: Distilled water (500 mL); Flow rate: 200 mL/min.

The Cs⁺ transport could not reach to 100% even after 18 h of operation (Figure 3.8). As shown in Table 3.6, the P value decreased with increasing Cs(I) concentration in the feed solution, suggesting a saturation effect. The acidity of strip phase was also measured as a

function of time interval and, as can be seen from the Table 3.7 acid transport is unaffected with the metal ion concentration in the feed.

Table 3.7: Effect of Cs(I) concentration in feed solution on its transport rate; Carrier: 1.0×10^{-3} M calix[4]arene-bis-naphthocrown-6; Feed: CsNO_3 in 3 M HNO_3 spiked with ^{137}Cs tracer (500 mL); Receiver: Distilled water (500 mL); Flow rate: 200 mL/min.

| [Cs], (g/L) | $P \times 10^6$ (cm/s) | %Transport (6 h) | $[\text{H}^+]$ in strip phase (6 h) |
|-------------|------------------------|------------------|-------------------------------------|
| Tracer | 15.6 ± 0.13 | > 99.9 | 0.30 mol/L |
| 0.1 | 9.48 ± 0.23 | 82.2 | 0.29 mol/L |
| 0.3 | 4.94 ± 0.17 | 62.1 | 0.28 mol/L |
| 0.5 | 3.04 ± 0.15 | 52.4 | 0.32 mol/L |
| SHLW | 6.47 ± 0.10 | 69.6 | 0.30 mol/L |

3.3.5 Transport of cesium from Simulated High Level Waste (SHLW)

After complete optimization of transport process through HFSLM, cesium transport was investigated from Simulated High Level Waste (SHLW) solution. SHLW contains 0.3 g/L of cesium at 3-4 M HNO_3 acidity. Hence, the transport studies were carried out with SHLW as the feed solution using 1×10^{-3} M CNC in the optimized membrane solvent. With SHLW as the feed, it took about 14 hours for ~ 90 % transport of cesium which was > 99 % in 6 hours when metal ion was taken at the tracer level. Figure 3.9 depicts the comparison between the transport profiles in the two cases.

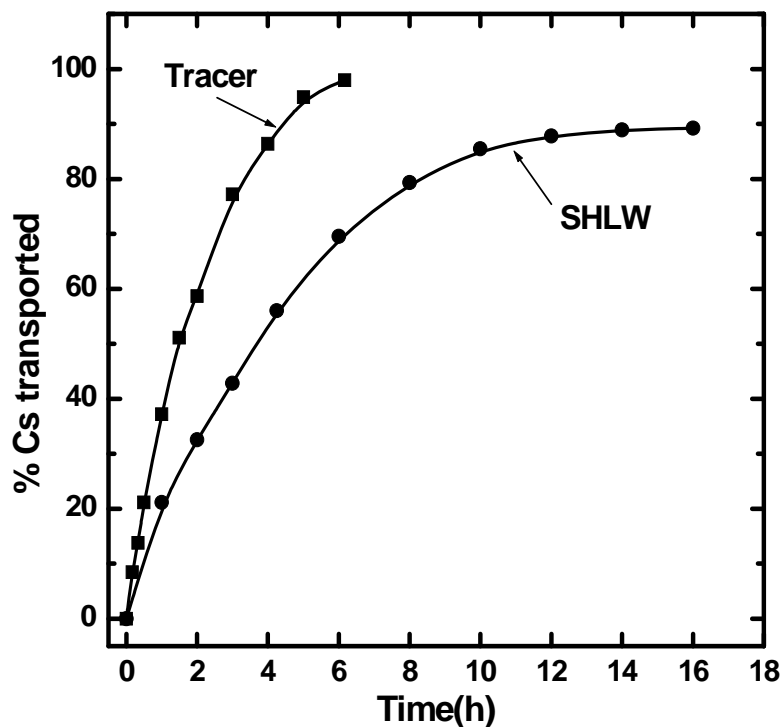


Figure 3.9 Transport profile of Cs(I). Strip: Distilled water; Carrier: 1.0×10^{-3} M CNC in 80% NPOE + 20% *n*-dodecane containing 0.4% Alamine 336; Flow rate: 200mL / min.

A plateau at higher time scale suggested quantitative transport of cesium was not achieved even after 14 hours of operation. To investigate this, acid titration of strip phase was carried out and the acid transport profile for the studies with SHLW as the feed is presented in figure 3.10. Continuous transport of acid was observed and it can be seen that after 14 hours, almost 0.52 M (17%) acid was transported into the strip phase. The accumulation of acid in the strip phase, as described earlier, can possibly be making the stripping of metal ion difficult resulting in saturation of the metal ion transport (figure 3.8) after 14 hours of operation. Although the direct evidence is not available with us, yet the further investigations have proven the role of acid transport in the overall transport profile of Cs through the membrane.

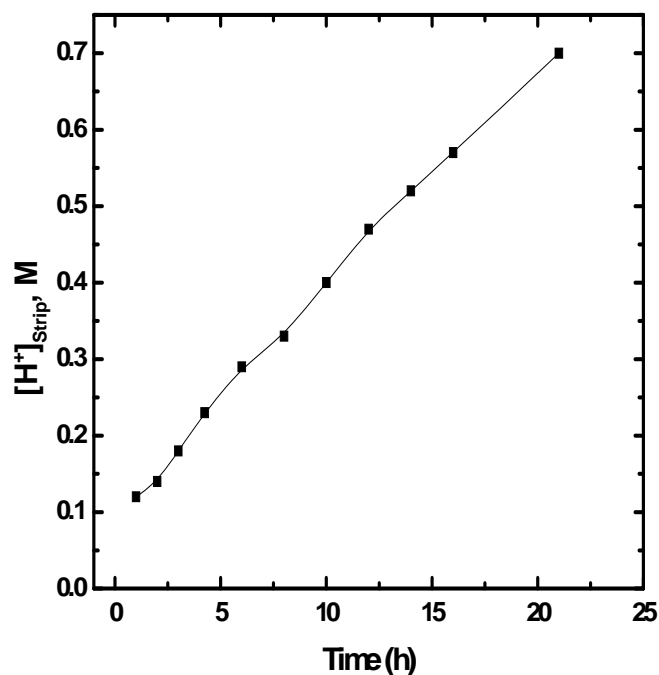


Figure 3.10 Acid transport profile with SHLW as feed (500 mL). Strip: Distilled water (500 mL), Carrier: 1.0×10^{-3} M CNC in 80% NPOE + 20% *n*-dodecane + 0.4% (v/v) Alamine 336, Flow rate: 200 mL/min.

Efforts have been made to increase the % Cs transport by changing the composition of the strip phase so that effect of acid transport can be minimized. To reduce the effect of acid in the receiver phase, 0.1 M acetate buffer (pH 5) was employed as the strip phase. However, it could not improve the transport rate of Cs(I) due to limited buffer capacity of the buffer solution (Figure 3.11). On the other hand, when the acidity of the receiver phase was neutralized with NaOH at regular time intervals (every 2 h), the transport profile improved remarkably and > 95% Cs(I) could be recovered in about 16 h of operation. This experimental observation suggested that selective recovery of Cs is possible by effectively neutralizing the acidity of strip phase by addition of equivalent amount of NaOH.

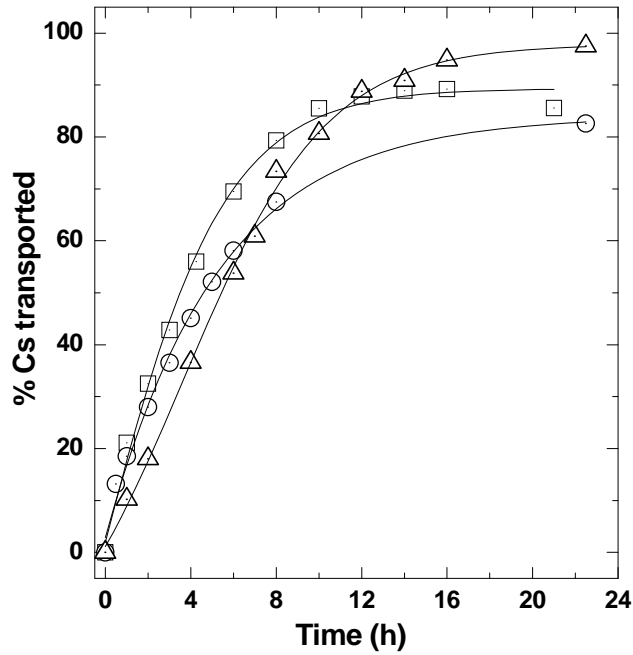


Figure 3.11 Transport of Cs from SHLW; Carrier: 1.0×10^{-3} M CNC; Feed: SHLW spiked with ^{137}Cs tracer (500 mL); Strip: Distilled water (500 mL); Flow rate: 200 mL/min; Strip phases: \square distilled water, \circ acetate buffer at pH 5, and Δ dist. Water neutralized with NaOH at 2 h intervals

3.3.6 Effect of the flow rate

The effect of flow rate on the transport behavior of cesium was also investigated by carrying out experiments at varying flow rates of 100 mL/min to 500 mL/min. The results of the Cs(I) permeation with the feed on the tube side at different flow rates are given in Fig. 3.12. The P value initially increased with the flow rate and then became independent of the flow rate. The P value can be described by the following equation [77];

$$P = \frac{k_d}{k_d \left(\frac{d_{aq}}{D_{aq}} \right) + \frac{d_m \tau}{D_m} \left(\frac{r_i - d_{aq}}{r_i} \right)} \quad (3.10)$$

As the flow rate increased, thickness of the aqueous boundary layer (d_{aq}) decreased, and hence the P value increased. Eventually, P becomes independent of the flow rate when $K_d(d_{aq}/D_{aq})$ terms in the equation becomes negligible at the optimum flow rate. As shown in Fig. 3.12, the permeability coefficient reaches a saturation value at a flow rate of 100 mL/min or higher. Thus, 200 mL/min was used as the flow rate for all subsequent experiments.

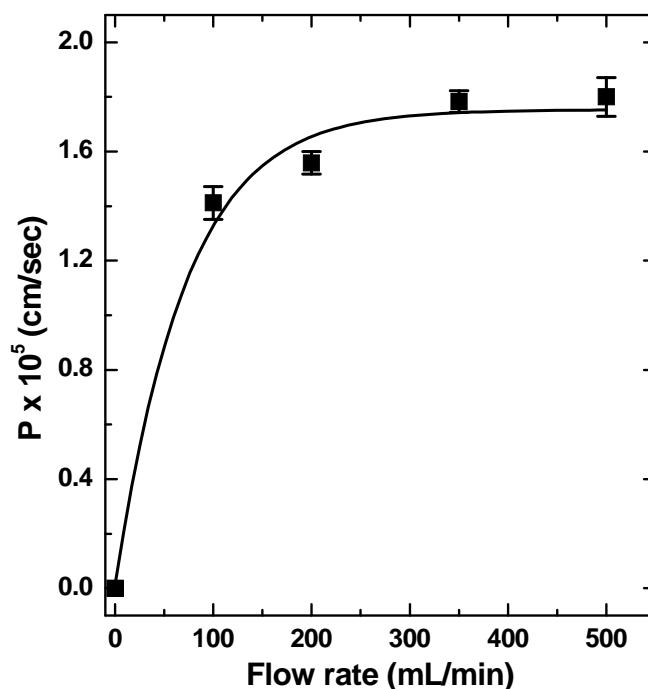


Figure 3.12 Variation of permeability coefficient (P) with flow rate; Carrier: 1×10^{-3} M of CNC; Feed: 3 M HNO_3 spiked with ^{137}Cs tracer (500 mL); Receiver: Distilled water (500 mL); Temperature: 25°C.

3.4 Conclusions

The HFSLM method has been developed in the present work for the recovery of Cs(I) from acidic feed solutions and PHWR-SHLW feed solution at 0.5 liter scale. Various experimental

conditions were studied and conditions were optimized. The results of the present studies can be summarized as follows

- It was evident from the results that Cs(I), at tracer level concentration, can be quantitatively transported in only 6 hours of operation from 3 M HNO₃ feed solution (0.5 L) into a receiver phase containing distilled water (0.5 L). Table 3.8 shows the comparison between transport rates of cesium and acid in the FSSLM and HFSLM configuration.

Table 3.8: Cs and acid transport data during the FSSLM and HFSLM transport studies using tracer. Feed: 3 M HNO₃ spiked with ¹³⁷Cs; strip: distilled water. Flow rate for HFSLM: 200 mL/min; Temperature: 25°C.

| Time (min) | % T in FSSLM (20mL scale) | | Time (min) | % T in HFSLM (500 mL scale) | |
|------------|---------------------------|------|------------|-----------------------------|------|
| | Cs | Acid | | Cs | Acid |
| 30 | 3.6 | 0.11 | 95 | 43.6 | 4.3 |
| 60 | 5.7 | 0.16 | 120 | 52.1 | 5.0 |
| 120 | 9.4 | 0.19 | 180 | 69.3 | 6.0 |
| 180 | 17 | 0.23 | 240 | 82.5 | 7.3 |
| 240 | 24 | 0.31 | 300 | 93.8 | 10.0 |
| 360 | 39 | 0.39 | | | |

- With PHWR-SHLW as the feed, ~ 90% recovery of cesium was achieved in 14 hours of operation after which a plateau was reached. The acid transport to the strip side by CNC was also examined in order to find the reason for the saturation in transport profile. Studies with PHWR-SHLW solution revealed that high acid uptake by the carrier plays a

crucial role in the transport behavior of Cs(I) ion. In order to get near quantitative recovery of cesium from SHLW conditions, various modifications of the strip phase composition were attempted. It was found that > 95% recovery of cesium is possible when acidity of strip phase is neutralized by intermittent spiking of NaOH thereby alleviating the problem of inefficient stripping. Acetate buffer (0.1 M at pH 5) was found to be ineffective in this regard probably due to insufficient buffer capacity.

- The membrane stability has been shown to be quite excellent up to few days (Table 3.3) and further investigations are also required. To use the HFSLM system on large scale various other aspects viz. hydrodynamic parameters, radiation stability, physical stability etc are also required to be examined.
- Radiation resistant membranes are also required to be explored as high radiation field associated with the actual high level nuclear waste solution may cause damage to the polymer matrix.

It can be concluded that the HFSLM method can be effectively applied for the recovery of cesium at liter scale with much faster mass transfer as compared to the FSSLM transport system. The HFSLM technique appears to be quite promising for the selective recovery of cesium from the acidic radioactive waste solution using calix-crown ligand as the carrier extractant.

CHAPTER 4: Studies on liquid membrane transport of strontium

4.1 INTRODUCTION

^{90}Sr , like ^{137}Cs , is produced in the nuclear reactor as a result of nuclear fission of ^{235}U by thermal neutrons. Though several isotopes of Sr are formed in this process (as described in Chapter 1), ^{90}Sr is the most important due to its long half-life and its significant contribution to the radioactivity of the high level waste. The β -decay of ^{90}Sr generates ^{90}Y which also is a pure beta-emitting radionuclide. Hence, the recovery of ^{90}Sr can not only reduce the risk due to degradation of disposal matrix by the presence of such a high heat generating radioisotope but also the recovered ^{90}Sr can be used for various useful purposes as detailed before (Chapter 1) [9].

The selective recovery of Sr from the mixture of metal ion has been demonstrated by various research groups [49-61] and this has also been described in Chapter 1. These methods include ion-exchange, precipitation by suitable reagents (e.g. antimoniac acid), solvent extraction using crown ethers and mixture of crown ethers with synergistic reagents. Out of the solvent extraction methods those involving crown ethers as extractant are found to be highly efficient with very high selectivity. Researchers at Argonne National Laboratory suggested a process for Sr recovery using 4,4'(5') di-tert-butyl-dicyclohexano-18-crown-6 (DtBuCH18C6) in 1-octanol [57]. High acid uptake was reported due to the presence of 1-octanol as diluent. Also, the aqueous solubility of this crown ether was a serious problem and structural modifications were carried out in order to minimize the solubility of crown ether in aqueous phase [55]. Horwitz *et al.* proposed a process called SREX (Strontium EXtraction) for strontium recovery by 4,4'(5')-di-tert-butyl-cyclohexano-18-crown-6 (DtBuCH18C6) in 1-octanol. In this process, strontium is extracted from acidic ($\geq 1 \text{ M HNO}_3$) solution using a 0.2 M solution of DtBuCH18C6 in 1-octanol. Extracted strontium is readily stripped from the organic phase using either water or ~

0.05M HNO₃. It extracts Sr(II) effectively from the simulated sludge solution (Sr = 1.3 × 10⁻³ M). Within three contacts, >99.7% Sr(II) recovery was achieved [57]. The solvent exhibits good radiolytic stability.

Out of various separation methods, liquid membrane technique seems to be quite attractive in view of certain advantages such as requirement of low ligand inventory, ease of handling, easy scale-up and low capital and operating cost, etc. There have been different liquid membrane based separation methods for Sr recovery using crown ethers as the carrier extractant [124-126]. Di-*tert*-butyl cyclohexano-18-crown-6 (DtBuCH18C6) has been used in several liquid membrane studies [127, 128] while dicyclohexano-18-crown-6 (DCH18C6) has also been used by several researchers [29-31]. The major disadvantages of these liquid membrane based Sr recovery methods include high acid co-transport leading to decreased Sr transport efficiency. Rawat et al. [129] investigated Sr transport using DtBuCH18C6 as the carrier and 0.5 M HNO₃ + 2 M Al(NO₃)₃ as the feed phase composition. Although they have reported quantitative Sr recovery in about 44 hours, the addition of large concentration of nitrate salts in the feed is not advisable. In another study, modification of carrier solvent composition has resulted in lower acid co-extraction [132] but flat-sheet supported liquid membrane (FSSLM) studies were not very promising [61] due to very high acid co-transport. Very recently, transport of Sr(II) through FSSLM containing DtBuCH18C6 in 80% NPOE + 20% *n*-dodecane has been reported and it has been found that almost 98 % of strontium can be recovered in about 24 hours of operation [133] with only 11% acid transport. Due to limited surface area available per unit volume, the FSSLM studies resulted in very slow mass transfer rates. Hence, it was required to use HFSLM technique which provides large surface area to volume ratio and is also associated with various other advantages viz. ease of operation, easy scale-up of process etc. Using HFSLM technique,

relatively higher mass transfer fluxes can be achieved and hence, the operation time could effectively be reduced.

Though ^{90}Sr recovered from high level waste, can be used as power source, it can also be used as a source of ^{90}Y which is used in radiopharmaceuticals. Many methods and reagents have been used for separation of ^{90}Y from a mixture of $^{90}\text{Sr} - ^{90}\text{Y}$. Wai and Du [134] reported the paper chromatographic method for the separation of ^{90}Y from ^{90}Sr using crown ether carboxylic acids. The major limitation of this method is that the paper can be only be used for one application.

Ion-exchange methods have also been used Dowex-50 has been used as cation exchange resin which retains ^{90}Sr while ^{90}Y is eluted with aqueous complexant such as acetate [135], lactate [136], EDTA [137] or citrate and oxalate [138]. The loss due to radiolytic degradation of ion-exchange material results in the poor loading capacity of resin. As a result, ion-exchange is considered suitable for sub-curie quantities of radioactivity, less than the quantities required for clinical applications. Finally, achieving high yields of ^{90}Y while minimizing ^{90}Sr breakthrough often requires the use of long ion-exchange columns and impractically large volumes of eluents [139].

Wike et al. [140] demonstrated a method involving solvent extraction of ^{90}Y by bis(2-ethylhexyl) phosphoric acid in *n*-dodecane as carrier extractant. The useful life of generator was found to be limited as the radiolytic products of the extractant accumulate in the product. Moreover complexity of process, which involves repeated stripping of extractant and repeated wet ashing of the stock solution to destroy dissolved organic phosphates, is quite prohibitive. This would also produce a large amount of secondary organic waste. Researchers have also used organo-ceramic hybrid materials implanted with extractant molecules (like organo-phosphorous

compounds) to avoid the leaching of material by repeated applications [141]. Hence, a method which require low ligand inventory and provides high throughput with fast mass transfer rate is quite necessary to achieve sufficiently large activity of ^{90}Y for use in radiopharmaceutical applications.

Flat sheet SLM methods have been employed for selective removal of ^{90}Y [142, 143] but these methods are not only much time consuming but also produce activity in low yield which are of less use for therapeutic purposes. Higher mass transfer rates can be achieved by using the system in HFSLM configuration. In this view, separation of ^{90}Y from a mixture of ^{90}Sr - ^{90}Y by using HFSLM containing PC88A in *n*-dodecane as the carrier solvent was also demonstrated and the purity of ^{90}Y obtained was ascertained by various methods. Hence, the present work was initiated to produce highly pure ^{90}Y with improved throughput as compared to flat sheet SLM methods using HFSLM technique.

4.2 DISTRIBUTION STUDIES

Major work involving solvent extraction of Sr from acidic feeds using the crown ether, DtBuCH18C6 (figure 4.1) in NPOE medium, has been carried out by Raut et al. [132] and they have optimized the system parameters and found that the distribution ratio for strontium (D_{Sr}) is approximately 3.13 ± 0.08 at 3 M HNO_3 with 0.1 M DtBuCH18C6 in 80% NPOE + 20% *n*-dodecane.

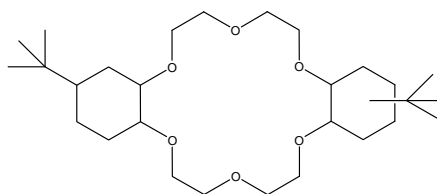
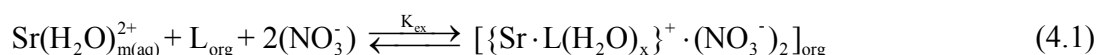


Figure 4.1 Structural formula of di-*tert*-butylcyclohexano 18-crown-6

From our previous experience, a solvent mixture of 80% NPOE + 20% *n*-dodecane has been proven to be an excellent solvent composition from membrane stability point of view and hence, the membrane transport experiments were carried out with this diluent composition containing 0.1 M DtBuCH18C6. The extraction equilibrium has been established and is given as follows [132]:



where, L represents DtBuCH18C6 molecule. The distribution ratio for Sr(II) was found to be increasing with the acidity of the aqueous phase. With distilled water as the aqueous phase, the D_{Sr} value was found to be $< 10^{-3}$ and hence, for the subsequent studies with supported liquid membranes, 3 M HNO₃ was taken as the feed phase while distilled was used as the strip phase.

4.3 HOLLOW FIBRE SUPPORTED LIQUID MEMBRANE STUDIES

In the present work, the transport behaviour of Sr(II) through HFSLM was thoroughly investigated and various system parameters were studied to optimize the experimental conditions. The results are discussed in the following section:

4.3.1 Transport of Sr(II) through HFSLM

The transport of Sr(II) through HFSLM impregnated with solvent comprising of 0.1 M DtBuCH18C6 in 80% NPOE + 20% *n*-dodecane was investigated, where, 3 M HNO₃ and distilled water were employed as the feed and the strip solutions, respectively. In view of possible application in ⁹⁰Sr recovery from the high level waste, which has the acidity of 3-4 M HNO₃, the feed used in the present study usually contained 3 M HNO₃ for possible comparison. The flow rate was kept constant at 200 mL / min the transport studies were performed in recycling mode. As can be seen from figure 4.2, almost 90% strontium was found to be

transported in about 3 hours of continuous operation. The permeability coefficient (P) was found to be 2.22×10^{-3} cm/min. In comparison to the work carried out by Raut et al. [133], where they have reported ~ 98% recovery of Sr in 24 hours using flat sheet SLM, the present work suggested possible recovery of Sr(II) under comparable experimental conditions with much lesser operational time and high throughput (500 mL feed volume).

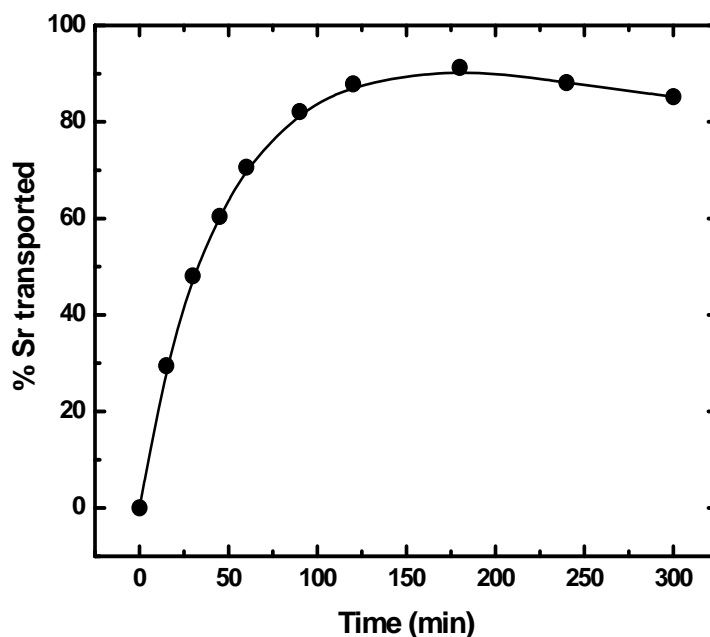
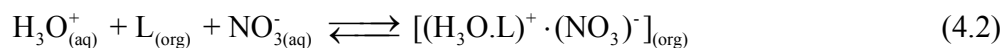


Figure 4.2 Transport profile of Sr(II) through HFSLM. Feed: 3 M HNO₃, Strip: Distilled water, Carrier: 0.1 M DtBuCH18C6 in 80% NPOE + 20% *n*-dodecane, Flow rate: 200 mL/min

It was surprising to observe that after 3 hours of operation, back transport of metal ion took place and the % Sr transport value decreases to ~ 85% after 5 hours (Fig. 4.1). As, the exact reason for the back transport was unknown, strip phase acidity was determined by titrimetric methods using NaOH and phenolphthalein (indicator). Crown ethers are well known [144, 145] for complexing with acid as hydronium ion as per the following equilibrium,



The acid transport profile is given in figure 4.3. As can be seen that after 3 hours of operation, ~ 14% (0.42 M) acid was transported to strip side after which the back transport of metal ion became apparent. This indicates the critical role of acid transport on the overall transport profile of Sr(II). In case of FSSLM, the acid transport was not prominent due to the rate of acid transport is slower due to lesser effective surface area available for mass transfer unlike HFSLM transport that provide much higher surface area per unit volume occupied.

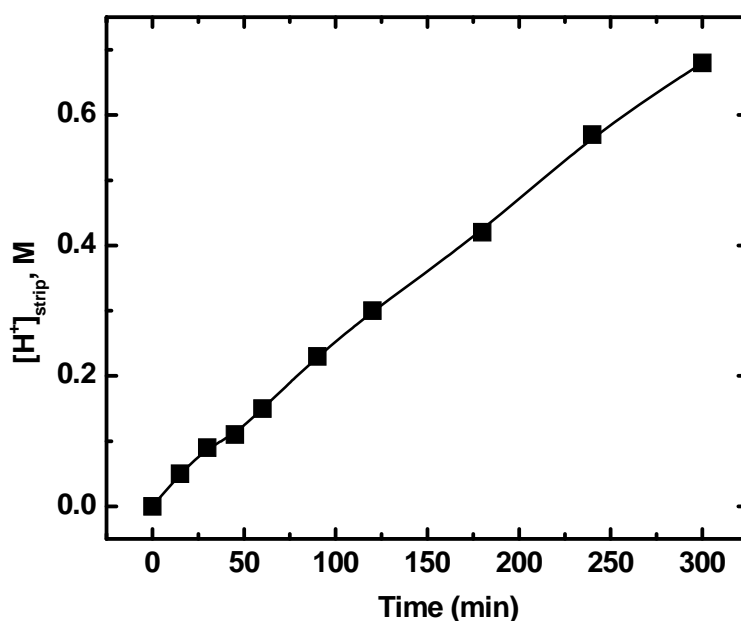


Figure 4.3 Transport of H⁺ by DtBuCH18C6 through HFSLM. Feed: 3 M HNO₃ spiked with ¹³⁷Cs; Strip: Distilled water; Carrier: 0.1 M DtBuCH18C6 in 80% NPOE + 20% *n*-dodecane; Flow rate: 200 mL / min.

The selectivity experiments were also carried out with SHLW as the feed where the inactive metal ions are present at the same concentration as present in PHWR-HLW (Table 4.1). The transport of Sr(II) was monitored by adding radioactive ^{85,89}Sr and after the optimum strontium transport, the strip solution was analyzed for various metal ion concentrations using ICP-AES.

Table 4.1: % Transport of various metal ions from PHWR-SHLW by HFSLM after 3 h of operation. Strip: Distilled water; Carrier: 0.1 M DtBuCH18C6 in 80% NPOE + 20% *n*-dodecane; Flow rate: 200 mL/min

| Elements | Initial ($\mu\text{g/mL}$) | Feed-Final ($\mu\text{g/mL}$) | Strip-Final ($\mu\text{g/mL}$) | % Transport |
|-----------------|--------------------------------------------------|-----------------------------------------------------|------------------------------------------------------|--------------------|
| Ba | 0.2125 | 0.07 | 0.1425 | 67.06 |
| Cr | 1.025 | 1.025 | 0.005 | 0.49 |
| Fe | 6.7 | 6.55 | 0.005 | 0.07 |
| La | 1.6875 | 1.625 | 0.005 | 0.30 |
| Mn | 3.95 | 3.925 | 0.025 | 0.63 |
| Mo | 0.57 | 0.57 | 0.005 | 0.88 |
| Nd | 0.9525 | 0.795 | 0.005 | 0.52 |
| Pd | 0.1925 | 0.1925 | 0.001 | 0.52 |
| Pr | 0.3975 | 0.1525 | 0.001 | 0.25 |
| Sm | 0.755 | 0.645 | 0.005 | 0.66 |
| Sr | 0.32 | 0.0625 | 0.2575 | 80.47 |
| Y | 2.0225 | 1.925 | 0.01 | 0.49 |
| Zr | 0.4825 | 0.4225 | 0.005 | 1.04 |
| Na | 42.1 | 35.75 | 6.35 | 15.08 |

It is seen from the table that along with Sr other metal ions like Ba and Na were also co-transported which results in the poor selectivity of crown ether for Sr compared to Ba and Na. Only 80 % transport of strontium metal ion takes place even after 3 hours of operation which

may be due to competition between various metal ions present for the extractant and hence less availability of the crown ether for Sr(II) transport.

4.3.2 Effect of the feed acidity

As per the equilibrium (1), with the increase in nitrate concentration in the solution, the equilibrium shifts towards right side and hence, more and more metal ion is extracted in the organic phase. In this context, it was important to see the effect of feed acidity on the Sr(II) transport profile. For this, feed solutions at different nitric acid concentrations viz. 1 M, 2 M, 3 M and 4 M HNO_3 were used while distilled water was employed as the strip phase. The carrier concentration was kept fixed at 0.1 M DtBuCH18C6 in 80% NPOE + 20% *n*-dodecane. The transport profiles of Sr(II) under these experimental conditions are shown in figure 4.4.

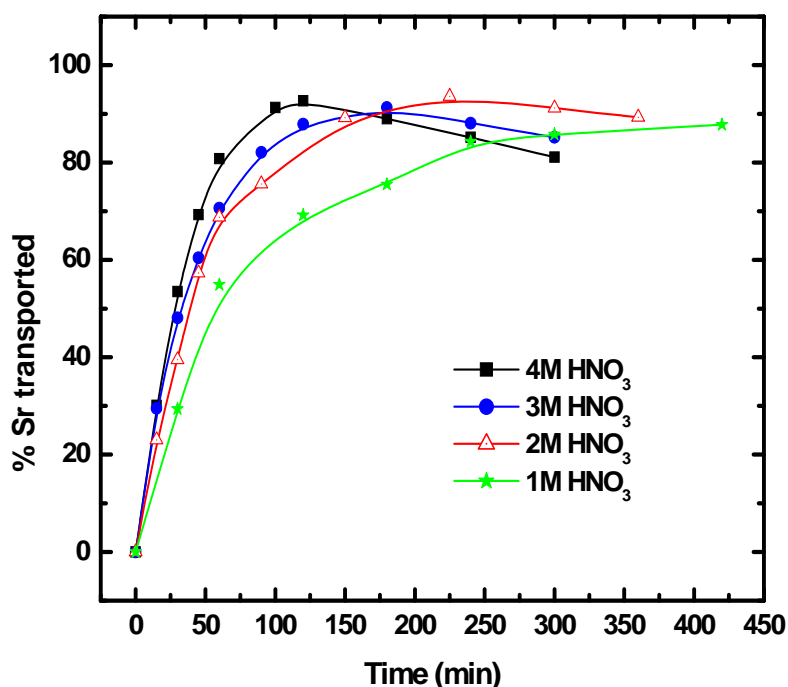


Figure 4.4 Transport profile of Sr(II) at different feed acidity. Strip: Distilled water, Carrier: 0.1 M DtBuCH18C6 in 80% NPOE + 20% *n*-dodecane, Flow rate: 200 mL/min.

As can be seen, with the increase in the feed phase acidity, the rate of Sr(II) transport increased initially (upto 2 hours). It was particularly important to observe that the point of maximum metal ion transport was obtained at much earlier time in case of feed acidity of 4 M HNO₃. To confirm the role of acid co-transport in this observation, strip phase acidity was measured and the results are listed in Table 4.2.

Table 4.2: Transport of H⁺ at varying feed acidity. Feed: HNO₃ at different concentration; Strip: Distilled water; Carrier: 0.1 M DtBuCH18C6 in 80% NPOE + 20% *n*-dodecane; Flow rate: 200 mL/min.

| 1 M HNO ₃ | | 2M HNO ₃ | | 3 M HNO ₃ | | 4 M HNO ₃ | |
|----------------------|------|---------------------|------|----------------------|------|----------------------|------|
| Time (min) | % T | Time (min) | % T | Time (min) | % T | Time (min) | % T |
| 0 | 0 | 0 | 0.0 | 0 | 0 | 0 | 0.0 |
| 30 | 1.3 | 15 | 1.0 | 15 | 1.7 | 15 | 3.9 |
| 60 | 2.7 | 30 | 2.0 | 30 | 3.0 | 30 | 5.1 |
| 120 | 4.7 | 45 | 3.0 | 45 | 3.7 | 45 | 7.4 |
| 180 | 7.0 | 60 | 4.0 | 60 | 5.0 | 60 | 9.4 |
| 240 | 9.3 | 90 | 5.7 | 90 | 7.7 | 100 | 14.3 |
| 300 | 11.0 | 150 | 9.3 | 120 | 10.0 | 120 | 17.2 |
| 420 | 14.0 | 225 | 13.3 | 180 | 14.0 | 180 | 26.0 |
| | | 300 | 17.0 | 240 | 19.0 | 240 | 29.9 |
| | | 360 | 20.7 | 300 | 22.7 | 300 | 35.4 |

It was found that in case of 4 M HNO₃ as the feed, the rate of acid transport was faster (fig. 4.4) as compared to that at lower acidity ranges as governed by the equilibrium (2). Hence,

the strip phase acidity increased continuously at a much faster rate in case of 4 M HNO₃. In only 2 hours of operation, the acidity of the strip phase was found out to be ≥ 0.42 M and after which back transport of Sr(II) was observed. It was important to note that in all the experiments, the back transport of Sr(II) started whenever the acidity of the strip phase has reached 0.42 M concentration. The exact reason for this fact is still unknown and further investigations are yet to be done to understand this aspect.

4.3.3 Effect of the metal ion concentration

The main aim of the present studies was to selectively recover strontium from high level waste. The concentration of strontium in typical PHWR-HLW is approximately 30 ppm and hence, it was our aim to study the effect of Sr concentration on the transport behaviour of Sr. In the present studies, experiments were carried out at varying concentrations of strontium in a feed containing 3 M HNO₃ and distilled water as the strip phase. 0.1 M DtBuCH18C6 in 80% NPOE + 20% *n*-dodecane was employed as carrier solvent and other system parameters were used as before. Fig 4.5 shows the transport profile of Sr at varying strontium concentrations in the feed solutions. A marginally small effect of Sr concentration (up to 50 ppm) was seen on the overall transport profile of Sr(II). Since 0.1 M DtBuCH18C6 in 80% NPOE + 20% *n*-dodecane has been used as the carrier solvent, the effective concentration of the free ligand remains almost unchanged even at 50 ppm concentration of metal ion in the feed, and hence, the extraction of the metal ion does not change much which leads to a very small effect on the transport behavior of the metal ion.

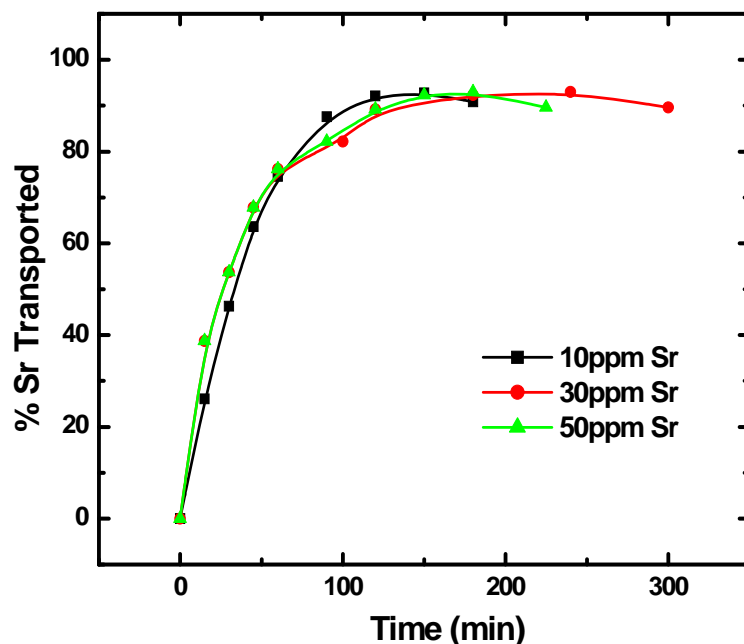


Fig 4.5 Sr transport profile at various metal ion loading. Feed: 3 M HNO₃ at varying HNO₃ acidity; Strip: Distilled water; Carrier: 0.1 M DtBuCH18C6 in 80% NPOE + 20% *n*-dodecane; Flow rate: 200 ml/min.

4.3.4 Transport of Sr from SHLW feed solution

The transport of Sr(II) from SHLW as feed solution was also investigated and the results are presented in figure 4.6. With SHLW as the feed (3-4 M acidity), the rate of metal ion transport was found to be slightly slower as compared to the case where Sr(II) is present in 3 M HNO₃ solution at tracer level concentration. This suggests the interference of other metal ions with the transport of Sr(II). As has been discussed in the Section 4.1, Na and Ba were also co-transported along with Sr to the strip phase. This would probably reduce the availability of the crown ether ligand for Sr transport which resulted in the slower transport rate of the metal ion.

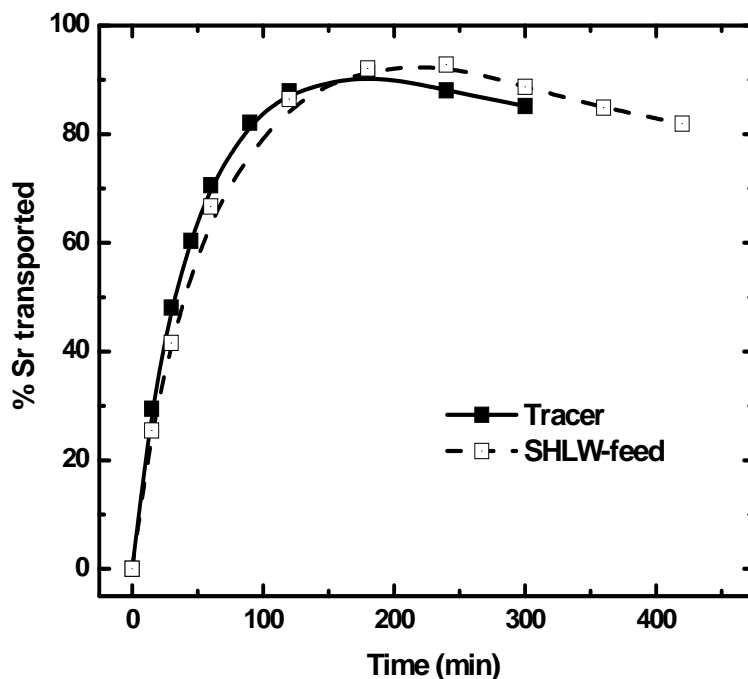


Fig 4.6 Comparative transport profile of Sr. Feed: SHLW or 3 M HNO₃; Strip: Distilled water; Carrier: 0.1 M DtBuCH18C6 in 80% NPOE + 20% *n*-dodecane; Flow rate: 200 mL/min.

The transport of acid in this case also has been found to be similar but slightly slower and hence the back transport of Sr(II) starts at slightly later time interval. As a result of this, we were able to get only 92% transport of strontium in about 4 hours of operation.

4.3.5 Effect of the acid co-transport on the transport of Sr(II)

The above studies indicated that the co-transport of acid in the strip phase renders the overall transport to be affected adversely. Hence, it was pertinent to see the effect of neutralization of the strip phase acidity. The strip phase acidity was neutralized by the addition of equivalent amounts of NaOH after each hour of operation.

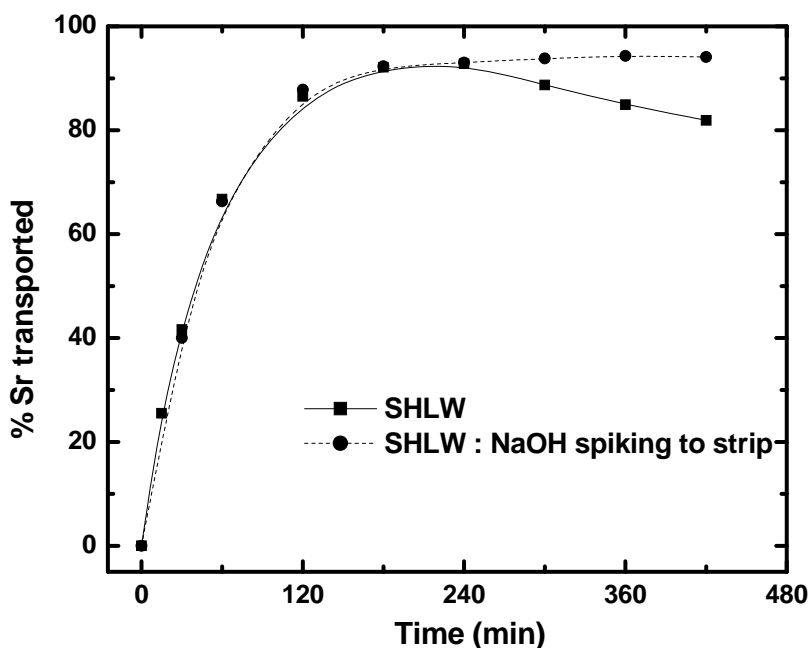


Figure 4.7 Transport profile of Sr without and with the neutralization of strip phase acidity by NaOH. Feed: SHLW solution; Strip: Distilled water; Carrier: 0.1 M DtBuCH18C6 in 80% NPOE + 20% *n*-dodecane; Flow rate: 200 mL/min.

Although, there is no direct evidence linking the acid build up in the strip phase to the back transport of Sr(II), neutralization of the strip phase acidity by NaOH has indicated no back transport of Sr(II) (Fig 4.7). Although the quantitative Sr transport was not observed, it was possible to achieve > 94% recovery of Sr(II) from SHLW solution.

Apart from this, to minimize the H^+ ion transport from feed solution, the composition of the feed phase was chosen in such a way that the transport of acid becomes negligible. A mixture of HNO_3 and $NaNO_3$ was taken as the feed phase such that the total nitrate concentration remains 3 M and the H^+ concentration was varied. Figure 4.8 depicts the experimental results. As per the equilibrium (2), rate of acid transport is expected to get slower with the decrease in H^+ concentration.

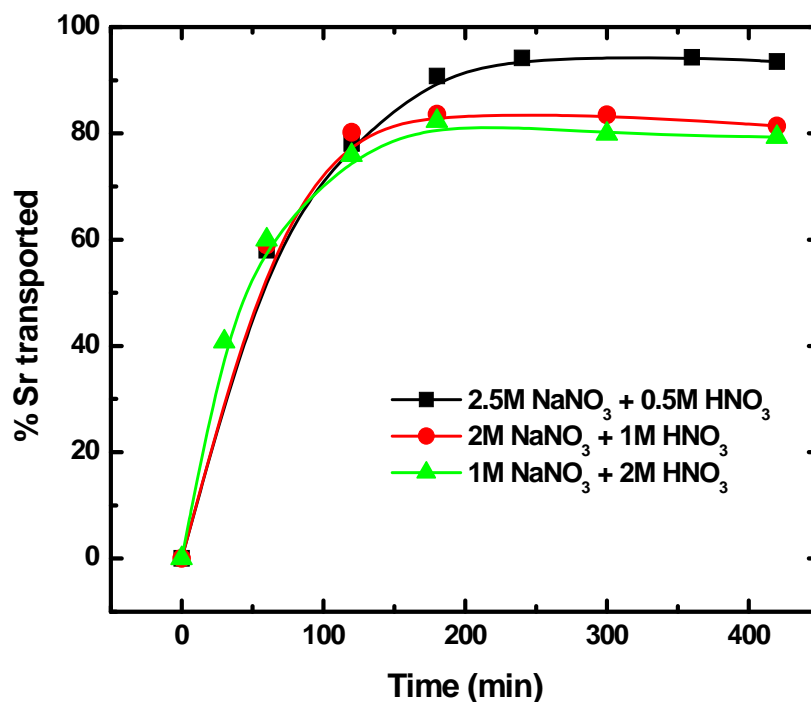


Figure 4.8 The effect of $[H^+]$ variation in feed on transport profile of Sr(II). Feed: Varying H^+ at fixed 3 M NO_3^- ; Strip: Distilled water, Carrier: 0.1 M DtBuCH18C6 in 80% NPOE + 20% *n*-dodecane. Flow rate: 200 mL/min.

It was seen that in the initial part of each case, the rate of Sr transport was similar but with the passage of time the transport profile become saturated in case of higher H^+ case whereas in case of 2.5 M $NaNO_3$ + 0.5 M HNO_3 , the maximum transport (~ 94 %) was observed without back transport of the metal ion. This again proved the role of H^+ ion in the back transport of the metal ion.

4.4 SEPARATION OF CARRIER FREE ^{90}Y FROM MIXTURE OF ^{90}Sr - ^{90}Y

The separation of ^{90}Y from the secular equilibrium mixture of ^{90}Sr + ^{90}Y was carried out by using bis-(2-ethylhexyl) phosphonic acid (PC-88A, Figure 4.9) in *n*-dodecane as the carrier solvent. PC-88A has been a well known extractant for trivalent lanthanide metal ions over mono- and divalent ions such as alkali metal and alkaline earth metal ions [142, 143]. Also, PC-88A has

been demonstrated to have higher loading capacity values for metal ions [146]. Therefore, it was required to investigate and develop HFSLM method using this system to selectively extract ^{90}Y with acceptable level of therapeutic purity with high throughput in lesser operational time.

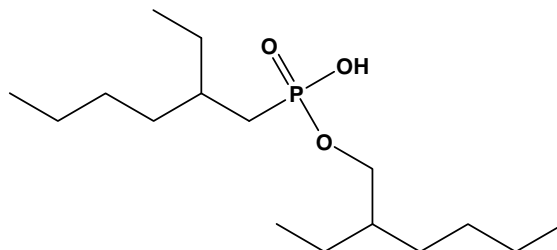
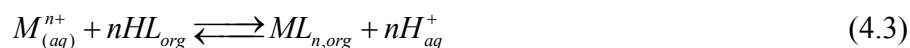


Fig 4.9 Structural formula of PC-88A

Solvent extraction studies were carried out in order to investigate the extraction system and to find the required experimental conditions for the liquid membrane transport process. Subsequently the liquid membrane transport studies were carried out and the purity of the desired product was checked by various methods. This has been discussed in the following sections.

4.4.1. SOLVENT EXTRACTION STUDIES

Batch distribution studies were carried out in the same way as described earlier in the experimental section (Chapter 2). Being a dialkyl phosphonic acid (PC-88A), the extraction equilibrium with acidic extractant is represented by the following equation [147, 148],



where, M^{n+} represents the metal ion, subscripts have the same meaning as explained earlier and HL_{org} denotes PC-88A in *n*-dodecane. The extraction equilibrium constant (K_{ex}) of the above equilibrium can be written as,

$$K_{ex} = \frac{[ML_n] \cdot [H^+]^n}{[M^{n+}] \cdot [HL]^n} \quad (4.4)$$

And the distribution ratio can be written as $K_{d,M} = [ML_n] / [M^{n+}]$ and hence equation (4.4) can be written as,

$$\log K_d = \log K_{ex} + n \cdot \log [HL]_{org} + n \cdot pH \quad (4.5)$$

As per equation (4.5), the extraction of metal ion depends upon various factors like PC-88A concentration, aqueous phase acidity, etc. Several experiments were carried out in order to establish the complete extraction system.

In the HFSLM separation process, the metal ion comes in contact with the ligand for a short time depending upon the flow rate of the feed solution. The extraction kinetics is, therefore, an important parameter for the supported liquid membrane transport processes. For extraction kinetics studies, aqueous and organic phases were equilibrated for varying time, followed by assaying the two phases for determining the distribution ratio of the metal ions as a function of time. The kinetics was monitored in terms of fractional attainment of the equilibrium expressed as follows,

$$F = K_{d,Y,t} / K_{d,Y,eq} \quad (4.6)$$

where $K_{d,Y,t}$ and $K_{d,Y,eq}$ are the distribution ratio of Y(III) at time 't' and at equilibrium, respectively. The kinetic data were plotted in terms of (1-F) values as a function of equilibration time and are shown in Fig. 4.10. The results suggested that the extraction equilibrium could be attained within 10 min of the equilibration, implying significantly fast complexation reaction between Y(III) and the ligand. It is worth mentioning that the extraction of Sr(II) was practically negligible with PC-88A under the chosen experimental conditions.

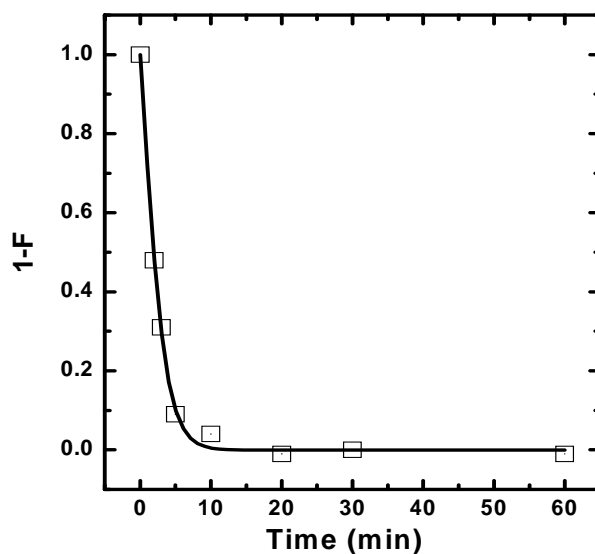


Fig 4.10 Kinetics of equilibrium for extraction of Y(III) by 0.63 M PC-88A in *n*-dodecane. Aq. phase: 0.5 M HNO₃

Stoichiometry of the metal-ligand complex was found out from the dependence of the distribution ratio of metal ion with varying PC-88A concentration at a fixed acidity of 0.5 M HNO₃. As shown in the figure 4.11, the log-log plot of $K_{d,Y}$ vs. PC88A concentration gave a slope of ~ 2 suggesting two ligand molecules are involved in the two-phase equilibrium.

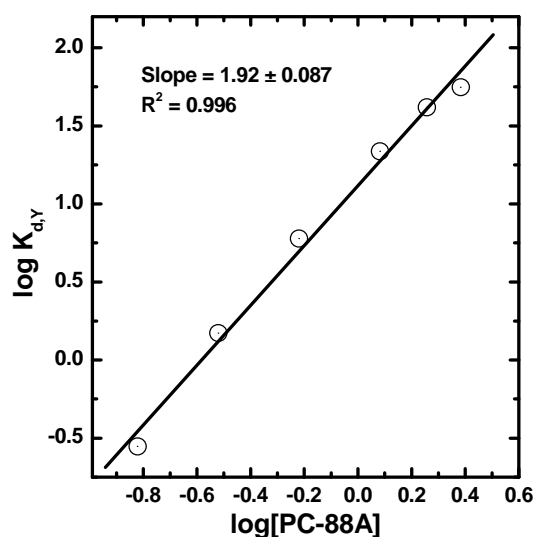
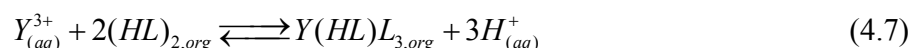


Fig 4.11 Plot of $\log K_{d,Y}$ vs. $\log[\text{PC-88A}]$. Aqueous phase: 0.5 M HNO₃; Equilibration time: 1hr.

The extraction of tri-positive metal ion by such an extractant cannot be explained because the charge neutralization is not possible. It is known that such phosphoric extractant (like HD2EHP or PC-88A) tend to exist as dimer in non-polar diluents like kerosene and *n*-dodecane etc. [149-151] and hence the equilibrium can be written in the form of the following equation,



The stoichiometry was further confirmed by estimating the $K_{d,Y}$ value at varying (H^+) at fixed nitrate (1 M $HNO_3/NaNO_3$) and 0.63 M PC-88A in *n*-dodecane as the extractant solution. A log-log plot of $K_{d,Y(III)}$ vs. H^+ ion concentration gave a slope value of ~ 3 (Figure 4.12), suggesting the involvement of two dimer molecules of PC-88A in the extraction of Y(III) confirming the equilibrium (4.7).

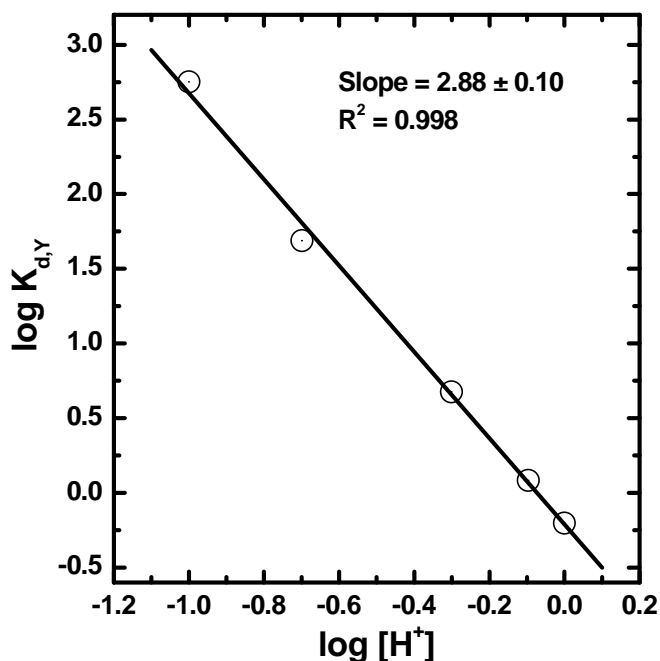


Fig 4.12 Plot of $\log K_{d,Y}$ vs. $\log [H^+]$. Organic Phase: 0.63 moles/L PC-88A in *n*-dodecane, Aqueous phase: 3 M NO_3^- ; Equilibration time: 1 hour.

Studies were also carried out to see the distribution behaviour of Y(III) and Sr(II) by PC-88A under different nitric acid concentration. Ratio of the distribution ratios for Y(III)/Sr(II) (known as the separation factor) was found to be increasing with increasing the acidity of nitric acid in the aqueous phase. In table 4.3, the distribution ratio data along with separation factor values are listed at various nitric acid concentrations.

From Table 4.3, it is clear that at 0.1 M HNO₃, maximum separation factor between Y and Sr is observed while at 3 M HNO₃ concentration, the distribution ratio for Y(III) as well as Sr(II) is very small. Hence, for subsequent membrane transport studies 0.1 M HNO₃ was used as the feed phase while the strip solution comprised of 3 M HNO₃.

Table 4.3: Extraction of Y(III) and Sr(II) with PC-88A; Organic phase: 0.63 M PC-88A; Aqueous phase: HNO₃; Diluent: *n*-dodecane; Temperature: 25°C

| [HNO ₃], M | K _{d,Y} | K _{d,Sr} | S.F. (K _{d,Y} /K _{d,Sr}) |
|------------------------|------------------|-------------------|---------------------------------------------|
| 3 | 0.05 | 0.0005 | 100 |
| 2 | 0.08 | 0.0012 | 67 |
| 1 | 0.58 | 0.0009 | 644 |
| 0.5 | 5.88 | 0.0023 | 2557 |
| 0.1 | 138 | 0.0016 | 86250 |
| 0.01 | 209 | 0.0063 | 33175 |
| 0.001 | 69 | 0.0382 | 1806 |
| 0.0001 | 102 | 0.0395 | 2582 |

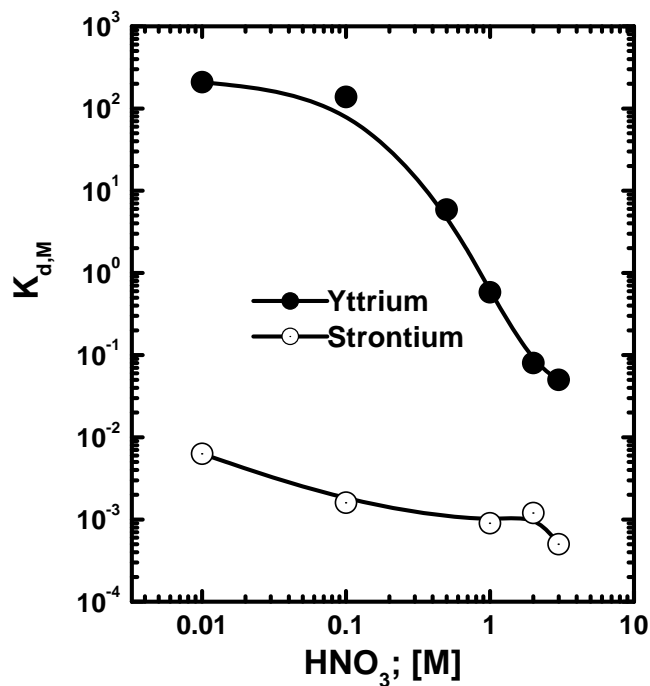


Fig 4.13 Distribution of Y(III) and Sr(II) from nitric acid medium by PC-88A. Organic phase: 0.63 M PC-88A; Diluent: *n*-dodecane; Equilibration time: 1 hour; Temperature: 25°C.

4.4.2. MEMBRANE STUDIES

4.4.2.1. Flat sheet SLM transport

After optimization of the feed and the strip phase conditions, the transport of Y(III) was investigated in flat sheet supported liquid membrane (FSSLM) mode using 0.63 M PC-88A in *n*-dodecane as the carrier solvent. 0.1 M HNO₃ was taken as the feed while the strip phase was 3 M HNO₃. As shown in fig. 4.14, the transport of Y(III) increased with time and ~ 80 % transport could be observed in 5 hrs.

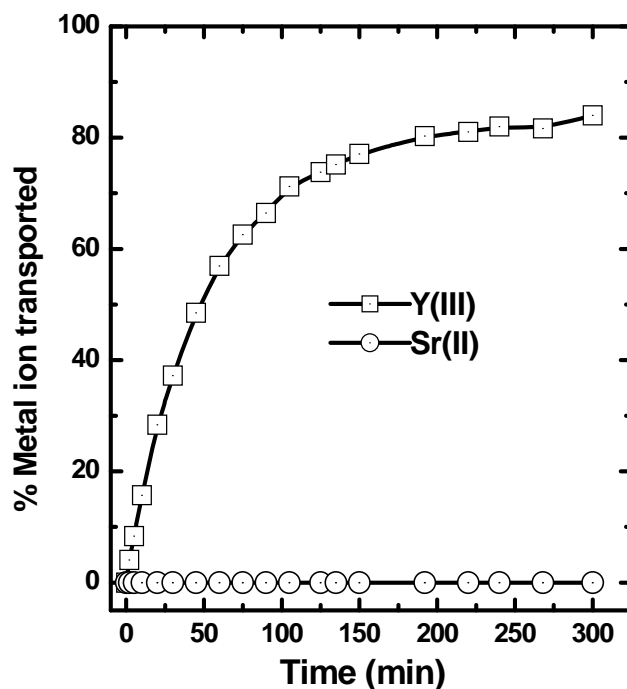


Fig 4.14 Transport of Sr(II) and Y(III) by PC-88A in FSSLM; Membrane support: 0.45 μ m PTFE; Carrier: 0.63 Mol/L PC88A; Diluent: *n*-dodecane; Feed: 0.1 M HNO₃ spiked with ⁹⁰Y and ^{85,89}Sr tracers (20mL); Strip: 3 M HNO₃ (20mL); Temperature: 25°C

The permeability coefficient which is a measure of the metal ion transported across the SLM was obtained experimentally by using the following equation [152],

$$\ln(C_t/C_0) = - P (Q/V) t \quad (4.8)$$

where, C_t and C_0 are the concentrations of the metal ion in the aqueous feed solution at time 't' and start of the experiment ($t = 0$), respectively. Q is the effective membrane area obtained from the total exposed membrane surface area A and the porosity ϵ ($Q = A \cdot \epsilon$), V is the volume of the feed solution in cm^3 , and t is the permeation time (seconds). Thus a plot of $\ln(C_t/C_0)$ versus time allows one to evaluate the permeability coefficient (P) from the slope of the linear fit. It should be noted that the above equation is valid only when carrier is not saturated and the flux decreases with time. In the present work, since all the experiments were carried out at tracer level

concentration, Eq. (4.8) was applied for the calculation of the permeability coefficient. The permeability coefficient of Y(III) was found to be $(2.49 \pm 0.11) \times 10^{-3}$ cm/sec. At the same time, no transport of Sr(II) was seen in the strip phase as reflected from its distribution ratio by PC-88A (Figure 4.13).

4.4.2.2. Hollow fibre SLM transport

In view of encouraging results obtained with FSSLM studies, HFSLM (hollow fibre supported liquid membrane) studies were carried out at 500 mL scale using 0.63 M PC-88A in *n*-dodecane as the carrier ligand. Similar to the FSSLM studies, the optimized condition for the feed solution was 0.1 M HNO₃ (containing a mixture of ^{85,89}Sr and ⁹⁰Y tracers), while the receiver phase was 3 M HNO₃. The transport results of Y(III) and Sr(II) by HFSLM are shown in fig. 4.15. As expected from the FSSLM transport studies, selective permeation of Y(III) was observed and >90% transport could be achieved in only 30 minutes of operation. Higher transport rate of Y(III) by HFSLM was ascribed not only to its large distribution ratio, but also due to the availability of large effective surface area as compared to FSSLM. On the other hand, practically no transport of Sr(II) (carried out using ^{85,89}Sr) was noticed. The permeability coefficient of Y(III) in HFSLM was calculated to be 2.61×10^{-3} cm/min. Ramanujam et al. [142], have performed SLM transport studies of ⁹⁰Y from the HLW through SLM at only 5 ml scale and found that ⁹⁰Y can be separated in 6 hours of operation. Also, Dhimi et al. [143] carried out two-stage SLM system (capacity 5 mL) using KSM-17 and CMPO as the two extractants. The yield of the generator was obtained to be ~ 95 %. Hence, HFSLM system seems to be quite promising encouraging due to much faster mass transfer rates and high throughput values achieved.

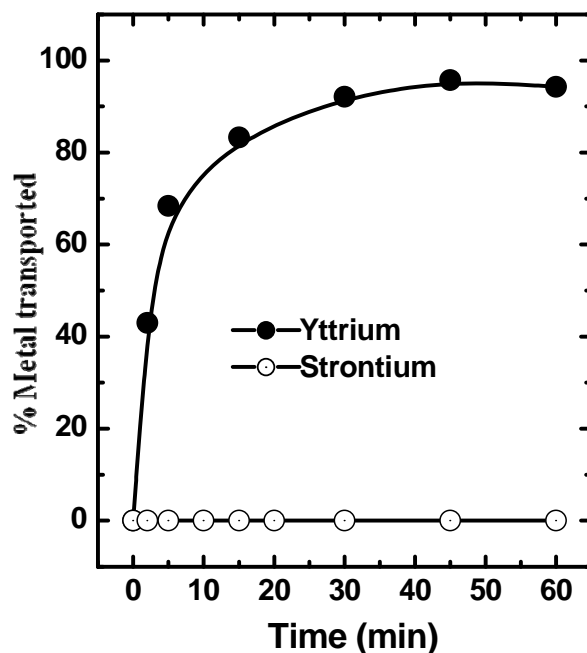


Fig 4.15 Transport of Y(III) and Sr(II) in HFSLM; Carrier: 0.63 M PC-88A; Diluent: *n*-dodecane; Feed: 0.1 M HNO₃ spiked with ⁹⁰Y and ^{85,89}Sr tracers (500 ml); Strip: 3 M HNO₃ (500 ml); Flow rate: 200 ml/min; Temperature: 25°C

As discussed earlier, assuming the strip side resistance to be negligibly small, the permeability coefficient and $K_{d,Y}$ are related to each other by the following relation,

$$\frac{1}{P} = \frac{1}{k_f} + \frac{r_i}{r_{lm} \cdot k_m \cdot K_{d,Y}} \quad (4.9)$$

where, the symbols have their usual meaning as stated earlier. The aqueous feed phase mass transfer coefficient (k_f) was obtained from the intercept of the linear fits of equation (4.9) by plotting $1/P$ vs. $1/K_{d,Y}$ (Fig. 4.16). Similarly, the value of membrane mass transfer coefficient (k_m) was obtained from the slope of the same plot (i.e. slope = $r_i/r_{lm} \cdot k_m$) as the radius of the hollow fibre is known. Experimental values show a good fitting of equation (4.9) with regression coefficient (R^2) of 0.993. The values of k_f and k_m were calculated to be 2.72×10^{-4} cm/s and

1.15×10^{-5} cm/s, respectively. The value of k_f was much higher as compared to k_m , suggesting that the membrane mass transfer is the rate controlling step.

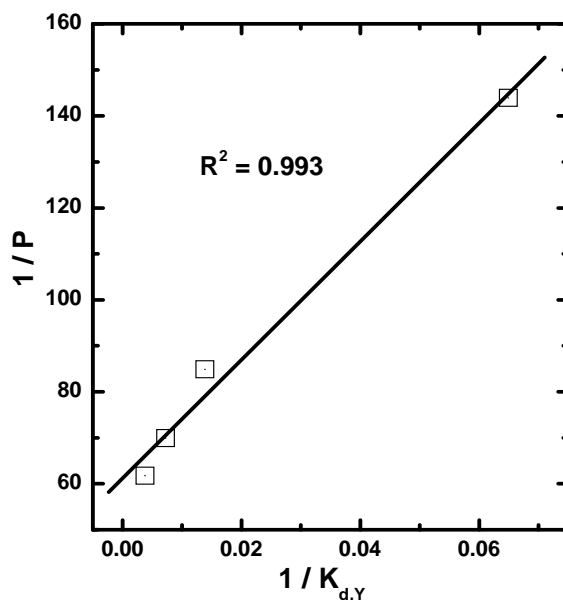


Fig 4.16 Plot of $1/P$ vs. $1/K_{d,Y}$ for the calculation of mass transfer coefficients.

4.4.2.3. Separation of ^{90}Sr and ^{90}Y and purity of the product

After demonstrating the possibility of the separation of Y(III) from the Y and Sr mixture in HFSLM, actual separation of ^{90}Sr and ^{90}Y was performed. A 500 mL stock solution containing a mixture of ^{90}Y and ^{90}Sr (activity of ^{90}Y and ^{90}Sr are equal due to secular equilibrium) at 0.1 M HNO_3 was employed as the feed and 3 M HNO_3 as the strip solution. The strip phase was collected after 30 minutes of operation and analyzed for the purity of the product. The purity of the separated ^{90}Y activity was analyzed by three different methods, viz., half-life method, paper chromatography method and radiometric analysis of the product after the complete decay of ^{90}Y . In the first method, the strip sample is regularly counted for beta-activity for many days and the half life is measured at each point of time. By plotting $\ln(N_t/N_0)$ vs. time 't' (where 'N' denotes

number of counts), we calculated the apparent decay constant (λ_{cal}) (Figure 4.17). Then the half life is calculated by using the following equation,

$$t_{1/2} = \frac{0.693}{\lambda_{\text{cal}}} \quad (4.10)$$

The half life method indicated significant contamination by ^{90}Sr as the decay profile showed an increase in the half-life with increasing number of days after the separation. Based on literature report, a Sr(II) specific extraction chromatography column containing a substituted crown-ether was used for subsequent purification [153].

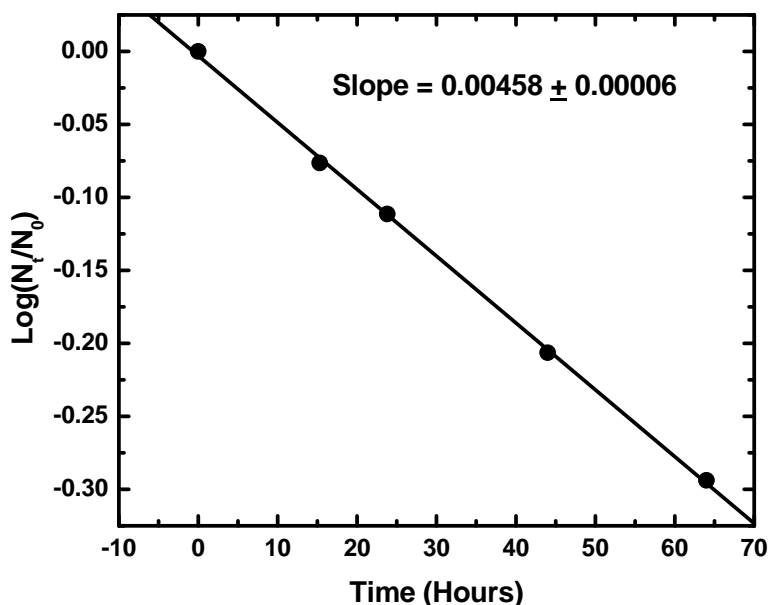


Figure 4.17 $\log(N_t/N_0)$ vs. time plot for calculation of half life of radionuclide.

The purity of the separated ^{90}Y after the extraction chromatographic purification step significantly improved with measured half-life of the product as 64.7 h as compared to the pure tracer which has half-life of 64.1 hrs (Fig. 4.18). In the radiometric methods, ^{90}Y is left to decay completely for more than 30 days (> 10 half lives) and then activity of ^{90}Sr is measured by beta-counting. As the half life of ^{90}Sr is very high (~ 28.5 years) we can safely assume the measured

beta-activity completely due to ^{90}Sr . Though half-life measurement method indicated still some amount of ^{90}Sr in the product, radiometric method involving complete decay of the ^{90}Y indicated a D.F. value $>10^4$ suggesting much better purity as indicated by the half-life method. This was further confirmed by paper chromatographic method where Y(III) selective reagents are immobilized on a special paper sheet and the strip solution is spotted at a particular place. ^{90}Y is complexed by the selective reagent on paper while ^{90}Sr moved along with the mobile phase. The paper pieces are then collected and counted for beta-activity. In this manner, the contamination due to ^{90}Sr was measured and the decontamination factor was also confirmed.

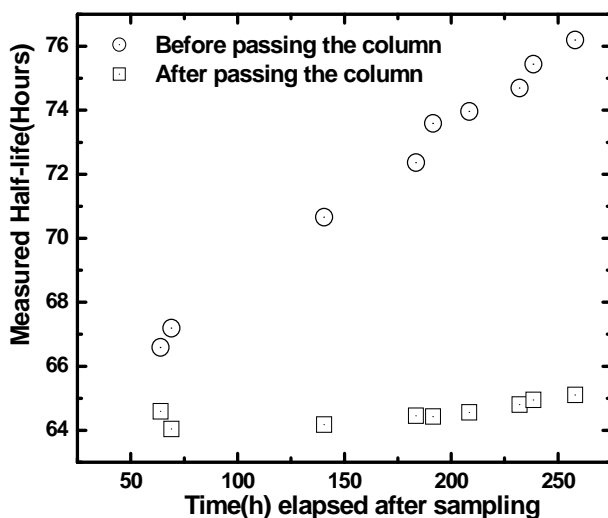


Fig 4.18 Purity analysis of ^{90}Y product after the HFSLM separation by the half-life method.

4.4.2.4. Radiation stability

The radiation stability of the ligand (PC-88A) was investigated after its irradiation with gamma rays from a ^{60}Co source at an exposure dose rate of $1.8 \text{ kGy}\cdot\text{h}^{-1}$. The distribution ratio of Y(III) at 0.1 M HNO_3 acidity along with permeability coefficient and percentage transport after 1 hr of measurement are summarized in Table 4.4. Subsequently, the irradiated ligand solution was used to measure the permeation of Y(III) by FSSLM and the results are shown in Fig. 4.19. No

significant effect of radiation on the distribution behaviour of Y(III) by PC-88A was seen under the experimental conditions upto 1000 kGy of absorbed dose (Table 4.4).

Table 4.4: Permeability coefficient (P) of Y(III) in FSSLM by irradiated solvent; Carrier: 0.63 Mol/L PC-88A in *n*-dodecane; Feed: 0.1 M HNO₃; Strip: 3 M HNO₃; Temperature: 25°C

| Dose (kGy) | K _{d,Y} value (at 0.1 M HNO ₃) | Px10 ³ (cm/sec) | %Transport (60 min) |
|------------|--------------------------------------------------------|----------------------------|------------------------|
| 0 | 138.56 ± 3.54 | 2.61 ± 0.13 | 76.9 |
| 100 | 122.26 ± 5.64 | 2.54 ± 0.11 | 77.2 |
| 200 | 130.15 ± 2.14 | 2.40 ± 0.12 | 75.1 |
| 350 | 140.28 ± 8.58 | 2.56 ± 0.11 | 77.7 |
| 500 | 128.96 ± 7.86 | 2.36 ± 0.10 | 73.1 |
| 1000 | 130.25 ± 5.62 | 2.49 ± 0.12 | 75.6 |

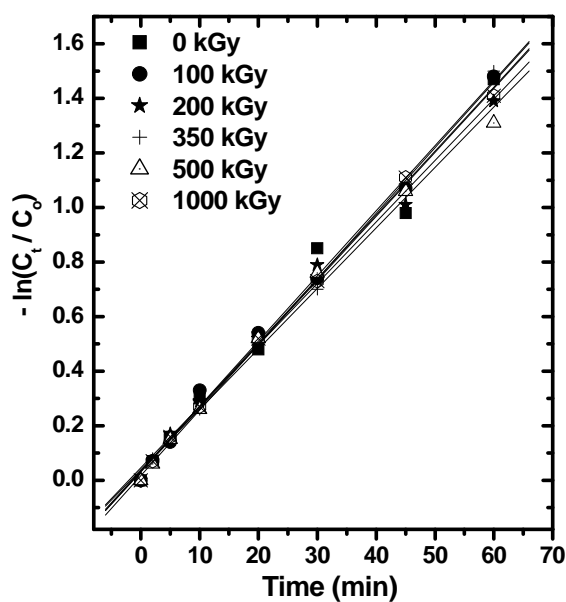


Fig 4.19 Effect of radiation dose on the permeation of Y(III) in FSSLM. Membrane support: 0.45 μm PTFE; Carrier: 0.63 M PC-88A; Diluent: *n*-dodecane; Feed: 0.1 M HNO₃ spiked with ⁹⁰Y and ^{85,89}Sr tracers (20 mL); Strip: 3 M HNO₃ (20 mL); Temperature: 25°C

Also, the transport studies indicated no change in transport profile or permeability (P) due to the absorbed radiation dose. The results suggested that the carrier can be used for the separation of the radio isotopes (^{90}Y) without any radiolytic degradation problem.

The radiation stability of the polymer matrix is also important as far as the large scale process scale up is important. The effect of radiation on hollow fiber module has been shown elsewhere [154], which suggested that the polypropylene hollow fibres can withstand a radiation dose up to 500 kGy dose without any significant deterioration in its performance. Hence, radiation resistant polymeric membranes are required to be developed in order to work with high levels of radioactivity.

4.5 CONCLUSIONS

During this work, exhaustive studies were carried out for the separation of Sr(II) from SHLW solution by HFSLM containing DtBuCH18C6 in NPOE - *n*-dodecane as the mobile carrier. Various experimental conditions were analyzed and the suitable conditions were optimized. The studies revealed that near quantitative (> 94 %) recovery of Sr(II) was possible from SHLW solution into a strip phase of distilled water. In addition to this, there was a need to develop a method for faster separation of ^{90}Y in high purity from a mixture of ^{90}Sr - ^{90}Y with high throughput. The main results of the present work can be summarized as follows:

- Faster Sr(II) transport rates were observed with HFSLM configuration and higher through-put was achieved. Acid transport has been found to play an important role in transport behaviour of Sr(II) through the membrane. Various experiments were carried out to minimize the effect of acid transport to strip side and suitable conditions were optimized.

- Sr(II) can be recovered using HFSLM containing 0.1 M DtBuCH18C6 in 80% NPOE + 20% *n*-dodecane from PHWR-SHLW as the feed solution into distilled water by effectively neutralizing the acidity build up in the strip phase with the addition of calculated amount of NaOH. Contamination of Na and Ba was also observed by our studies which need to be seriously addressed. Table 4.5 summarizes the literature work and results obtained from our studies.

Table 4.5: Overview of the various literature reports and results obtained with present system

| System | Remarks | Ref. |
|---------------------------------------------------------------------------------------------------|-----------------------------------------------------------------------------------------------------------------------------------------------------------------------------------------------------------------|---------------------|
| 0.2 M DtBuCH18C6 in 1-octanol | Higher acid uptake by 1-octanol. | [4.10] |
| 0.01 M DtBuCH18C6 in 1-octanol | ~ 100 % in 44 h, where 2 M Al(NO ₃) ₃ + 0.5 M HNO ₃ was employed as feed phase. | [4.20] |
| 0.01 M DtBuCH18C6 in 20% 1-octanol + 80% toluene | ~ 50% recovery of Sr in 7 hours due to significant acid transport by 1-octanol. | [4.23] |
| 0.1 M DtBuCH18C6 in 80% 2-nitrophenyl octyl ether + 20% <i>n</i> -dodecane in FSSLM configuration | > 98% in 24 hours (at tracer metal ion concentration) but the experiments were carried out at 20 ml scale. | [4.24] |
| 0.1 M DtBuCH18C6 in 80% 2-nitrophenyl octyl ether + 20% <i>n</i> -dodecane in HFSLM configuration | > 99% Sr recovery in 3 hours at tracer level, while > 94% Sr recovery possible with SHLW feed conditions (500 mL scale), Acidity of strip phase has to be neutralize with NaOH to prevent back transport of Sr. | Present work |

- Recovery of ^{90}Y from mixture of $^{90}\text{Sr} - ^{90}\text{Y}$ by PC-88A was also demonstrated. The product (^{90}Y) was found to be very slightly contaminated with ^{90}Sr which was then further purified by conventional method to get acceptable level of purity. The present investigations indicate the possible application of HFSLM technique for the selective separation of ^{90}Y from a mixture of $^{90}\text{Sr}-^{90}\text{Y}$. HFSLM technique seems to be quite promising in these regard.

CHAPTER 5: Mathematical modeling for mass transport in liquid membranes

5.1 INTRODUCTION

Liquid membranes have been applied in various lab scale metal ion separation and are found to be quite interesting in view of the very low carrier solvent inventory [70-74]. There have been large scale use of membranes in industries such as biomedical, food processing, water treatment, gas separation, etc and process development has been proven to be promising. Before going to actual process scale-up, various parameter optimization experiments have to be performed for arriving at the suitable experimental conditions. This would, of course, require large human efforts and investment of money as well as time. Therefore, understanding of the various chemical equilibria and also transport process is very important before any scaling up can be attempted.

Mathematical modeling of the process is a tool by which the process optimization can be done with less human efforts and experimental trials as well. It also helps in better understanding of the process. Various mathematical models have been presented in literature that describes the process of mass transport through liquid membranes [77-86]. Many of them appear simple and treat the process by several approximations. While the others are so rigorous and difficult to handle that solutions are not easily achievable. Hence, it was pertinent to develop a model for mass transfer through liquid membranes which can satisfactorily predict the transport profiles of metal ions permeating through the membranes with moderate approximations to yield results with reasonable levels of accuracy. In this Chapter, we have described a detailed description of the mathematical model which we have developed based on various parameters. The model has been validated by simulating various different transport systems and the results are discussed.

5.2 MODEL DEVELOPMENT

5.2.1 Basic process of mass transport

The basic metal ion transport process is schematically presented in figure 5.1. Across the membrane surfaces, aqueous boundary layers are assumed which result from the removal of metal ion from feed phase into the membrane phase thereby creating the concentration gradient.

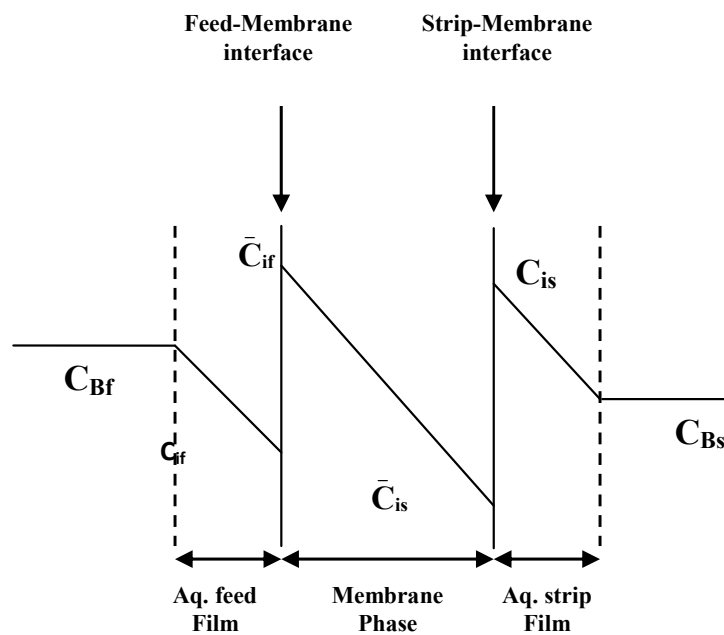


Figure 5.1 Schematic diagram showing concentration profiles across various zones of the supported liquid membrane transport system.

The mass transfer process in liquid membranes (particularly through FSSLM and HFSLM) is composed of various steps. The metal ion diffuses through the bulk of feed solution to the feed-membrane interface. At the interface, complexation of metal ion with the extractant molecule takes place and the metal ion is transferred into the membrane phase. Due to its concentration gradient, the metal-extractant complex diffuses through the membrane and reaches the strip-membrane interface. At the strip-membrane interface, the decomplexation of the metal-

extractant complex takes place releasing the metal ion into the strip phase. The free extractant then diffuses back to the feed-membrane interface and the cycle continues till the entire amount of the metal ion is transferred from the feed to the receiver phase. This is schematically represented in fig.5.2.

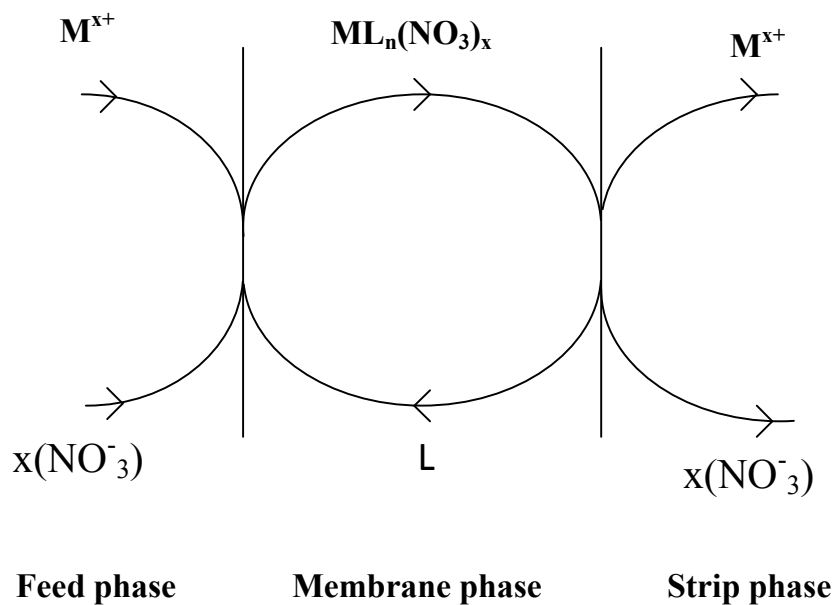


Figure 5.2 Schematic diagram showing the metal ion transport process by neutral extractant across a supported liquid membrane. M^{x+} represents the metal ion; L stands for the carrier ligand

In FSSLM experiments, the feed and the strip phases are agitated for homogenization of the aqueous solutions and to minimize the thickness of boundary layer in order to reduce the resistance offered by the layers. The aqueous mass transfer coefficient (k_{aq}) depends on the diffusivity of the metal ion in the aqueous phase and the thickness of aqueous boundary layer. The thickness of the boundary layers depends on the stirring speed according to the following relation [155],

$$\begin{aligned} \frac{r}{d_{aq}} &= 0.285 \left(\frac{\rho \omega r^2}{\eta} \right)^{0.55} \left(\frac{\eta}{\rho D_{aq}} \right)^{0.33} & \text{Re} < 32000 \\ \frac{r}{d_{aq}} &= 0.443 \left(\frac{\rho \omega r^2}{\eta} \right)^{0.75} \left(\frac{\eta}{\rho D_{aq}} \right)^{0.33} & \text{Re} > 32000 \end{aligned} \quad (5.1)$$

where, r is the radius of permeation cell, ω is stirring speed, η and ρ are the viscosity and density of the aqueous feed film. ‘Re’ represents Reynolds number which gives an indication about the flow pattern of the fluid. The lower value of Reynolds number indicates the laminar flow where viscous forces are predominant, while higher value of Reynolds number suggests the turbulent flow of fluid which is governed by inertial forces. The membrane phase mass transfer coefficient k_{org} is dependent on the diffusivity of the metal-extractant complex (D_o), thickness of the membrane (d_m) and the tortuosity factor of the membrane (τ). It is independent of the stirring speed of the feed phase. Thus, in a well stirred cell the thickness of boundary will be narrower and the aqueous mass transfer coefficients (k_{aq}) will be higher compared to membrane mass transfer coefficient (k_{org}).

In the case of HFSLM, the flow of feed and strip phases through the fibre leads to small (or no) effective change in the transport process as the diffusion is not affected by the flow of liquids. The flow of liquids affects the thickness of boundary layers which, in turn, affects the flux through the aqueous boundary layers. The higher flow rates may reduce the thickness of the boundary layers thereby reducing the resistances for mass transport. The feed side aqueous boundary layer thickness was calculated by considering the laminar flow inside the fibers. In that case, the following relation, called Leveque approximation [156], was used to calculate the aqueous diffusion layer thickness (d_{aq}),

$$Sh = 1.62Gz^{0.33}$$

This on simplification gives,

$$\frac{R_t}{d_{aq}} = 1.62 \left(\frac{d^2 v}{LD_{aq}} \right)^{0.33} \quad (5.2)$$

where, Sh , Gz are the Sherwood and Graetz numbers, respectively while d , L and v represents inner diameter, length of fiber and linear flow velocity of feed through the fiber, respectively. Sherwood number (which is a dimensionless quantity) is defined as the ratio of convective mass transfer coefficient to the diffusive mass transfer coefficient. On the other hand, Graetz number, in case of fluid flow, is defined as the ratio of momentum diffusion to the mass diffusion when there is a flow in the fluid. As can be seen from equation 5.2, the value of d_{aq} depends upon the flow rate of feed solution. Hence, the higher the flow rate, the narrower will be aqueous boundary layer thickness. For a flow rate of 200 mL/min, the value of d_{aq} was calculated to be 4.4×10^{-3} cm.

5.2.2 Conditions for transport modeling

The transport processes across the liquid membranes are very complex in nature. In order to simplify the process for our understanding and formulation of process into mathematical equations, we need to have certain assumptions on some real grounds. Following assumptions are made to simplify the process:

- i. The concentration gradients across the boundary layer and membrane are linear
- ii. The interfacial reactions are much faster compared to the diffusion through the boundary layers hence reaction resistances are negligible
- iii. The stripping process at the membrane-strip phase interface is fast enough to ensure that there is no mass-accumulation at the interface

- iv. At dynamic equilibrium, pseudo-steady state exists i.e. the loss of number of moles of metal ions from the feed phase is equal to the number of moles of metal ion passing through the membrane phase which, in turn, equal to the increase in the number of moles of the metal ion in the strip phase
- v. The diffusion process across the membrane phase is the rate limiting process (this will be justified later in the section)
- vi. In the case of HFSLM, the flow through the fibre is assumed to be Newtonian and laminar so that the Fick's law of diffusion can be applied for flux calculations in a simplified way.

Based on these assumptions, mathematical model is developed and the equations obtained are solved using mathematical software. The simulation results are compared with the experimental data produced. The results are discussed in this Chapter.

5.2.3 Diffusion and factors affecting diffusion

The basic process of mass transfer in the case of liquid membranes is diffusion. The diffusion of the species of interest takes place by various driving forces e.g., it can be due to pressure gradient or concentration gradient. Diffusion through the solutions depends upon various factors viz., temperature, viscosity of medium, size of diffusing species etc. Following are some empirical correlations that have been used to calculate diffusion coefficients (also called 'diffusivity') of metal ion or metal-ligand complexes.

5.2.3.1 Wilke-Chang equation

After carrying out various experimental investigations, Wilke and Chang [157], gave a generalized correlation (5.3) which gives diffusion coefficient of species through the fluid medium,

$$D_o = 7.4 \times 10^{-8} \frac{\chi^{1/2} T M^{1/2}}{\eta V_M^{0.6}} \quad (5.3)$$

where, χ , T , M , η and V_m are association parameters of diluent, absolute temperature, molecular weight of solvent, viscosity of solvent (extractant + diluent, in centipoises) and molar volume of extractant, respectively. The association parameter (χ) is 1 for non-dissociating diluents while it is 2.6 for water as medium.

5.2.3.2 Stokes-Einstein correlation

This is another most commonly used correlation for calculating diffusion coefficient in a solution which assumes that the diffusion to be limited by viscous drag forces offered by the medium. Although the correlation has been modified for various other geometries, the simple equation which has been widely used is given below,

$$D_o = \frac{k_B T}{6\pi\eta R} \quad (5.4)$$

where, k_B is the Boltzman's constant (1.3806×10^{-23} J/K) and R represents radius of the diffusing specie.

5.2.4 Mathematical modeling of Cesium transport through FSSLM

In the case of a neutral ligand (e.g. calix-crown ethers), a counter anion is co-transported with metal ion to neutralize the charge on complex and the extraction reaction is given as per the equilibrium [44],



where, $CNC_{(org)}$ and $(Cs.CNC)^+ \cdot (NO_3)_{org}^-$ denote the carrier extractant and the metal-carrier complex, respectively; NO_3^- the is counter-anion, which gets transported from the feed to the

strip along with Cs^+ ; and K_{eq} stands for the two phase extraction constant. The species with subscript 'org' indicate those in the organic phase and those with 'aq' represent species in the aqueous phase. Considering fast chemical reaction between the metal ion and the carrier extractant [152, 158], local equilibrium at interface is reached and concentrations at interface are related as,

$$K_{eq} = \frac{\bar{C}_i}{C_i X_f E} = \frac{K_d}{X_f E} \quad (5.6)$$

where, \bar{C}_i denotes the concentration of $(CsCNC)^+ \cdot (NO_3)^-_{org}$ at the organic side of the feed-membrane interface while C_i is the concentration of Cs^+ at the aqueous side of the feed-membrane interface; E represents concentration of free carrier in the membrane phase and X_f is the activity of nitrate ion in the feed solution (activity = molality of nitric acid \times activity coefficient) and distribution ratio (K_d) is defined as,

$$K_d = \frac{[(CsCNC)^+ (NO_3)^-]_{org}}{[Cs^+]_{aq}} = \frac{\bar{C}_i}{C_i}$$

Flux at the aqueous feed film J_{aq} and the liquid membrane flux J_{org} for metal ion (Cs^+) can be obtained by the application of Fick's first law of diffusion [Fig. 5.1],

$$J_{aq} = k_{aq} (C_{Bf} - C_{if}) \quad (5.7)$$

$$J_{org} = k_{org} (\bar{C}_{if} - \bar{C}_{is}) \quad (5.8)$$

where, C_{Bf} is the concentration of cesium in the bulk feed solution; \bar{C}_{if} denotes the concentration of $(CsCNC)^+ \cdot (NO_3)^-_{org}$ at the membrane-strip interface; k_{aq} & k_{org} denote the mass transfer

coefficients of the aqueous feed film & that of the organic membrane, respectively ($k = D / d$; where, D signifies diffusivity & d denotes length of diffusing path). Considering distribution coefficient of cesium at the membrane-strip interface to be much lower than that at the feed-membrane interface, equation (5.8) can be rewritten as,

$$J_{\text{org}} = k_{\text{org}} \overline{C}_{\text{if}} \quad (5.9)$$

Considering the definition of $K_d (= \overline{C}_{\text{if}} / C_{\text{if}})$ and coupling this with equations (5.7) and (5.9) under the assumption of pseudo steady state ($J_{\text{aq}} = J_{\text{org}} = J$), flux expression for Cs^+ can be given as,

$$J = -\frac{V}{Q} \left(\frac{dC_B}{dt} \right) = \frac{K_d C_B}{(K_d k_{\text{aq}}^{-1} + k_{\text{org}}^{-1})} \quad (5.10)$$

where, V is the volume of the aqueous feed solution and Q represents the effective membrane area computed by multiplying the geometrical membrane area (A) with the membrane porosity (ε), and k^{-1} represents the mass-transfer resistance of respective layer. Using $J = P.C_B$ (P being the overall permeability) from equation (5.10), permeability can be obtained as,

$$P = \frac{K_d}{(K_d k_{\text{aq}}^{-1} + k_{\text{org}}^{-1})} \quad (5.11)$$

Considering one mole of CNC attached with one mole of cesium complex [106], mass balance of the carrier at the membrane-feed interface can be written as,

$$E_T = E + \overline{C}_i \quad (5.12)$$

where, E_T is the total carrier concentration in membrane phase and E denotes the free carrier concentration.

By combining equations (5.7), (5.9), (5.10) and (5.12), one gets final mass-balance equation as follows,

$$\left(\frac{k_{\text{org}}^{-1} K_d C_B}{K_d k_{\text{aq}}^{-1} + k_{\text{org}}^{-1}} \right) + \left(\frac{K_d}{X_f K_{\text{eq}}} \right) - E_T = 0 \quad (5.13)$$

For one mole of Cs^+ transport, one mole of NO_3^- is transported from the feed to the strip side to preserve electrical neutrality [31]. Therefore, time-functionality of NO_3^- present in the feed can be written in terms of reduction of feed cesium concentration:

$$X_f = X_{f_0} - (C_{B_0} - C_B) \quad (5.14)$$

where, C_{B_0} & X_{f_0} denote initial concentrations of cesium ion and nitrate ion in the bulk feed solution, respectively. Substituting X_f from equation (5.14) into equation (5.13), one gets,

$$\left(\frac{k_{\text{org}}^{-1} K_d C_B}{K_d k_{\text{aq}}^{-1} + k_{\text{org}}^{-1}} \right) + \left(\frac{K_d}{(X_{f_0} - C_{B_0} + C_B) K_{\text{eq}}} \right) - E_T = 0 \quad (5.15)$$

Now, rearranging equation (5.10) one can obtain,

$$\left(\frac{dC_B}{dt} \right) = - \left(\frac{Q}{V} \right) \left(\frac{K_d C_B}{K_d k_{\text{aq}}^{-1} + k_{\text{org}}^{-1}} \right) \quad (5.16)$$

Equation (5.15) is then differentiated with respect to time and the resulting equation along with equation (5.16) form a set of equations in two variables K_d and C_B , which can be solved to get the variation of cesium ion concentration with time during permeation. In order to solve,

initial condition, K_{do} can be calculated by equation (5.15) at known k_{aq} , k_{org} , X_{fo} , K_{eq} , E_T , and C_{Bo} . The differential equations are solved using the numerical integration by computational program.

5.2.5 Mathematical modeling of Cesium ion transport in HFSLM mode

The flux equations have been written in much the same way as done in the previous section. Now, the mass balance for a single hollow-fibre over differential length of Δz and time Δt under no mass accumulation (Fig 5.3) gives,

$$\dot{V} C_{B|z} \Delta t = \dot{V} C_{B|z+\Delta z} \Delta t + J_{org} (2\pi R \varepsilon \Delta z) \Delta t \quad (5.17)$$

where, \dot{V} denotes volumetric flow rate, C_B , the metal concentration in the bulk feed solution flowing through the fibre lumens, Δt is infinitesimally small time interval, R and ε are inner radius and porosity of hollow fibre, respectively and other symbols are as described in the earlier section.

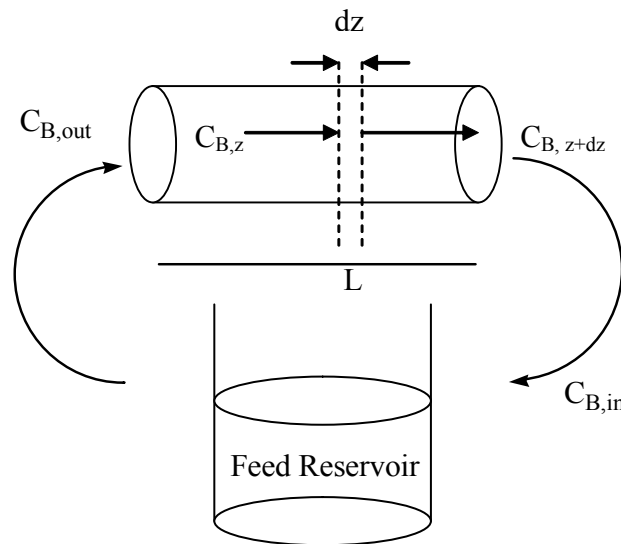


Figure 5.3 Schematic diagram showing mass balance in fibre and feed tank

Simplifying Eq. (5.17) one gets,

$$J_{\text{org}} = - \frac{Rv}{2\varepsilon} \frac{dC_B}{dz} \quad (5.18)$$

where, v is the linear feed flow velocity. Considering pseudo-steady state in cylindrical geometry, [$J_{\text{aq}} = \{R\varepsilon / (R-d_{\text{aq}})\} J_{\text{org}}$] and combining equation (5.18) with the equations from Fick's law (as written earlier), we get,

$$\frac{dC_B}{dz} = - \frac{2\varepsilon}{Rv} \frac{K_d C_B}{(k_{\text{aq}}^{-1} K_d + k_{\text{org}}^{-1})} \quad (5.19)$$

where, k represents the mass-transfer coefficients in HFSLM mode and is given as,

$$k_{\text{aq}}^{-1} = \frac{R \varepsilon d_{\text{aq}}}{(R - d_{\text{aq}}) D_{\text{aq}}} \quad \& \quad k_{\text{org}}^{-1} = \frac{d_{\text{org}} \tau}{D_{\text{org}}}$$

Further, integrating eq. (5.19) for single passage of solution through a single fibre, we get

$$\int_{C_{\text{Bin}}}^{C_{\text{Bout}}} \frac{dC_B}{C_B} = - \frac{2\varepsilon}{Rv} \frac{K_d}{(k_{\text{aq}}^{-1} K_d + k_{\text{org}}^{-1})} \int_0^L dz$$

or,

$$C_{\text{B,out}} = C_{\text{B,in}} \cdot e^{\left(- \frac{2\varepsilon}{Rv} \frac{K_d L}{(k_{\text{aq}}^{-1} K_d + k_{\text{org}}^{-1})} \right)} \quad (5.20)$$

where, L is the effective fibre length (referring to fig. 5.2). Considering mass balance for the feed reservoir, one can get

$$\frac{dC_B}{dt} = \frac{\dot{V}}{V_f} \cdot (C_{\text{B,out}} - C_{\text{B,in}}) \quad (5.21)$$

where, V_f is the volume of the feed solution in the reservoir.

Combining Eqs. (5.20) and (5.21) one gets

$$\frac{dC_B}{dt} = \frac{\dot{V}}{V_f} \cdot C_B \cdot \left(e^{\left(- \frac{2\varepsilon}{Rv} \frac{K_d L}{(k_{\text{aq}}^{-1} K_d + k_{\text{org}}^{-1})} \right)} - 1 \right) \quad (5.22)$$

Here $C_{B,in}$ is same as C_B at time t . Now, integrating equation (5.22), one can obtain,

$$\int_{C_0}^{C_t} \frac{dC_B}{C_B} = \int_0^t \frac{\dot{V}}{V_f} \left(e^{\frac{2\varepsilon}{Rv} \left(\frac{K_d L}{(k_{aq}^{-1} K_d + k_{org}^{-1})} \right)} - 1 \right) dt$$

$$\ln \left(\frac{C_t}{C_0} \right) = \frac{\dot{V}}{V_f} \int_0^t \left(e^{\frac{2\varepsilon}{Rv} \left(\frac{K_d L}{(k_{aq}^{-1} K_d + k_{org}^{-1})} \right)} - 1 \right) dt$$

$$\ln \left(\frac{C_t}{C_0} \right) = \frac{\dot{V}}{V_f} \left(e^{\frac{2\varepsilon}{Rv} \left(\frac{K_d L}{(k_{aq}^{-1} K_d + k_{org}^{-1})} \right)} - 1 \right) t \quad (5.23)$$

where, C_t , C_0 is the metal concentration of feed solution at a time 't' and initial concentration, respectively. Equation (5.23) has been used to get the time variation of bulk metal concentration in feed reservoir.

Accuracy of prediction was measured as the error associated with the predicted data from the experimentally obtained one. The error was calculated using the following equation,

$$\text{Deviation}(\%) = \frac{100}{p} \sum_{m=1}^p \left(\frac{|y_{\text{Expt},m} - y_{\text{Pred},m}|}{y_{\text{Expt},m}} \right) \quad (5.24)$$

where, p is the number of data points.

5.3 PROCEDURE OF SOLVING DIFFERENTIAL EQUATIONS IN MATLAB

MATLAB is a software package for high-performance numerical computation and visualization. The name MATLAB stands for MATrix LABoratory. It has numerous built-in functions for technical computation and many other purposes. It provides an excellent tool for data analysis, numerical solution of ordinary differential equations (ODEs), etc. The software

package has been used for solving the differential equation derived in the earlier section. Many differential equation solvers are present in the library of MATLAB. For the present case, solver ODE-45 has been used which is based on the Runge-Kutta fourth order method for solving the ordinary differential equation.

Runge-Kutta 4th order method is a numerical technique used to solve ordinary differential equation of the form

$$\frac{dy}{dx} = f(x, y), y(0) = y_0$$

So, only first order ordinary differential equations can be solved by using the Runge-Kutta 4th order method. The Runge-Kutta 4th order method is based on the following methodology.

$$y_{i+1} = y_i + (a_1k_1 + a_2k_2 + a_3k_3 + a_4k_4)h \quad (5.25)$$

where, knowing the value of $y = y_i$ at x_i , we can find the value of $y = y_{i+1}$ at x_{i+1} , and

$$h = x_{i+1} - x_i \quad (5.26)$$

Equation (5.25) is equated to the first five terms of Taylor series,

$$y_{i+1} = y_i + \frac{dy}{dx} \Big|_{x_i, y_i} (x_{i+1} - x_i) + \frac{1}{2!} \frac{d^2y}{dx^2} \Big|_{x_i, y_i} (x_{i+1} - x_i)^2 + \frac{1}{3!} \frac{d^3y}{dx^3} \Big|_{x_i, y_i} (x_{i+1} - x_i)^3 + \frac{1}{4!} \frac{d^4y}{dx^4} \Big|_{x_i, y_i} (x_{i+1} - x_i)^4 \quad (5.27)$$

Knowing that $\frac{dy}{dx} = f(x, y)$ and $x_{i+1} - x_i = h$

$$y_{i+1} = y_i + f(x_i, y_i)h + \frac{1}{2!} f'(x_i, y_i)h^2 + \frac{1}{3!} f''(x_i, y_i)h^3 + \frac{1}{4!} f'''(x_i, y_i)h^4 \quad (5.28)$$

Based on equating Equation (5.26) and Equation (5.27), one of the popular solutions used is

$$y_{i+1} = y_i + \frac{1}{6}(k_1 + 2k_2 + 2k_3 + k_4)h \quad (5.29)$$

where, $k_1 = f(x_i, y_i)$ (5.30)

$$k_2 = f\left(x_i + \frac{1}{2}h, y_i + \frac{1}{2}k_1h\right)$$
 (5.31)

$$k_3 = f\left(x_i + \frac{1}{2}h, y_i + \frac{1}{2}k_2h\right)$$
 (5.32)

$$k_4 = f(x_i + h, y_i + k_3h)$$
 (5.33)

This procedure is used by ODE-45 solver in MATLAB for solving the differential equations. Simultaneous differential equations are also solved using this procedure. This can be illustrated as follows.

If there are two variables x and y which depend on time 't' (say), then one can write,

$$dx/dt = f_1(x,y)$$
 (5.34)

$$dy/dt = f_2(x,y)$$
 (5.35)

Above two equations form a set of simultaneous equations which can be integrated by ODE solvers in MATLAB by which we can have a profile of how x and y vary with time.

5.4 MODEL PREDICTION AND COMPARISON RESULTS

5.4.1 Modeling of mass transfer across FSSLM

5.4.1.1 Solvent extraction studies

Batch solvent extraction studies were carried out to obtain some required basic data for mass-transfer modeling (such as equilibrium constant, k_{eq} ; mass transfer coefficients k_{aq} and k_{org} etc). Equation (5.6) can be rewritten as,

$$K_d = K_{eq} \cdot X_f \cdot E$$
 (5.36)

The value of K_{eq} was obtained by calculating the K_d (distribution coefficient) for different ligand concentration at a fixed nitrate concentration. The average value of K_{eq} was found to be 867 M^{-2} (Figure 5.4).

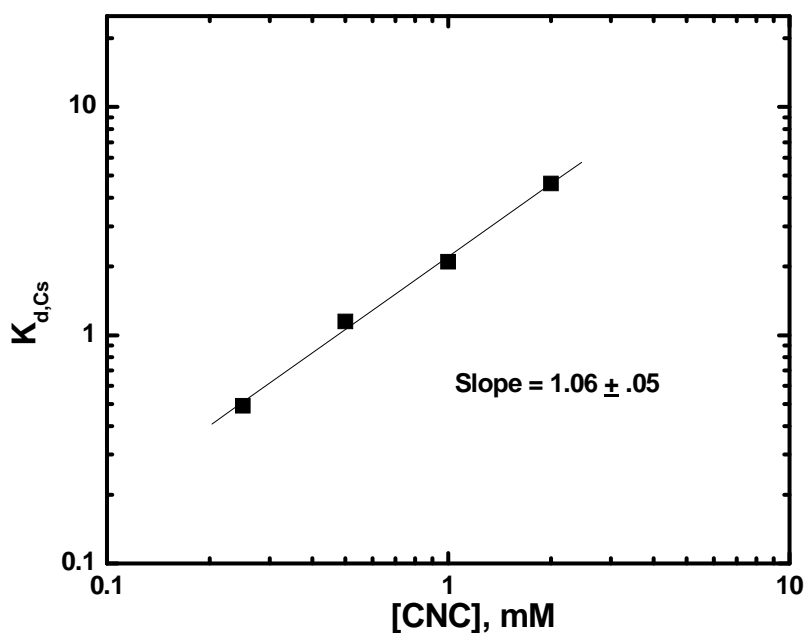


Fig. 5.4 Log-log plot of variation of $K_{d,Cs}$ with the ligand concentration. Aqueous phase: 3 M HNO_3 spiked with ^{137}Cs ; Organic phase: Varying concentration of CNC in 80% NPOE + 20% *n*-dodecane as the diluent.

5.4.1.2 Liquid membrane studies

5.4.1.2.1 Calculation of mass transfer coefficients

When the metal ion concentration is at the tracer level, equation (5.11) can be written as,

$$\frac{1}{P} = k_{aq}^{-1} + \frac{k_{org}^{-1}}{K_d} \quad (5.37)$$

The mass transfer coefficients were calculated by plotting a graph between $1/P$ and $1/K_d$ (Figure 5.5). Permeability coefficient was calculated by the metal ion transport experiment in

FSSLM mode at different ligand concentrations which change the K_d value at the feed-membrane interface.

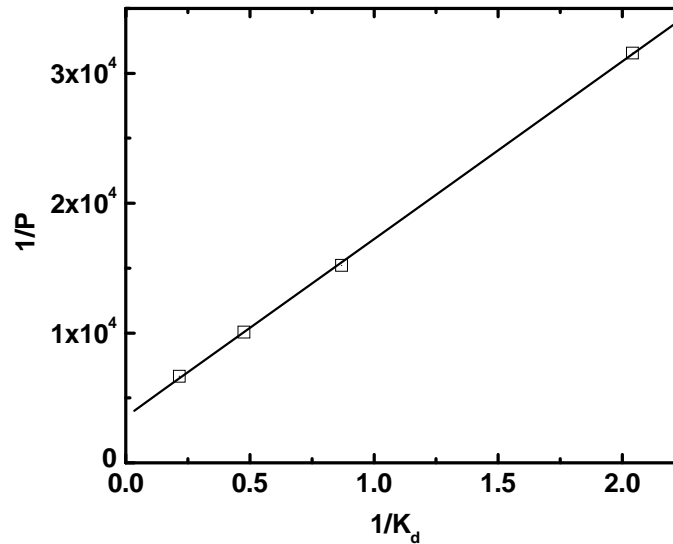


Figure 5.5 Calculation of mass transfer coefficients. Feed: 3 M HNO_3 ; Strip: Distilled water; Carrier: 1.0×10^{-3} CNC in 80% NPOE + 20% *n*-dodecane.

The values of mass transfer coefficients k_{aq} and k_{org} were obtained as 2.67×10^{-4} cm/s and 7.65×10^{-5} cm/s, respectively. As expected, the membrane mass transfer coefficient was found to be lower as compared to the aqueous feed film mass transfer coefficient. Diffusivity is related to the mass-transfer coefficient by the following relation,

$$k_{org} = D_o/d_o \cdot \tau \quad (5.38)$$

where, τ = tortuosity factor of the membrane. The value of membrane diffusivity (D_o) was found to be 9.2×10^{-7} cm²/s. The diffusivity was also estimated by using the empirical Wilke-Chang equation (Eq. 5.3) as 4.7×10^{-7} cm²/s which is reasonably close to the value obtained experimentally. These values were used as input for the model prediction.

5.4.1.2.2 Model validation using transport experiments

The validity of Equations (5.15) and (5.16) was demonstrated by performing experiments under various operating conditions. Flat-sheet SLM experiments were performed and were simulated based on the developed model. Four different sets of experiments were carried out as the case studies:

5.4.1.2.2.1 Effect of carrier concentration

In the first set of experiments, the feed was 3 M HNO₃ containing the cesium tracer (¹³⁷Cs) and distilled water was used as the strip solution in the receiver compartment while the carrier (CNC) concentration was varied from 2.5×10⁻⁴ M to 3.0×10⁻³ M. Almost 90% Cs transport was observed in 24 h when the membrane contained 3.0×10⁻³ M CNC in 80% NPOE + 20% *n*-dodecane. The % Cs transport decreased from 90% to 40% in 24 h as the CNC concentration in membrane phase decreased from 3.0×10⁻³ M to 2.5×10⁻⁴ M. This can be easily explained as the transport rates are dependent on K_d which in turn depend on the carrier concentration.

For model prediction, effect of viscosity on the diffusivity was taken into account. With the increase in the ligand concentration in the organic phase there would be a significant increase in the viscosity of the medium and the diffusivity (D_o) of species/complex in the membrane phase will decrease by the following relation (Eq. 5.4),

$$D_o \propto (1/\eta) \quad (5.39)$$

where, η represents viscosity of the medium. Viscosity was measured for different concentration of ligand by the method described earlier in experimental section (Table 5.1) and the diffusivity of metal-ligand complex was already estimated for the case of 1.0×10⁻³ M CNC ligand concentration of solution (as discussed above). The diffusivity values at other ligand

concentrations were calculated by taking ratios of their viscosities as indicated in Eq. 5.37 and the data are presented in Table 5.1.

Table 5.1: Variation of membrane mass-transfer coefficient and the viscosity of solvent with the variation in carrier concentration. Feed: 3 M HNO₃; Strip: Distilled water; Diluent: 80% NPOE + 20% *n*-dodecane

| [Ligand] ×10 ³ M | k _{org} (cm/s) | Viscosity (cP) |
|-----------------------------|-------------------------|----------------|
| 0.25 | 8.4×10 ⁻⁵ | 11.1 |
| 0.5 | 8.2×10 ⁻⁵ | 11.3 |
| 1 | 7.65×10 ⁻⁵ | 12.2 |
| 2 | 7.2×10 ⁻⁵ | 13.0 |
| 3 | 6.9×10 ⁻⁵ | 13.5 |

Using these parameters, computational results are shown by solid and dotted lines in Figure 5.6 which are in good agreement with the experimentally found transport data shown by solid symbols in the same figure. The observed trend can easily be explained by looking at equation (5.16). Increased concentration of CNC led to higher distribution ratio value (K_d) for Cs which in turn makes the right hand side of the equation 5.16 more negative and hence the metal concentration reduces with much faster rate at higher ligand concentration.

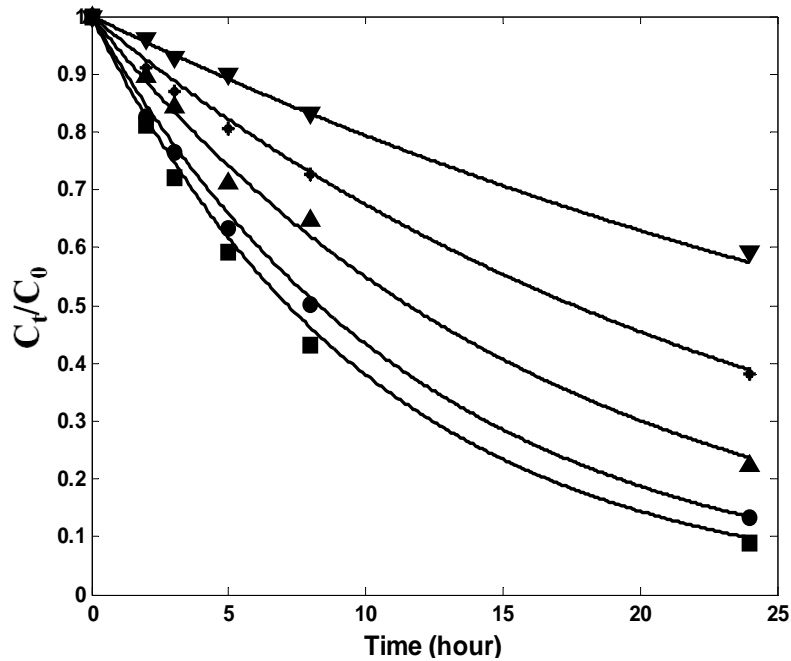


Fig 5.6 Transport of Cs under varying ligand concentrations. Symbols ▼, +, ▲, ● and ■ are for 0.25×10^{-3} M, 0.5×10^{-3} M, 1×10^{-3} M, 2×10^{-3} M and 3×10^{-3} M concentrations of CNC, respectively. Feed: 3 M HNO₃, Strip: Distilled water; Diluent: 80% NPOE + 20% *n*-dodecane + 0.4% Alamine 336.

5.4.1.2.2.2 Effect of feed acidity on transport profile of Cs(I)

As the metal ion transport is dependent on the counter anion concentration, increase in the latter's concentration is expected to enhance the transport rates. Therefore, transport experiments were carried out at varying feed nitric acid concentration keeping other parameters constant. The distribution coefficient is expected to decrease as the acidity of feed (Eq. 5.36) is lowered which in turn decrease the extraction of metal ion from the feed side and hence decrease the rate of transport of the metal ion. Experimental and simulation results are shown in Figure 5.7.

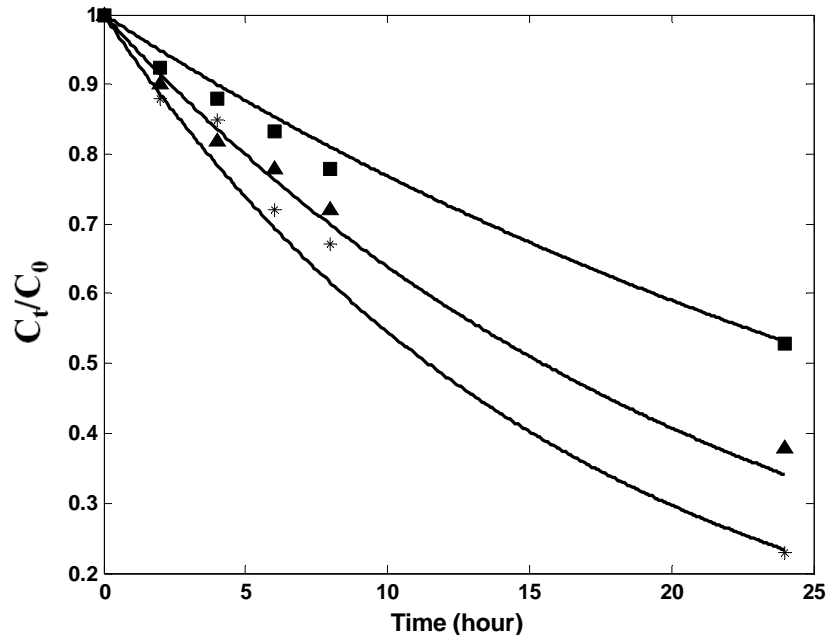


Fig 5.7 Effect of feed acidity on transport of cesium. Symbols ■, ▲ and * represents 1, 2 and 3 M feed acidity respectively. Strip: Distilled water; Carrier solvent: 1.0×10^{-3} M CNC in 80% NPOE + 20% *n*-dodecane+ 0.4% Alamine 336.

The model takes into account the effect of the increasing feed acidity on the distribution ratio of metal ion which increases the permeability (Eq. 5.11) because the denominator of the equation is mainly governed by k_{org}^{-1} which is independent of K_d . Hence, at higher acidity of feed phase, the rate of Cs transport increased according to equation 5.16. As can be seen, the model predicts the experimental results reasonably well with minor deviations.

5.4.1.2.2.3 Effect of feed metal ion concentration

The effect of the metal ion concentration in the feed phase on the Cs transport rates was also investigated using varying concentrations of Cs carrier in the range of 0.05 g/L to 0.3 g/L while keeping the feed acidity constant at 3 M HNO₃. The extractant concentration in the membrane phase was kept at 1.0×10^{-3} M CNC in 80% NPOE + 20% *n*-dodecane containing

0.4% Alamine 336 and distilled water was used as the strip solution in the receiver phase. It was observed that the rate of Cs transport increases with increasing the metal ion concentration in the feed phase. Usually, an increase in the metal ion concentration in the feed enhances the flux through the membrane (according to Fick's law) but the % transport is decreased at a particular time as the metal ion concentration is also large so it takes long time for the transport of metal ion [159, 160].

Table 5.2: Distribution ratio of cesium at different cesium concentration in the feed. Carrier: 1.0×10^{-3} M CNC in 80% NPOE + 20% *n*-dodecane + 0.4% Alamine 336

| Cesium concentration, g/L | $K_{d,Cs}$ |
|---------------------------|-----------------|
| Tracer | 2.15 ± 0.03 |
| 0.01 | 1.99 ± 0.02 |
| 0.1 | 1.15 ± 0.01 |
| 0.2 | 0.61 ± 0.01 |
| 0.3 | 0.42 ± 0.01 |
| 0.5 | 0.25 ± 0.01 |

At higher metal ion concentration, the availability of free extractant becomes increasing lesser and, as per equation (5.36), the distribution ratio (K_d) for metal ion decreases at higher metal ion loading (Table 5.2) thereby affecting the transport rate (Table 5.3). Table 5.3 lists the results of simulation and the Figure 5.8 depicts the experimental and prediction results and as can be seen there is good match between them. The model which was first described by Danesi et al. [77] was applicable when the metal ion concentration is at tracer level. The presented model can

be used for higher concentration of metal ion. Although various models have been used for such conditions [85, 86] but the complexity of solution of simultaneous equations is a difficult task.

Table 5.3: The simulation results of cesium ion transport at different cesium concentration in feed. Simulation parameters: Feed: 3 M HNO₃; Strip: distilled water; Carrier: 1.0×10⁻³ M in 80% NPOE + 20% *n*-dodecane + 0.4% Alamine 336; Flow rate: 200 mL/min

| Time (Hours) | Metal ion concentration (M) × 10 ³ | | |
|-----------------|-----------------------------------------------|--------------------------|---------------------------|
| | [Cs] ₀ = 1.50 | [Cs] ₀ = 0.75 | [Cs] ₀ = 0.375 |
| 0 | 1.50 | 0.75 | 0.375 |
| 2 | 1.43 | 0.71 | 0.351 |
| 4 | 1.39 | 0.67 | 0.308 |
| 6 | 1.31 | 0.62 | 0.285 |
| 8 | 1.24 | 0.56 | 0.252 |
| 10 | 1.21 | 0.51 | 0.235 |
| 12 | 1.21 | 0.49 | 0.212 |
| 14 | 1.15 | 0.46 | 0.205 |
| 16 | 1.04 | 0.43 | 0.192 |
| 18 | 0.98 | 0.41 | 0.184 |
| 20 | 0.92 | 0.39 | 0.165 |
| 22 | 0.86 | 0.36 | 0.158 |
| 24 | 0.82 | 0.34 | 0.150 |

* [Cs]₀ represents the initial metal ion concentration in feed phase

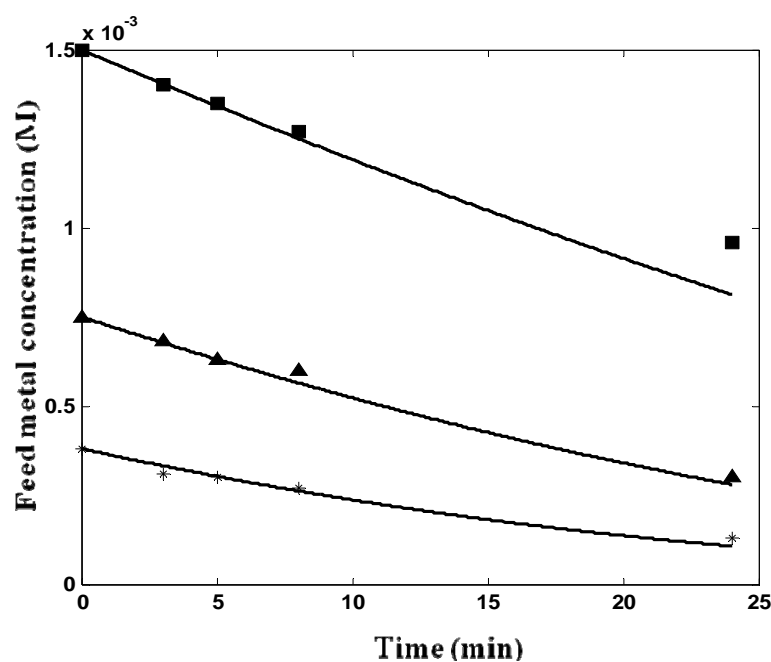


Fig 5.8 Figure showing the effect of loading of cesium ion on the transport. Symbols ■, ▲ and * represents the case of 0.3 g/L, 0.1 g/L and 0.05 g/L feed cesium ion concentration. Carrier: 1.0×10^{-3} M CNC in 80% NPOE + 20% *n*-dodecane + 0.4% Alamine 336.

5.4.1.2.2.4 Effect of diluent (NPOE and *n*-dodecane) composition

In a different set of experiments, various compositions of the diluents were tested viz., 50-50%, 60-40%, 80-20% NPOE-*n*-dodecane mixture and 100% NPOE were taken as the diluents and its effect on transport rate was seen. As the diluent composition was changed, the equilibrium constant and viscosity of medium also changed accordingly. Both these factors were considered while modeling the transport experiment. Batch experiments were separately performed to calculate the extraction equilibrium constant (K_{ex}) at various compositions of the diluent. The effect of viscosity was reflected in the membrane mass transfer coefficient (Table 5.4). Both these factors have a major effect on the rate of the metal ion transport as seen in Figure 5.9 where the experimentally obtained data points are presented along with the simulation

results. There seems to be more deviation in the experimental data points in case of diluent mixture of 80% NPOE and 20% *n*-dodecane which is within the experimental error limits.

Table 5.4: Variation of extraction equilibrium constant (K_{eq}) and membrane mass-transfer co-efficient (k_{org}) with the variation in diluent composition. [CNC]: 1.0×10^{-3} M.

| Diluent composition (NPOE- <i>n</i> -dodecane) | $K_{eq}(M^{-2})$ | $k_{org}(cm/s)$ |
|---------------------------------------------------|------------------|-----------------------|
| 50-50 % | 180 | 1.18×10^{-4} |
| 60-40 % | 320 | 1.00×10^{-4} |
| 80-20 % | 867 | 7.65×10^{-5} |
| 100-0 % | 1500 | 6.25×10^{-5} |

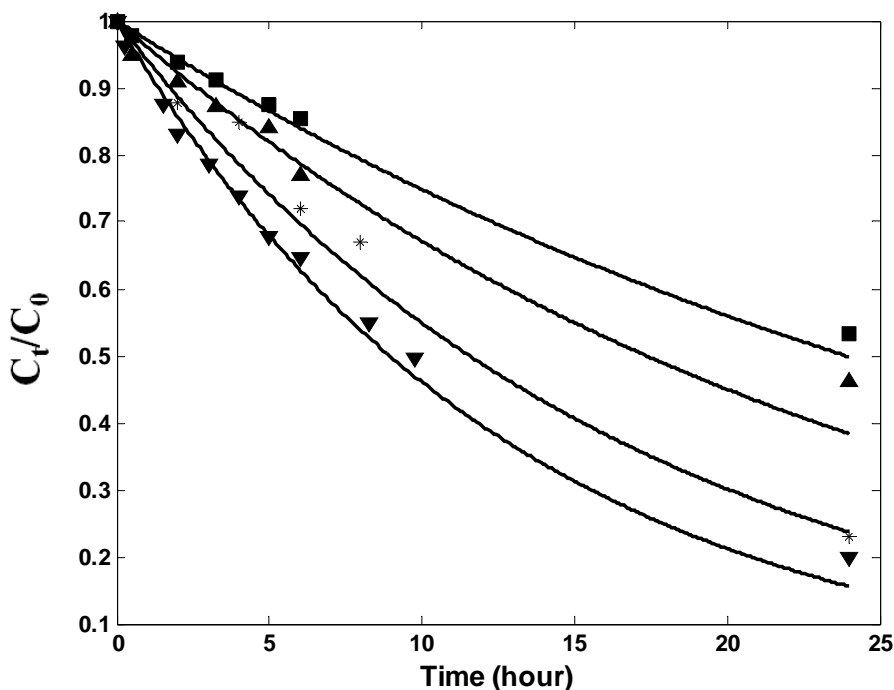


Fig 5.9 Transport profile of Cs(I) at varying diluent composition. Symbols \blacksquare , \blacktriangle , $*$ and \blacktriangledown represents the diluent composition of 50-50%, 60-40%, 80-20% of NPOE- *n*-dodecane and 100 % pure NPOE. Carrier solvent: 1.0×10^{-3} M CNC; Feed: 3 M HNO_3 ; Strip: distilled water.

5.4.2 Modeling of mass transfer across HFSLM

Experiments were also performed using HFSLM method under various operating conditions to validate the model prediction. The same experiments were simulated based on developed mathematical model. Basic parameters were used from the previous experiments while others were calculated in this present case. The various experimental and simulation results are discussed as follows:

5.4.2.1 Effect of carrier concentration

In the first set of experiments, transport behavior of cesium was investigated at different carrier concentrations. The feed was 3 M HNO₃ with cesium tracer and distilled water as strip. Almost 98% cesium transport was observed in 6 hours when the membrane phase was taken as 1.0x10⁻³ M of CNC in 80% NPOE + 20% *n*-dodecane + 0.4% Alamine 336. As seen from the Fig. 5.9, the concentration drop is fast which gets slow with time. This can be attributed to the fact that the rate of mass transfer depends upon the concentration of metal ion present at any given time (Equation 5.22). With the passage of time, the metal ion concentration was found to decrease leading to slower transport rates. Further, it was found that % transport decreased from 98% to 60% in 6 hours as the CNC concentration in the membrane phase was decreased from 1.0x10⁻³ M to 2.5x10⁻⁴ M.

The effect of viscosity on the diffusivity was considered while simulating the process of diffusion. Diffusivity of the species at different carrier concentrations has been calculated in the same way as described in the earlier section (Table 5.1). Using these parameters, transport profile of Cs(I) were simulated. In Figure 5.10, the computational results are shown by solid and

dotted lines. With the increasing CNC concentration, the rate of Cs transport is found to be increasing rapidly which is quite obvious from the Equation (5.22). K_d value of metal ion increased with increasing CNC concentration in organic phase, which make the term in the left hand side of Equation (5.22) more negative which suggested that faster rate of metal ion transfer at higher ligand concentrations.

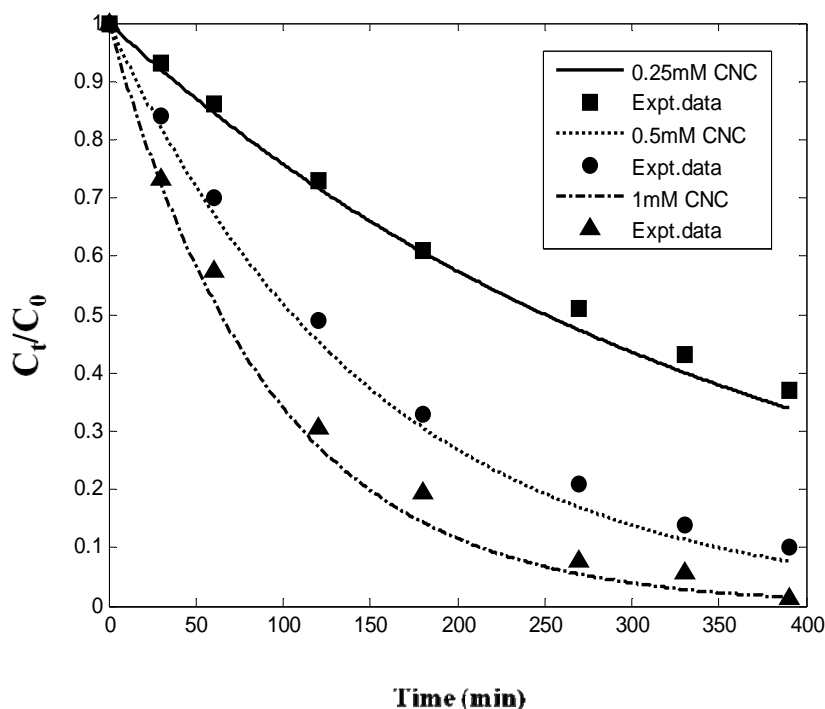


Figure 5.10 Transport of Cs(I) through HFSLM. Feed: Cs(I) in 3M HNO₃; Strip: distilled water; Carrier solvent: Varying concentration of CNC in 80% NPOE + 20% *n*-dodecane + 0.4% Alamine 336; Flow rate: 200ml/min.

5.4.2.2 Effect of the feed acidity

The effect of feed phase acidity was also studied using 1 M, 2 M and 3 M nitric acid as the feeds. It was observed that at lower feed acidity the rate of metal ion transport decreased (Figure 5.11). As discussed earlier, the distribution ratio is expected to decrease at lower feed acidity which in turn decreases the rate of transport of the metal ion. The model takes into

account the effect of the feed acidity on the distribution ratio of metal ion at feed-membrane interface. According to eq. 5.22, as the distribution ratio decreases the value inside the bracket becomes less negative and hence the rate of cesium transport with time gets slower. Experimental and simulation results are shown in Fig. 5.11 which indicates acceptable level of deviations of the predicted values from the experimental data points.

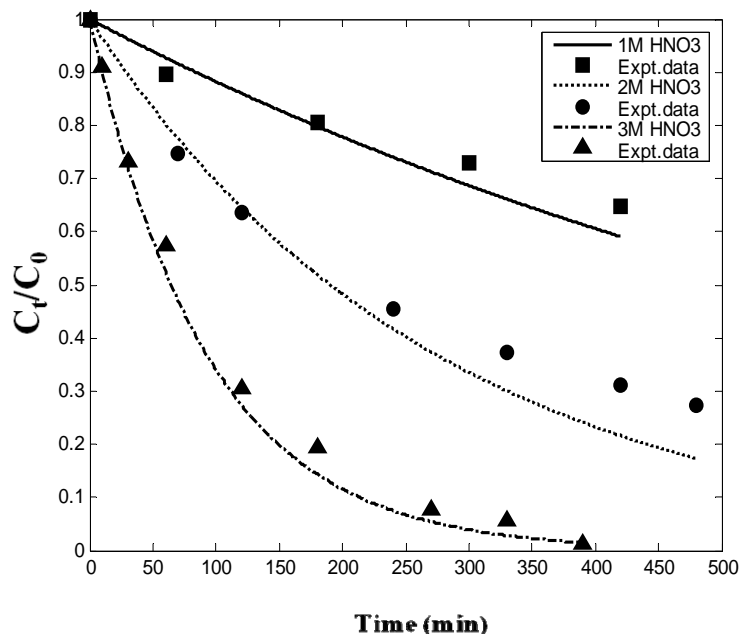


Figure 5.11 Transport of Cs(I) at different feed acidity. Feed: Cs(I) in different conc. Of HNO₃; Strip: Distilled water; Carrier solvent: 1.0×10^{-3} M CNC in 80% NPOE + 20% *n*-dodecane + 0.4% Alamine 336; Flow rate: 200 ml/min.

5.4.2.3 Effect of feed metal ion loading

In HFSLM configuration, experiments were also performed at different feed metal ion concentration of 0.1g/L, 0.3g/L and 0.5g/L. The carrier solvent was 1.0×10^{-3} M in 80% NPOE + 20% *n*-dodecane containing 0.4% Alamine 336 and distilled water was used as the strip phase. As observed with the FSSLM experiments, the rate of cesium transport was faster as the metal ion concentration increased, while the % transport values decreased. Figure 5.12 depicts the

experimental and prediction results indicating reasonably good match. Other research groups have also found similar trend by both by experimental and mathematical models [161, 162]. Variation in the transport profile with metal ion loading was also simulated by Kittisupakorn et al. [161], where the removal efficiency of HFSLM system was investigated for copper using D2EHPA as the carrier extractant. They have also reported the rate of removal to be decreasing with metal ion loading.

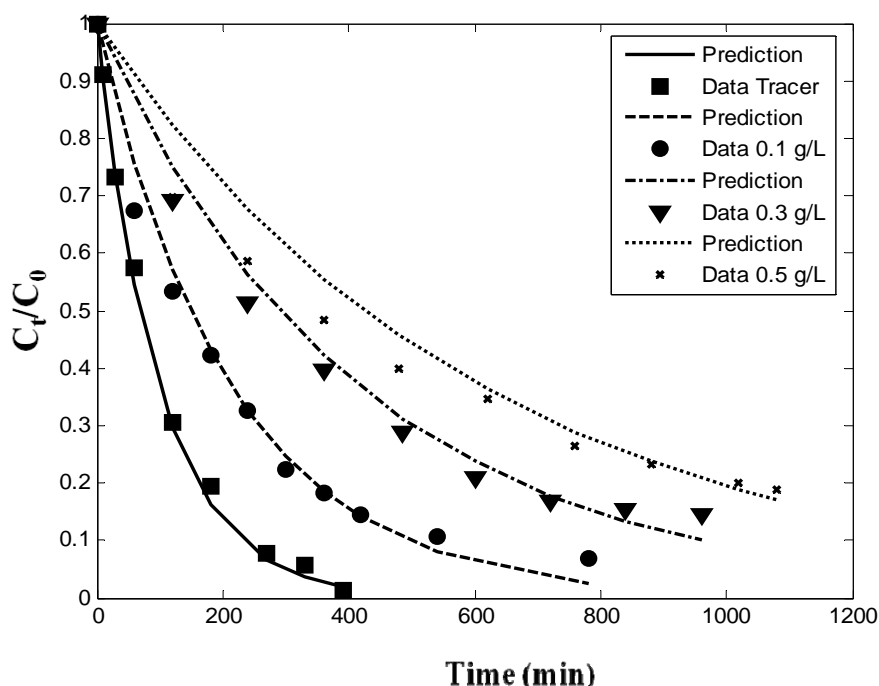


Figure 5.12 Cs(I) transport profile at varying CsNO_3 concentration in feed. Feed: Cs(I) in 3 M HNO_3 ; Strip: Distilled water; Carrier solvent: 1.0×10^{-3} M CNC in 80% NPOE + 20% *n*-dodecane + 0.4% Alamine 336; Flow rate: 200 ml/min.

5.4.2.4 Effect of flow rate

A mathematical prediction was also done to see the effect of feed side flow rate. It was seen that the effect of flow rate is almost negligible on the rate of metal ion transport. This can be explained by understanding the process of diffusion in membrane. The rate determining step in

the overall transport is the membrane diffusion. Since the organic phase mixture has significantly high viscosity, the rate of metal ion transport was mainly governed by the membrane diffusion step. Since diffusion inside the membrane was unaffected by the flow rate, there was only marginal change in the rate of metal ion transport through the membrane. Alternatively, from Equation (5.22), the term inside the bracket has negligible effect of k_{aq}^{-1} because the factor k_{org}^{-1} is very large due to high viscosity and lower diffusion coefficient of metal-ligand complex. The flow rate affects the aqueous diffusion layer thickness thereby reducing the aqueous mass transfer resistance which does not change the sum of $(K_d.k_{aq}^{-1} + k_{org}^{-1})$ leading to little change in the transport profile. This has been observed experimentally also.

5.5 MODELING OF OTHER MEMBRANE TRANSPORT SYSTEM

The modeling studies of cesium transport have shown excellent results that matches well with our experimental finding for both the cases of FSSLM and HFSLM. Apart from this, attempts were also made to validate the model for other transport systems.

The transport of strontium has been studied and discussed in Chapter 4. The results of those studies were simulated using the developed model. The primary data required were calculated or taken from the literature. Figure 5.13 shows the comparison of the model prediction and experimental data points.

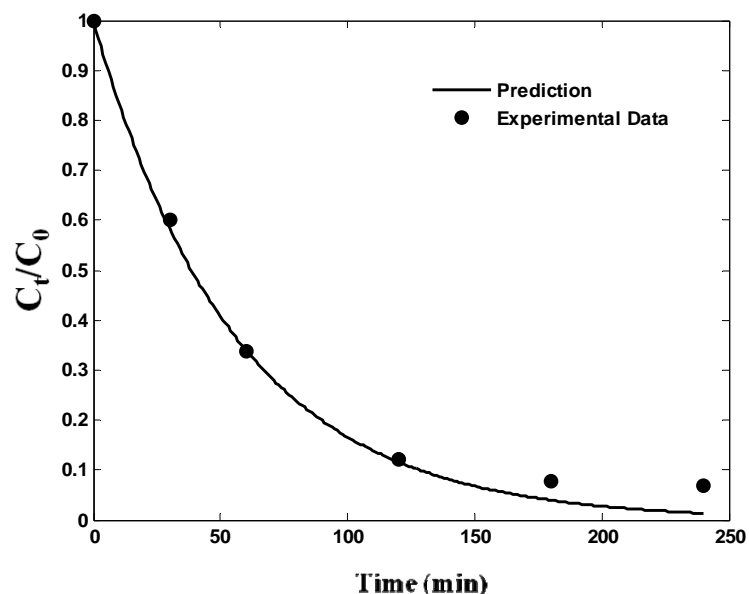


Figure 5.13 Experimental and prediction results for Sr(II) transport through HFSLM containing 0.1 M DtBuCH18C6. Feed: 3 M HNO₃; Strip phase: Distilled water.

Model prediction was excellent in the initial region of time but with passage of time, slight deviation was observed which was attributed to acid co-transport to the strip side. The effect of the increased strip phase acidity has not been taken care of in the model and hence the deviation can be justified.

5.6 CONCLUSIONS

In this Chapter we have described the formulation of a mathematical model for simulation and prediction of mass-transfer of metal ions across liquid membranes. The model is developed on the basis of diffusional mass-transport phenomenon. Fundamental equations are written on the basis of certain assumptions and mass-conservation laws. Equations derived from such treatment represent the actual transport process solving which gives us the results which matches well with the experimental findings carried out independently. Mathematical software was used

to get the solutions of differential equations so produced. The following conclusions can be made:

- The model is purely on fundamental ground and represents the transport process well for FSSLM and HFSLM. Various basic parameters were calculated which can be used for any other experimental conditions and provide useful information about the process.
- Validation of the models was performed by carrying out the experiments and comparing the results with the simulations. In almost all cases, a good agreement was seen except in some cases where large acid uptake by the ligand render the transport significantly affected.
- Although the model prediction is quite well, the major drawback of this model has been the lack of incorporation of effect of acid transport. The systems where acid transport plays crucial role (e.g. transport of Sr^{2+} by DtBuCH18C6), significant deviation has been observed. In the present case, for simplification, we have neglected the acid transport part for simplification but it can be taken care of by incorporating some extra parameters.

CHAPTER 6: Development of alternative diluent system for simultaneous recovery of cesium and strontium by CCD and PEG mixture

6.1 INTRODUCTION

The major radioactivity of high level waste (HLW) after sufficiently long cooling period is due to the two radioisotopes viz. ^{137}Cs ($t_{1/2}=30.1$ years) and ^{90}Sr ($t_{1/2}=28.5$ years). It had been estimated that after 30 years of time period, ~ 98 % of radioactivity of HLW is due to these two radioisotopes [45]. This high level of radioactivity poses problem in handling and vitrification of HLW in the repositories. Selective removal of these radionuclides from HLW is one of the possible option for the alleviation of problems associated with the radioactive waste management including the MANREM issues. Further, the recovered ^{90}Sr and ^{137}Cs can find use in many applications as mentioned in Chapter 3 and 4. The extraction of alkali / alkaline earth metal ion by crown ethers has been proven to be promising but the radiolytic degradation of these reagents restrict their use for the recovery of Cs and Sr from HLW. In this regard, chlorinated cobalt dicarbollide (CCD) has been suggested to be more resistant towards acid hydrolysis and radiation [163, 164].

The first transition metal dicarbollide (e.g. iron dicarbollide, $\text{Fe}(\text{B}_9\text{C}_2\text{H}_{11})_2^-$) was synthesized by Hawthorne et al. [165, 166] in 1965. They had reported the degradation of carborane ($\text{B}_{10}\text{C}_2\text{H}_{12}$) to dicarbadodecahydroundecaborate (-1) ion ($\text{B}_9\text{C}_2\text{H}_{11}^-$) which on complexation with Fe^{3+} ion resulted in the iron dicarbollide. The 1,2-dicarbollide ion and transition metal bis-dicarbollide complex ion have the structures as shown in figure 6.1. Several metal dicarbollides were synthesized including chromium dicarbollide, iron dicarbollide, nickel dicarbollide and cobalt dicarbollide [167].

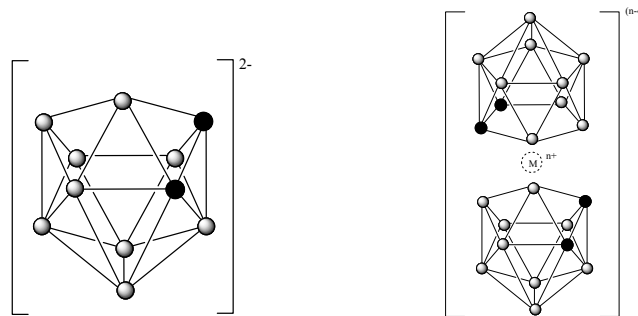


Figure 6.1 Structural representation of (a) 1,2-dicarbollide dianion and (b) transition metal bis-dicarbollide complex ion.

Cobalt dicarbollide (fig. 6.2) has been studied most widely because of the easy extraction of its sodium salt from the aqueous solution into ether and it has been extensively tested for the extraction of various radionuclides. Various research groups have reported that radionuclides like ^{137}Cs can be extracted in organic phase comprising of cobalt dicarbollide in polar diluents (like nitrobenzene or halogenated diluents) due to the solubility of cesium-cobalt dicarbollide in various water-immiscible diluents [47, 168]. Rais et al. [168] first reported the applicability of cobalt dicarbollide in solvent extraction processes for the extraction of cesium.

CCD has been found to be a highly selective extractant for cesium from acidic medium. Czech researchers reported that strontium could also be extracted along with cesium by the addition of polyethylene glycol (PEG) to CCD dissolved in nitrobenzene [169]. Cesium ion is one of the least hydrated ions in aqueous solutions compared to other metal ions and combines to the poorly hydrated CCD anion and gets transferred to the organic phase. Addition of PEG is considered to dehydrate Sr^{2+} and thereby

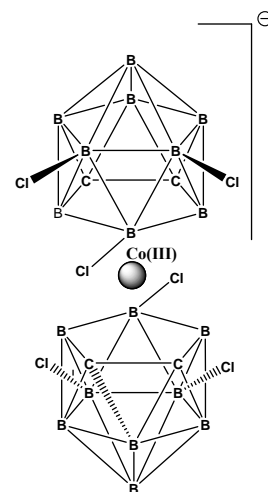


Fig. 6.2 Structural formula of chlorinated cobalt dicarbollide (CCD)

facilitating the extraction of Sr along with Cs. Rais et al. [168, 170] have reported a large synergistic effect on the extraction of micro-quantities of Ca^{2+} , Sr^{2+} , Ba^{2+} , and Pb^{2+} in the presence of polyethylene glycols (PEG) and CCD.

This unique extraction properties of CCD/PEG mixtures permits the removal of Cs and Sr from acidic high activity wastes (HAW). However, the industrial use of this process was not feasible due to the lack of an appropriate diluent for CCD. Acceptable diluents for use in radioactive waste treatment must have high chemical and radiation stability, low aqueous solubility, low viscosity, and a density substantially different from the aqueous process solutions. Further, the extractants (CCD and PEG), and their solvated metal complexes, must be readily soluble in the diluent and the formation of an immiscible third phase should not be seen under loading conditions or otherwise. Finally, the diluent should be nontoxic, inexpensive, and readily available or produced.

Collaborative efforts of the KRI and INEEL were started in 1994 to investigate the applicability of the CCD/PEG process as applied to INEEL tank and dissolved calcine wastes. This early testing used nitroaromatic diluents and hydrazine as a strip reagent, both unacceptable in the United States for commercial use because of their hazardousness. Ongoing efforts have been focused on development and demonstration of the UNiversal solvent EXtraction (UNEX) process to extract all the major radionuclides (^{137}Cs , ^{90}Sr and minor actinides) from INEEL wastes [171-174], simultaneously. The UNEX process incorporates a mixture of 0.08 M CCD + 0.1 % (v/v) PEG-400 + 0.2 M CMPO in nitrobenzene or trifluoro methyl phenyl sulfone (FS-13) to simultaneously extract the radionuclides [48, 175-179].

The major limitation of the UNEX process has been the use of toxic / corrosive diluents which are environmentally hazardous. Hence, there is a need for alternative diluent system for CCD and PEG mixture for Cs and Sr co-recovery from radioactive high level nuclear waste on the larger scale. In the present work, we have investigated the mixture of NPOE in *n*-dodecane as the suitable diluent for the co-recovery of Cs and Sr from the acidic solutions. Preliminary experiments were carried out and the results have been found to be encouraging. Solvent extraction studies and supported liquid membrane transport studies have been performed and the results are discussed in this Chapter.

6.2 SOLVENT EXTRACTION STUDIES

The extraction of Cs(I) and Sr(II) by CCD in FS-13 (or in nitrobenzene) has already been established by various groups [180, 181]. In this work, a mixture of NPOE – *n*-dodecane has been investigated as an alternative diluent for extraction of Cs(I) and Sr(II) by the mixture of CCD and PEG. Distribution studies were carried out to investigate the basic extraction process.

6.2.1 Diluent composition optimization

Diluent plays an important role in the extraction of metal ions into the organic phase. Presently, we have used a mixture of 2-nitrophenyloctyl ether (NPOE) and *n*-dodecane as diluent because the high viscosity of NPOE may lead to the slower mass transfer rates. Figure 6.3 shows the variation of $K_{d,Cs}$ values with the varying diluent composition. A steady decrease in the distribution ratio was observed with an increase in the NPOE content in the diluent mixture e.g., $K_{d,Cs}$ value of 7.30 was obtained from 1 M HNO_3 using 0.01 M CCD in 40% NPOE + 60% *n*-dodecane as the diluent which decreased to 4.80 when pure NPOE was taken as the diluent. It was not possible to reduce the NPOE fraction beyond 40% because of solubility limitations of

CCD. This decrease in distribution ratio with increasing NPOE percentage can be explained by considering the interaction of CCD molecule with NPOE which may be affecting the free ligand concentration. A detailed investigation is required to understand this phenomenon.

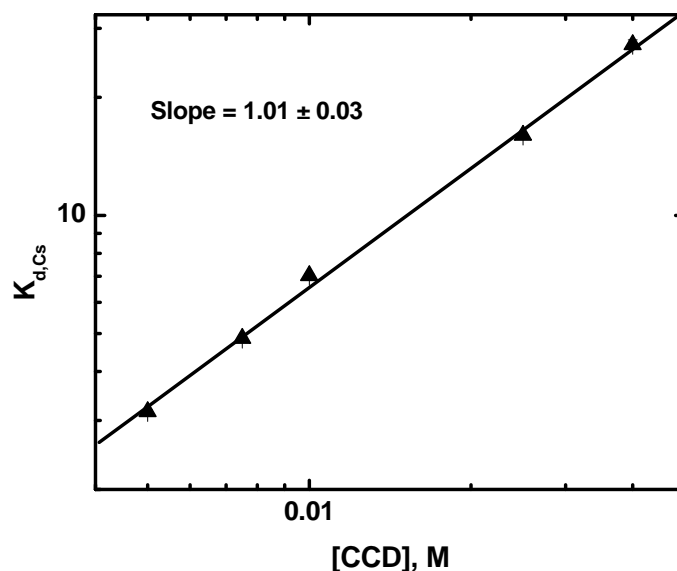


Figure 6.3 Variation of distribution ratio of Cs(I) with varying diluent composition. Aqueous phase: 1 M HNO₃ containing ¹³⁷Cs tracer; Organic phase: 0.01 M CCD in NPOE + *n*-dodecane; Equilibration time: 1 hour.

In case of 20% NPOE + 80% *n*-dodecane as solvent, a red colored third phase appeared in between the organic and the aqueous phases which may be the CCD rich NPOE phase due to the solubility limitation of CCD in the particular diluent composition. Hence, subsequent solvent extraction experiments were performed with the diluent composition of 40% NPOE + 60% *n*-dodecane. This helps in two ways: firstly due to less viscosity (Table 6.1) of this composition, the mass transfer is relatively faster as compared to the diluent composition of 80% NPOE + 20% *n*-dodecane and secondly, in supported liquid membrane systems (where hydrophobic polymeric support such as PTFE or PP is used) this optimized diluent system may be helpful in better membrane stability as will be discussed below. Moreover, this diluent composition

resulted in higher $K_{d,Cs}$ values at lower CCD concentrations as compared to those observed in the UNEX process [180]. This can reduce the ligand inventory and reduce the secondary organic waste generation.

Table 6.1: Measured value of viscosity of various compositions of NPOE and *n*-dodecane.

| Diluent composition | Viscosity (mPa.s) |
|-----------------------------------|-------------------|
| 40% NPOE + 60% <i>n</i> -dodecane | 3.014 |
| 60% NPOE + 40% <i>n</i> -dodecane | 7.048 |
| 80% NPOE + 20% <i>n</i> -dodecane | 11.088 |
| 100% NPOE | 13.417 |

6.2.2 Kinetics of equilibrium

The extraction kinetics study was carried out using 0.01 M CCD in 40% NPOE + 60% *n*-dodecane diluent mixture as the solvent system and the results have been shown in figure 6.4.

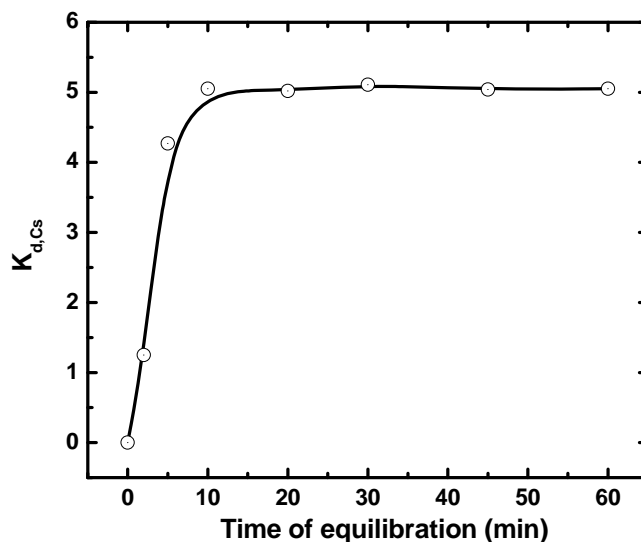


Figure 6.4 Kinetics of extraction of Cs(I) by CCD. Aqueous phase: 1 M HNO₃ spiked containing ¹³⁷Cs; [CCD]: 0.01 M in 40% NPOE + 60% *n*-dodecane.

It was observed that the equilibrium $K_{d,Cs}$ values were obtained in about 10 minutes. Apparently, as anticipated, the lower viscosity of this diluent composition helps in the faster mass transfer rates.

6.2.3 The effect of HNO_3 concentration

The acidity of the aqueous phase plays a key role in the extraction of the metal ion. Experiments were carried out with different feed nitric acid concentrations keeping other experimental parameters constant. Increasing the acidity decreased the $K_{d,Cs}$ which suggested the ion-exchange type extraction mechanism as per the following equation [179, 182],

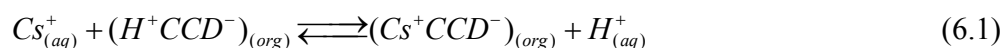


Figure 6.5 shows the comparative experimental results in the form of the plots showing $K_{d,Cs}$ vs. HNO_3 concentration at 0.01 M CCD in 40% NPOE + 60% *n*-dodecane and FS-13 as diluent. A steep fall in $K_{d,Cs}$ with increasing acidity has been observed with the diluent mixture which becomes $< 10^{-2}$ at acidity > 6 M HNO_3 . Similar trend was observed with FS-13 as the diluent but the respective values of $K_{d,Cs}$ are found to be quite lower than that with the diluent mixture. The acidity of SHLW is usually in the range of 3-4 M HNO_3 [183]. As mentioned above, the $K_{d,Cs}$ values are quite low when 0.01 M CCD is used as extractant. On the other hand, the distribution ratio for Cs is found to be sufficiently high (7.07 ± 0.16) for 1 M HNO_3 feed solutions. Therefore, process application of the solvent system required to adjust the acidity of SHLW to 1 M HNO_3 by appropriate dilution for Cs recovery.

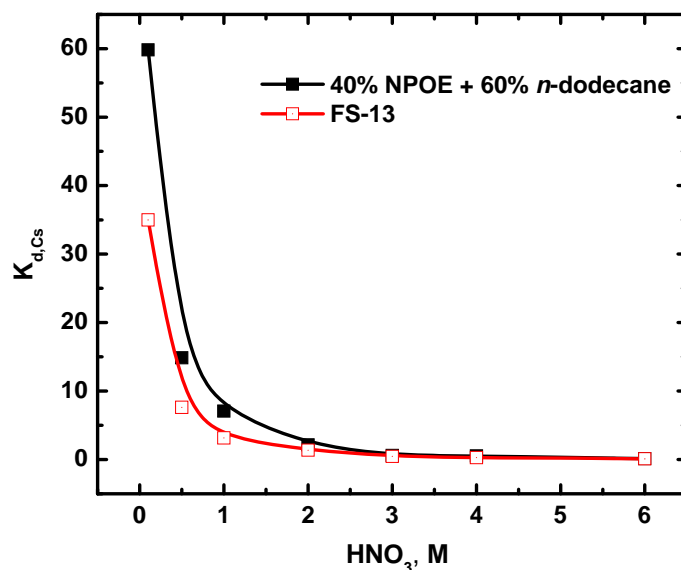


Figure 6.5 Variation of $K_{d,Cs}$ with the nitric acid concentration. Organic phase: 0.01 M CCD in FS-13 or 40% NPOE + 60% *n*-dodecane; Aqueous phase: Varying concentration of HNO_3 containing ^{137}Cs tracer; Equilibration time: 1 hour.

6.2.4 The effect of CCD concentration

The stoichiometry of the metal-CCD complex was ascertained by measuring $K_{d,Cs}$ values as a function of ligand concentration. The slope of the log-log plot between ligand concentration and distribution ratio of metal gives the average number of CCD molecules associated with the extracted species. For these experiments, CCD concentration was varied from 0.005 M to 0.04 M in 40% NPOE + 60% *n*-dodecane while the aqueous phase acidity was 1 M HNO_3 . A steady decrease in the distribution ratio ($K_{d,Cs}$) was observed with decreasing CCD concentration. Figure 6.6 shows the log-log plot of $K_{d,Cs}$ vs. CCD concentration which showed a linear dependence. The straight line plot in Fig. 6.6 has a slope value of ~ 1 suggesting the involvement of one CCD molecule per Cs^+ ion as already showed in the equation 6.1, which also indicated that the equilibrium will shift towards the left side with increasing acidity of aqueous phase. Thus, the

metal-ligand complex will become destabilized at higher acidity resulting in the effective stripping of the metal ion.

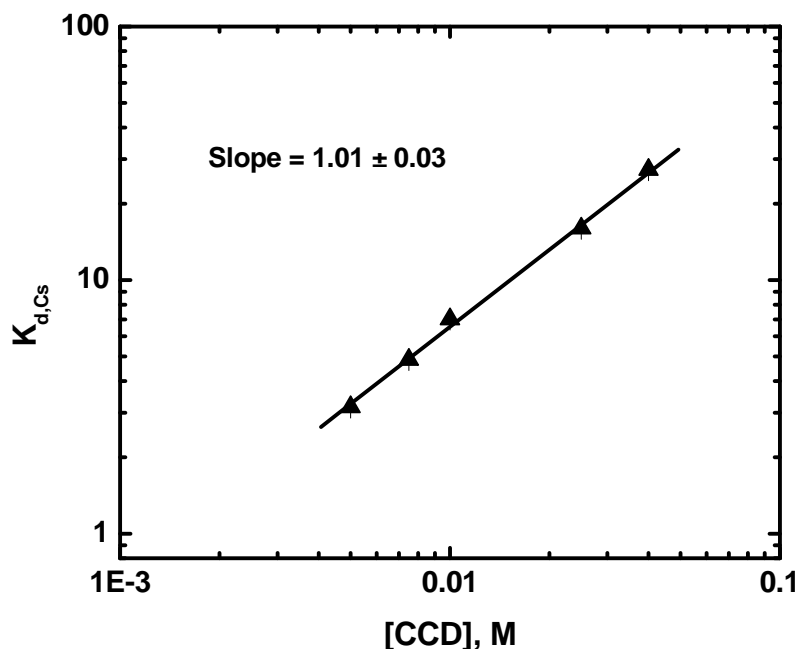


Figure 6.6 log-log plot of $K_{d,Cs}$ vs. CCD concentration. Aqueous phase: 1 M HNO_3 ; Diluent: 40% NPOE + 60% *n*-dodecane; Equilibration time: 1 hour.

6.2.5 Addition of PEG-400 with CCD

One of the objectives of the UNEX process is the simultaneous extraction of Cs and Sr. Co-recovery of Cs and Sr requires the addition of polyethylene glycol (PEG)-400 with the CCD in the organic phase [178]. PEG-400 is reported to be dehydrating the Sr^{2+} in the aqueous phase by removing water molecules from its inner coordination sphere and making a 'wrapped around' complex with the glycolic 'O' atoms which can be extracted in the organic phase with the CCD anion. To investigate the role of PEG-400 in the co-extraction of Sr with Cs, the organic phase PEG-400 concentration was varied keeping the CCD concentration fixed in the 40% NPOE + 60% *n*-dodecane diluent mixture. Extraction of Cs(I) and Sr(II) was carried out from 1 M HNO_3

acidity and Figure 6.7 shows the experimental results. With the increasing PEG-400 concentration, the distribution ratio of Sr(II) was found to increase while that for Cs(I) seem to be decreasing. This can be explained because of less availability of CCD for Cs(I) extraction due to increased extraction of Sr(II) with the addition of PEG-400. After 0.2 % PEG-400 concentration, a saturation plateau was observed leading to a constant value of $K_{d,Sr}$ of ~ 30 thereafter.

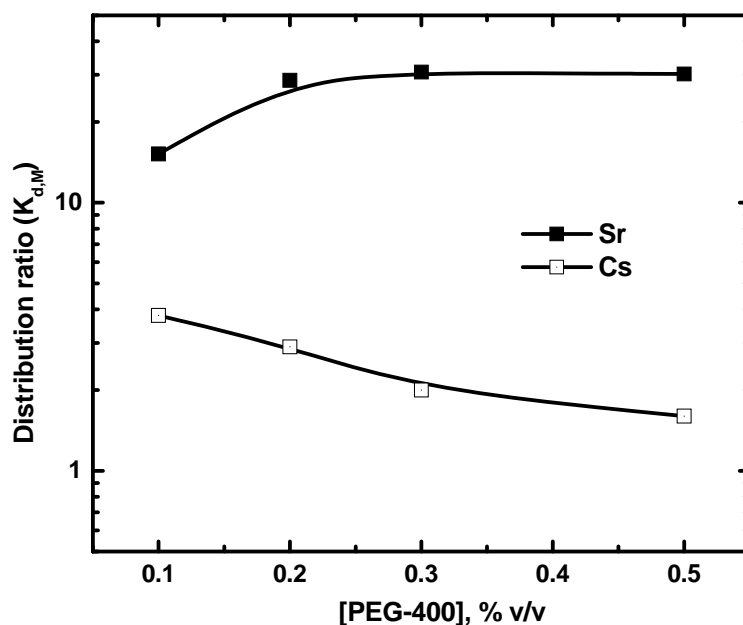


Figure 6.7 Extraction of Cs(I) and Sr(II) by a mixture of CCD and PEG-400. Aqueous phase: 1 M HNO_3 ; Organic phase: 0.01 M CCD + varying concentration of PEG-400; Equilibration time: 1 hour.

In another set of experiments, CCD concentration was varied from 0.005 M to 0.05 M in 80% NPOE + 20% *n*-dodecane at a constant PEG-400 concentration. Distribution ratio values for Sr(II) were determined from 1 M HNO_3 and Figure 6.8 shows the log-log plot of $K_{d,Sr}$ vs. CCD concentration.

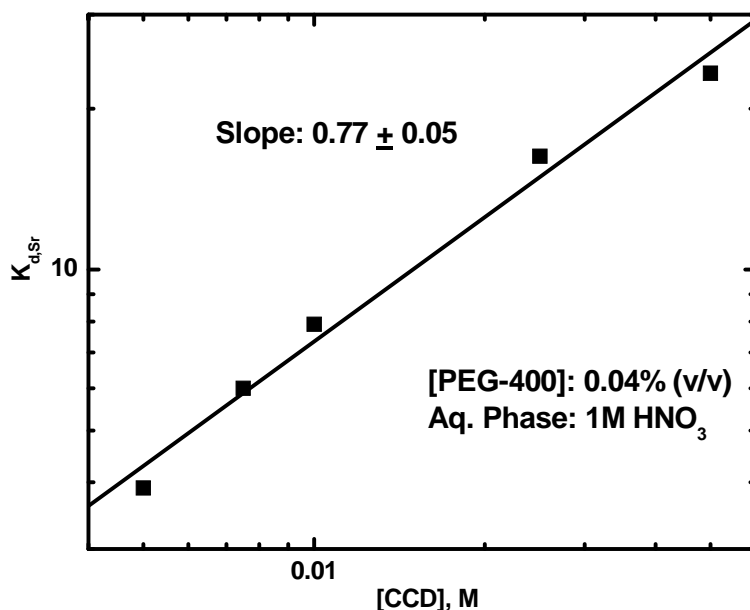
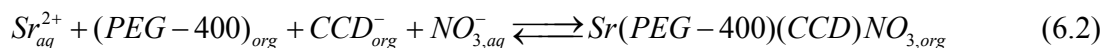


Figure 6.8 Log-log plot of $K_{d,Sr}$ vs. CCD concentration. Aqueous phase: 1 M HNO_3 ; Organic phase: Varying concentration of CCD + 0.04% (v/v) PEG-400; Equilibration time: 1 hour.

The linear fit of the data points gave a slope of 0.77 ± 0.05 suggesting the involvement of approximately one CCD molecule in the extraction of Sr^{2+} . To neutralize the partial residual charge on the complex formed, other counter anion such as NO_3^- can take part thereby facilitating the extraction of Sr^{2+} in to the organic phase. The extraction equilibrium is represented as:



Zalupski et al. [184] have performed calorimetric studies with the similar system and reported the extraction of such kind of species where $Sr(NO_3)^+$ have been extracted by a mixture of CCD and PEG-400 in FS-13. The results of the calorimetric studies suggested that the PEG-400 functions as a stoichiometric phase transfer reagent rather than acting simply as a phase transfer catalyst or phase modifier.

6.2.6 Co-current extraction of Cs(I)

For quantitative extraction of metal ion from feed solution by solvent extraction techniques, it is required to repeatedly contact the aqueous phase containing the metal ion with fresh organic phases. This way, the metal ion from the feed solution is transported into the organic phase by multiple contacts. Co-current extraction studies were carried out for the removal of Cs(I) from aqueous solution and the results are given in Table 6.2. As indicated, > 99.5 % extraction of Cs(I) is achieved in 4 contacts of the aqueous feed with fresh organic phases.

Table 6.2: Co-current extraction of Cs(I) by CCD. Aqueous phase: 1 M HNO₃; Organic phase: 0.01 M CCD in 40% NPOE + 60% *n*-dodecane, Equilibration time: 1 hour.

| No. of contact | % Extraction of Cs(I) | Cumulative extraction (%) |
|----------------|-----------------------|---------------------------|
| 1 | 87.0 | 87.0 |
| 2 | 86.3 | 97.7 |
| 3 | 73.4 | 99.2 |
| 4 | 65.5 | 99.5 |

6.2.7 Reusability of the solvent

The applicability of the separation process on a large scale is commercially viable if the reagents can be repeatedly used for processing leading to the minimization of secondary waste generation. The low solubility of the extractant in the aqueous phase is a criterion for better reusability of the process solvent. Experiments were carried out by repeatedly using the same organic phase in extraction and stripping stages and the results are represented in the following bar chart (Figure 6.9). A small but gradual decrease in $K_{d,Cs}$ is observed with increasing number

of cycles of reusing the solvent which may be due to the leaching out of CCD in the aqueous phase arising from the partial solubility of CCD in aqueous phase.

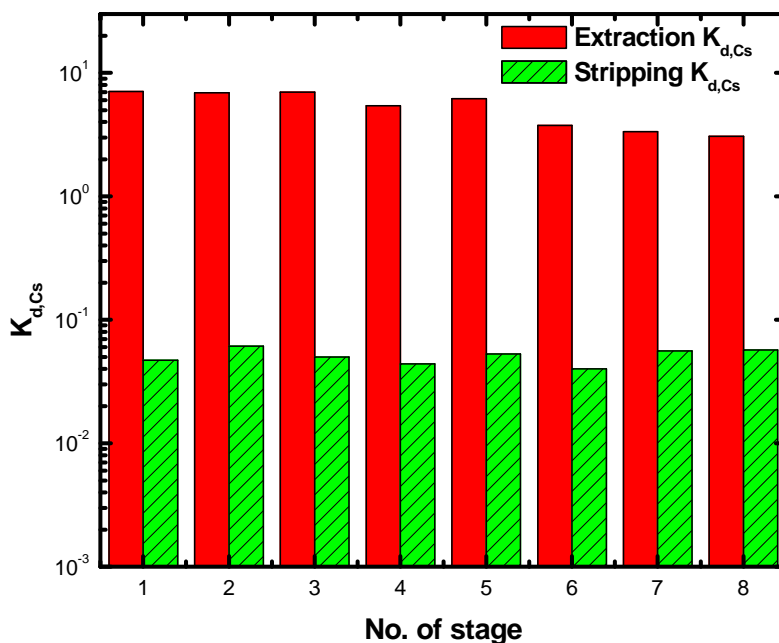


Figure 6.9 Successive extraction and stripping distribution ratio values using the fresh feed and strip solutions but regenerated solvent. Aqueous phase: 1 M HNO₃; Organic phase: 0.01 M CCD in 40% NPOE + 60% *n*-dodecane; Equilibration time: 1 hour.

6.2.8 Radiation stability of the solvent

The effect of radiation on the solvent is important while employing the solvent system for Cs/Sr recovery from the actual nuclear waste solutions. The radiation degradation effect on the solvent system developed in this work was also investigated. Table 6.3 lists the effect of different radiation doses on the extraction behavior of Cs(I) ion. It was observed that with increasing radiation dose, the $K_{d,Cs}$ values decreased significantly leading to poorer extraction values at higher absorbed doses (> 10 Mrad). This may be due to the degradation of diluent NPOE in the radiation field leading to radical formation which may adversely affect the extraction of metal

ion. Further investigation of the degradation products is required to investigate the effect of radiation on the solvent into more detail.

Table 6.3: The effect of radiation dose on the distribution ratio of Cs(I) ion by CCD. Aqueous phase: 1 M HNO₃; Organic phase: 0.01 M CCD in 40% NPOE + 60% *n*-dodecane.

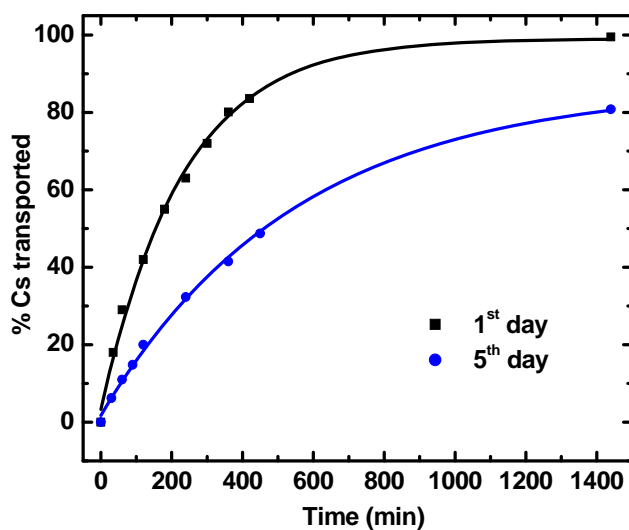
| Radiation dose (Mrad) | K_{d,Cs} |
|------------------------------|-------------------------|
| 0 | 7.10 |
| 3.76 | 2.95 |
| 7.23 | 1.24 |
| 10.56 | 0.46 |
| 15.25 | 0.12 |
| 21.53 | 0.08 |

6.3 MEMBRANE TRANSPORT STUDIES

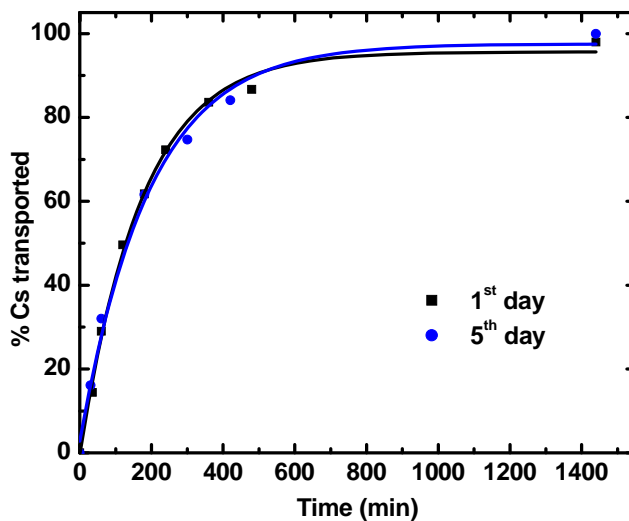
After optimizing conditions for the recovery of Cs and Sr using CCD and PEG-400 in NPOE and *n*-dodecane mixture from acidic feeds, it was required to evaluate the supported liquid membrane technique for the metal on recovery from the same feed solutions. For these experimental studies, feed and strip conditions were optimized by solvent extraction studies. Basic SLM experiments were performed to show the viability of the transport system for the Cs and Sr recovery. In most of the experiments, 1 M and 8 M HNO₃ were employed as the feed and the strip phases, respectively, while 0.01 M CCD was taken as the membrane phase. The diluent composition was optimized and suitable composition was used for further experiments as detailed in the following sections.

6.3.1 Diluent composition optimization

To optimize the suitable diluent composition for the supported liquid membrane studies, various combinations of NPOE and *n*-dodecane were examined. Figure 6.10 presented the transport profiles of Cs through FSSLM containing 0.01 M CCD in different composition of NPOE and *n*-dodecane while other experimental conditions were maintained identical.

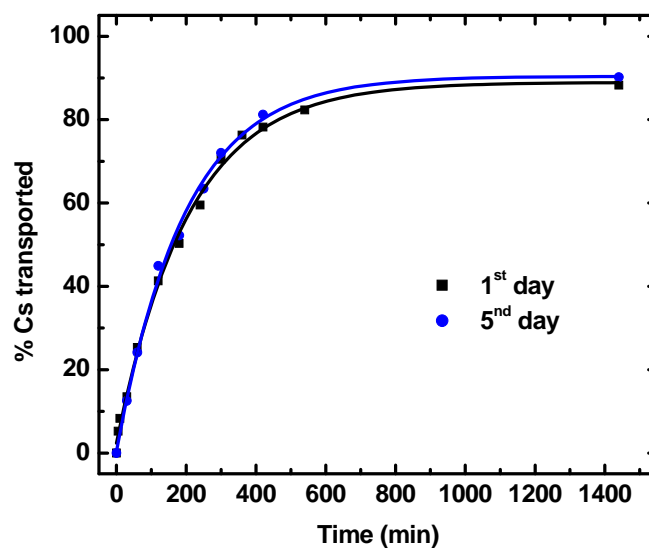


(a)

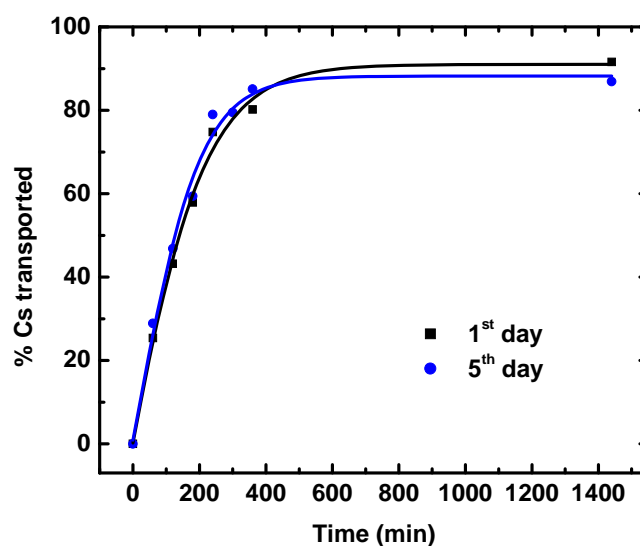


(b)

(Continued...)



(c)



(d)

Figure 6.10 Comparison of transport profile of Cs(I) through FSSLM at 1st and 5th day. Feed: 1 M HNO₃; Strip: 8 M HNO₃; Carrier: 0.01 M CCD in (a) 40% NPOE + 60% *n*-dodecane, (b) 60% NPOE + 40% *n*-dodecane, (c) 80% NPOE + 20% *n*-dodecane and (d) 100% NPOE.

Although lower percentage of NPOE is preferred due to lower viscosity leading to higher mass transfer rates, the poor membrane stability with diluent composition of 40% NPOE + 60% *n*-dodecane renders the use of this diluent composition in membrane studies. Table 6.4 lists the

% transport of Cs(I) in 6 hours in case of diluent compositions of 40% NPOE + 60% *n*-dodecane, 60% NPOE + 40% *n*-dodecane and 80% NPOE + 20% *n*-dodecane.

Table 6.4: % transport of Cs(I) after 6 hours through FSSLM. Feed: 1 M HNO₃ spiked with Cs; Strip: 8 M HNO₃; Carrier: 0.01 M CCD in varying composition of NPOE + *n*-dodecane.

| Time elapsed | % Transport of Cs (6 h) | | |
|----------------------|-------------------------|----------|-----------|
| | 40% NPOE | 60% NPOE | 80 % NPOE |
| 1 st day | 80 | 78 | 76 |
| 5 th day | 55 | 77 | 77 |
| 10 th day | 29 | 75 | 74 |
| 19 th day | - | 72 | 73 |

A stable supported liquid membrane system was obtained with 60% NPOE + 40% *n*-dodecane as the diluent. Increasing the NPOE content in the diluent increased the carrier stability in the membrane but decreased the rate of mass transfer to some extent. Hence, all subsequent experiments were carried out with 60% NPOE + 40% *n*-dodecane as the diluent composition. The permeability coefficient (P) has been calculated to be $(6.18 \pm 0.18) \times 10^{-4}$ cm/s in case of 0.01 M CCD in 60% NPOE + 40% *n*-dodecane while the same was $(3.86 \pm 0.08) \times 10^{-4}$ cm/s in case of 40% NPOE + 60% *n*-dodecane as the diluent composition.

6.3.2 Effect of feed acidity on the transport profile of Cs(I)

The acidity of the feed phase plays an important role in the overall transport of Cs(I) in the SLM studies. Using 0.01 M CCD in 60% NPOE + 40% *n*-dodecane as the membrane carrier phase and 8 M HNO₃ as the strippant, transport experiments were carried out by varying the feed

acidity from 0.1 M HNO₃ to 3 M HNO₃. The results of the transport experiments have been presented in figure 6.11. A rapid fall in the rate of mass transfer was observed when the feed acidity was increased from 0.1 M to 3 M HNO₃. As discussed in the previous Section, increasing the acidity of the feed solution lowered the distribution ratio of metal ion at the feed-membrane side which, in turn, decreased the extraction rate resulting in slow transport rate of the metal ion.

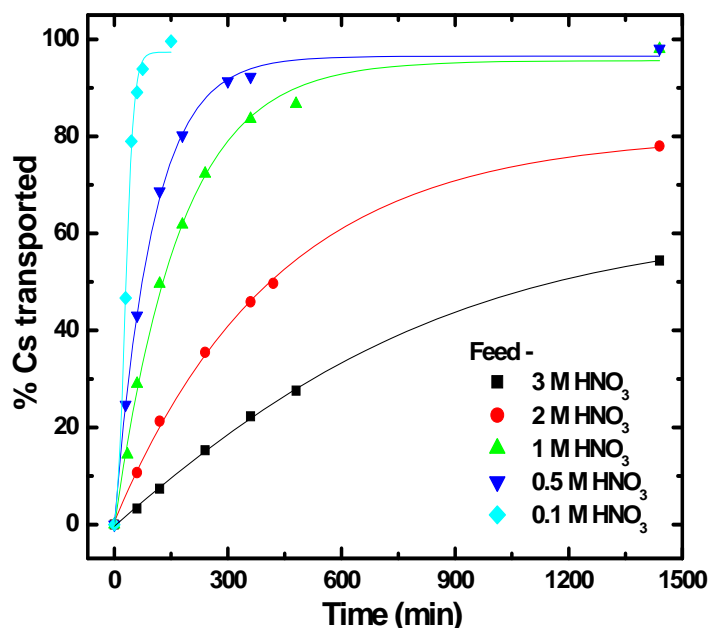


Figure 6.11 Transport profile of Cs(I) at different feed acidity. Feed: HNO₃ at varying concentration; Strip: 8 M HNO₃; Carrier: 0.01 M CCD in 60% NPOE + 40% *n*-dodecane.

With 3 M HNO₃ as the feed solution, only 52% of Cs(I) gets transported in 24 hours while > 95% Cs(I) recovery was possible in the same time interval with 1 M HNO₃ as the feed acidity. With further reduction in the acidity to 0.1 M, only 2 hours were sufficient for > 99% Cs(I) transport through the membrane. Hence, subsequent FSSLM transport studies were carried out with 1 M HNO₃ as the feed phase and 8 M HNO₃ as the strip phase.

6.3.3 Effect of CCD concentration on the transport of Cs(I)

Supported liquid membrane transport experiments were also carried out with varying concentrations of CCD in the organic phase. 1 M HNO₃ was used as the feed solution while the strip solution was 8 M HNO₃. The results are presented in figure 6.12 which indicate that the transport rate was increasing with increasing CCD concentration in the membrane phase. This can be explained using Equation (6.1), which indicated that higher metal ion extraction is favoured at higher carrier concentration which resulted in higher permeability coefficient (P), as can be seen from the following relation,

$$P = K_{d,Cs} \times k_{org} \quad (6.3)$$

(The above equation is valid when the aqueous mass transfer coefficient is very large compared to membrane mass transfer coefficient viz., $k_{aq} \gg k_{org}$).

This, in turn, increases the metal ion transport rate according to the following relation [77],

$$\ln\left(\frac{C_t}{C_0}\right) = -P\left(\frac{Q}{V}\right)t \quad (6.4)$$

where, Q and V represents the effective surface area of membrane (cm²) and volume of the feed solution (in mL), respectively. From these experiments, it can be suggested that 0.01 M CCD is quite sufficient for the quantitative recovery (~ 98%) of Cs(I) from a feed solution of 1 M HNO₃ into a receiver phase of 8 M HNO₃ in 24 hours of operation. Higher concentration of CCD is not advisable as it can lead to large organic waste generation. Mohapatra et al. [185], reported faster Cs transport rates using 0.025 M CCD in FS-13 as the carrier solvent, 1 M HNO₃ as the feed and 8 M HNO₃ as the strippant.

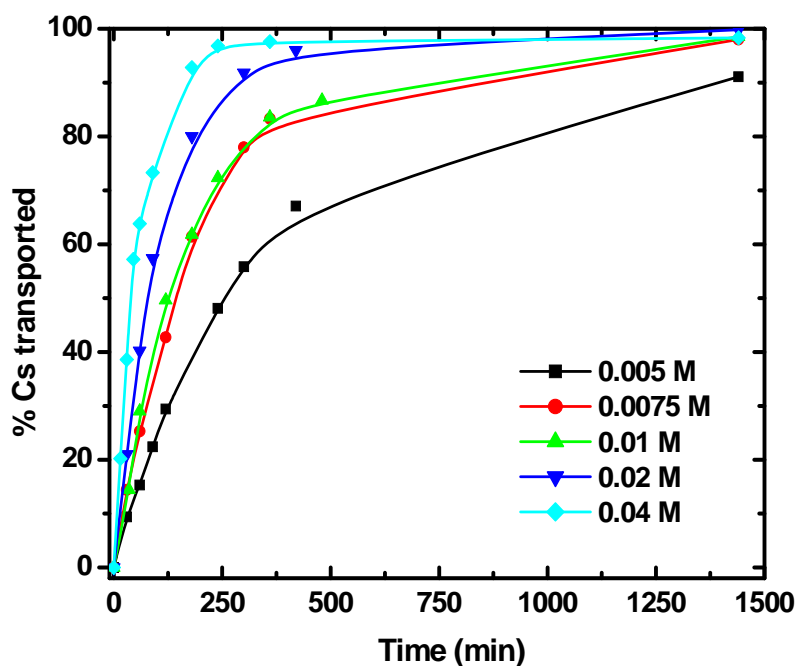


Figure 6.12 Transport profile of Cs(I) at varying CCD concentration. Feed: 1 M HNO₃; Strip: 8 M HNO₃; Carrier: CCD in 60% NPOE + 40% *n*-dodecane.

6.3.4 Membrane thickness variation

The rate controlling step in membrane transport experiments is diffusion through membrane (as described in Section 5.2.2 of Chapter 5). With the increase in the membrane thickness, the flux through the membrane decreased as indicated by the Fick's law expression,

$$J_{org} = -D_o \frac{\Delta C}{d_m \tau} \quad (6.5)$$

where, ΔC represents change in concentration across membrane, and other symbols have their usual meaning. Experiments were carried out by varying the thickness of the membrane by sticking two or more membranes onto each other after impregnation of the carrier solution. Table 6.5 lists the experimental values of % transport of Cs(I) after 6 hours along with the calculated permeability coefficients.

Table 6.5: Variation of % transport after 6 hours and permeability coefficient with the membrane thickness. Feed: 1 M HNO₃; Strip: 8 M HNO₃; Carrier: 0.01 M CCD in 60% NPOE + 40% *n*-dodecane.

| Thickness of membrane (μm) | % Transport of Cs(I), (6 h) | P × 10 ⁴ (cm/s) |
|----------------------------|-----------------------------|----------------------------|
| 85 | 83.6 | 5.9 ± 0.17 |
| 170 | 59.5 | 2.79 ± 0.05 |
| 255 | 36.6 | 1.81 ± 0.01 |
| 340 | 30.5 | 1.62 ± 0.13 |

6.3.5 Calculation of diffusivity by time-lag method

The diffusion coefficient of Cs-CCD complex is the main membrane transport parameter that governs the rate of metal ion transport through the membrane phase. There are various empirical relations in the literature (as given in Chapter 5) that can be used for the calculation of diffusion coefficient of metal-ligand complex across the organic layer. Time-lag experiment has also been described [186] in which the permeation of metal-ligand complex is observed through the membrane (FSSLM) and the time after which the metal is detected in the strip phase is noted down. The diffusivity of the complex is then estimated from the following relation,

$$D_o = \frac{d^2}{6t_{lag}} \quad (6.6)$$

where, '*d*' represents the diffusive path length and '*t_{lag}*' denotes the time-lag which is the time interval after which metal ion starts appearing in the strip side of membrane.

FSSLM transport experiments were carried out with 1 M HNO₃ as the feed and 8 M HNO₃ as the strip solution while 0.01 M CCD was used as the carrier extractant. PTFE flat sheet membrane (thickness of the membrane was 85 micron and tortuosity was 1.5) was used as

membrane support. Figure 6.13 presents the strip concentration profile of ^{137}Cs and the time-lag was found to be 160 seconds and using equation 6.6, the diffusivity of Cs-CCD complex was calculated to be $1.7 \times 10^{-7} \text{ cm}^2/\text{s}$.

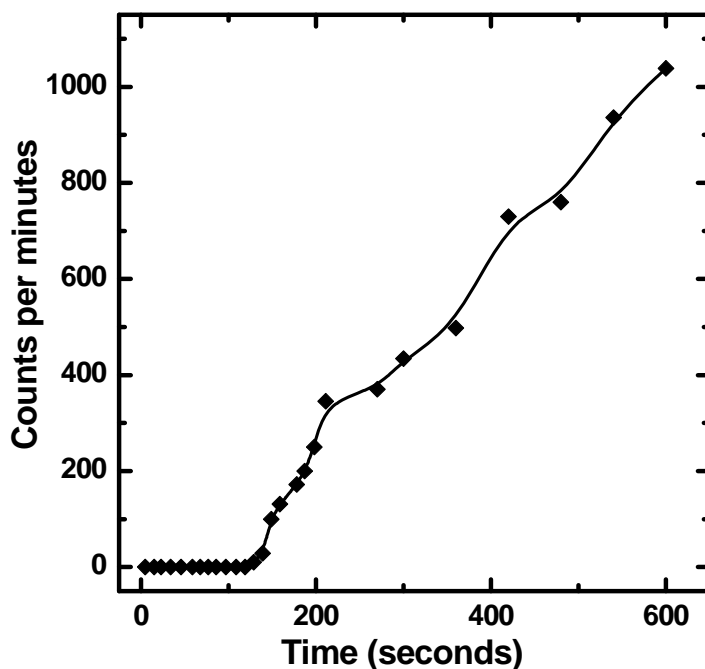


Figure 6.13 Transport profile of ^{137}Cs as a function of time. Feed: 1 M HNO_3 ; Strip: 8 M HNO_3 ; Carrier: 0.01 M CCD in 60% NPOE + 40% *n*-dodecane.

6.3.6 Transport of Cs and Sr by CCD and PEG-400 mixture

The co-recovery Cs and Sr requires the addition of PEG-400 along with CCD as discussed in Section 6.2.5. FSSLM transport studies were carried out to simultaneously extract Cs and Sr by 0.01 M CCD + 0.04% (v/v) PEG-400 in 60% NPOE + 40% *n*-dodecane as the carrier solvent. Cesium transport was found to be similar to those observed without the addition of PEG-400 but, surprisingly, no strontium transport was observed. This is shown in figure 6.14, where the transport profiles of both the metal ions is presented.

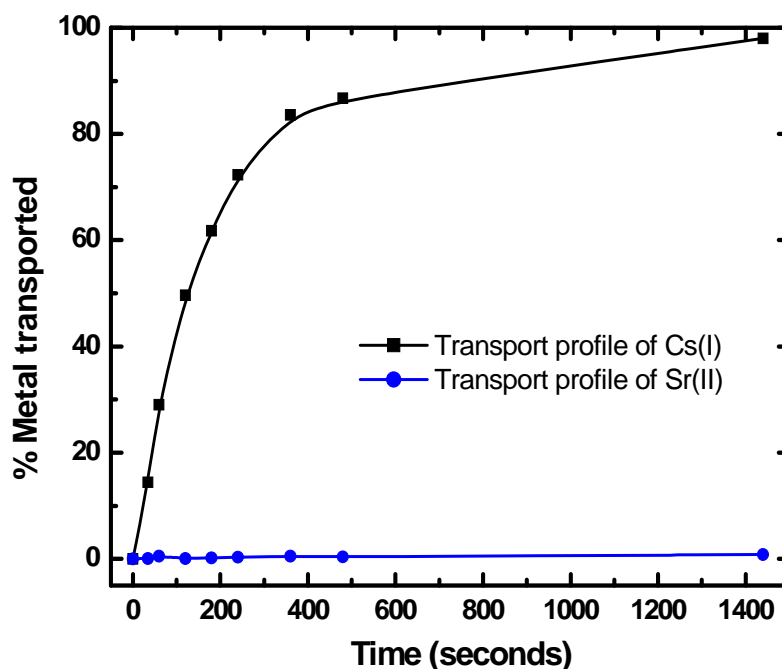


Figure 6.14 Transport profile of Cs and Sr. Feed: 1 M HNO₃; Strip: 8 M HNO₃; Carrier: 0.01 M CCD + 0.04% (v/v) PEG-400 in 60% NPOE + 40% *n*-dodecane.

PEG-400 has a partition coefficient of 1.5×10^{-5} between hexane and water [187] indicating that only 1.5 parts of PEG-400 is present in hexane per 1,00,000 parts in water. In SLM transport experiments, 20 mL of each of the feed and the strip phases was used. The high solubility of PEG-400 in aqueous solution may lead to leaching out of PEG-400 from the impregnated organic layer in the pores of membrane thereby leading to ineffective transport of Sr. Further investigation are required to arrest the leaching out of the extractant from the membrane pores. It may require to carry out strip dispersion [188] studies for effective Sr transport. Plasma polymerization surface coating is another method as described by Yang et al. [189], where they have reported that a coating of heptylamine on the stripping side of a polypropylene membrane to be very effective in providing better membrane stability. Wijers et al. [190] have reported a method to improve membrane life-time by applying one stabilization layer on strip side or two

stabilization layers on either side of flat sheet supported liquid membrane. In future, such methods must be applied to address the issue of poor membrane stability.

6.4 CONCLUSIONS

The present studies deal with the recovery of Cs(I) and Sr(II) from acidic feed solutions. We have reported the possible methods for the recovery of Cs(I) and Sr(II) from a solution of 1 M HNO₃ acidity using 0.01 M CCD in 40% NPOE + 60% *n*-dodecane. It is interesting to find that sufficiently large distribution ratio value were obtained for Cs and Sr even at a very low concentration (0.01 M) of CCD compared to 0.08 M CCD used in the UNEX process solvent. The membrane studies were also carried out and revealed the possibility of applying liquid membrane based techniques for the simultaneous extraction of Cs and Sr from the PHWR-SHLW feed conditions. Although the present experiments were performed with FSSLM configuration, the process can be applied in the HFSLM mode which can provide higher mass transfer rates with easy scale-up options. The major observations can be summarized as follows:

- With 0.01 M CCD in 40% NPOE + 60% *n*-dodecane, Cs and Sr can be co-extracted from 1 M HNO₃ solution. Stripping of metal ions can be performed by using relatively higher concentrations of nitric acid (> 6 M HNO₃).
- 99.5 % Cs(I) can be extracted from 1 M HNO₃ solution by giving 4 contacts with 0.01 M CCD solution in the optimized diluent mixture of 40% NPOE + 60% *n*-dodecane..
- FSSLM transport studies were carried out using 0.01 M CCD in 60% NPOE + 40% *n*-dodecane as the carrier solvent where 1 M HNO₃ was employed as the feed phase while 8 M HNO₃ was used as the strip phase. Our studies revealed that the supported liquid membrane system was quite stable upto 19 days (Table 6.4) of continuous operation

indicating reasonably high stability which can make it an attractive option for the simultaneous recovery of Cs and Sr from HLW.

- > 98% Recovery of Cs(I) was possible by FSSLM containing 0.01 M CCD in 60% NPOE + 40% *n*-dodecane as carrier extractant thereby suggesting the possibility of liquid membrane techniques for recovery of Cs from the acidic radioactive waste solutions. HFSLM based methods seems to be promising for the recovery of Cs using this solvent system as it can provide faster mass transfer rates and high throughput.
- However, co-recovery of Sr was not possible due to leaching out of the PEG-400 from the membrane pores, strip-dispersion studies may be one of the solution of this problem. Also, surface modification by adhesion of polymeric layers on membrane surface can also improve the membrane stability and can be investigated as possible solution of the present problem.

CHAPTER 7: Summary and Conclusions

Recovery of valuables such as ^{137}Cs and ^{90}Sr has been the main objective of this Thesis work. These radioisotopes are produced in the nuclear reactor as a result of fission reaction of ^{235}U by thermal neutrons. Moderately long lived fission products ^{137}Cs ($t_{1/2}= 30.1$ y) and ^{90}Sr ($t_{1/2}=28.5$ y), due to their large heat output (^{137}Cs : 0.42 W/g and ^{90}Sr : 0.90 W/g), can cause degradation of the glass matrix thereby increasing the risk of leaching out of the radionuclides from the vitrified blocks. Also, leaching out of radioactive elements from the repositories can be extremely harmful for the environment. Therefore, the removal of such radionuclides can reduce the waste volume and hence can minimize the MANREM problem.

Long half-life and high energy beta/gamma rays emitted from ^{90}Sr and ^{137}Cs make these radionuclides viable alternative sources for various energy sources as described in the Chapter 1. Amongst many reagents, crown ethers and calix-crowns have been known for their high selectivity for a particular metal ion and simplicity of operation. Hence, substituted 18 crown 6 ethers have been used in the present work for selective extraction of Sr(II) from acidic solution. Also, calix-[4]arene-bis(2,3-naphtho)-crown-6 has been evaluated as a selective extractant for Cs(I) ion even in the presence of large excess of other alkali metal ion like Na^+ or K^+ . Due to the hazardous nature of the diluents like nitrobenzene or 1-octanol, high cost and carcinogenic nature of crown ethers, less harmful chemicals and separation methods with low ligand inventory were the main aim of this Thesis work. Liquid membrane techniques were explored to be one of the possible options in view of very low solvent inventory.

Apart from these, the objectives of present work include the search for alternative diluent systems for the co-recovery of Cs and Sr by the CCD + PEG-400 mixture. 2-nitrophenyloctyl

ether (NPOE) and *n*-dodecane mixture has been investigated as an alternative to the conventionally used fluorinated solvent or nitrobenzene based solvent systems. In addition to this, HFSLM technique was also successfully demonstrated for the separation of high purity carrier free ^{90}Y from a mixture of ^{90}Sr - ^{90}Y by using PC-88A as the carrier extractant. A mathematical model was developed for simulation of mass-transfer of the metal ion through supported liquid membranes (FSSLM and HFSLM).

The summary of the results are briefly given below.

1. Solvent extraction and membrane transport studies on Cs(I) have been carried out under various experimental conditions. At tracer level concentration of cesium, with 1.0×10^{-3} M calix[4]arene-bis(2,3-naphtho)-crown-6 (CNC) in 80% NPOE + 0.4% (v/v) + 20% *n*-dodecane and 3 M HNO_3 acidity, the distribution ratio for cesium was found to be 2.1 while the same was $< 10^{-2}$ with distilled water as aqueous phase. In flat sheet supported liquid membrane (FSSLM) configuration, it took about 24 hours for $\sim 90\%$ transport of Cs(I) from 3 M HNO_3 into distilled water with the optimized carrier solvent. The FSSLM experiments have been carried out at only 20 mL scale and the transport rates were rather slow. Hence, the present work dealt with the development of hollow fibre supported liquid membrane (HFSLM) technique to achieve higher mass transfer rates and throughput. With the similar experimental conditions as used with FSSLM, HFSLM transport experiment was carried out taking 0.5 L of 3 M HNO_3 solution as feed and distilled water as strip phase. In 6 hours of continuous operation in recycling mode, $> 99\%$ cesium was transported when cesium ion was present at tracer level of concentration. Other experiments were carried out by varying feed phase acidity, varying carrier concentration and varying the concentration of cesium ion in the feed phase. Increasing the feed acidity was found to provide higher mass transfer rates

upto 3 M HNO₃ acidity above which, a decrease in the transport rate was observed which was attributed to the competition of H₃O⁺ for CNC against Cs⁺ which affects the availability of free CNC carrier molecule for cesium transport. Under the same experimental conditions, with SHLW as the feed (3-4 M acidity), it took ~ 14 hours for only 88% Cs(I) transport which was attributed to the significantly high acid co-transport by the carrier to the strip phase. Various conditions of feed and strip were investigated to achieve maximum possible cesium recovery. Acetate buffer (0.1 M) at pH 5 was used as the strip solution but no significant improvement was observed in transport profile which may be due to limited buffer capacity of the strip solution. In a separate experiment, > 94% cesium transport was possible when the strip phase acidity was neutralized by the addition of equivalent amount of NaOH. Hence, near quantitative recovery of Cs(I) from SHLW as feed solution was demonstrated.

2. The recovery of Sr(II) by hollow fibre supported liquid membrane technique was carried out by using 0.1 M DtBuCH18C6 in 80% NPOE + 20% *n*-dodecane. 3 M HNO₃ was taken as feed while distilled water was used as the strippant in the receiver phase. With tracer level concentration of Sr, it took about 3 hours for ~ 90% transport of strontium. Afterwards, the back transport of metal ion was observed leading to a decreased transport of Sr to 85% in 6 hours. The back transport of metal ion was attributed to the co-transport of acid by the crown ether which was indirectly confirmed by various subsequent experiments. With SHLW as the feed solution, similar observations were seen. In order to increase the % transport of Sr, the strip phase acidity was neutralized by the addition of NaOH to the strip phase and it was found that > 94 % of Sr recovery is possible without observing the back transport of the metal ion. Sodium and barium were also found to be co-transported along with Sr.

3. A method was also developed to separate ^{90}Y from a mixture of ^{90}Sr - ^{90}Y . ^{90}Y is an important radioisotope which has been used in radiopharmaceuticals for the treatment of various types of cancers. HFSLM technique has been applied to get high throughput of ^{90}Y in sufficiently less time of operation as compared to methods previously applied for the same purpose. Bis-(2-ethylhexyl) phosphonic acid (PC-88A) was used as a selective extractant for ^{90}Y over ^{90}Sr . Solvent extraction experiments were carried out to get optimized condition for membrane studies. With 0.1 M HNO_3 as aqueous phase and 0.63 M PC-88A (20% v/v) in *n*-dodecane as extractant, the highest separation factor was achieved for Y over Sr. Subsequently, for HFSLM transport experiments, ^{90}Sr - ^{90}Y in 0.1 M HNO_3 was used as feed and strip was 3 M HNO_3 . It was observed that more than 90% transport of ^{90}Y can be achieved in only 30 minutes of operation leaving bulk of ^{90}Sr and unextracted ^{90}Y in the feed phase. Purity analysis using half-life method indicated contamination due to ^{90}Sr in the product which was further purified by passing the strip solution through a Sr.Spec® column leading to significant increase in the purity of the product. Decontamination factor value 10^4 was found which indicated the possible application of HFSLM based technique for obtaining high purity carrier free ^{90}Y .
4. Mathematical modeling of mass transfer through the liquid membranes was also performed which was important from many aspects. Various mathematical models have been described in literature but the complexity of those models leads to cumbersome treatment of equations rendering the use of models very difficult. A mathematical model was developed which was used to simulate the mass transport profiles of metal ion. Certain assumptions were made to simplify the process of mass transfer through the supported liquid membranes and the equations governing the transport, were written based on Fick's law of diffusion. The

differential equations were solved using numerical integration solvers in MATLAB software. The model was tested for various systems under various experimental conditions. Although simple in nature, the model predicted the experimental findings with acceptable error limits. Strip phase resistance has been neglected in the model which makes us unable to see the effect of the strip composition. Another disadvantage of the model has been the lack of incorporation of acid co-transport which can be done by assuming the complexation of acid (H_3O^+) with the carrier molecule.

5. Towards the development of an alternative diluent system for CCD/PEG extractant mixture for the co-recovery of Cs and Sr, a mixture of NPOE diluted with *n*-dodecane has been evaluated as a viable alternative. Encouraging results were obtained by solvent extraction studies which reveal the possibility of extraction of Cs and Sr by 0.01 M CCD + 0.05 % (v/v) PEG-400 in 40% NPOE in *n*-dodecane from 1 M HNO_3 as the aqueous solution. At > 6 M HNO_3 , D_{Cs} value was found to be $< 10^{-2}$ which suggested the possible striping of metal ions with this acidity. With this information, supported liquid membrane studies were carried out with the FSSLM configuration where 1 M HNO_3 was employed as feed phase while strip phase was 8 M HNO_3 . With 0.01 M CCD in 60% NPOE + 40% *n*-dodecane, $> 98\%$ cesium transport was reported in 24 hours of operation. The membrane stability with this diluent system was found to be quite good and after 19 days of repeated experiments, the permeability of metal ion was not significantly affected indicating the solvent system quite promising and can be used for the recovery of Cs using the membrane based separation techniques.

Future perspectives

In this thesis work, HFSLM technique has been explored as an emerging technique for the separation of valuable radionuclides from acidic feed solutions. Various advantages of the technique include much lower inventory of expensive or toxic compounds for treatment of radioactive wastes. The following points can be made as future directions

- The major challenge in recovery of valuables from high level waste would be the radiation degradation of polymer matrix of hollow fibers. The degradation of the polymer matrix (polypropylene) was noticed after 500 kGy of radiation dose. Hence, it is pertinent to develop hollow fibers with radiation resistant polymers which can withstand high radiation exposure as encountered in actual high level waste solutions.
- Simultaneous recovery of Cs and Sr can be achieved by using CCD + PEG-400 in NPOE/*n*-dodecane mixture as the solvent system. More extensive studies are required to investigate the extraction system. FSSLM transport experiments were carried out for Cs transport which suggested a very stable membrane system but the poor mass transfer rates can be overcome by using the system in HFSLM configuration. Further investigations are needed to explore this area of research in more detail.

The simple mathematical model can predict the transport profiles of metal ions. However, correction for acid co-transport is necessary for the cases where significantly higher acid uptake is observed. Also, the selectivity of system can also be visualized by performing the membrane transport simulation by the model. An important modification in the model will be if one can incorporate the strip phase equilibrium in the overall metal ion transport process. This would probably enable us to see the effect of strip phase composition on the net transport profile.

REFERENCES

1. IAEA Nuclear technology Review, 2009, IAEA, Vienna, (2009) p. 3.
2. Ansari, S.A., Mohapatra, P.K. and Manchanda, V.K., *Ind. Eng. Chem. Res.*, 48, (2009) 8605-8612.
3. U.S. Department of Health and Human services, Public health service, *Agency for toxic substances and disease registry, CESIUM CAS #7440-46-2*.
4. Technical Report Series No.356, *Feasibility of separation and utilization of cesium and strontium from high level liquid waste*, IAEA, Vienna, (1993) p.5.
5. Report on the accident at the Chernobyl nuclear power station, *Report NUREG-1250 rev. 1*, U. S. Government Printing Office, Washington, DC (1988).
6. *Strontium*, Human Health Fact Sheet (November 2006), Argonne National Laboratory, EVS, U.S.A.
7. Sadat, R., Ross, A. and Leveziel, H., Food irradiation: A global scenario, *in proceedings of International Conference on Applications of Radioisotopes and Radiation in Industrial Development (ICARID-94)*, February-1994, (1994).
8. Shor, R., Lafferty, R.H., Jr. Baker P.S., *Strontium-90 heat sources, ORNL-11C-36* (May, 1971).
9. Schulz, W.W. and Bray, L.A., *Sep. Sci. Technol.*, 22, (1987) 191-214.
10. Singh, S.P.N., *U.S. DOE Report SD-RE-PCP-011*, Rockwell Hanford Operations, Richland, WA (1983).

11. Rupp, A. F., *Proceedings of the Intemtional Conference on the Peaceful Uses of Atomic Energy, Volume 14: General Aspects of the Use of Radioactive Isotopes: Dosimetry* (1955) pp. 68-84.
12. Barton, G. B., Hepworth, J. L., McClanahan, E. D., Moore, R. L. and Van Tuyl., H. H., *Industrial and Engineering*, 50, (1958) 212-216.
13. Mimura, H., Akiba, K., *In the proceedings of WM'02 Conference*, Tucson, AZ, 24-28, (2002) p. 3.
14. Scasnar, V., Koprda, V., *Radiochem. Radioanal. Letters*, 39, (1979) 75-86.
15. Bortun, A.I., Bortun, L.N., Stepin, A.A., Pekhamkina, N. P., *J. Radioanal. Nucl. Chem.*, 174, (1993) 279-289.
16. Anthony, R.G., Dosch, R.G., Gu, D. and Philip, C.V., *Ind. Eng. Chem. Res.*, 33, (1994) 2702-2705.
17. Zheng, Z., Philip, C. V., Anthony, R. G., Krumhansl, J. L., Tradell, D. E . and Miller, J. E., *Ind. Eng. Chem. Res.*, 35, (1996) 4246-4256.
18. Mann, N.R. and Todd, T.A., Removal of Cesium from Acidic Radioactive Tank Waste Using IONSIV IE-911, accepted for publication in *Separation Science and Technology*, (2004).
19. Walker, D.D., WSRC-TR-2000-00362 (December 2000).
20. Smit, J., Van, R., *J. Nature*, 181, (1958) 1530-1531.

21. John, J., Sebesta, F., Motl, A., *Chemical Separation Technologies and Related Methods of Nuclear Waste Management*, G. R. Choppin, M. K. Khankhasayev (eds), Kluwer Academic Publishers, Dordrecht (1999).
22. Sebesta, F., John, J. and Motl, A., Phase II Report on the Evaluation of Polyacrylonitrile (PAN) as a Binding Polymer for Absorbers Used to Treat Liquid Radioactive Wastes, SAND96-1088 (1996).
23. Buchwald, H. and Thistlethwaite, W.P., *J. Inorg. Nucl. Chem.*, 5, (1958) 341-343.
24. Smit, J.V.R., Robb, W. and Jacobs, J.J., *J. Inorg. Nucl. Chem.*, 12, (1959) 104–112.
25. Satyanarayana, J., Murthy, G. S., Sasidhar, P., *J. Radioanal. Nucl. Chem.*, 242, (1999) 11-16.
26. Todd, T. A., Mann, N. R., Tranter, T. J., Sebesta, F., John v and Motl, A., *J. Radioanal. Nucl. Chem.*, 254, (2002) 47-52.
27. Tranter, T. J., Herbst, R.S., Todd, T.A., Olson, A.L., Eldredge, H.B., *Advances in Environmental Research*, 6, (2002) 107-121.
28. Ding N. and Kanatzidis, M.G., *Nature Chemistry*, 2, (2010) 187-191.
29. Mohsen Shahinpoor, *Bioinsp. Biomim.*, 6, (2011) 046004 (11pp).
30. Pederson, C. J., The discovery of crown ethers, *Science*, 241, (1988) 536-540.
31. Gerow, I.H., Smith, G.E. and Davis, M.W., *Sep. Sci. Technol.*, 16, (1981) 519-548.
32. Kinard, W.F., McDowell, W.J. and Shoun, R.R., *Sep. Sci. Technol.*, 15, (1980) 1013-1024.

33. McDowell, W.J., Case, G.N., McDonough, J.A. and Bartsch, R.A., *Anal. Chem.*, 64, (1992) 3013-3017.
34. Blasius, E. and Nilles, K.H., *Radiochem. Acta.*, 35(3), (1984) 173-182.
35. Blasius, E. and Nilles, K.H., *Radiochem. Acta.*, 36(4), (1984) 207-214.
36. Schuler, R. G., Bowers Jr., C. B., Smith, Jr., J. E., Brunt, V. V. and Davis Jr., M. W., *Solv. Extr. Ion Exch.*, 3, (1985) 567-604.
37. Zinke, A. and Ziegler, E., *Chem. Ber.*, 77, (1944) 264-272.
38. Izatt, S.R., Hawkins, R.T., Christensen, J.J. and Izatt, R.M., *J. Am. Chem. Soc.*, 107, (1985) 63-66.
39. Thuery, P., Nierlich, M., Lamare, V., Dozol, J.F., Asfari, Z. and Vicens, J., *J. Incl. Phenom. Macrocycl. Chem.*, 36, (2000) 375-408.
40. Casnati, A., Pochini, A., Ungaro, R., Ugozzoli, F., Arnaud, F., Fanni, S., Schwing, M.J., Egberink, R.J.M., de Jung, F. and Reinhoudt, R.N., *J. Am. Chem. Soc.* 117, (1995) 2767-2777.
41. Asfari, Z., Wenger, S. and Vicens, J., *Pure Appl. Chem.* 67, (1995) 1037-1043.
42. Ungaro, R., Casnati, A., Ugozzoli, F., Pochini, A., Dozol, J.F., Hill, C. and Rouquette, H., *Angew. Chem. Int. Ed. Eng.* 33, (1994) 1506-1509.
43. Haverlock, T.J., Sachleben, R.A., Bonnesen, P.V. and Moyer, B.A., *J. Incl. Phenom.*, 36, (2000) 21-37.
44. Raut, D.R., Mohapatra, P.K., Ansari, S.A. and Manchanda, V.K., *J. Membr. Sci.*, 310, (2008) 229-236.

45. Hawthorne, M.F. and Dunks, G.B., *U.S. Patent no. 5698169*, dated Dec.16, 1997 (1997).
46. Kyrs, M., *J. Radioanal. Nucl. Chem. Letters*, 187, (1994) 185-195.
47. Kyrs, M. and Selucky, P., *J. Radioanal. Nucl. Chem. Ar.*, 174, (1993) 153-165.
48. Rais, J., Plesek, J. and Selusky, P., *J. Radioanal. Nucl. Chem. Ar.*, 148, (1991) 349-357.
49. Bray, L.A., *U.S. AEC Report HW-79286*, General Electric Co., Richland, WA (1963).
50. Aubertin, C. and Lefevre, J., *French Patent 1469088*, (1967).
51. Lefevre, J., *French report CEA-Conf. 1092*, (1969).
52. Mann, N.R., Todd, T.A., *Sep. Sci. And Technol.*, 39, (2004) 2351-2357.
53. Horner, D.E., Brown, K.B., Crouse, D.J. and Weaver, B., Oak Ridge national Laboratory report, ORNL-3518, UC-4, TID-4500 (23rd ed.), (1963).
54. Richardson, G.L., *U.S. AEC Report HW-80686*, General Electric Co., Richland, WA (1964).
55. Horwitz, E.P., Dietz, M.L. and Fisher, D.E., *Solv. Extr. Ion Exch.*, 9, (1991) 1-25.
56. Mohapatra, P.K. and Manchanda, V.K., *Radiochim. Acta*, 55, (1991) 193-197.
57. Horwitz, E.P., Dietz, M.L. and Fisher, D.E., *Solv. Extr. Ion Exch.*, 8, (1990) 557-572.
58. Wood, D.J., Tranter, T.J. and Todd, T.A., *Solv. Extr. Ion Exch.*, 13, (1995) 829-844.
59. Horwitz, E. P. and Schulz, W. W., *Metal-Ion Separation and Preconcentration: Progress and Opportunities*, A. H. Bond, M. L. Dietz, R. D. Rogers (eds), ACS Symposium Series 716, Washington D.C. (1999).

60. Kumar, A., Mohapatra, P.K., Pathak, P.N. and Manchanda, V.K., *Talanta*, 45, (1997) 387-395.
61. Raut, D.R., Mohapatra, P.K. and Manchanda, V.K., *Sep. Sci. Technol.*, 45, (2010) 204–211.
62. Sekine, T. and Hasegawa, Y. (Eds.), “Solvent Extraction Chemistry: Fundamentals and Applications”, Marcel Dekker, New York (1977), p. 60.
63. Bagawade, S.V., Rao, P.R.V., Ramakrishna, V.V. and Patil, S.K., *J. Inorg. Nucl. Chem.*, 40, (1978) 1913-1918.
64. Small, H., *Ion chromatography*. New York: Plenum Press, ISBN 0-306-43290-0. (1989).
65. Wei, Y., Kumagai, M., Takashima, Y., Modolo, G. and Odoj, R., *Nuclear Technology*, 132, (2000) 413-423.
66. Lumetta, G.J., Wester, D.W., Morrey, J.R. and Wagner, M.J., *Solv. Extr. Ion Exch.*, 11, (1993) 663-682.
67. Horwitz, E.P., Dietz, M.L. and Chiarizia, R., *J. Radioanal. Nucl. Chem.*, 161, (1992) 575-583.
68. Dietz, M.L., Horwitz, E.P., Chiarizia, R. and Diamond, H., Topic J-4, at the *International Solvent Extraction Conference, ISEC'93, York, England*, (September 9-15, 1993). (Same as: CONF930945-3).
69. Lee, K., Evans, D.F. and Cussler, E.L., *AIChE J.*, 24, (1978) 860-868.
70. Danesi, P.R., *Sep. Sci. Technol.*, 19, (1984-85) 857-894.

71. Dworzak, W.R. and Naser, A.J., *Sep. Sci. Technol.*, 22, (1987) 677-689.
72. Guerreiro, R., Meregalli, L. and Zhang, X., *Hydrometallurgy*, 20, (1988) 109-120.
73. Kopunec, R. and Manh, T.N., *J. Radioanal. Nucl. Chem.*, 183, (1994) 181-204.
74. Urugami, T., “*Membrane Science and Technology*”, Eds., Y. Osada, , T. Nakagawa, , Marcel Dekker: New York (1992).
75. Parthasarathy, N., Pelletier, M., Buffle, J., *Anal. Chim. Acta*, 350, (1997) 183-195.
76. Prasad, R., Sirkar, K.K., *J. Membr. Sci.*, 50, (1990) 153-175.
77. Danesi, P. R.: *J. Membr. Sci.*, 20, (1984) 231-248.
78. Lin, S.H. and Juang, R.S., *J. Membr. Sci.*, 188, (2001) 251–262.
79. Gupta, S.K., Rathore, N.S., Sonawane, J.V., Pabby, A.K., Janardan, P., Changrani, R.D., *J. Membr. Sci.*, 300, (2007) 131–136.
80. D’Elia, N.A., Dahuron, L. and Cussler, E.L., *J. Membr. Sci.*, 29, (1986) 309–319.
81. Kim, J.I. and Stroeve, P., *Chem Eng Sci.*, 43, (1988) 247–257.
82. Kim, J.I. and Stroeve, P., *Chem Eng Sci.*, 44, (1989) 1101–1111.
83. Kim, J.I. and Stroeve, P., *J. Membr. Sci.*, 45, (1989) 99–114.
84. Kim, J.I. and Stroeve, P., *J. Membr. Sci.*, 49, (1990) 37–53.
85. Alhousseini, A. and Ajbar, A., *Math. Comput. Model.*, 32, (2000) 465–480.
86. Komasaawa, I., Otake, T., and Yamashita, T., *Ind. Eng. Chem. Res. Fund.*, 22, (1983) 127–131.

87. Garea, A., Urtiaga, A.M., Ortiz, M.I., Alonso, A.I. and Irabien, J.A., *Chem. Eng. Commun.*, 120, (1993) 85–97.
88. Evans, R.D., “The atomic nucleus”, (1955) p. 479.
89. Mathur, J.N., Murali, M.S., Natarajan, P.R., Badheka L.P. and Banerji, A., *Talanta*, 39, (1992) 493-496.
90. Knoll, G.F., *J. Radioanal. Nucl. Chem.*, 243, (2000) 125-131.
91. Knoll, G.F. , “Radiation detection and measurement”, 3rd ed., John Willy and sons, New York (2000), p. 406.
92. McDowell, W.J., “Organic scintillators and liquid scintillation counting”, D.L. Horrocks, L.T. Peng (Eds.), Academic Press, Inc., New York (1971), p. 937.
93. Ihle, H., Karayannis, M. and Murrenhoff, A. , “Organic scintillators and liquid scintillation counting”, D.L. Horrocks, L.T. Peng (Eds.), Academic Press, Inc., New York (1971), p. 879.
94. Thompson, M. and Walsh, J.N., ‘Inductively Coupled Plasma Spectrometry’, Blackie (1989).
95. Moore, V. G. L., ‘Introduction to Inductively Coupled Plasma Atomic Emission Spectroscopy’, Elsevier, Amsterdam (1989), ISBN: 0-444-43029-6.
96. Danesi, P.R., Horwitz, E.P., Rickert, P.G., *J. Phys. Chem.*, 87, (1983) 4708-4715.
97. Baker, R.W., Tuttle, M.E., Kelly, D.J., Lonsdale, H.K., *J. Membr. Sci.*, 2, (1977) 213–233.
98. Ibanez, J.A., Victoria, L., Hernandez, A., *Sep. Sci. Technol.*, 24, (1989) 157–164.

99. Kiani, A., Bhave, R.R., Sirkar, K.K., *J. Membr. Sci.*, 20, (1984) 125–145.
100. Prasad, R., Kiani, A., Bhave, R.R., Sirkar, K.K., *J. Membr. Sci.*, 26, (1986) 79–97.
101. Zha, F., Fane, A.G., Fell, C.J.D., *Ind. Eng. Chem. Res.*, 34, (1995) 1799–1809.
102. Ren, Z., Zhang, W., Dai, Y., Yang, Y., Hao, Z., *Ind. Eng. Chem. Res.*, 47, (2008) 4256–4262.
103. Yang, Q., Kocherginsky, N.M., *J. Membr. Sci.*, 297, (2007) 121–129.
104. Tranter, T.J., Vereshchagina, T.A., Utgikar, V., *Solv. Extr. Ion Exch.*, 27, (2009) 199–218.
105. Banerjee, D., Rao, M.A., Gabriel, J., Samanta, S.K., *Desalination*, 232, (2008) 172–180.
106. Talanov, V.S., Talanov, G.G., Gorbunova, M.G., Bartsch, R.A., *J. Chem.Soc., Perkin Trans.*, 2, (2002) 209–215.
107. Dietz, M.L., Horwitz, E.P., Rhoads, S., Bartsch, R.A., Palka, A., Krzykawski, J., *Solv. Extr. Ion Exch.* 14, (1996) 1–12.
108. Dietz, M.L., Horwitz, E.P., Jensen, M.P., Rhoads, S., Bartsch, R.A., Palka, A., Krzykawski, J., Nam, J., *Solv. Extr. Ion Exch.* 14, (1996) 357–384.
109. Gutsche, C. D., *Calixarenes*, The Royal Society of Chemistry, Cambridge, England (1989).
110. Böhmer, V., *Angew. Chem. Int. Ed. Engl.* 34, (1995) 713-745.
111. Ghidini, E., Ugozzoli, F., Ungaro, R., Harkema, S., El-Fadl, A., Reinhoudt, D.N., *J. Am. Chem. Soc.*, 113, (1990) 6979–6985.

- 112.** Sachleben, R.A., Bryan, J.C., Engle, N.L., Haverlock, T.J., Hay, B.P., Urvoas, A., and Moyer, B.A., *Eur. J. Org. Chem.*, (2003), 4862-4869.
- 113.** Ugozzoli, F., Ori, O., Casnati, A., Pochini, A., Ungaro, R. and Reinhoudt, D. N., *Supramol. Chem.*, 5, (1995) 179-184.
- 114.** Fujimoto, T., Yanagihara, R., Kobayashi, K. and Aoyama, Y., *Bull. Chem. Soc. Jpn.*, 68, (1995) 2113-2124.
- 115.** Leonard, R. A., Conner, C., Liberatore, M. W., Sedlet, J., Aase, S. B., Vandegrift, G. F., Delmau, L. H., Bonnesen, P. V., Moyer, B. A., *Sep. Sci. Technol.*, 36, (2001) 743-766.
- 116.** Mohapatra, P.K., Ansari, S.A., Sarkar, A., Bhattacharyya, A., Manchanda, V.K., *Anal. Chim. Acta*, 571, (2006) 308–314.
- 117.** Asfari, Z., Bressot, C., Vicens, J., Hill, C., Dozol, J. F., Rouquette, H., Eymard, S., Lamare, V. and Tournois, B., *Anal. Chem.* 67, (1995) 3133-3139.
- 118.** Raut, D.R., Mohapatra, P.K., Ansari, S.A., Sarkar, A. and Manchanda, V.K., *Desalination*, 232, (2008) 262–271.
- 119.** Bonnesen, P. V., Delmau, L. H., Haverlock, T. J., Moyer, B. A., Report No. ORNL/TM-13704, Oak Ridge National Laboratory, Oak Ridge, Tennessee, USA (Dec., 1998).
- 120.** Raut, D. R., Mohapatra, P. K., Ansari, S. A., Manchanda, V. K.: *Sep. Sci. Technol.*, 44, (2009) 3664-3678.
- 121.** Urtiaga, A.M., Ortiz, M.I. and Salazar, E., *Ind. Eng. Chem. Res.*, 31, (1992) 877-886.

122. Kriz, J., Dybal, J., Makrlik, E. and Budka, J., *Magn. Res. Chem.*, 46, (2008) 235-243.
123. Kriz, J., Dybal, J., Makrlik, E., Budka, J. and Vanura, P., *Monatshefte für Chemie*, 138, (2007) 735-740.
124. Eroglu, I., Kalpakci, R., Gunduz, G., *J. Membr. Sci.*, 80, (1993) 319–325.
125. Shamsipur, M. and Raoufi, F., *Sep. Sci. Technol.*, 37, (2002) 481–492.
126. Mikulaj, V., Hlatby, J., Vasekova, L., *J. Radioanal. Nucl. Chem.*, 101, (1986) 51–57.
127. Walkowiak, W., Kozlowski, C. A., *Desalination* 240, (2009) 186-197.
128. Dozol, J.F., Casas, J. and Sastre, A.M., *Sep. Sci. Technol.*, 28, (1993) 2007–2022.
129. Rawat, N., Mohapatra, P.K., Lakshmi, D.S., Bhattacharyya, A., Manchanda, V.K., *J. Membr. Sci.*, 275, (2006) 82–88.
130. Mohapatra, P.K., Lakshmi, D.S. and Manchanda, V.K., *Desalination*, 198, (2006) 166-172.
131. Ramadan, A. and Danesi, P.R., *Solv. Extr. Ion Exch.*, 6, (1988) 157-166.
132. Raut, D.R., Mohapatra, P.K., and Manchanda, V.K., *Radiochim. Acta.*, 97, (2009) 565-570.
133. Raut, D.R., Mohapatra, P.K. and Manchanda, V.K., *J. Membr. Sci.*, 390–391, (2012) 76– 83.
134. Wai, C. M., Du, H. S., *Anal. Chem.*, 62, (1990) 2412-2414.
135. Kawashima, T., *J. Appl. Radiat. Isot.*, 20, (1969) 806-808.
136. Rane, A., and Bhatki, K.S., *Anal. Chem.*, 38, (1966) 1598-1601.

137. Skraba, W.J., Arino, H. and Kramer, H.H., *J. Appl. Radiat. Isot.*, 29, (1978) 91-96.
138. Suzuki, Y., *Int. J. Appl. Radiat. Isot.*, 15, (1964) 599-602.
139. Chinol, M. And Hnatowich, D., *J. Nucl. Med.*, 28, (1987) 1465-1470.
140. Wike, J.S., Guyer, C.E., ramey, D.W. and Phillips, B.P., *Appl. Radiat. Isot.*, 41, (1990) 861-865.
141. Lee, J.S., Park, U.J., Son, K.J., Han, H.S., *Appl. Radiat. Isot.*, 67, (2009) 1332-1335.
142. Ramanujam, A., Achuthan, P. V., Dhami, P. S., Kannan, R. Gopalakrishnan, V., Kansra, V. P., Iyer, R. H., Balu, K., *J. Radioanal. Nucl. Chem.*, 247, (2001) 185-191.
143. Dhami, P. S., Naik, P. W., Dudwadkar, N. L., Kannan, R., Achuthan, P. V., Moorthy, A. D., Jambunathan, U., Munshi, S. K. and Dey, P. K., *Sep. Sci. Technol.*, 42, (2007) 1107-1121.
144. Kolthoff, I.M., Wang, W-Ji and Chantooni, M.K. Jr., *Anal. Chem.*, 55, (1983) 1202-1204.
145. Liou, C.C. and Brodbelt, J.S., *J. Am. Chem. Soc.*, 114, (1992) 6761-6764.
146. Narayanan, P., Nair, V. R., and Moharana, L. N., Proc. of the International Symposium on Solvent Extraction, ed. by V. N. Mirsa, S. C. Das and K. S. Rao, (Allied Publishers PVT Ltd., New Delhi, 2002) 227-234.
147. Lee, MS., Lee, GS., Lee, JY., Kim, S.D. and Kim, J.S., *Materials Transactions*, 46, (2005) 64-68.
148. Kao, H.C., Yen, PS and Juang, RS, *Chemical Engineering Journal*, 119, (2006) 167-174.

149. Lee, T.W., Ting, G., *Isotopes in Environmental and Health Studies*, 27, (1991) 269-273.
150. Qiu, D., Zheng, L. and Ma, R., *Solvent Extr. Ion Exch.*, 7, (1989) 937–950.
151. Plucinski, P., Nitsch, W., *J. Membr. Sci.*, 39, (1988) 43–59.
152. Danesi, P.R., Horwitz, E.P. and Rickert, P.G., *J. Phys. Chem.*, 87, (1983) 4708-4715.
153. Pandey, U., Dhama, P.S., Jagasia, P., Venkatesh, M. and Pillai, M.R.A., *Anal. Chem.*, 80, (2008) 801-807.
154. Ansari, S.A., Bhattacharyya, A., Raut, D.R., Mohapatra, P.K. and Manchanda, V.K., *Radiochim. Acta.*, 97, (2009) 149-153.
155. De, S., Dias, J.M. and Bhattacharya, P.K. *Chem. Eng. Comm.*, 159, (1997) 67-89.
156. Leveque, M.A., Les, L., *Ann. Mines.* 13, (1928) 201–239.
157. Wilke, C. R. and Chang, P., *A. I. Ch. E. Journal*, 1, (1955) 264-270.
158. Huang, T. and Huang, C., *J. Membr. Sci.* 29, (1986) 295-308.
159. Panja, S., Mohapatra, P.K., Tripathi, S.C. and Manchanda, V.K., *Sep. Sci. Technol.* 46, (2011) 94-104.
160. Panja, S., Mohapatra, P.K., Dakshinamoorthy, A. and Manchanda, V.K., *Sep. Sci. Technol.* 45, (2010) 1112-1120.
161. Kittisupakorn, P., Weerachaipichaskul, W and Thitiyasook, P., *J. Ind. Eng. Chem.*, 13, (2007) 903-910.
162. Harrington, P.J. and Stevens, G.W., *J. Membr. Sci.*, 192, (2001) 83–98.

163. Makrlík, E. and Vanura, P., *Talanta*, 32, (1985) 423–429.
164. Hawthorne, M.F., Andrews, T.D., *J. Chem. Soc., Chem. Commun.*, 19, (1965) 443–444.
165. Hawthorne, M.F., Young, D.C., Wegner, P.A., *J. Am. Chem. Soc.*, 87, (1965) 1818–1819.
166. Callahan, K.P. and Hawthorne, M.F., *Adv. Organomet. Chem.*, 14, (1976) 145-186.
167. Rais, J., *Czech Patent No. 153933*.
168. Rais, J.; Selucky, P.; Kyrs, M., *J. Inorg. Nucl. Chem.*, 38, (1976) 1376–1378.
169. Selucky, P.; Vanura, P.; Rais, J.; Kyrs, M., *Radiochem. Radional. Lett.*, 38, (1979) 297–302.
170. Romanovskiy, V.N., Smirnov, I.V., Babain, V.A., *Solvent Extr. Ion Exch.*, 19, (2001) 1-21.
171. Smirnov, I.V., Babain, V.A., Shadrin, A.Y., Proceedings from the International Conference on Decommissioning and Decontamination and on Nuclear and Hazardous Waste Management, Spectrum'98, Denver, Colorado (1998).
172. Todd, T.A., Law, J.D., Herbst, R.S., Brewer, K.N., Romanovsky, V.N., Esimantovsky, V.M., Smirnov, I.V., Babain, V.A., Zaitsev, B.N., Kuznetsov, G.I., Shklyar, L.I., Proceedings from the International Conference on Decommissioning and Decontamination and on Nuclear and Hazardous Waste Management, Spectrum'98, Denver, Colorado (1998).

- 173.** Law, J.D., Herbst, R.S., Todd, T.A., Law, J.D., Romanovskiy, V.N., Esimantovskiy, V.M., Smirnov, I.V., Babain, V.A., Zaitsev, B.N., *Proceedings from Global '99*, Jackson, Wyoming (1999).
- 174.** Law, J.D., Herbst, R.S., Todd, T.A., Romanovskiy, V.N., Esimantovskiy, V.M., Smirnov, I.V., Babain, V.A., Zaitsev, B.N., Report INEEL/EXT-99-00954 (October 1999).
- 175.** Makrlík, E., Vanura, P., Selucky, P., *J. Radioanal. Nucl. Chem.*, 288, (2011) 177–180.
- 176.** Romanovsky, V.N., *J. Nucl. Sci. Technol. Suppl.*, 3, (2002) 8–13.
- 177.** Herbst, R.S., Law, J.D., Todd, T.A., *Solvent. Extr. Ion Exch.*, 20, (2002) 429–445.
- 178.** Herbst, R.S., Peterman, D.R., Tillotson, R.D. and Delmau, L.H., *Solv. Exch. Ion Exch.*, 26, (2008) 163–174.
- 179.** Mason, C.F.V., Reilly, S.D., Smith, P.H., Report LA-11695, Los Alamos, N.Mex.: Los Alamos National Laboratory, USA (1990).
- 180.** Herbst, R. S., Law, J. D., Todd, T. A., Romanovskii, V. N., Babain, V. A., Esimantovski, V. M., Zaitsev, B. N. and Smirnov, I. V., *Sep. Sci. Technol.*, 37, (2002) 1807-1831.
- 181.** Luther, T. A., Herbst, R. S., Peterman, D. R., Tillotson, R. D., Garn, T. G., Babain, V. A., Smirnov, I. V., Stoyanov, E. S. and Antonov, N. G., *J. Radioanal. Nucl. Chem.*, 267, (2006) 603-613.
- 182.** Dozol, J. F., Dozol, M. and Macias, R. M., *J. Incl. Phenom. Macro.*, 38, (2000) 1–22.

- 183.** Ansari, S.A., Mohapatra, P.K., Prabhu, D.R. and Manchanda, V.K., *J. Membr. Sci.*, 298, (2007) 169–174.
- 184.** Zalupski, P. R., Herbst, R. S., Delmau, L. H., Martin, L. R., Peterman, D. R. & Nash, K. L., *Solv. Extr. Ion Exch.*, 28, (2010) 161-183.
- 185.** Mohapatra, P.K., Bhattacharyya, A. and Manchanda, V.K., *J. Membr. Sci.*, 181, (2010) 679–685.
- 186.** Crank, J., *The Mathematics of Diffusion*, 2nd ed., Oxford University Press Inc., New York (1975), p. 414.
- 187.** Ma, T. Y., Hollander, D., Krugliak, P. and Katz, K., (1990). *Gastroenterology* 98, (1990) 39–46.
- 188.** Ho, W.S.W., Wang, B., U.S. Patent, No. US 6291705 B1.
- 189.** Yang, X.J., Fane, A.G., Bi, J. and Griesser, H.J., *J. Membr. Sci.*, 168, (2000) 29-37.
- 190.** Wijers, M.C., Jin, M., Wesseling, M. and Strathmann, H., *J. Membr. Sci.*, 147, (1998) 117-130.

LIST OF PUBLICATIONS

1. Selective cesium transport using hollow fibre supported liquid membrane containing calix[4]arene-bis-naphthocrown-6 as the carrier extractant. **P. Kandwal**, P.K. Mohapatra, S.A. Ansari and V.K. Manchanda, *Radiochim. Acta*, 98 (2010) 493-498.
2. Separation of carrier free ^{90}Y from ^{90}Sr by hollow fiber supported liquid membrane containing bis(2-ethylhexyl) phosphonic acid. **P. Kandwal**, S.A. Ansari, P.K. Mohapatra and V.K. Manchanda, *Sep. Sci. Technol.*, 46(6), (2011) 904-911.
3. Mathematical modeling of Cs(I) transport through flat sheet supported liquid membrane using calix-[4]-bis(2,3-naphtho)-18-crown-6 as the mobile carrier. **P. Kandwal**, S. Dixit, S. Mukhopadhyay, P.K. Mohapatra, V.K. Manchanda, *Desalination*, 278 (2011) 405-411.
4. Mass transport modeling of Cs(I) through hollow fiber supported liquid membrane containing calix-[4]-bis(2,3-naphtho)-crown-6 as the mobile carrier. **P. Kandwal**, S. Dixit, S. Mukhopadhyay, and P.K. Mohapatra, *Chemical Engineering Journal*, 174 (2011) 110– 116.
5. Transport of cesium using hollow fiber supported liquid membrane containing calix[4]arene-bis(2,3-naphtho)crown-6 as the carrier extractant: Part II. Recovery from simulated high level waste and mass transfer modeling. **P. Kandwal**, S.A. Ansari and P.K. Mohapatra, *J. Membr. Sci.*, 384 (2011) 37-43.
6. A Highly Efficient Supported Liquid Membrane System for Near Quantitative Recovery of Radio-strontium from Acidic Feeds: Part II. Scale up and Mass Transfer

Modeling in Hollow Fiber Configuration. **P. Kandwal**, S.A. Ansari and P.K. Mohapatra, *J. Membr. Sci.*, 405-406, (2012) 85-91.

7. Selective Recovery of Am(III) over Eu(III) by Hollow Fiber Supported Liquid Membrane Using Cyanex 301 in the Presence of Synergists as the Carrier. A. Bhattacharyya, S. A. Ansari, **P. Kandwal**, P. K. Mohapatra, and V. K. Manchanda, *Sep. Sci. Technol.*, 46 (2011) 205–214.*
8. A ‘cold’ actinide partitioning run at 20 L scale with hollow fibre supported liquid membrane using diglycolamide extractants. S. A. Ansari, R. B. Gujar, P. K. Mohapatra, **P. Kandwal**, A. Sengupta, S. K. Thulasidas and V. K. Manchanda, *Radiochim. Acta*, 99 (2011) 815-821.*
9. Pertraction of plutonium in the +4 oxidation state through a supported liquid membrane containing TODGA as the carrier. S. Panja, P.K. Mohapatra, **P. Kandwal**, S.C. Tripathi, V.K. Manchanda, *Desalination*, 262 (2010) 57-63.*
10. Evaluation of polymer inclusion membranes containing calix[4]-bis-2,3-naphtho-crown-6 for Cs recovery from acidic feeds: Transport behavior, morphology and modeling studies. D.R. Raut, **P. Kandwal**, G. Rebello, P.K. Mohapatra, *J. Membr. Sci.*, 407– 408 (2012) 17– 26.*

(* not included in the thesis.)

SYMPOSIUMS

1. Separation of ^{90}Y from ^{90}Sr using hollow fiber supported liquid membrane containing PC-88A as the carrier. **P. Kandwal**, D.R. Raut, P.K. Mohapatra, and V.K. Manchanda, in the proceedings of conference *NUCAR-2009* held in SVKM's Mithibai college during January 7-10, 2009.
2. Effect of radiation on Transport of ^{90}Y across Supported Liquid Membrane Using PC-88A as the Carrier Ligand. **Pankaj Kandwal**, P.K. Mohapatra and V.K. Manchanda, in the proceedings of *NSRP-2009* held in Kumaun University during March 12-14 2009.
3. Selective recovery of radio-caesium on litres scale with calix[4]arene-bis-naphthocrown-6 using Hollow Fibre Supported Liquid Membrane technology. **Pankaj Kandwal**, P.K. Mohapatra, S.A. Ansari and V.K. Manchanda, in the proceedings of "*National Seminar on Solvent Extraction*" held at IGCAR, Kalpakkam, during June 23-24, 2009.
4. Studies on transport of Cesium ion by Calix[4]arene-bis-(2,3-naphtho)-18-crown-6 using Flat Sheet Supported Liquid Membrane. **P. Kandwal**, Smita Dixit, S. Mukhopadhyay, P.K. Mohapatra and V.K. Manchanda, in the proceedings of symposium *SESTEC-2011*, held in IGCAR, Kalpakkam during March 1-4, 2010.
5. Effect of Synergists on Separation of Am(III) and Eu(III) with Cyanex-301 Using Hollow Fibre Supported Liquid Membrane. A. Bhattacharya, S.A. Ansari, **P.**

Kandwal, P.K. Mohapatra and V.K. Manchanda, in the proceedings of symposium *SESTEC-2011*, held in IGCAR, Kalpakkam during March 1-4, 2010.

6. Transport and Modeling Studies of U pertraction Using TEHDGA as the carrier across a supported Liquid membrane. **Pankaj Kandwal**, S. Panja, P.K. Mohapatra, S.C. Tripathi, P.K. dey, S.K. Munshi, V.K. Manchanda, in the proceedings of conference *NUCAR-2011* held in Visakhapatnam during February 22-26, 2011.
7. Modeling of transport of Cs(I) through Hollow Fibre Supported Liquid membrane using Calix[4]arene-bis-2,3-naphtho-crown-6 (CNC) as the carrier. **P. Kandwal**, S. Dixit, S. Mukhopadhyay, P.K. Mohapatra and V.K. Manchanda, in the proceedings of conference *NUCAR-2011* held in Visakhapatnam during February 22-26, 2011
8. Modeling of Cs(I) transport Data Across polymer Inclusion Membrane Containing Calix[4]arene-bis-2,3-naphtho-crown-6 (CNC) as the carrier. **P. Kandwal**, D.R. Raut, P.K. Mohapatra and V.K. Manchanda, in the proceedings of conference *NUCAR-2011* held in Visakhapatnam during February 22-26, 2011.
9. Recovery of cesium from nuclear waste using hollow fibre supported liquid membrane containing calix[4]arene-bis-(2,3-naphtho)-crown-6. **P. Kandwal**, P.K. Mohapatra, in the proceedings of conference *GLOBAL-2011* held during December 11-16, 2011 in Makuhari Messe, Japan.
10. Use of Chlorinated Cobalt Dicarbollide in 2-nitrophenyloctyl Ether as a Promising Alternative to FS-13 Based Solvents. **P. Kandwal** and P.K. Mohapatra, in the proceedings of conference *SESTEC-2012* held in SVKM's Mithibai College during February 27 – March 1, 2012.

- 11.** Cesium Transport across Flat Sheet Supported Liquid Membrane Containing CCD in NPOE-Dodecane mixture. **P. Kandwal**, P.K. Mohapatra, in the proceedings of conference *SESTEC-2012* held in SVKM's Mithibai College during February 27 – March 1, 2012.

- 12.** Studies on the Transport behaviour of Sr(II) through Hollow Fibre Supported Liquid Membrane containing di-*tert*-butylcyclohexano 18-crown-6 as mobile carrier. **P. Kandwal**, P.K. Mohapatra, in the proceedings of conference *SESTEC-2012* held in SVKM's Mithibai College during February 27 – March 1, 2012.